THE MECHANISM AND PHYSIOLOGICAL FUNCTION OF EPIDERMAL

LIPOXYGENASE-3

By

Yuxiang Zheng

Dissertation

Submitted to the Faculty of the

Graduate School of Vanderbilt University

in partial fulfillment of the requirements

for the degree of

DOCTOR OF PHILOSOPHY

in

Pharmacology

December, 2010

Nashville, Tennessee

Approved:

Professor Alan R. Brash

Professor Tina M. Iverson

Professor F. Peter Guengerich

Professor David L. Hachey

Professor Claus Schneider

ACKNOWLEDGMENTS

TABLE OF CONTENTS

LIST OF FIGURES

# LIST OF ABBREVIATIONS

| | |
|---|---|
| AA | arachidonic acid |
| AA/lyso PA | 1-arachidonoyl-lysophosphatidic acid |
| ARCI | autosomal recessive congenital ichthyosis |
| APCI | atmospheric pressure chemical ionization |
| BDE | bond dissociation energy |
| BHA | butylated hydroxyanisole |
| CE | cornified cell envelope |
| CLE | corneocyte lipid envelope |
| diH(P)ETE | dihydro(pero)xyeicosatetraenoic acid |
| eLOX3 | epidermal lipoxygenase-3 |
| EFA | essential fatty acid |
| ENU | N-ethyl-N-nitrosourea |
| EOS | esterified omega-hydroxyacyl-sphingosine |
| GC-MS | gas chromatography mass spectrometry |
| H(P)ETE | hydro(pero)xyeicosatetraenoic acid |
| H(P)ODE | hydro(pero)xyoctadecadienoic acid |
| KODE | ketooctadecadienoic acid |
| KETE | ketoeicosatetraenoic acid |
| LA | linoleic acid |
| LA/lyso PC | 1-linoleoyl-lysophosphatidylcholine |
| LH or FA | fatty acid |
| LC-MS | liquid chromatography mass spectrometry |

| | |
|---|---|
| LOX | lipoxygenase |
| Mn-LOX | manganese lipoxygenase |
| NDGA | nordihydroguaiaretic acid |
| OS | omega-hydroxyacyl-sphingosine |
| $PGE_2$ | prostaglandin $E_2$ |
| PPAR | peroxisome proliferator-activated receptor |
| ROOH or LOOH | fatty acid hydroperoxide |
| RP-HPLC | reversed phase high pressure liquid chromatography |
| SP-HPLC | straight phase high pressure liquid chromatography |
| TPP | triphenylphosphine |

# CHAPTER I

# INTRODUCTION

**Lipoxygenase catalysis: reactions with polyunsaturated fatty acids**

Widely expressed in plants and animals, lipoxygenases (LOX) are a class of non-heme iron dioxygenases that incorporate a molecule of oxygen into polyunsaturated fatty acids with at least one 1Z,4Z-pentadiene unit, yielding fatty acid hydroperoxides (1). The hydoperoxide products, being relatively unstable, will often undergo further transformation to bioactive molecules such as leukotrienes, which are pro-inflammatory lipid mediators in inflammatory diseases such as asthma (2,3).

Within the LOX family, soybean LOX-1 and rabbit reticulocyte 15-LOX are the best studied mechanistically (4,5). The same catalytic mechanism has been proposed for the two enzymes (**Figure 1**). Briefly, the active site $Fe^{3+}$, together with one of its six ligands, a hydroxide ion, abstracts a hydrogen atom from the fatty acid substrate, forming a $Fe^{2+}$-$H_2O$ complex and a fatty acid radical. The fatty acid radical then combines with a triplet $O_2$ diradical to form a peroxy radical. Finally, the peroxy radical obtains the hydrogen atom back from the $Fe^{2+}$-$H_2O$ complex, forming the hydroperoxide product and regenerating the ferric enzyme, thus completing a catalytic cycle.
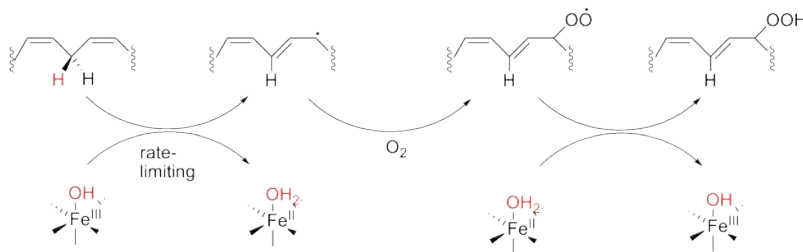


**Figure 1**: The catalytic cycle of LOX enzymes

Molecular oxygen in the atmosphere exists in the triplet state, and triplet oxygen does not react with covalently complete hydrocarbon molecules (6). To overcome this difficulty, either molecular oxygen or the hydrocarbon substrate has to be activated. LOX enzymes employ the latter strategy to activate the polyunsaturated fatty acid substrate to a fatty acid radical, which will then readily react with triplet molecular oxygen. The chemistry of this substrate activation involves the homolytic cleavage the bisallylic C-H bond in the fatty acid substrate by the active site $Fe^{3+}$-OH complex. The moderately high bond dissociation energy (BDE) of the bisallylic C-H bond (e.g., ~ 73 kcal/mol for $C_{11}$-H in linoleic acid (7)) dictates that the redox potential of the active site iron should be moderately high for the bond cleavage to occur (6). Indeed, a moderately high redox potential, ~ 600 mV, has been demonstrated experimentally in soybean LOX-1 (8).

A remarkable feature of LOX catalysis is that the incorporation of molecular oxygen is often regio- and stereospecific; each LOX usually makes a single optically active hydroperoxide. This implies two facets of enzymatic control: 1) only one hydrogen atom on the substrate will be abstracted, and 2) on the subsequently formed pentadienyl radical, only one side of one reactive carbon will be preferentially accessible to molecular oxygen. The first facet can be explained if the substrate adopts a relatively rigid conformation in the enzyme active site so that only one of the hydrogens is placed in proximity to the iron and thus available for abstraction. As to the second facet, however, a considerable debate continues, centering on the means by which oxygen access is controlled in the enzyme active site. $O_2$ channels have been proposed (9,10), yet simple steric shielding of $O_2$ by amino acid residues within the fatty acid binding cavity is also a

possibility (11). It is foreseeable that this conflict of views may eventually be resolved when xenon gas is successfully used to probe LOX enzymes in the years to come.

In 2004, this laboratory made the discovery that the regio- and stereospecificity of LOX enzymes is partly controlled by an active site residue, conserved as Gly in *R*-LOX (i.e., LOX enzymes that make products in the *R* configuration) and Ala in *S*-LOX (12). Swapping the two residues by site-directed mutagenesis almost always results in swapping of stereospecificity along with a shift in regiospecificity in the product (13-16); for example, the Ala-to-Gly mutation in 8*S*-LOX leads to a switch of oxygenation specificity from 8*S* to 12*R*. To explain this, a model has been proposed (**Figure 2**) (14). In essence, this model states that the Ala/Gly residue is aligned with one of the two reactive terminal carbons on the activated pentadiene unit, and that whereas the smaller Gly allows $O_2$ to react at this site, the bigger Ala blocks the space for $O_2$ thus causing a switch of oxygen insertion to the other reactive terminal carbon. Recently, based on a high-resolution crystal structure of coral 8*R*-LOX, Newcomer and colleagues propose a new model where the space for $O_2$ is made available by a nearby Leu residue (rather than by the Ala/Gly directly), which alternates between two positions. This controls the position of $O_2$ within the active site depending on whether the neighboring residue is Ala or Gly (17). At present, with no crystal structure of LOX enzymes with bound fatty acid substrate available, it is difficult to ascertain which model depicts more accurately the role of the Ala/Gly residue in the control of oxygen access.
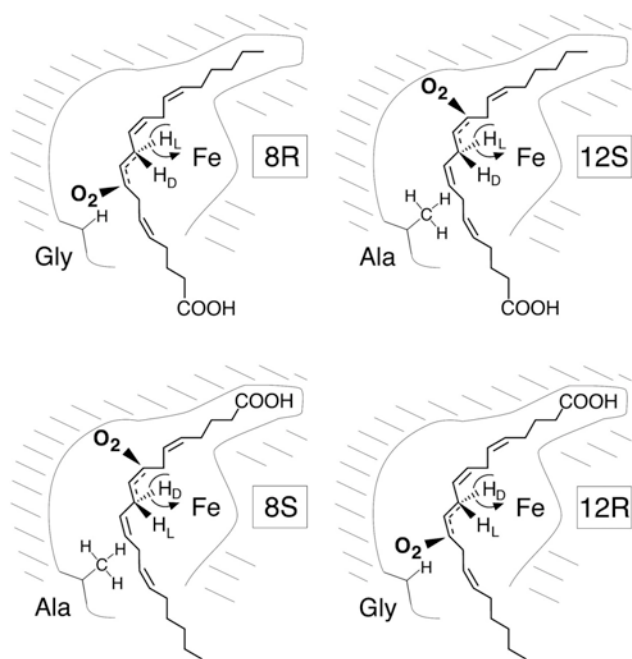
**Figure 2**: A model to explain the *R* or *S* specificity of LOX enzymes. Reproduced from (14).

**Reactions of lipoxygenases with fatty acid hydroperoxides**

In addition to catalyzing oxygenation of polyunsaturated fatty acids, LOX enzymes also react with fatty acid hydroperoxides, especially with their own product from the oxygenation reaction. One such reaction common to all LOX enzymes occurs at the initial stage of LOX-catalyzed oxygenation of polyunsaturated fatty acids, known as the activation step. For soybean LOX-1, for example, the ferrous enzyme will be transformed by an equimolar amount of 13*S*-hydroperoxylinoleic acid (13*S*-HPODE) to a ferric species (18), which is the catalytically active form in the oxygenation reaction (19). Because the native LOX is usually in the ferrous state, a kinetic lag phase is commonly observed in the oxygenation reaction of the native enzyme; the reaction is usually started with a trace amount of fatty acid hydroperoxides present in the substrate solution, and only when sufficient hydroperoxide product accumulates will the native ferrous enzyme be fully activated to the ferric form and reach the maximal rate. Consistent with this, the lag phase can be abolished by pre-incubation of the enzyme with an appropriate fatty acid hydroperoxide or, conversely, can be prolonged in the presence of a reagent that reduces hydroperoxides (e.g., glutathione and glutathione peroxidase or $SnCl_2$) (20).

*Fe(II) soybean LOX-1 + 13S-HPODE → Fe(III) soybean LOX-1 + unknown products*

It is important to recognize at this point that this type of reaction of LOX with fatty acid hydroperoxides is a single turnover event rather than a self-propagating catalytic reaction; once the enzyme is oxidized the ferric form, it will no longer react with the fatty acid hydroperoxide. Because of this single turnover nature of the reaction, the

products are formed in minute amounts and have not been identified. Although substantial evidence suggests that an alkoxyl radical is produced (21), the fate of this alkoxyl radical is poorly understood.

Fueled by the potential clinical applications, investigations into LOX inhibitors led to the discovery of a novel mechanism of inhibition in the late 1980s and early 1990s (22-26). Several antioxidants, including butylated hydroxyanisole (BHA) and nordihydroguaiaretic acid (NDGA), are effective LOX inhibitors, yet these antioxidants inhibit LOX enzymes by reducing the catalytically active, ferric enzyme to the catalytically inactive, ferrous form (27), instead of by scavenging the enzyme-bound radicals as originally proposed (4). After one year into the research, I realized that this class of redox-based LOX inhibitors would afford an opportunity to obtain the products from the LOX activation reaction in large amounts. As shown in **Figure 3**, whereas the fatty acid hydroperoxide oxidizes the ferrous enzyme to the ferric enzyme, a redox-based inhibitor such as NDGA will in turn reduce the ferric enzyme back to the ferrous enzyme. Thus, a catalytic cycle is established in the presence of NDGA and now the fate of the fatty acid hydroperoxide can be easily followed with a catalytic amount of enzyme.
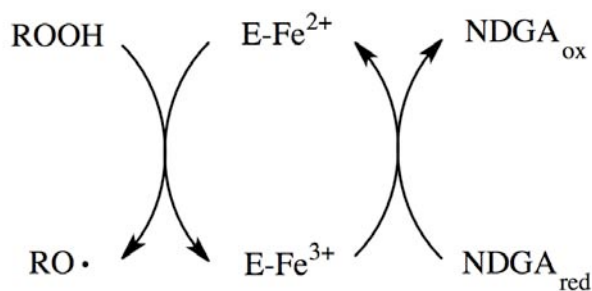


**Figure 3** LOX-catalyzed redox reaction between a fatty acid hydroperoxide (ROOH) and NDGA, a redox-based LOX inhibitor.

Under anaerobic conditions, a fatty acid substrate reacts with a LOX the same way as does NDGA, i.e., it will effectively reduce the ferric LOX to the ferrous form (28). Recall that in the LOX catalytic cycle (**Figure 1**), $O_2$ enters the reaction pathway after the hydrogen abstraction step (29). In the absence of the reacting $O_2$, the fatty acid radical formed from hydrogen abstraction will eventually escape from the enzyme active site, leaving the enzyme in the ferrous state. If a fatty acid hydroperoxide is also present in the incubation, it would in turn oxidize the ferrous enzyme back to the ferric form with itself being converted to an alkoxyl radical. Thus, under anaerobic conditions, LOX enzymes will catalyze a redox reaction between a fatty acid and a fatty acid hydroperoxide (**Figure 4**). A well-known example is the anaerobic reaction of soybean LOX-1 with linoleic acid and 13S-HPODE, which gives a complex mixture of products, including fatty acid dimers, ketones and aldehydes (30,31). In analyzing this complexity, one should realize that the enzyme generates only two species, the linoleic acid radical and the 13S-HPODE-derived alkoxyl radical, and the complexity arises only when these two radicals are released into the solution and allowed to react on their own (32).
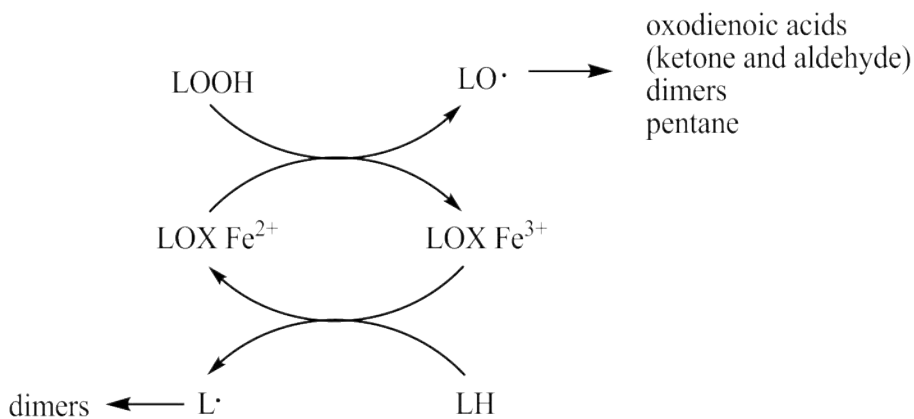


**Figure 4** LOX-catalyzed redox reaction between a fatty acid hydroperoxide (LOOH) and a fatty acid (LH) under anaerobic conditions.

7

A linoleic acid-independent anaerobic reaction of soybean LOX-1 with 13*S*-HPODE or 9*S*-HPODE has also been reported (33). This reaction is ~ 1500 fold slower than the linoleic acid-dependent reaction and gives a different set of products, mainly epoxyalcohols. A variation of this reaction is the so-called purple enzyme degradation (34). The purple enzyme refers to a complex between ferric soybean LOX-1 (or some other LOX enzymes such as soybean LOX-3) and 13*S*-HPODE, formed and spectroscopically detected at high concentrations of enzyme (e.g., 100 μM) and 2-3 higher concentrations of 13*S*-HPODE (18). The purple color stems from a charge transfer complex between the ferric iron and the hydroperoxide anion. This purple enzyme is metastable and will revert to the free ferric enzyme concomitant with conversion of 13*S*-HPODE to mainly a single epoxyalcohol with 70% retention of both oxygens from the hydroperoxide group (**Figure 5**) (34). It is found that $O_2$ inhibits this degradation process (35). Therefore, under aerobic conditions, the degradation occurs with a lag phase during which $O_2$ is gradually consumed (and $O_2$ will eventually all be consumed because the enzyme and the fatty acid hydroperoxide are both at high concentrations relative to $O_2$, i.e., > 240 μM). It is estimated that the specific epoxyalcohol is mostly formed under anaerobic conditions (35).
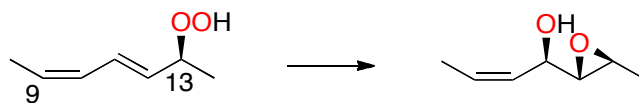


**Figure 5**: Formation of a single epoxyalcohol during the purple enzyme decomposition.

**Epidermal lipoxygenase-3: an atypical lipoxygenase exhibiting a prominent**

**hydroperoxide isomerase activity**

Human epidermal lipoxygenase 3 (eLOX3) is phylogenetically related to the LOX enzymes, hence "LOX" in its name. Unlike conventional lipoxygenases, however, eLOX3 is claimed to be "totally lacking" dioxygenase activity with polyunsaturated fatty acids such as arachidonic acid (36,37). It appears that all the well-conserved sequences, including the five amino acid ligands of the iron, remain intact in eLOX3. Thus, it is unclear why eLOX3 does not react with polyunsaturated fatty acids.

In 2003, this laboratory discovered in eLOX3 a novel hydroperoxide isomerase activity that converts fatty acid hydroperoxides into epoxyalcohols and ketones (36,37). This reaction of eLOX3 with fatty acid hydroperoxides exhibits all the hallmarks of true enzyme catalysis: speed, substrate selectivity, and product specificity. For example, human eLOX3 converts its best substrate, 12*R*-HPETE (12*R*-hydroperoxyarachidonic acid), to a single epoxyalcohol isomer and a ketone with a turnover number of 5 s$^{-1}$. Even more remarkably, mass spectrometric analysis of the products from the reaction of eLOX3 with an $^{18}$O-labeled 15*S*-HPETE indicated that both oxygen atoms in the epoxyalcohol product originate from the hydroperoxide group; thus this is truly an isomerase activity. By analogy to the hematin-catalyzed conversion of fatty acid hydroperoxides (38), a mechanism for eLOX3 catalysis has been proposed (**Figure 6**). First, Fe$^{2+}$ eLOX3, the proposed active species, homolytically cleaves the hydroperoxide substrate into an alkoxyl radical, and a "HO·" trapped in the iron center in the form of a hydroxide ion (specifically, the Fe$^{2+}$ donates an electron to the "HO·", forming a Fe$^{3+}$-OH complex) (step 1); the alkoxyl radical may isomerize to an epoxyallylic radical (step 2),

which then combines with the trapped "HO·" to form the epoxyalcohol product (step 3); alternatively, the alkoxyl radical may lose a hydrogen atom, probably to the $Fe^{3+}$-$^-$OH complex, forming the ketone product (step 4).
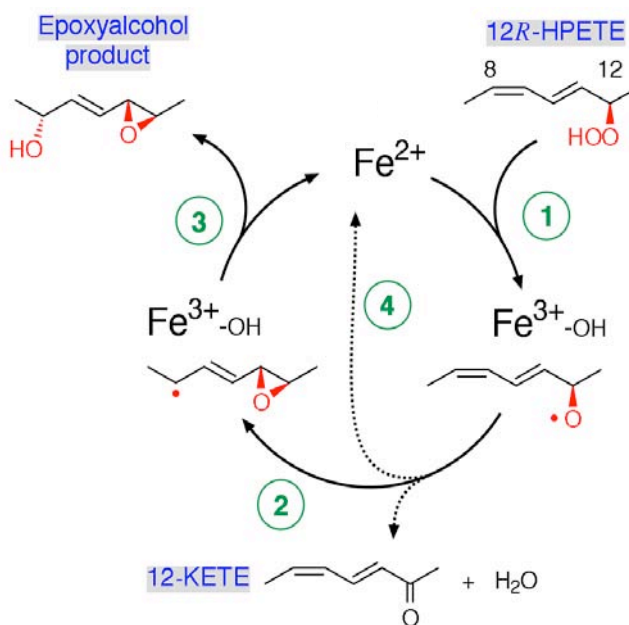


**Figure 6:** Proposed mechanism for eLOX3 catalysis. From (37).

Although unprecedented among LOX enzymes, the chemistry of the hydroperoxide isomerase activity is not new. As mentioned above, hematin catalyzes similar reactions, albeit with no specificity. In fact, the first chemical step (step 1 in **Figure 5**), involving homolytic cleavage of the O-O bond, is a facile reaction of ferrous ion (or other transition metals at the lower oxidation state, such as $Cu^{2+}$), whether it is in aqueous solutions, in model complexes or in proteins (39). The ferrous form of typical LOX enzymes is no exception; as noted in the previous section, the LOX activation step, common to all LOX enzymes, uses the same chemistry to give the same alkoxyl radical intermediate. Thus, the difference between eLOX3 and typical LOX enzymes lies in the fate of the alkoxyl radical, one resulting in preservation of the ferrous state of the enzyme

via the "oxygen rebound" mechanism, the other resulting in oxidation/activation of the enzyme via an yet unknown mechanism.

It may not be merely a coincidence that oxygenase activity is absent while an unusual hydroperoxide isomerase activity is present in eLOX3. Conceivably, certain steric factors of the enzyme active site may create a local environment that is depleted of $O_2$, which may account for both the lack of oxygenase activity and the possession of the hydroperoxide isomerase activity, the latter being easily understood by recalling that the linoleic acid-independent reaction of soybean LOX-1 with 13$S$-HPODE under anaerobic conditions also gives epoxyalcohols (33,34).

It is also possible the active site iron of eLOX3 may have a lower than normal redox potential (37). As noted earlier, this redox requirement is imposed by the first chemical step of the dioxygenase cycle, which involves homolytic cleavage of a bisallylic C-H in the fatty acid substrate by the active site $Fe^{3+}$-OH complex. Therefore, if tuned to a lower redox potential, the iron in eLOX3 may not be able to perform hydrogen abstraction. It is worth noting that although a lower than normal redox potential may explain the lack of dioxygenase activity in eLOX3, it does not explain why the hydroperoxide isomerase activity is uniquely present in this enzyme.

Having read a few textbooks and dozens of papers, I decided in Aug 2007 that I should try some experiments on eLOX3. The first experiment was to test the lack of active site oxygen hypothesis, by seeing if eLOX3 would react with arachidonic acid in the presence of the fatty acid hydroperoxide 12$R$-HPETE. Since a similar reaction occurs with soybean LOX-1 under anaerobic conditions, this should work for eLOX3 if its active site is indeed anaerobic. After a trial or two, disappointed by the seemingly

negative results, I quickly abandoned the experiment. (When this experiment was revisited and more rigorously done in 2010, to my own surprise, positive results were obtained).

My attention then shifted to the low redox potential hypothesis. To test this, I questioned whether the unusual fatty acid I studied in my rotation project, 20:3-9*E*,11*Z*,14*Z* (structure in **Figure 7**), is a substrate of eLOX3. The organic chemistry textbook I had read tells that this fatty acid is easier to oxidize than arachidonic acid, because the fatty acid radical derived from it is stabilized by one more resonance structure than the corresponding arachidonic acid radical (**Figure 7**). The reaction worked. Thus with this momentum I wrote the proposal, passed the Phase II exam, and formally began my dissertation research. (The second part of my research, on the physiological function of 12*R*-LOX and eLOX3, was not yet in the plan at the time.)
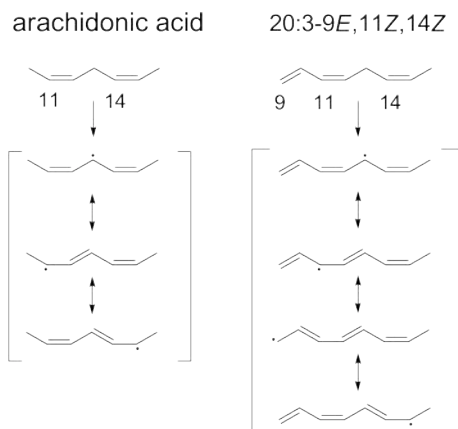


**Figure 7** Resonance structures of the fatty acid radicals derived from arachidonic acid and 20:3-9*Z*,11*Z*,14*Z*.

**The physiological role of 12*R*-LOX and eLOX3 in the skin**

The barrier function of the skin

Our skin provides a barrier that protects us from dehydration and invasion by foreign substances. Without this skin barrier, humans would not survive on dry land. With an impaired skin barrier, most often due to genetic mutations, humans would have ichthyosis, a heterogeneous group of disorders of dry scaly skin (40). The fish-like scales characteristic of ichthyotic skin result from hyperproliferation of skin cells (keratinocytes), which is a compensatory response to the impaired barrier function (40).

The skin can be dissected into epidermis (the outer layer), dermis (the middle layer), and subcutaneous tissue (the inner layer). The epidermis can be further divided, from the innermost to the outermost, into stratum basale (the basal layer), stratum spinosum (the spinous layer), stratum granulosum (the granular layer), and stratum corneum (the horny layer) (**Figure 8**). Though seemingly a static structural tissue, the epidermis undergoes constant changes. In the short life span of a keratinocyte (~ one month), it will undergo drastic morphological and cellular changes as it migrates through the multiple layers towards the surface, will serve the barrier function for a few days when arriving at the stratum corneum, and eventually will be shed off from the skin surface as it is replaced by a newly arrived, younger cell. To enable this constant self-renewal, the epidermis in fact stores a large number of stem cells in its basal layer and thus is also of interest to researchers studying stem cells (41). Here, however, the focus will be given instead to the barrier layer, the stratum corneum.
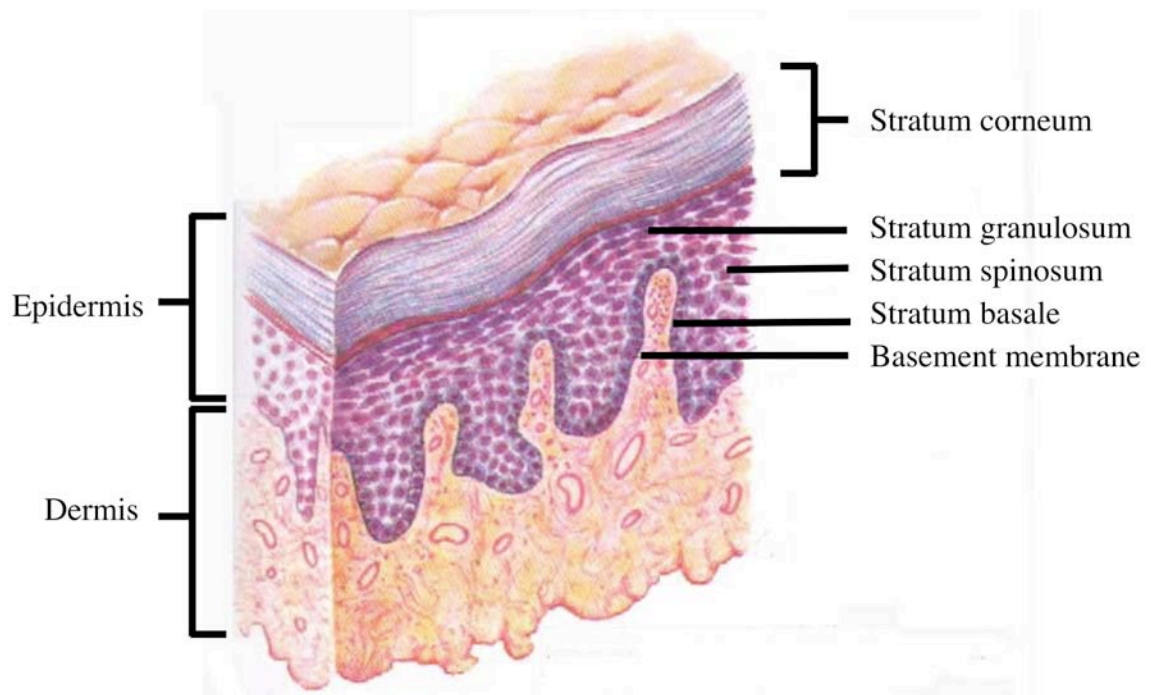
**Figure 8** Anatomy of the skin. From Shier, Butler, & Lewis (1999) *Hole's of Human Anatomy & Physiology*, 8th edition.

How does the stratum corneum provide the barrier function? This can be explained by the "bricks and mortar" model to a satisfactory degree of accuracy (42). In this model, "bricks" refer to the cells in the stratum corneum, a.k.a. corneocytes. These cells, anucleate and filled with keratin bundles, provide the framework and the required mechanical strength of the barrier. The other component, "mortar", refers to the lipids that fill the intercellular spaces, consisting of an approximately equimolar mixture of ceramides, cholesterol, and free fatty acids. Notably, phospholipids are not a component. These lipids are organized into stacked membrane sheets. These hydrophobic membrane sheets confer the essential water impermeable properties of the skin barrier. As we shall see later, the skin barrier function is critically dependent on these membrane sheets in the correct, ordered, structure, which in turn relies not only on the correct lipid composition, but also on the presence of a unique lipid-protein structure at the surface of corneocyte.

Formation of the skin barrier

As mentioned earlier, keratinocyte differentiation involves a complex program of morphological and cellular changes. Here we will focus on the final stage of keratinocyte differentiation, i.e., the transition from the granular cell to the corneocyte, during which the skin barrier is being formed (**Figure 9**).
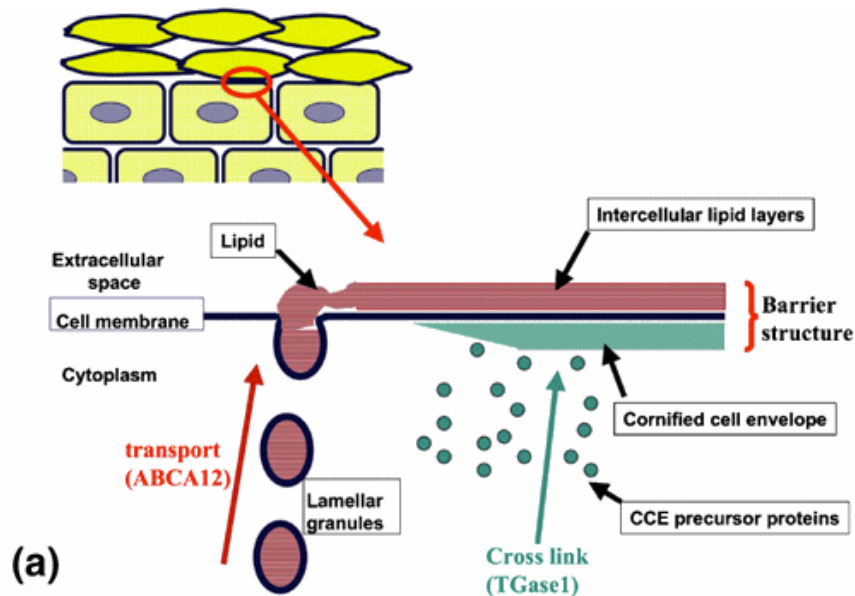


**Figure 9** Skin barrier formation. The barrier properties are mainly conferred by the ordered lamellar membranes outside the cell, the cross-linked cornified protein envelope beneath the cell surface, and the monolayer of lipid envelope at the cell surface. The plasma membrane composed of phospholipids is eventually replaced by the lipid envelope composed mainly of ω-hydroxyceramides covalently bound to proteins (not shown). From Ref. (43).

The granular cell, as its name implies, is marked by the occurrence of granules in the cytoplasm, including lamellar granules. The lamellar granules are secretory organelles loaded with lipids that are organized into stacked coin-like disks, together with numerous hydrolytic enzymes that will be activated once secreted into the extracellular space. The

15

coin-like disks in the lamellar granules appear to be flattened membrane vesicles composed of phospholipids, glucosylceramides, cholesterol, and free fatty acids.

As the granular cell transforms into the corneocyte, the lamellar granules will migrate to the apical side of the cell, and then the bounding membrane of the lamellar granules will fuse with the plasma membrane, while the contents, including the membrane disks and the hydrolytic enzymes, will be released into the intercellular space. Subsequently, several enzymatic reactions will come into play (44). Inside the cell, just beneath the plasma membrane, proteins such as involucrin and loricrin will be extensively crosslinked by sulfhydryl oxidases and transglutaminase-1, ultimately forming a 10 nm- thick protein envelope. Outside the cell, the polar lipids of the extruded membrane disks will be processed by the activated hydrolytic enzymes to less polar lipids, in particular free fatty acids and ceramides; glycerophospholipids will be all degraded to furnish free fatty acids, and glucosylceramides and sphingomyelins will be converted into ceramides. At the cell surface, the phospholipids will also be degraded, and one major lipid class originating from the bounding membrane of lamellar granules, acylglucosylceramides (see below), will be processed to ω-hydroxyceramides which in turn will be covalently coupled to the protein envelope via an ester bond between the ω-hydroxyl groups on the ceramides and glutamine/glutamate side chains on the proteins. The covalent coupling is thought be catalyzed by transglutaminase-1 (45). This monolayer of covalently bound ω-hydroxy-ceramides is distinct from the original plasma membrane, which is a phospholipid bilayer, although both appear in similar dimensions (~ 5 nm thick). To distinguish the two, the monolayer of covalently bound ω-hydroxy-ceramides is given the name corneocyte lipid envelope (CLE).

Upon formation of the corneocyte lipid envelope and lipid maturation catalyzed by hydrolytic enzymes, the extruded membrane disks in the extracellular space will fuse edge-to-edge to form ordered, elongated, lamellar membranes sheets (46), which are essential for the structural integrity of the water barrier. It is hypothesized that the lipid envelope serves as a scaffold for the deposition of lipids, thereby facilitating the formation of ordered, elongated, lamellar membrane sheets (47).

<u>Essential fatty acids and skin barrier function</u>

It has been known for 80 years that essential fatty acid deficiency leads to dry scaly skin (48,49). The skin phenotype induced by essential fatty acid deficiency, as in ichthyosis, reflects an underlying defect in the skin water barrier. Consistent with this, essential fatty acid deficient animals, including humans, show significantly increased transepidermal water loss compared to their normal counterparts (50-52).

There was once a debate on which essential fatty acid, arachidonic or linoleic acid, is responsible for normal functioning of the skin. Both fatty acids are effective in reversing the scaly skin defect from essential fatty acid deficiency, either when fed to the animals (53) or when topically applied to the skin (54). The prostaglandin $PGE_2$ derived from arachidonic acid was once considered as a mediator of the epidermal effect of essential fatty acids, since a group reported that cutaneous application of $PGE_2$ partially alleviated the scaliness of the skin of essential fatty acid deficient animals (55). However, the involvement of $PGE_2$ in the barrier function was ruled out later, when it was shown that the level of transepidermal water loss remains unchanged upon $PGE_2$ application, that indomethacin, a potent cyclooxygenase inhibitor, does not inhibit the curative effect of arachidonic or linoleic acid, and that columbinic acid (5*trans*,9*cis*,12*cis*-18:3), which

17

cannot be converted to prostaglandins, is equally effective in reversing the scaly skin condition (54,56). Even the involvement of $PGE_2$ in preventing keratinocyte hyperproliferation (i.e., scaliness) *per se* has been called into question, since the initial result could not be reproduced in a prominent lab studying essential fatty acids (54). The lesson here is that scaliness is an effect secondary to the primary barrier defect, and any conclusion regarding whether or not a molecule is involved in the barrier function should be made only from direct, rigorous, functional assays such as measurement of transepidermal water loss.

A major breakthrough pointing to a role of linoleic acid in skin barrier function came when two novel classes of sphingolipids, acylglucosylceramides and acylceramides, both of which contain esterified linoleate, were discovered in the granular layer and the stratum corneum respectively (**Figure 10**) (57-63). In essential fatty acid deficient animals, the linoleate moiety on the two classes of sphingolipids is substituted by oleate (64). When either arachidonic or linoleic acid is fed to essential fatty acid deficient rats, a correlation is seen between restoration of transepidermal water loss and specific incorporation of linoleic acid, but not arachidonic acid, into acylglucosylceramides and acylceramides (53). Further evidence suggests that arachidonic acid will be retroconverted into linoleic acid under essential fatty acid deficient conditions (65), whereas the reverse conversion from linoleic acid to arachidonic acid cannot occur in the skin because the Δ-6 and Δ-5 desaturase enzyme activities required for the conversion is absent (66). It is inferred, therefore, that the action of essential fatty acids in the skin barrier formation is exerted via the unique linoleate-containing acylglucosyceramides and acylceramides.
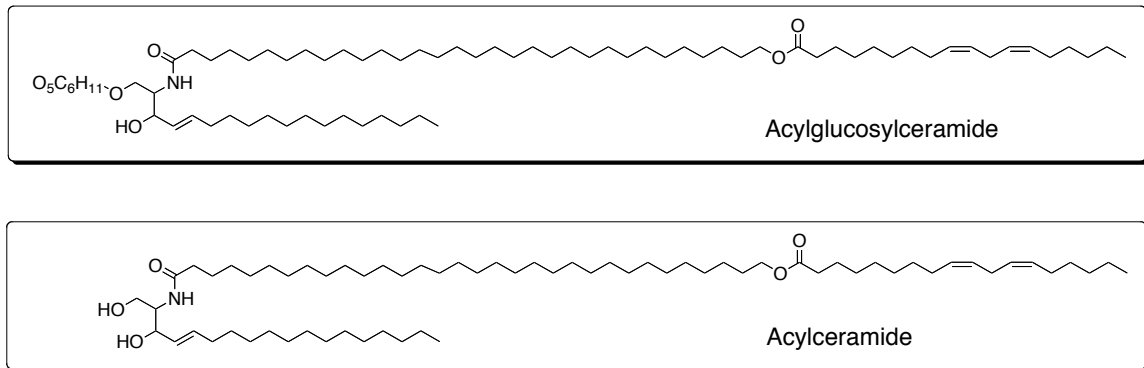
**Figure 10** Structure of a typical species of acylglucosylceramide and acylceramide.

It has been demonstrated by Houtsmuller and coworkers that topical application of several other n-6*cis*,n-9*cis* fatty acids in addition to linoleic and arachidonic acids is equally effective in reversing the scaly skin condition of essential fatty acid deficient rats (54). These results are best explained if, similar to arachidonic acid, these other effective fatty acids are first converted to linoleic acid, which is then incorporated into the linoleate-containing acylglucosylceramides and acylceramides to exert the function. The only known exception is columbinic acid (5*trans*,9*cis*,12*cis*-18:3), which itself is incorporated into acylglucosylceramides and acylceramides to a significant extent (53).

The exact mechanism through which linoleate-containing acylglucosylceramides and acylceramides help establish and maintain the skin barrier, however, is not completely understood. Acylglucosylceramides, which are localized to the lamellar granules in the granular cells, are proposed to function by promoting the formation of the stacked coin-like disk structures in lamellar granules (**Figure 11**) (58). Consistent with this, it is found *in vitro* that acylglucosylceramides readily induce flattening of phospholipid liposomes to membrane disks similar to what is observed in lamellar

granules (67). The problem with this hypothesis, however, is that stearate-containing acylglucosylceramides are as effective as linoleate-containing acylglucosylceramides in *in vitro* experiments. Acylceramides, formed from deglycosylation of the extruded acylglucosylceramides by β-glucocerebrosidase, reside instead in the intercellular space of the stratum corneum. Biophysical studies suggest that the presence of acylceramides is essential for the correct phase separation of the intercellular lamellar membrane sheets (68). Yet oleate-containing acylceramides show only subtle differences from linoleate-containing acylceramides in this respect (68). Taken together, it appears that a new hypothesis is needed to fully explain the specific requirement for linoleate in acylglucosylceramide and acylceramides (See below).
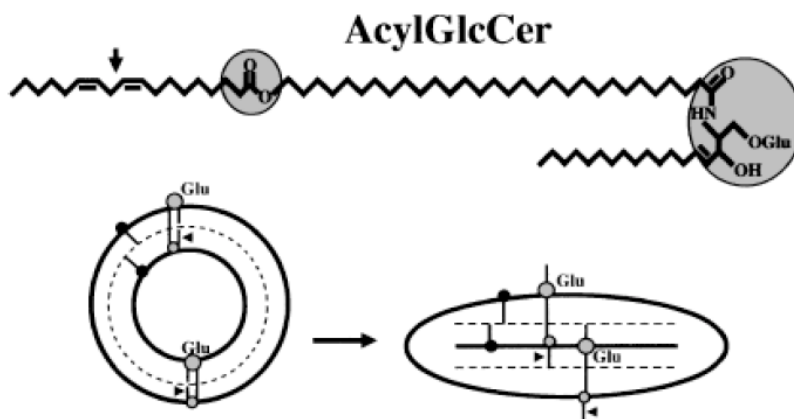


**Figure 11** Proposed model of acylglucosylceramide function in the flattening and stacking of lipid vesicles to generate the double bilayer structure of the internal lamellae of lamellar granules. From Ref. (47).

A few years after the discovery of acylglucosylceramides and acylceramides, it was realized that in addition to free extractable lipids, there are also covalently bound lipids in the stratum corneum (69,70), which can be liberated by mild-alkaline hydrolysis. These bound lipids, including ω-hydroxyceramides, ω-hydroxy very long chain fatty acids and saturated fatty acids, constitute the corneocyte lipid envelope (71), a unique

cellular structure essential for the barrier function (see above). Meanwhile, it was observed in pig epidermis that the proportion of acylglucosylceramides among all glucosylceramide species, ~50%, is considerably higher than that of acylceramides among all ceramides, ~ 10% (72). Since acylceramides in the stratum corneum derive exclusively from deglycosylation of the extruded acylglucosylceramides from the granular cells (73,74), this observation implies that a fraction of acylceramides is further metabolized, possibly to ω-hydroxyceramides that will then be covalently attached to proteins. This proposed intermediacy of acylceramides to the bound ω-hydroxyceramides is further supported by a study on the time course of lipid synthesis in pig epidermis pulsed with $[1-^{14}C]$-acetate (75), and another study that analyzed the lipids of mouse epidermis at different embryonic stages (76). In both studies, the level of glucosylacylceramides transiently reaches a peak value at an early time point and then declines monotonously, concomitant with an increase in the level of ω-hydroxyceramides. Acylceramides, as expected from a metabolic intermediate, either maintains a steady-state level (75) or declines concomitantly with glucosylacylceramides (76).

As to how acylceramides are converted to the bound ω-hydroxyceramides, it is presumed that the linoleate would be cleaved off and recycled (47), or that some transesterification reaction would directly couple the ω-hydroxyl group to glutamate/glutamine residues on proteins (44). The latter proposition is inherently flawed in that for transesterification to occur, invariably one nucleophile (the ω-hydroxyl group on acylceramides) has to be replaced by another (which cannot be the electrophilic glutamate/glutamine carbonyl group), whereas the electrophile (linoleate) has to remain

the same. The former proposition is comparatively more attractive, and it seemingly represents an ideal mechanism for the skin to conserve the essential fatty acid, linoleic acid. However, it is still a matter of debate whether linoleic acid is recycled or not. On the one hand, recycling of linoleic acid is suggested by a study on an organotypic murine keratinocyte culture model of the skin (77). On the other hand, extensive oxygenation of linoleic acid instead is noted when the fatty acid is topically applied to essential fatty acid deficient rats to correct the skin defect (54).

The extensive oxygenation of linoleic acid noted by Houtsmuller and colleagues is consistent with a new hypothesis I will propose in this dissertation, necessitating linoleate oxygenation by the two LOX enzymes, 12$R$-LOX and eLOX3, during the conversion of acylceramides to $\omega$-hydroxyceramides. Another piece of evidence relevant in the present context is that in the epidermis of essential fatty acid deficient hairless rats, where the linoleate moiety in acylceramides is replaced by oleate, the amount of protein-bound $\omega$-hydroxyceramides is significantly reduced compared to that of normal rats, pointing to a defect in the metabolic pathway from acylceramides to bound $\omega$-hydroxyceramides caused by the fatty acid substitution (78). This stringent structural requirement for linoleate in acylceramides can be well explained if LOX enzymes are involved in the pathway, because linoleate is a LOX substrate, but oleate is not.

<u>12*R*-LOX and eLOX3 and skin barrier function</u>

It has long been suspected that the effect of essential fatty acids on skin barrier formation might be mediated via LOX enzymes. Since the findings that feeding of ETYA, a COX/LOX inhibitor, to rats also induces extremely dry scaly skin similar to that seen in essential fatty acid deficiency (79), and that COX/prostaglandins are not involved in skin barrier formation (see the previous section), scientists in search of potential mediators of the effect of essential fatty acids have naturally shifted their attention to LOX enzymes and products.

In an elegant study in 1985, Nugteren and coworkers demonstrated that when [1-$^{14}$C]-linoleic acid was topically applied to the skin of essential fatty acid deficient rats, some of the radioactivity was incorporated into a novel class of lipids, polyoxyacyl ceramides, which were deduced by the team to be LOX metabolites of the linoleate-containing acylceramides (80). Furthermore, this conversion was not seen in their negative controls using either the LOX inhibitor ETYA or the linoleic acid analogues 9*trans*,12*cis*-18:2, 9*cis*,12*trans*-18:2, and 9*trans*,12*trans*-18:2, none of which is a LOX substrate. Despite these control experiments, questions have been raised over the enzymatic nature of the polyoxyacyl ceramide formation (81). It can be argued, for example, that ETYA at the high concentrations used in the study serves also as an antioxidant, or that 9*trans*,12*cis*-18:2 or 9*cis*,12*trans*-18:2 is more difficult to autoxidize than linoleic acid. This issue would have been resolved if regio- and stereospecificity of the conversion could be demonstrated. Unfortunately the structures of the putative LOX metabolites, the polyoxyacyl ceramides, were not characterized in detail due to technical limitations at that time. Although the polyoxyacyl ceramides appeared to be a mixture on

TLC, it is possible that the mixture could result from unintended hydrolysis during the workup even if there was only a single LOX metabolite *in vivo*. Some epoxyalcohols would easily hydrolyze to a nonspecific mixture at pH < 3. Thus, to analyze this type of products, care should be taken to avoid acid-catalyzed hydrolysis.

It is also worth mentioning that at the time, in the 1980s, the LOX enzymes in the skin were yet to be discovered. It was inferred from product analysis of incubations of human or rat epidermis with $[1-^{14}C]$linoleic or arachidonic acid that there must be a 15-LOX and a 12-LOX in human or rat epidermis (82), yet-as we will understand later-this type of classical biochemical experiment cannot detect LOX enzymes that prefer an ester to a free acid as substrate (e.g., murine 12*R*-LOX) or that do not use fatty acid/ester substrates at all (e.g., eLOX3).

Since the 1990s, when molecular cloning became a commonplace technology, our knowledge of mammalian LOX enzymes has expanded exponentially. It is now known that all the LOX enzymes (e.g., the six in humans, **Figure 12**) are expressed in the epidermis to various degrees, yet only three of them, 12*R*-LOX, eLOX3, and 15-LOX-2 (in humans, the mouse homologue of which is 8*S*-LOX) are specific to epithelial cells. Among these three, 12*R*-LOX and 15-LOX-2 were cloned, expressed, and characterized for the first time in our laboratory (83,84). As noted earlier (Chapter I-2), following its discovery eLOX3 immediately presented itself as a puzzle because, unlike other LOX enzymes, eLOX3 appeared not to react with polyunsaturated fatty acids. So what is the function of this strongly expressed (85) enzyme in the skin if it has no activity? (As we will see in Chapter II, the dioxygenase activity of eLOX3 is now uncovered, ten years after the enzyme was first cloned and expressed. However, this dioxygenase activity is

24

exhibited only under unusual circumstances, and we suspect that the physiological relevance of the enzyme residues in its unusual hydroperoxide isomerase activity.)
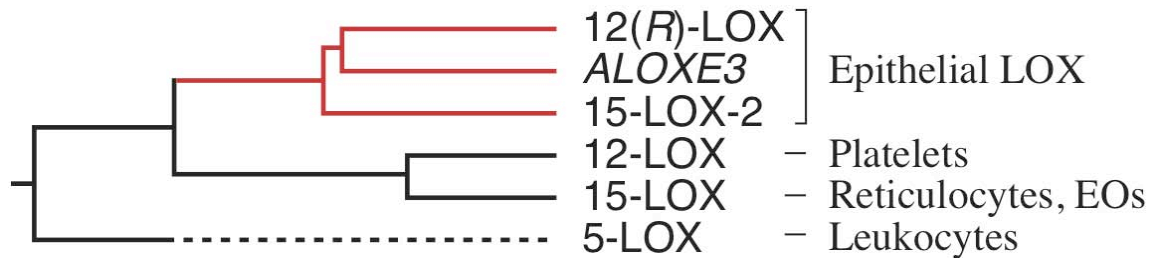


**Figure 12** Phylogenetic tree of human LOX enzymes

The next advances towards a better understanding of the LOX enzymes in the epidermis came when a group of geneticists made a splendid discovery and proposed an unconventional pathway (86), which was then further shown by the former graduate student Zheyong Yu in this laboratory to be biochemically sound and feasible (37). In the human genetic study, mutations in 12$R$-LOX (*ALOX12B)* and eLOX3 (*ALOXE3*) were identified in non-bullous congenital ichthyosiform erythroderma (NCIE). The authors concluded that "it seems likely that the product of one of these enzymes may be the substrate of the other, and that they belong to the same metabolic pathway". This suggestion by the geneticists led to the discovery in this laboratory of a new type of activity in eLOX3; instead of incorporating molecular oxygen into fatty acids, eLOX3 shows a prominent hydroperoxide isomerase activity that converts fatty acid hydroperoxides into epoxyalcohols and ketones. Notably, the 12$R$-LOX metabolite of arachidonic acid, 12$R$-HPETE, was by far the best substrate among all the HPETEs examined. Thus, the genetic and biochemical evidence agree with each other, suggesting

a novel metabolic/signaling pathway in which 12*R*-LOX and eLOX3 work in tandem in the epidermis.

More recent findings over the five years reinforced the importance of the 12*R*-LOX/eLOX3 pathway for a competent skin barrier function. More inactivating mutations in 12*R*-LOX or eLOX3 in humans have now been identified, and the scope of affected patients has been extended to autosomal recessive congenital ichthyosis (ARCI), of which NCIE is a subtype (87,88). Knockout mouse models of both 12*R*-LOX and eLOX3 have been generated (89,90). Both the 12*R*-LOX -/- and eLOX3 -/- mice die soon after birth due to excessive transepidermal water loss. A 12*R*-LOX functional knockout mouse has also been identified in an ENU genetic screen, which showed an identical phenotype (91). The more severe phenotype in the mice than in the patients is probably because mice have a larger surface area-to-volume ratio, or because mice have an inherently weaker barrier than humans.

<u>The arachidonate-derived hepoxilin connection in the epidermis?</u>

Since the discovery of the 12*R*-LOX/eLOX3 pathway in the skin, it was assumed that arachidonic acid is the natural substrate of this pathway, being converted via 12*R*-HPETE to 8*R*-hydroxy-11*R*,12*R*-epoxyeicosa-5*Z*,9*E*,14*Z*-trienoic acid, one of the isomers of hepoxilin $A_3$. [The name hepoxilin refers to two general classes of epoxyalcohols, hepoxilin A-type and hepoxilin B-type (**Figure 13**) (92)]. This assumption apparently agrees with the observation that a large amount of 12*R*-HETE is produced in human psoriatic scales (93). Yet psoriasis is an inflammatory, pathological condition that is not caused by an underlying barrier defect, and 12*R*-HETE or the hepoxilin $A_3$ isomer has never been detected in normal skin.

Following the discovery of the hepoxilin A₃ produced by the combined action of 12*R*-LOX and eLOX3 on arachidonic acid, it was shown that this compound at μM concentrations activates PPARα *in vitro* (94). However, if this is the 12*R*-LOX/eLOX3 pathway in the skin, the PPARα-/- mice should show the same phenotype as the 12*R*-LOX-/- or eLOX3-/- mice. However, in the PPARα-/- mice, a normal permeability barrier is formed at a late embryonic stage despite an initial delay (95).
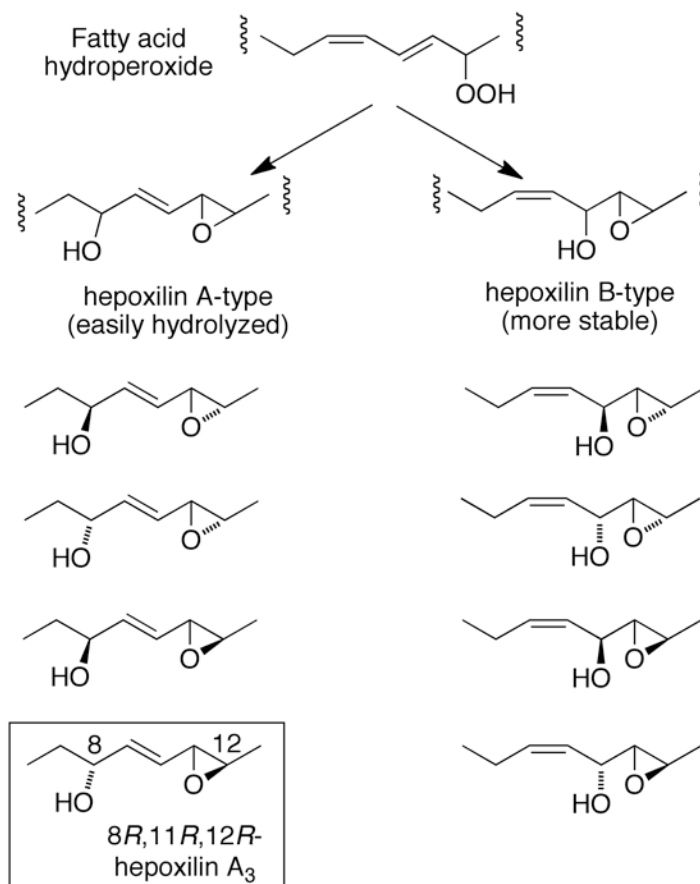


**Figure 13** General structures of hepoxilin A-type and B-type. Nonenzymic transformation from racemic hydroperoxide could lead to formation of all the individual isomers shown (plus the corresponding *cis*-epoxides, not shown). 12*R*-LOX and eLOX3 form exclusively the 8*R*-OH-11*R*,12*R*-epoxy-hepoxilin A₃ (boxed). From ref. (96).

A major problem for the arachidonate-derived hepoxilin hypothesis is that mouse 12*R*-LOX does not use free fatty acids (including arachidonic acid) as substrate, with the

long chain ω-3 fatty acid DHA being the only known exception (97). Instead, the enzyme prefers fatty esters. It was once postulated 8*S*-LOX might take the place of 12*R*-LOX in the hepoxilin pathway in mouse skin (98). This hypothesis is now rejected as the 12*R*-LOX -/- mouse model clearly demonstrates the indispensable role of mouse 12*R*-LOX in skin barrier formation (89).

<u>A new hypothesis on the role of 12*R*-LOX and eLOX3 in the skin</u>

While there is little doubt that 12*R*-LOX and eLOX3 function in tandem in the same pathway in the skin, in this dissertation I am challenging the assumption that arachidonic acid is the responsible fatty acid substrate of 12*R*-LOX in the pathway. Also, since 12*R*-LOX and eLOX3 are expressed at precisely the moment when the skin barrier is about to form (89), I consider it more likely that these two enzymes play a role in building the barrier rather than in signaling for further cell differentiation.

As noted earlier, linoleic acid is generally accepted as the essential fatty acid in the skin. In the barrier layer, stratum corneum, and its immediate precursor, the granular layer, linoleic acid is largely esterified into two classes of sphingolipids, acylceramides and acylglucosylceramides, respectively. In normal skin, the esterified fatty acid is almost exclusively linoleic acid. In essential fatty acid deficiency, the linoleate moiety is replaced by oleate, or the *trans* double bond isomers of linoleate, 9*trans*,13*cis*-18:2, 9*cis*,13*trans*-18:2 or 9*trans*,13*trans*-18:2, if these fatty acids are topically applied (and these *trans* fatty acids cannot reverse the essential fatty acid deficient state) (64,80). Since neither oleate nor any of the *trans* double bond isomers of linoleate is a LOX substrate, this specific requirement for linoleic acid in acylceramides and acylglucosylceramides for skin barrier function can be explained if acylceramides and/or

acylglucosylceramides are to be metabolized by LOX enzymes, as originally proposed by Nugteren and colleagues in 1985 (80).

If so, I questioned further, what functions would LOX metabolites of acylceramides and acylglucosylceramides provide? A possible answer can be deduced from two recent developments in studies of essential fatty acid deficiency and the 12*R*-LOX-/- mouse model respectively. As noted earlier, in essential fatty acid deficient skin, where the linoleate moiety of acylceramides and acylglucosylceramides is replaced by oleate, the covalently bound ω-ceramides that are a major component of the corneocyte lipid envelope are significantly decreased compared to those in normal skin (78). Coincidentally, in 12*R*-LOX-/- mouse skin the covalently bound ω-ceramides also appeared to be absent (89). Combining these two lines of evidence and considering that the bound ω-ceramides derive from acylceramides and/or acylglucosylceramides, I propose that the metabolites of 12*R*-LOX and eLOX3 are obligatory intermediates in the conversion of acylceramides and/or acylglucosylceramides to covalently bound ω-ceramides. In other words, the action of 12*R*-LOX and eLOX3 on the linoleate moiety makes possible the cleavage of the ester bond between the carboxyl of linoleate and the ω-hydroxyl of the very long chain fatty acid on the ceramides, thus freeing the ω-hydroxyl group for covalent coupling to the proteins of the cornified protein envelope. This new hypothesis is summarized in **Figure 14**.
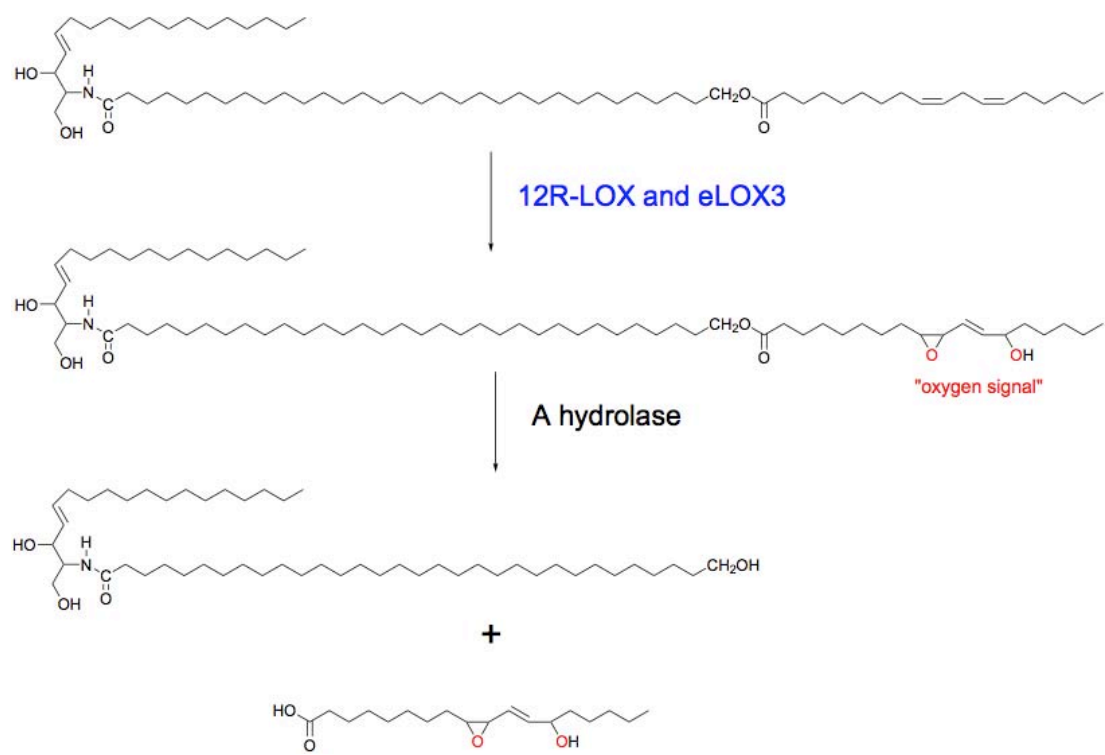
**Figure 14** 12*R*-LOX/eLOX3 pathway in the epidermis proposed in this dissertation.

# CHAPTER II

## DIOXYGENASE ACTIVITY OF ELOX3 UNVEILED: TYPICAL AND ATYPICAL FEATURES

### Introduction

Epidermal lipoxygenase-3 (eLOX3) is one of the two lipoxygenases (LOX) involved in skin barrier formation (96,99). Inactivating mutations in either the gene encoding human eLOX3 or the gene encoding 12$R$-LOX lead to impaired skin barrier function that manifests itself in the disease, autosomal recessive congenital ichthyosis (86,100). The scaly skin phenotype of this disease is a compensatory response to the fundamental defect in the barrier function (40). Targeted gene knockouts in mice confirm the role of these two LOX enzymes, and in both cases the mice die soon after birth due to severe transepidermal water loss (89,90).

In addition to its involvement in skin barrier formation, eLOX3 also attracts attention because of its unusual enzymology. It is classified as a LOX based on its amino acid sequence (e.g. 58% identity to 12$R$-LOX) yet its name eLOX3 lacks the usual designation such as 5-, 12- or 15-LOX. The reason is the enzyme appears to be devoid of typical dioxygenase activity with polyunsaturated fatty acid substrates such as arachidonic acid (37,101). Instead, it displays a novel hydroperoxide isomerase activity that efficiently converts fatty acid hydroperoxides, the usual LOX products, to epoxyalcohols and ketones (37). This hydroperoxide isomerase activity, acting on a hydroperoxide product of 12$R$-LOX, has been proposed to be the physiological function

of eLOX3 (96).

The non-heme iron in the active site of LOX enzymes exists in two oxidation states, ferrous and ferric. Native LOX are usually in the ferrous state, yet only the ferric enzyme is catalytically active as a dioxygenase (19). Therefore, to enter the catalytic cycle the ferrous enzyme has to be oxidized to the ferric form first, usually by one equivalent of their own hydroperoxide product. This process, commonly known as the activation step, accounts for the initial lag phase in the progress curve of LOX reactions (20,102). Because the reaction between typical LOX and fatty acid hydroperoxides is only a single turnover event, no significant products would accumulate unless an iron reducing agent such as nordihydroguaiaretic acid (NDGA) is given to regenerate the ferrous enzyme (27) (**Figure 15A**).

Unlike typical LOX, eLOX3 does not require iron reducing agents for its hydroperoxide isomerase activity. That this reaction is catalysis, rather than a single turnover, implies that the ferrous state of eLOX3 is largely preserved. However, NDGA does speed up the reaction (37), suggesting that the enzyme can be oxidized by fatty acid hydroperoxides to some extent. I reasoned that the activation step of the LOX activity in eLOX3, if it does occur, would be very inefficient, requiring many molecules of fatty acid hydroperoxide to oxidize one molecule of eLOX3 (**Figure 15B**). In other words, higher than usual concentrations of fatty acid hydroperoxide might be required to activate eLOX3. This inefficiency in the activation step of eLOX3 could potentially account for its apparent lack of dioxygenase activity, which must be performed by the activated, ferric enzyme.

An additional explanation for the lack of dioxygenase activity in eLOX3 might be

that the active site iron has a low redox potential. This redox requirement is imposed by the first chemical step of the dioxygenase cycle, which involves homolytic cleavage of a bisallylic C-H bond in the fatty acid substrate by the active site Fe(III)-OH complex (29). The moderately high bond dissociation energy (BDE) of this C-H bond (e.g., ~ 73 kcal/mol for $C_7$-H, $C_{10}$-H or $C_{13}$-H in arachidonic acid (7)) dictates that the redox potential of the active site iron should also be moderately high for the bond cleavage to occur (6). Indeed, a moderately high redox potential of ~ 600 mV has been demonstrated experimentally in the prototypical LOX, soybean LOX-1 (8). Unfortunately, a direct test of this hypothesis, by measuring the redox potential of eLOX3 for comparison with soybean LOX-1, is not yet possible due to difficulties in preparing multi-milligrams of purified eLOX3 for EPR spectroscopy.

In this study, I set out to test indirectly the redox potential hypothesis by incubating eLOX3 with a panel of synthetic fatty acids with extended conjugation. Because of the extended conjugation, these fatty acids are easier to oxidize than typical polyunsaturated fatty acids such as arachidonic acid (7) and thus might be accepted by eLOX3 as substrate. The study on this panel of synthetic fatty acids revealed some unusual characteristics of eLOX3 that prompted me to consider the other possibility that eLOX3 does not react with natural fatty acids because it is deficient in the activation step. To further test this possibility, I reexamined the reaction of eLOX3 with arachidonic acid using high concentrations of hydroperoxide activator. I also studied the effect of an Ala-to-Gly mutation in the active site that is known to affect oxygenation specificity (12,14) and investigated the effect of substrate orientation on product specificity using the large ester arachidonoyl-lysophosphatidic acid (AA/lyso PA). The Discussion section ties the

findings together and proposes a model with mechanistic relevance to the understanding

of LOX enzymes in general.
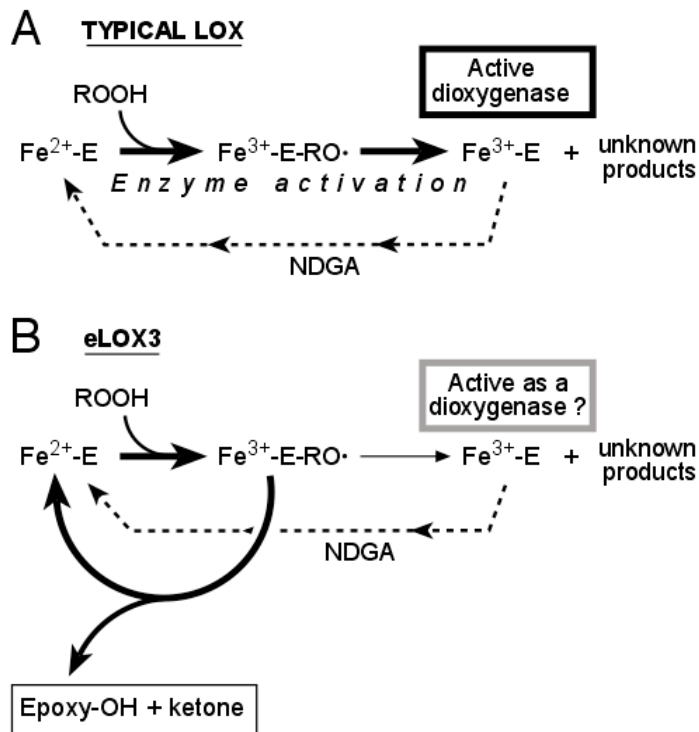


**Figure 15**: Comparison of typical LOX and eLOX3 reactions with fatty acid hydroperoxide (ROOH). **(A)** For typical LOX, one equivalent of ROOH oxidizes the $Fe^{2+}$ enzyme to the $Fe^{3+}$ form, via the $Fe^{3+}$ enzyme-alkoxyl radical (RO•) intermediate. NDGA reduces the $Fe^{3+}$ enzyme back to $Fe^{2+}$ and thus inhibits dioxygenase activity. **(B)** For eLOX3, more than one equivalent of ROOH is required to oxidize the $Fe^{2+}$ enzyme, because the $Fe^{3+}$ enzyme-RO• intermediate usually undergoes hydroperoxidase isomerase cycling with formation of epoxyalcohols and ketones. Occasionally, the $Fe^{3+}$ enzyme-RO• intermediate converts to the free $Fe^{3+}$ enzyme. NDGA reduces the $Fe^{3+}$ enzyme and thus stimulates hydroperoxide isomerase activity.

## Experimental procedures

Materials

Arachidonic acids were purchased from NuChek Prep Inc. (Elysian, MN). 15*S*-HPETE or 13*S*-HPODE was synthesized by reacting soybean LOX-1 with arachidonic acid or linoleic acid at pH 9 followed by SP-HPLC purification (103). 12*R*-HPETE was synthesized by autoxidation (37). 4-Hydroxy TEMPO was purchased from Sigma Aldrich (St. Louis, MO). AA/lyso PA was purchased from Avanti Polar Lipids, Inc. (Alabaster, AL).

Chemical synthesis of conjugated fatty acids

9*E*,11*Z*,14*Z*-20:3ω6 was synthesized by Dr. Jin K. Cha at Wayne State University, as previously described (16). 8*Z*,11*Z*,13*E*–20:3ω7 was a kind gift from Dr. K. C. Nicolaou at the Scripps Research Institute. 11*Z*,14*Z*,16*E*-20:3ω4 and 12*E*,14*Z*,17*Z*-20:3ω3 were synthesized by alkaline isomerization (104) of 11*Z*,14*Z*,17*Z*-20:3ω3 (NuChek Prep Inc., Elysian, MN), and 9*Z*,12*Z*,14*E*-18:3ω4 by alkaline isomerization of α-linolenic acid (NuChek Prep Inc., Elysian, MN)). Briefly, 10 mg of the precursor fatty acid was dissolved in 1 ml of 1 N KOH in ethylene glycol, flushed with argon, and placed in an oven at 144 °C. The extent of the reaction was monitored every 10 minutes by UV spectrophotometry assay of an aliquot, and the reaction was stopped when UV absorbance at 235 nm ceased to increase (The total reaction time was about 20 to 30 minutes). The reaction mixture was then acidified by 1 N HCl to pH 3 and extracted by methylene chloride. The extract was analyzed by silver ion chromatography and the two desired products were identified based on their UV (identical to that of 9*E*,11*Z*,14*Z*-

20:3ω6) and $^1$H and $^1$H,$^1$H-COSY NMR spectra.

Expression and purification of human eLOX3

The cDNA of human eLOX3 with an N-terminal His tag was subcloned into the pCW vector, and the protein was expressed and purified according to a previously published protocol (105). Flat-bottomed 500-ml flasks, which were found to give a higher yield of eLOX3 than baffled flasks, were used for the 50-ml cultures.

Reaction incubations

The room temperature reaction with 9$E$,11$Z$,14$Z$-20:3ω6 was monitored by UV spectrophotometry. By contrast, 0 °C reactions and the room temperature reaction with arachidonic acid were not monitored under UV. For the latter, incubation was typically conducted in a 5-ml reactivial. First, the fatty acid substrate and the auxillary components to be investigated (e.g., hydroperoxide activators, 4-hydroxy TEMPO) were added to an empty vial and then taken to dryness under a stream of N$_2$. Next, 2 ml of 100 mM sodium phosphate buffer pH 7.5 was added, the vial capped and subjected to vortex mixing. Next, enzyme was added to start reaction. Finally, reaction was quenched by the addition of methanol (usually 1 ml). For time course experiments with arachidonic acid, at specified time points, an aliquot (usually 150-200 μl) of the incubation mixture was taken out and immediately added to a separate vial containing 833 ng of 9$E$,11$Z$,14$Z$-20:3ω6, the internal standard, in 0.5 ml of methanol. The 0 °C reaction with AA/lyso PA was performed under the same conditions as the 0 °C reaction with arachidonic acid. The lyso phospholipid was chosen for this study because of its better solubility in aqueous solutions than those of diacyl phospholipids (106).

<u>Extraction of reaction products</u>

The incubation mixture was acidified to pH 5 using 1 N HCl, treated with more than one molar equivalent of $SnCl_2$ on ice for 10 minutes, and then extracted by an Oasis HLB cartridge (Waters Corp.).

<u>HPLC analysis</u>

For reaction with 9*E*,11*Z*,14*Z*-20:3ω6, straight phase HPLC analysis used a Beckman silica column (0.46 × 25 cm), a solvent system of hexane/isopropyl alcohol/acetic acid (100:1.5:0.1, by volume), and a flow rate of 1 ml/min. Chiral phase HPLC analysis used a Daicel Chiralpak AD column (0.46 × 25 cm), a solvent system of hexane/ethanol/acetic acid (100:5:0.05), and a flow rate of 1 ml/min.

For reaction with arachidonic acid, reversed phase HPLC analysis of HETE products was performed using a Waters Symmetry C18 column (0.46 × 25 cm), a solvent system of methanol/water/acetic acid (80/20/0.01), and a flow rate of 1 ml/min. For time course experiments, reversed phase HPLC analysis used the same column, methanol/water/acetic acid (95/5/0.01), and 1 ml/min. The remaining arachidonic acid substrate and accumulated 9- and 5-HPETE products in the time course experiments were quantified by comparison of their corresponding peak area with that of the internal standard, 9*E*,11*Z*,14*Z*-20:3ω6. To avoid rearrangement of bisallylic HETEs, which may occur under even mildly acidic conditions (107), HPLC analyses with no acid-containing solvent systems were also performed on reaction extract pre-treated with ethereal diazomethane, which converts free acids to methyl esters. 7-HETE and 11-HETE methyl esters were separated using a Beckman silica column (0.46 × 25 cm), an isocratic solvent system of hexane/isopropyl alcohol (100:2, by volume), and a flow rate of 1 ml/min. The

relative abundance of each HETE product was estimated based on the 205 nm absorbance. (This is justified by a previous study showing that the radioactive trace of [1-$^{14}$C]HETEs matches well with the corresponding UV trace at 205 nm (107).) Chiral analysis used a Daicel Chiralpak AD column (0.46 × 25 cm), isocratic solvent of hexane/methanol (100:1.5, v/v), and a flow rate of 1ml/min. The stereo-configuration of methyl 7-HETE enantiomers on chiral HPLC was deduced based on the finding that bisallylic HETEs would undergo mainly "suprafacial" rearrangement upon mild acid treatment (107). Briefly, the two enantiomers (1-2 μg) were purified by chiral HPLC, repeatedly (4-5 cycles) treated with 1 ml of methanol/water/acetic acid (75:25:1) followed by evaporation under N$_2$, and then subjected to chiral HPLC analysis. For example, the second peak of 7-HETE methyl ester on chiral HPLC was found to rearrange mainly to 5*S*-HETE and 9*R*-HETE methyl esters and was thus deduced to be 7*R*, since 7*R* hydroxyl sits on the same face of the double bond system in the fully extended configuration as does 5*S* or 9*R* hydroxyl.

For reaction with AA/lyso PA, the products were transmethylated after extraction using a previously published protocol (108), followed by reversed phase HPLC analysis using a Waters Symmetry C18 column (0.46 × 25 cm), an isocratic solvent system of methanol/water (80/20), and a flow rate of 1 ml/min.

<u>Derivatization and GC-MS analysis</u>

Catalytic hydrogenations were performed in 100 μl of ethanol using about 1 mg of palladium on alumina and bubbling with hydrogen for 2 min at room temperature. The hydrogenated products were recovered by the addition of water and extraction with ethyl acetate. TMS ether derivatives were prepared by treatment with *bis*(trimethylsilyl)-

trifluoracetamide (10 μl) and pyridine (2 μl) at room temperature for 2 hr. Subsequently, the reagents were evaporated under a stream of nitrogen and the samples were dissolved in hexane for GC-MS.

Analysis of the methyl ester trimethylsilyl ether derivatives of the products was carried out in the positive ion electron impact mode (70 eV) using a Thermo Finnigan Trace DSQ ion trap GC-MS with the Xcalibur data system. Samples were injected at 150 °C, and after 1 min the temperature was programmed to 300 °C at 20 °C/min. Spectra collected during elution of the GC peak (typically about 20 spectra) were averaged for calculation of the isotopic compositions.

**RESULTS**

Dioxygenase activity of eLOX3 with 9E,11Z,14Z-20:3ω6

To examine the potential oxygenase activity of eLOX3, we tested eLOX3 with a series of synthetic fatty acids with extended conjugation (their structures shown in **Figure 16**). Among these fatty acids, only 9*E*,11*Z*,14*Z*-20:3ω6 turned out to be a good substrate. The initial reactions of eLOX3 (0.1 μM) with 9*E*,11*Z*,14*Z*-20:3ω6 (18 μM) were conducted at room temperature and monitored by scanning UV spectrometry. The substrate contains a conjugated diene chromophore and absorbs strongly at 235 nm (**Figure 17A**, dotted line). Upon addition of enzyme, the UV absorbance of the substrate gradually decreased while a new chromophore typical of conjugated trienes came to prominence ($\lambda_{max} \sim 270$ nm, **Figure 17A**). Monitoring of the rate of reaction at 235 nm revealed a pronounced lag phase of ~ 5 min during which time no significant reaction is

apparent (**Figure 17B**); addition of exogenous hydroperoxide activator (1 μM 13*S*-HPODE) almost eliminated the lag phase. Kinetic measurements of initial rates over a range of substrate concentrations gave estimates of $K_m$ and $k_{cat}$ as 50 μM and 1.6 s$^{-1}$, respectively (**Figure 17C**).
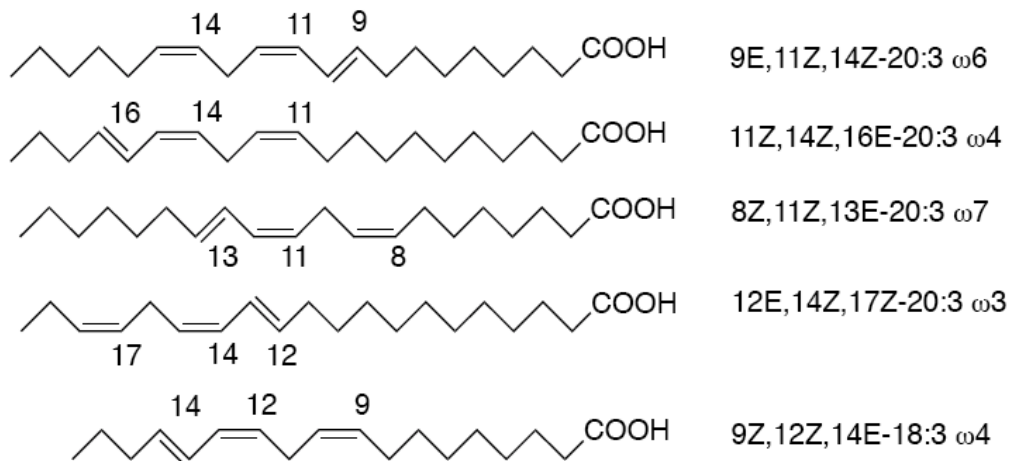


**Figure 16**: Tested synthetic fatty acids with extended conjugation.

Products of the 9E,11Z,14Z-20:3ω6 reaction at room temperature

Straight phase and reversed phase HPLC analyses revealed a complex product pattern including at least four products with $\lambda_{max}$ at 270 nm, four at 235 nm and four at 320 nm (data not shown). We reasoned that the substrate was first oxygenated to conjugated triene hydroperoxides ($\lambda_{max}$ 270 nm), which were then further converted by the hydroperoxide isomerase activity of eLOX3 to epoxyalcohols and ketones ($\lambda_{max}$ 235 nm and 320 nm). The fact that the epoxyalcohol products also absorb at 235 nm explains why a substantial UV absorbance at 235 nm remained upon completion of the reaction (**Figure 17A**).
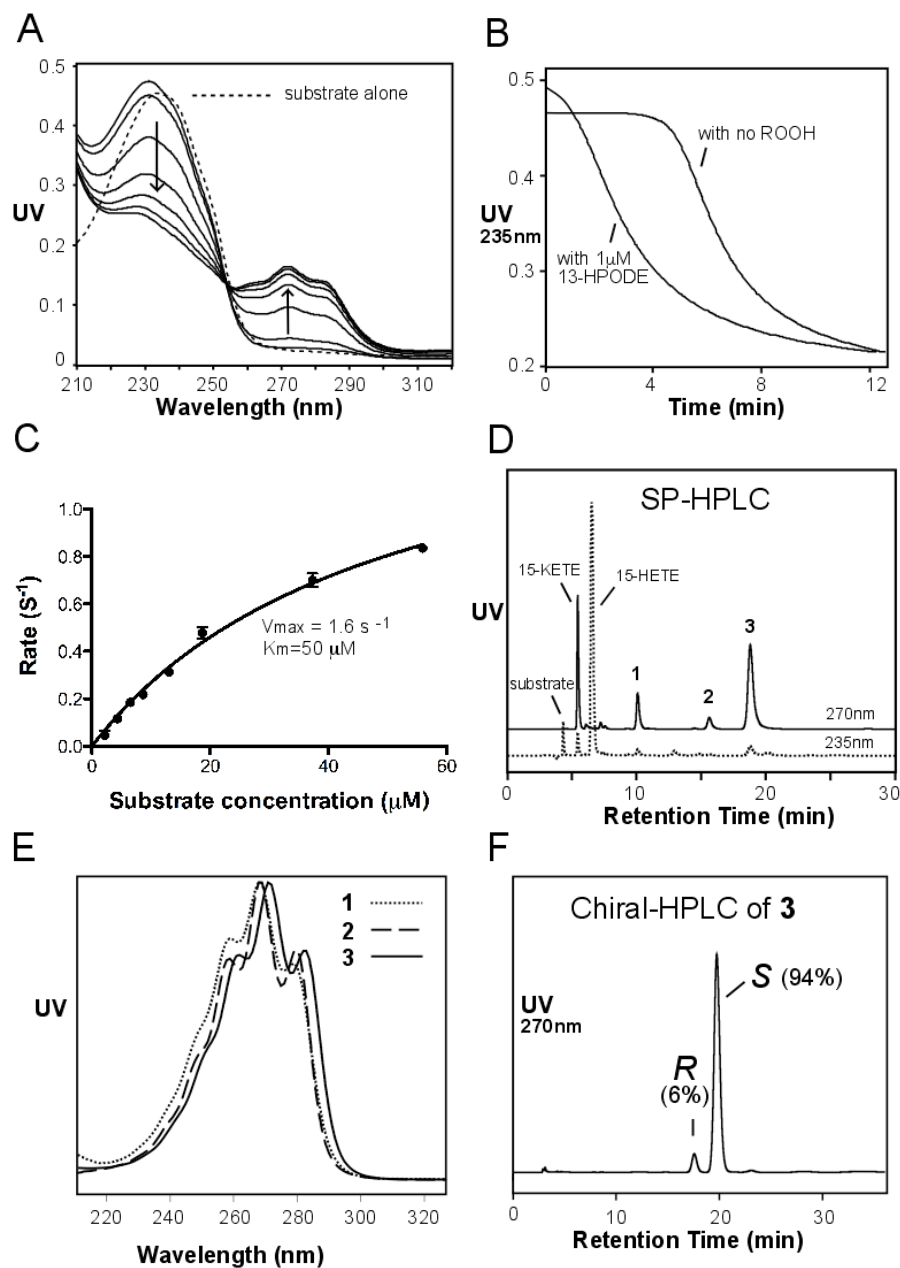
**Figure 17**: Dioxygenase activity of eLOX3 with 9*E*,11*Z*,14*Z*-20:3ω6. **(A)** UV scans of the room temperature reaction of eLOX3 (0.1 μM) with 9*E*,11*Z*,14*Z*-20:3ω6 (18 μM). To 1 ml of phosphate pH 7.5 buffer, the substrate was added and a UV scan taken (dotted line). After the enzyme was added and mixed (for ~15 s), a second scan was taken. Further scans shown were taken after 3 min, 4 min, 5 min, 6 min, 7 min and 8 min. **(B)** Progress curves of the reaction in the absence or presence of 13S-HPODE, monitored at 235 nm. The reaction conditions are the same as in panel **A**. **(C)** Dependence of maximal rate on substrate concentration. Maximal rates were taken from the steepest part of progress curves. **(D)** Straight phase-HPLC analysis of the primary products. Here, the reaction of eLOX3 (0.13 μM) with 9*E*,11*Z*,14*Z*-20:3ω6 (33 μM) was performed at 0 °C, in the presence of 15*S*-HPETE (150 μM) and 4-hydroxy TEMPO (1.5 mM). The reaction was completed within 30 minutes. **(E)** UV spectra (in straight phase solvent) of products **1**, **2** and **3**, as designated in panel **D**. **(F)** Chiral HPLC analysis of product **3**.

Trapping of the primary products

To focus on the primary LOX reaction, we identified three key factors that almost eliminated secondary product formation: (i) incubation at 0 °C preferentially reduces hydroperoxide isomerase activity compared to dioxygenase activity (109-112); (ii) an excess of 15$S$-HPETE included in the incubation competes with the conjugated triene hydroperoxide products for the hydroperoxide isomerase activity, and the excess 15$S$-HPETE helps keep the enzyme in the ferric state (see below); and (iii), addition of 4-hydroxy-TEMPO (1.5 mM), a water-soluble antioxidant, prevents non-enzymatic lipid peroxidation without causing significant enzyme inhibition (113). At the end of the incubation, SnCl$_2$ was added to convert hydroperoxides to the more stable alcohols and the products were extracted and analyzed by SP-HPLC with a diode-array detector (**Figure 17D and 17E**). By comparison with authentic standards obtained in a previous study (16) and by GC-MS analysis, the major peak **3** (76%) was identified as 9-hydroxy-10$E$,12$E$,14$Z$-eicosatrienoic acid, and the two minor products **1** and **2** as positional and geometric isomers of **3**. (**1** and **2** both have a 15-hydroxyl group, but differ in double bond configuration, data not shown). Chiral phase HPLC resolved product **3** into the $R$ and $S$ isomers with a ratio of 6:94 (**Figure 17F**). Thus, 9$E$,11$Z$,14$Z$-20:3ω6 was oxygenated by eLOX3 in a regio- and stereospecific fashion to its 9$S$-hydroperoxy derivative, 9$S$-hydroperoxy-10$E$,12$E$,14$Z$-eicosatrienoic acid. The 9$S$-oxygenation occurs four carbons removed from the site of bis-allylic hydrogen abstraction at C-13. None of the other conjugated fatty acids tested were significantly oxygenated, indicating substrate selectivity of eLOX3.

Dioxygenase activity of eLOX3 with arachidonic acid

The pronounced lag phase seen with 9*E*,11*Z*,14*Z*-20:3ω6 led us to question whether there might be an even longer lag phase with arachidonic acid, which might be overcome using fatty acid hydroperoxide activator. As shown in **Figure 18A**, in the absence of fatty acid hydroperoxides, eLOX3 (0.4 μM) showed only weak, slow activity with arachidonic acid (42 μM) as monitored by RP-HPLC assay of the remaining substrate. In the presence of high concentrations of fatty acid hydroperoxides, however, the rate of conversion of arachidonic acid was greatly accelerated, more so in the presence of 13*S*-HPODE than in the presence of 12*R*-HPETE. Also, the effect of fatty acid hydroperoxides is concentration-dependent, as 65 μM 13*S*-HPODE proved to be more effective than 27 μM 13*S*-HPODE. In fact, the reaction initiated with 27 μM 13*S*-HPODE was found to stall when 13*S*-HPODE was fully consumed and resume only after a second dose of 13*S*-HPODE (58 μM) was given. Therefore, the reaction of eLOX3 with arachidonic acid coincided with and was likely driven by its reaction with fatty acid hydroperoxides.

Dioxygenase activity of Ala451Gly eLOX3 with arachidonic acid

The stereospecificity of oxygenation in LOX enzymes is partly controlled by an active site residue conserved as Ala in *S*-LOX and Gly in *R*-LOX (14). eLOX3 has Ala in this position. Recently Oliw and colleagues reported that mutation of the natural Gly to Ala in Mn-LOX strongly augments hydroperoxide isomerase activity (114). Accordingly, it was of interest to examine whether changing Ala451 to Gly in eLOX3 would produce the opposite effect, i.e., a switch from hydroperoxide isomerase to dioxygenase activity. Therefore, we mutated Ala451 to Gly and incubated the mutant enzyme (0.5 μM) with

arachidonic acid (42 μM). Unlike wild-type eLOX3, Ala451Gly eLOX3 reacted well with arachidonic acid even in the absence of fatty acid hydroperoxides, yet only after an unusually long lag phase of ~ 20 minutes (**Figure 18B**). This lag phase could be eliminated by addition of 11 μM 13*S*-HPODE at the beginning of the reaction (**Figure 18B**).
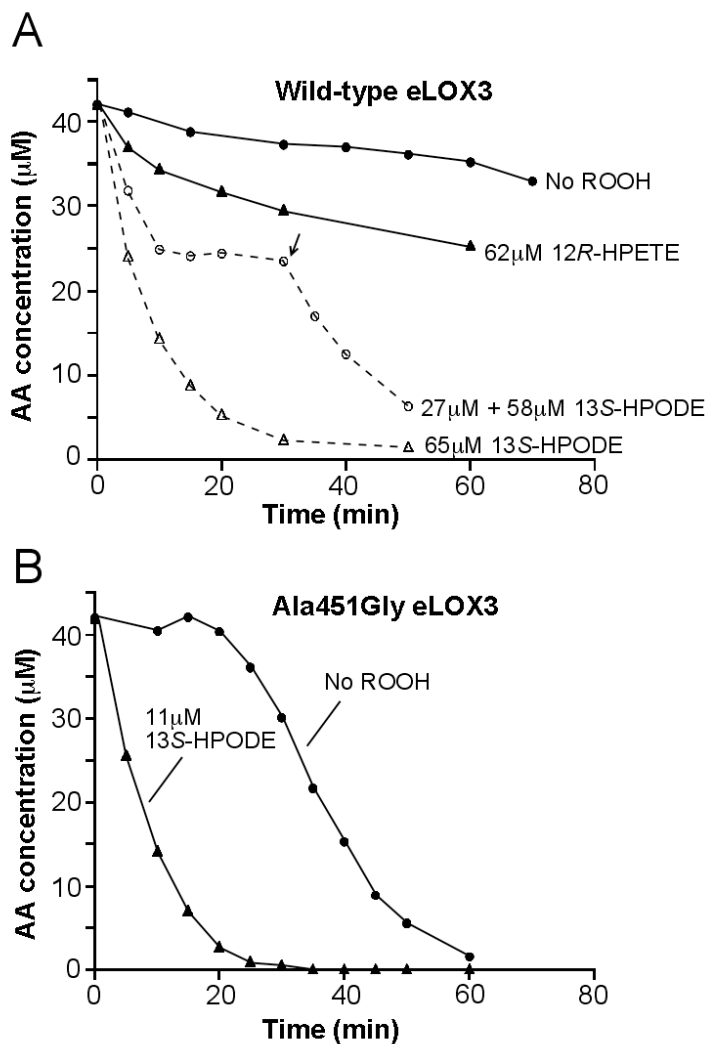


**Figure 18**: Effect of fatty acid hydroperoxide on dioxygenase activity of wild-type eLOX3 (0.4 μM) (panel **A**) or Ala451Gly eLOX3 (0.5 μM) (panel **B**) with arachidonic acid (42 μM) at room temperature. Arachidonic acid and fatty acid hydroperoxides were added first to phosphate pH 7.5 buffer, and then addition of enzyme started the reactions. At specified time points, an aliquot was taken and the unreacted arachidonic acid substrate was quantified by reversed phase HPLC.

44

Effect of temperature on accumulation of HPETE products

In the room temperature reactions mentioned above, the expected HPETE products occurred only as transient intermediates with either the wild-type or Ala451Gly eLOX3 (**Figure 19A and 19C**); the primary hydroperoxide products are further converted to epoxyalcohols and ketones by the hydroperoxide isomerase activity of eLOX3 (results not shown). However, similar to the observations with 9*E*,11*Z*,14*Z*-20:3ω6, when reaction with arachidonic acid was performed at 0 °C and in the presence of excess 13*S*-HPODE, the HPETE products continued to accumulate during the entire course of the reaction (**Figure 19B and 19D**) and the epoxyalcohol and ketone secondary products were formed only in negligible amounts.

Identification of the HPETE products

After the reaction, the HPETE products from the 0°C incubation were reduced with SnCl$_2$, extracted using a C$_{18}$ cartridge, and subjected to RP- and SP-HPLC analyses. As shown in **Figure 20A**, the products consisted of predominantly 7-, 9-, and 5-H(P)ETEs (25%, 29%, and 22%, respectively) that resulted from C-7 hydrogen abstraction, followed by 15- and 11-H(P)ETEs (8% and 9% respectively) from C-13 hydrogen abstraction. 12- and 8-H(P)ETEs were formed only in minor amounts (less than 3% each). The identity of the unusual bis-allylic 7-H(P)ETE product was unequivocally established by GC-MS analysis of its methyl ester TMS ether derivative, before and after catalytic hydrogenation (**Figure 21 and Figure 20C**).

Consistent with this lack of positional specificity, further analysis by chiral HPLC indicated no remarkable stereospecificity in any of the positional isomers (**Figure 22A, 22C, 22E**). Among the three major products, 7-H(P)ETE showed the highest degree of
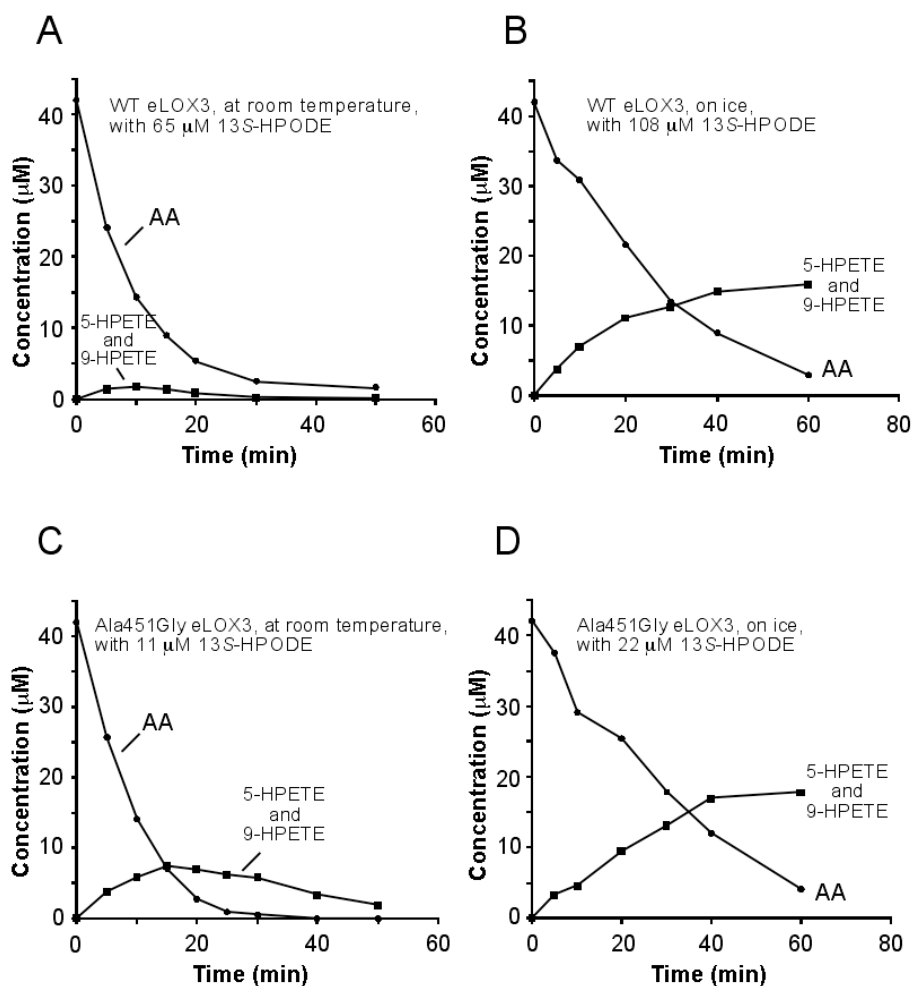
**Figure 19**: Effect of temperature on accumulation of HPETE products in the reaction of wild-type eLOX3 (0.4 μM) or Ala451Gly eLOX3 (0.5 μM) with arachidonic acid (42μM). 5-HPETE and 9-HPETE shown on the plots represented over 50% of the total products and could be readily quantified by reversed phase HPLC analysis. **(A)** Wild-type eLOX3 reaction at room temperature in the presence of 65 μM 13S-HPODE. **(B)** Wild-type eLOX3 reaction at 0 °C in the presence of 108 μM 13S-HPODE. **(C)** Ala451Gly eLOX3 reaction at room temperature in the presence of 11 μM 13S-HPODE. **(D)** Ala451Gly eLOX3 reaction at 0 °C in the presence of 22 μM 13S-HPODE.

46
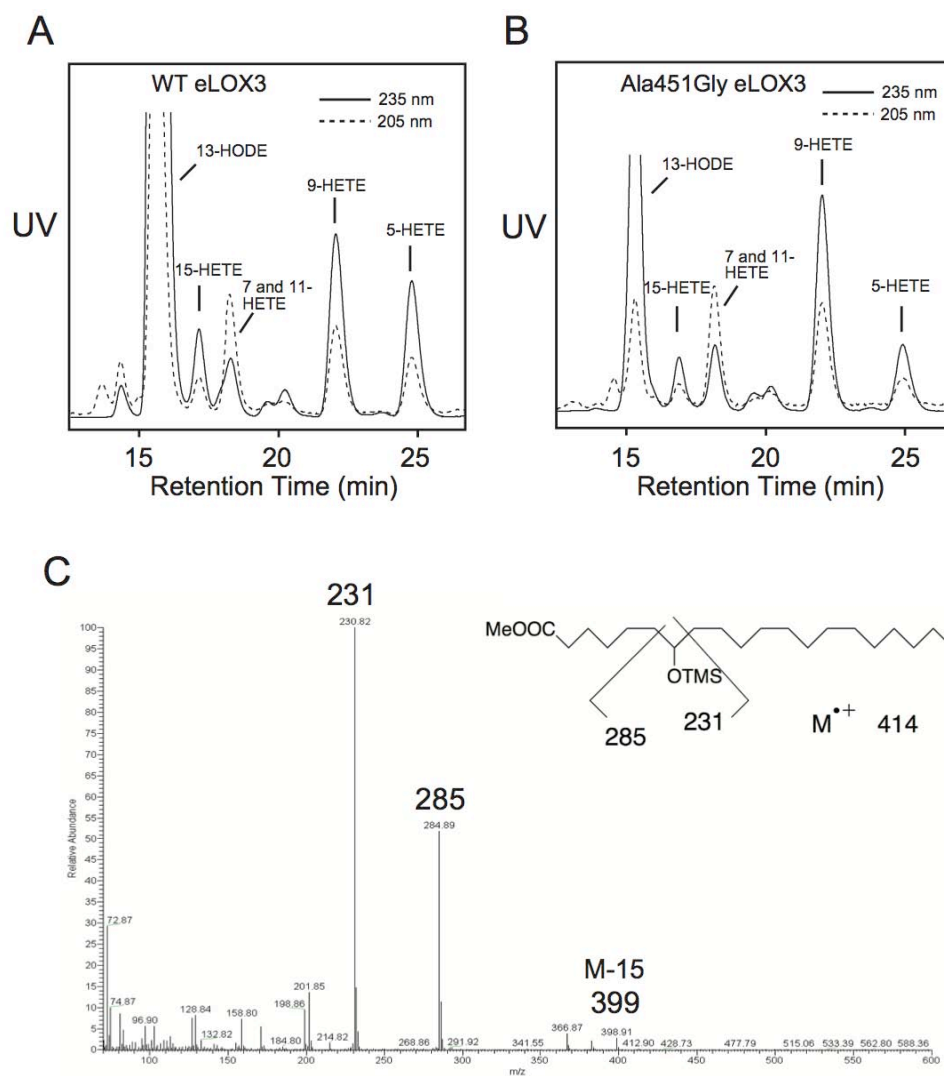
**Figure 20**: Identification of products from reactions of wild-type eLOX3 and Ala451Gly eLOX3 with arachidonic acid. The incubation conditions were the same as in **Fig. 19B** and **19D**. **(A) & (B)** Reversed phase-HPLC analysis of products from wild-type and Ala451Gly eLOX3 respectively. **(C)** GC-MS analysis of TMS ether methyl ester derivative of hydrogenated 7-HETE product. Before hydrogenation and derivatization, the 7-HETE product had been further purified by SP-HPLC.
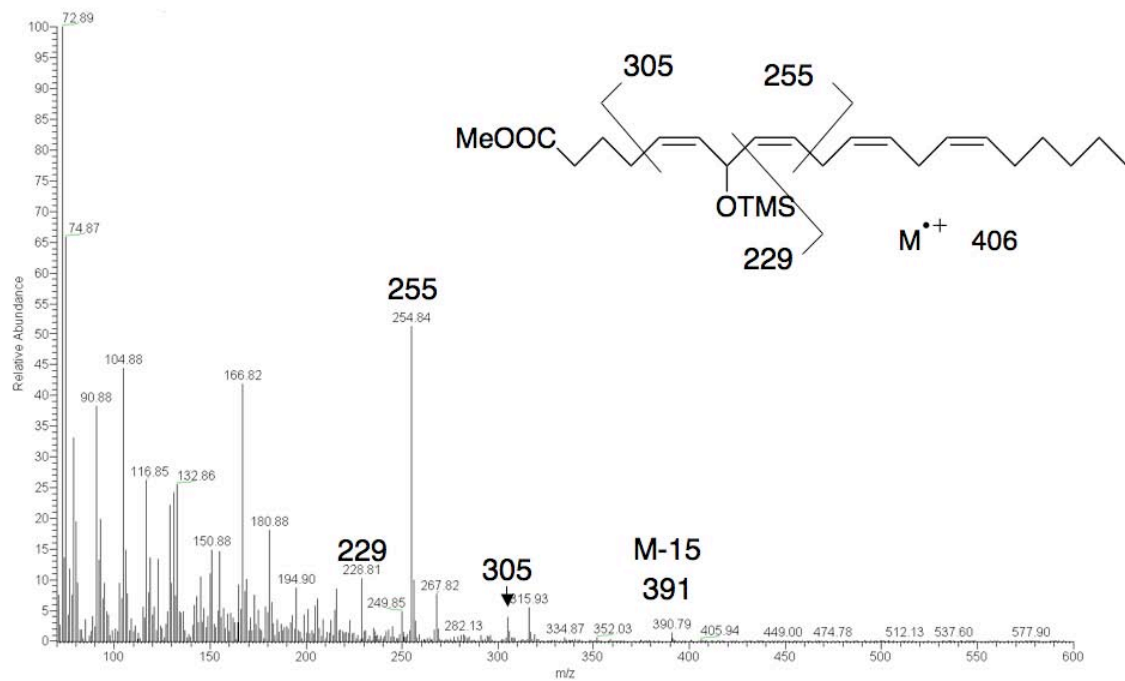
**48**: GC-MS analysis of TMS ether methyl ester derivative of the 7-HETE product.

stereospecificity, being 73% 7*R*. The 5-H(P)ETE product ranked the second, being 62% 5*R*, and the 9-H(P)ETE product was essentially racemic.

The active site Ala-Gly substitution in other LOX enzymes can lead to relatively dramatic changes in product profile (13,14,16) or mainly to changes in stereochemistry (115). The most noticeable effect of the Ala451Gly mutation in eLOX3 was a switch towards more 9-H(P)ETE, increased from 28.9 ± 1.4% (mean ± s.e.m., n = 4) to 38.5 ± 1.0%, seemingly at the expense of 5-H(P)ETE, decreased from 21.7 ± 0.8% to 11.6 ± 1.0%  (cf. **Figure 20A, 20B**). These differences were statistically significant (p < 0.01) for both wild-type and mutant eLOX3. Chiral HPLC analysis further revealed that the 9-H(P)ETE in the Ala451Gly eLOX3 reaction was 67% 9*R* (**Figure 22F**), an improvement in stereospecificity compared to the racemic 9-H(P)ETE product of wild-type eLOX3 (**Figure 22E**).

Dioxygenase activity of eLOX3 with AA/lyso PA

Experiments using AA/lyso PA as substrate, a molecule with a bulky ester on the arachidonate carboxyl, were used to gain insight into the possible "tail first" or "head-first" substrate binding orientation (11,116). Reaction occurred at less than 0.1% of the rate with free arachidonic acid and products arising mainly from C-13 hydrogen abstraction were formed (**Figure 23**). These results strongly suggest that the "tail first" orientation of substrate binding is mainly associated with H-13 abstraction in the reaction of wild-type or Ala451Gly eLOX3 with AA/lyso PA. It can be further inferred that the "head first" orientation is associated with H-7 abstraction and is the preferred orientation in the reaction of eLOX3 with free arachidonic acid.
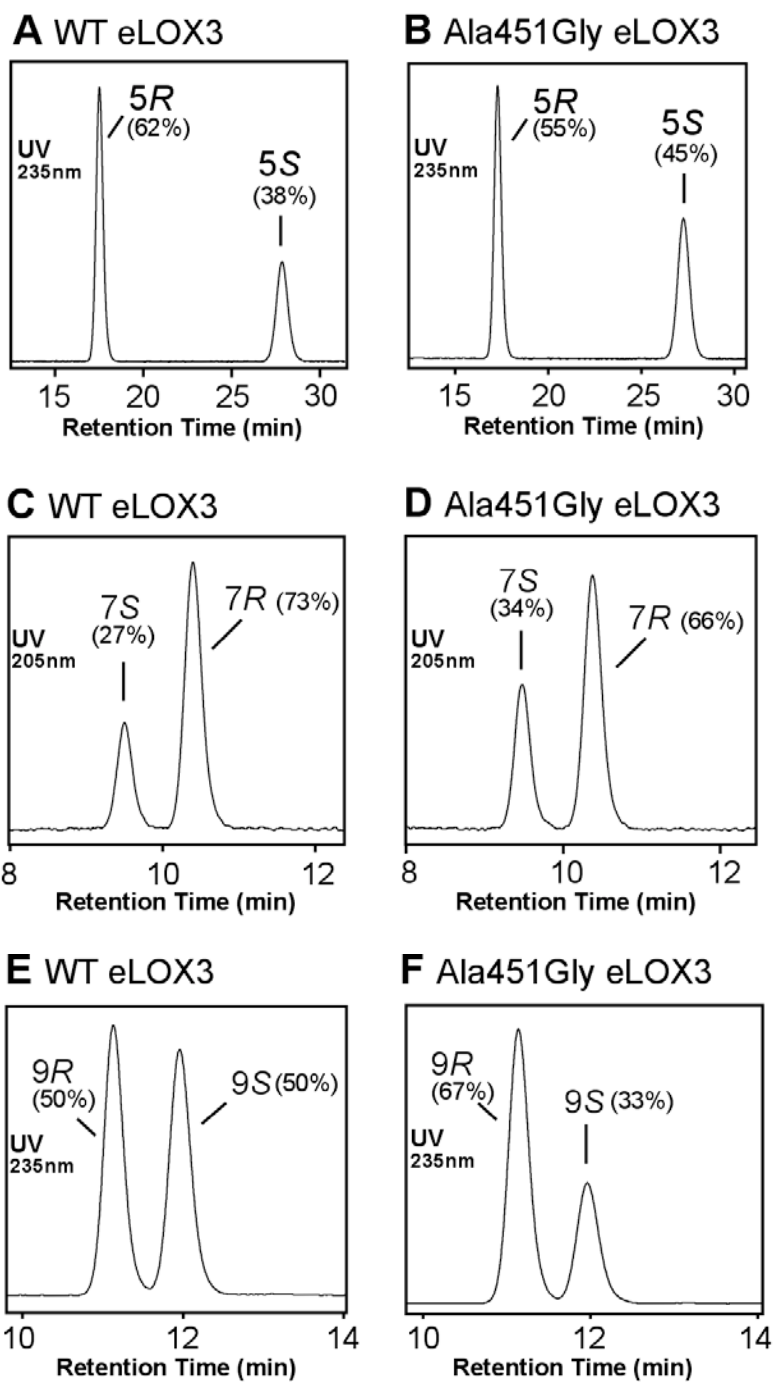
**Figure 22**: Chiral HPLC analysis of individual HETE products from reactions of wild-type eLOX3 and Ala451Gly eLOX3 with arachidonic acid. **(A)** Wild-type eLOX3, 5-HETE methyl ester. **(B)** Ala451Gly eLOX3, 5-HETE methyl ester. **(C)** Wild-type eLOX3, 7-HETE methyl ester. **(D)** Ala451Gly eLOX3, 7-HETE methyl ester. **(E)** Wild-type eLOX3, 9-HETE methyl ester. **(F)** Ala451Gly eLOX3, 9-HETE methyl ester.
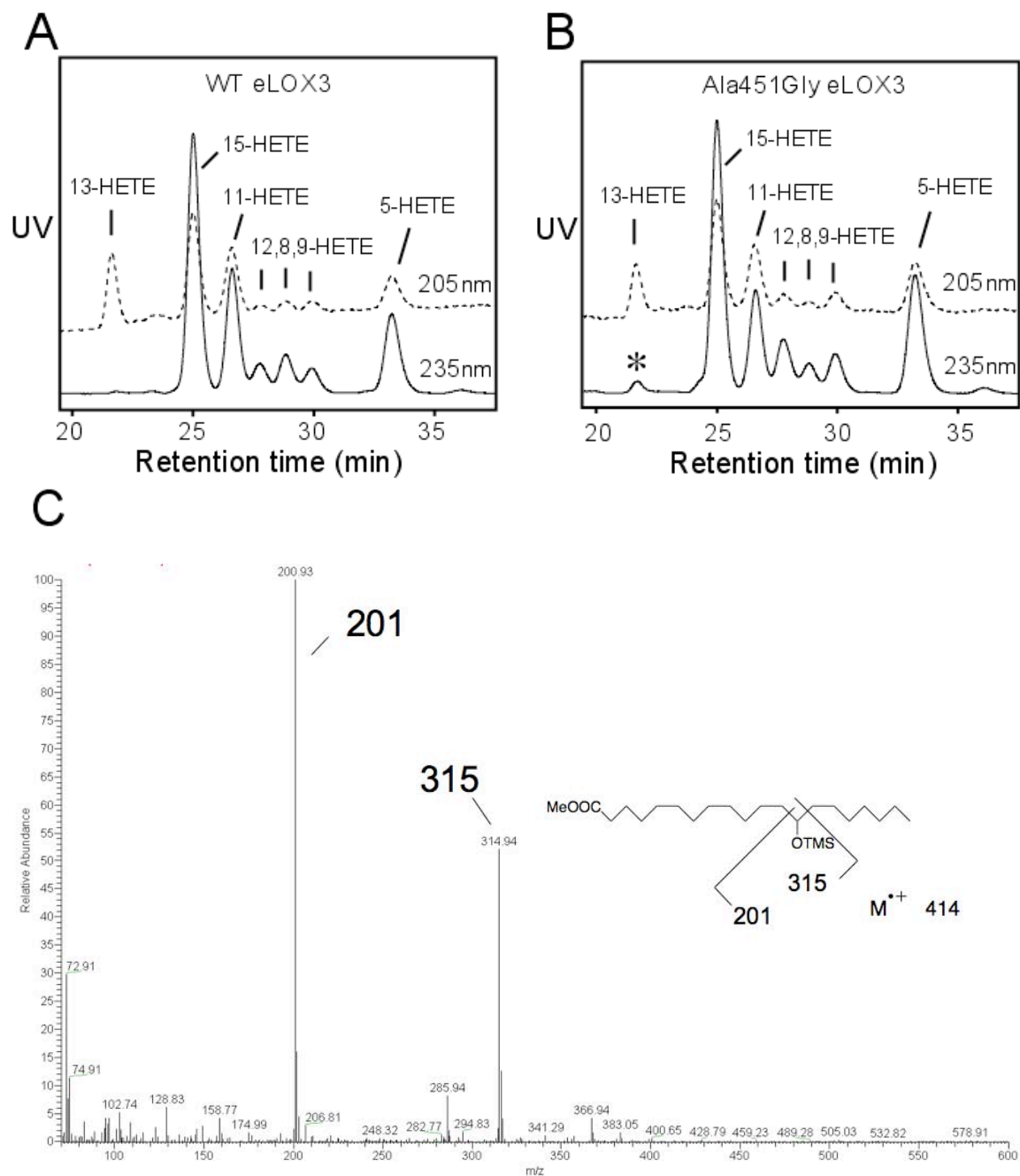
**Figure 23**: Identification of products from reactions of wild-type eLOX3 and Ala451Gly eLOX3 with AA/lyso PA. Note that whereas AA/lyso PA usually implies a tail-first orientation, the orientation of a free fatty acid substrate could be influenced by pH (117). **(A) & (B)** Reversed phase-HPLC analysis of trans-methylated products from wild-type and Ala451Gly eLOX3 respectively. **(C)** GC-MS analysis of TMS ether methyl ester derivative of hydrogenated 13-HETE product. * The slight UV absorbance at 235 nm was caused by an unknown 235 nm-absorbing compound that co-chromatographed with 13-HETE methyl ester.

**DISCUSSION**

Discovery of dioxygenase activity in eLOX3

This study demonstrates that eLOX3 in its active form is capable of oxygenating polyunsaturated fatty acids to the fatty acid hydroperoxides. As summarized in **Figure 24**, eLOX3 oxygenates 9*E*,11*Z*,14*Z*-20:3ω6 in a regio- and stereospecific fashion to give the 9*S* hydroperoxide. Although the reaction with arachidonic acid is much slower and exhibits considerably less specificity (**Figure 24**), the enzymatic nature of this reaction is confirmed by the formation of 7-HPETE, which cannot be formed non-enzymatically under the conditions used in this study. Such bis-allylic hydroperoxides are formed from the corresponding peroxyl radical only in the presence of a highly efficient hydrogen atom donor (118,119), which in this case is not present in the incubation buffer and thus must be part of the enzyme machinery, most likely the Fe(II)-$H_2O$ complex. eLOX3 joins Mn-LOX (120) and the recently characterized mini-LOX from cyanobacterium Cyanothece sp. (121) in the ability to make a bis-allylic hydroperoxide.

Unusual aspects of eLOX3 and reasons for its elusive dioxygenase activity

Our study also reveals aspects of eLOX3 that may explain why its dioxygenase activity has remained undetected for years: (i) With fatty acid substrate alone, the reaction shows an unusually long lag phase. This ranged from 4-5 min with 9*E*,11*Z*,14*Z*-20:3ω6 (**Figure 17B**) to over 1 hour with arachidonic acid (**Figure 18A**). (ii) Compared to typical LOX reactions, high concentrations of fatty acid hydroperoxide are required to abolish the lag phase. (iii) As known with other LOX enzymes (122-124), not every fatty

acid hydroperoxide is equally effective in the enzyme activation. The best substrate for

the hydroperoxide isomerase activity of eLOX3, 12*R*-HPETE, turns out to be only
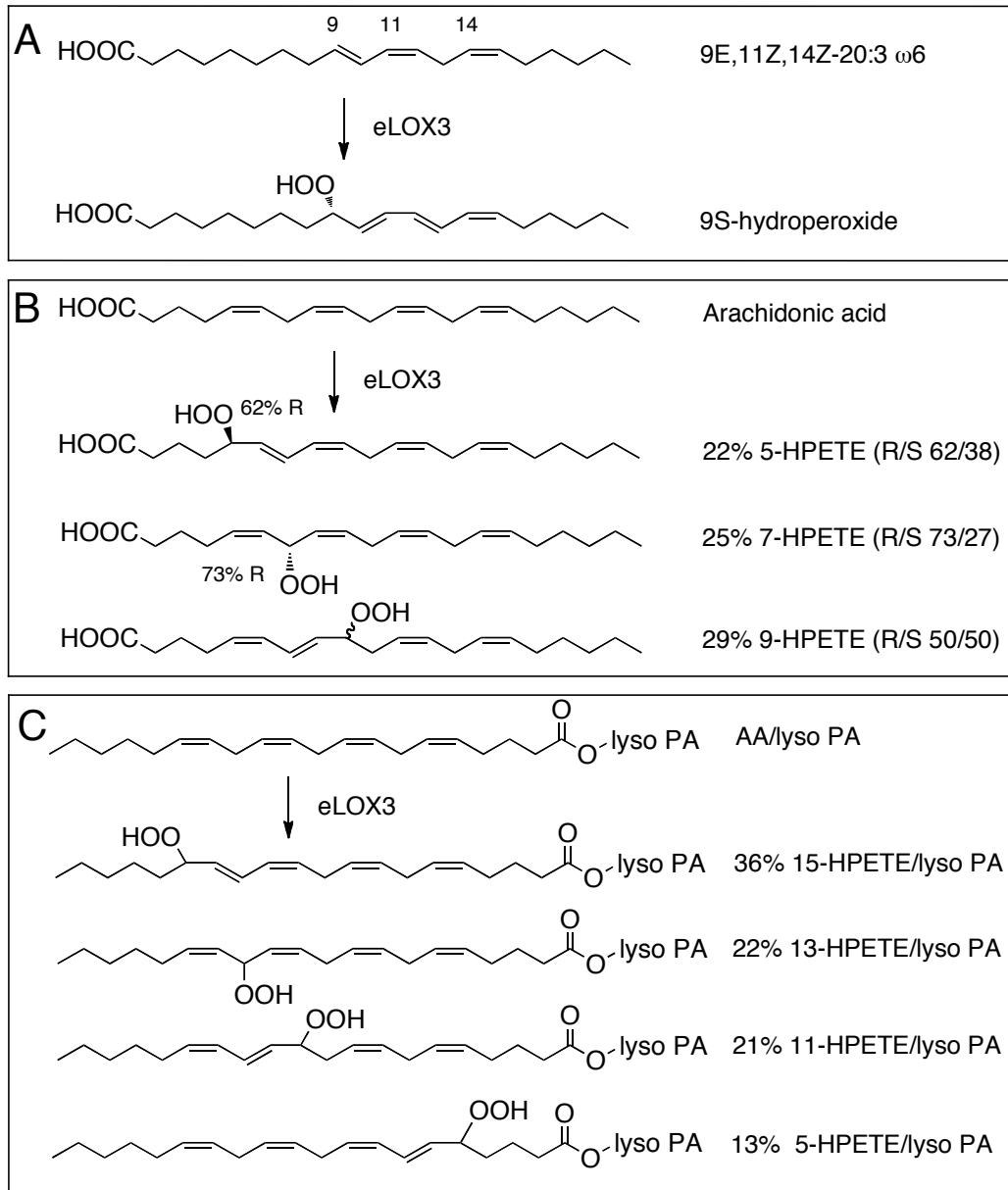


**Figure 24**: Dioxygenase activity of eLOX3.

marginally effective. This is not a coincidence, as 12*R*-HPETE allows for efficient

hydroperoxide isomerase cycling of eLOX3. (iv) At room temperature (as opposed to at 0

°C), the primary oxygenation products occur only as transient intermediates, i.e., they

will be further converted to epoxyalcohols and ketones by the hydroperoxide isomerase

activity. Therefore, the reaction gives no signal with the usual spectrophotometric (UV

235 nm) or HPLC-UV assays.

Our interpretations of the unusual aspects

The evidence points to a deficiency in the activation of eLOX3. Whereas one

equivalent of fatty acid hydroperoxide activator is sufficient in the activation step of

typical LOX, many equivalents are required in the activation step of eLOX3, hence the

pronounced lag phase and the requirement for high concentrations of a fatty acid

hydroperoxide activator. At room temperature, the concurrent hydroperoxide isomerase

activity producing epoxyalcohols and ketones from the primary hydroperoxide products

implies that a significant fraction of eLOX3 exists in the ferrous state even after the lag

phase. This is probably because, during the dioxygenase cycling of eLOX3, a significant

fraction of the free radical intermediates escape from the enzyme active site, leaving the

enzyme in the ferrous state.

The deficiency in the activation step of eLOX3 is somewhat relieved by the

Ala451Gly mutation. Ala451Gly eLOX3 appears to stand at the midpoint between wild-

type eLOX3 and typical LOX. On the one hand, Ala451Gly eLOX3 still shows a

pronounced lag phase in its reactions with arachidonic acid in the absence of fatty acid

hydroperoxides. On the other hand, the lag phase of Ala451Gly eLOX3 is much shorter

than that of wild-type eLOX3 and can be eventually overcome by only trace amounts of fatty acid hydroperoxide present in the substrate preparation.

Explaining the difference between eLOX3 and typical LOX

When the hydroperoxide isomerase activity of eLOX3 was originally characterized, our group had speculated that the enzyme fails to oxygenate natural fatty acids because the active site iron has a lower redox potential than the iron in typical LOX (37). As already outlined in the Introduction, hydrogen abstraction on typical fatty acid substrates, which is the first step of LOX catalysis, calls for a moderately high redox potential, and conceivably the redox potential could be exceptionally low in eLOX3 due to some unfavorable protein environment of the enzyme active site. However, this is not immediately evident on inspection of the protein sequence, as all the typical conserved features of LOX enzymes including the conserved amino acid ligands to the iron are retained in eLOX3. Most importantly, this issue is now addressed as we have demonstrated in this study that arachidonic acid can be oxidized by eLOX3 (with H-7 preferentially abstracted by the iron complex) thus definitively ruling out this low redox potential possibility.

To account for the atypical dioxygenase activity of eLOX3, we invoke an alternative explanation, that oxygen access is limited in the enzyme active site. Since molecular oxygen is one of the two substrates in LOX catalysis, limited oxygen access to the reacting fatty acid radical intermediate would undoubtedly impede catalysis. In the extreme scenario, when molecular oxygen is not available at all either because oxygen access is completely blocked or because the atmosphere is rendered anaerobic, even though the initial C-H bond cleavage step may proceed normally, the fatty acid radical

thus produced would eventually escape from the enzyme active site in the absence of reacting molecular oxygen, leaving the enzyme in the inactive ferrous state (**Figure 25**). Such a single turnover event would be undetectable in typical enzyme assays. Under such circumstances, redox cycling can occur only if the ferrous enzyme is re-oxidized by hydroperoxide back to the ferric form (**Figure 25**, dotted line), as seen classically in the anaerobic reaction of soybean LOX with linoleic acid and 13S-HPODE (30,125). However, under the usual aerobic conditions, such an extreme scenario hardly applies to typical LOX, indicating that molecular oxygen is readily accessible to the reacting fatty acid radical in their active site. For example, it is estimated that free radical leakage occurs only once per hundred turnovers in the reaction of soybean LOX-1 with linoleic acid (102). We suggest that limited oxygen access is the actual case in eLOX3, based on the following interpretations of the evidence:

(i) *Carbon radicals escape from the active site during dioxygenase cycling* - In the transformation of arachidonic acid at room temperature, the hydroperoxide isomerase activity is persistent throughout the reaction and HPETE products fail to accumulate (cf. **Figure 19, panel A and C**), indicating that the ferrous enzyme is constantly produced. Also, the reaction of eLOX3 with arachidonic acid is clearly driven by 13*S*-HPODE, (**Figure 18A**, the curve with two doses of 13*S*-HPODE), just as the anaerobic conversion of linoleic acid by soybean LOX-1 is driven by 13*S*-HPODE. These observations can be explained if a significant portion of fatty acid carbon radical intermediates escapes from the active site, which could be the result of lack of reacting oxygen (cf. **Figure 25**). Although leakage of peroxyl radical instead of carbon radical is also conceptually plausible, we consider this rather unlikely, because the subsequent trapping of peroxyl

radical by the enzyme is remarkably efficient as indicated by formation of the bis-allylic product, 7-HPETE.

(ii) *Lack of regio- and stereo-specificity within the active site* - The lack of oxygenation specificity with arachidonic acid is not entirely due to radical leakage and subsequent non-enzymatic oxygenation in solution. This is indicated by the appearance of 7-HPETE, which must be generated entirely within the enzyme active site. The *R/S* ratio of 73/27 in 7-HPETE must reflect a combination of the differences in oxygen supply to the two faces of C-7 and in trapping efficiency of the respective 7*R* and 7*S* peroxyl radicals. Indeed, it is likely that oxygen is added non-selectively to every reacting site on the delocalized pentadienyl radical (e.g., C-5, C-7 and C-9 when H-7 is abstracted), suggesting that oxygen supply is similarly low in every reacting site.

(iii) *The Ala451Gly mutation augments dioxygenase activity* - Ala451Gly eLOX3 shows "improved" specificity in its reaction with arachidonic acid compared to wild-type eLOX3, in that both the proportion of 9-HPETE among all isomers and its *R/S* ratio increase considerably. We deduce that the Ala-to-Gly mutation opens up space and introduces an oxygen "pocket" that is aligned with the "9*R*" site on arachidonic acid.

(iv) *eLOX3 readily oxygenates 9E,11Z,14Z-20:3ω6* – This synthetic fatty acid with extended conjugation is  a much better substrate than arachidonic acid, and is oxygenated regio- and stereospecifically to the 9*S* hydroperoxide. This is consistent with the availability of an oxygen pocket in this unusual 9*S* position, which is four carbons removed from the site of hydrogen abstraction at C-13. Obviously, such a pocket or channel would play no role in the oxygenation of typical pentadienyl fatty acids that

require oxygen to be delivered to sites that are two carbons removed from the site of hydrogen abstraction.

The connection between oxygen access and enzyme activation

The natural question at this point is how our proposed difference of eLOX3 from typical LOX, i.e., limited oxygen access, would lead to a deficiency in the enzyme activation step. A kinetic study of rabbit reticulocyte 15-LOX-1 suggests that molecular oxygen is in fact directly involved in the LOX activation step (126). We have evidence from comparison of soybean LOX-1 and eLOX3 that agrees with this proposition and further suggests that molecular oxygen is actually a driving force in the activation step. Therefore, it is not surprising that the activation step would be impaired when oxygen access in the active site becomes limited.

Concluding remarks

In this study we have unveiled dioxygenase activity of eLOX3 with fatty acids and investigated both the usual and unusual aspects. The usual aspects suggest that the basic machinery for LOX catalysis is fully functional in eLOX3, whereas the unusual aspects of eLOX3 point to the possibility that eLOX3 has limited oxygen access in the active site. It may be useful to consider a spectrum of activities among LOX enzymes that are partly dependent on the availability of molecular oxygen within the respective enzyme active sites. At one end of the spectrum are the conventional LOX, exemplified by soybean LOX-1, in which dioxygenase activity is dominant. Towards the other end of the spectrum, with limited access to molecular oxygen and radical leakage from the active sites, are atypical LOX enzymes such as eLOX3, plant type-2 lipoxygenases

(127,128), moss and maize LOX with hydroperoxide isomerase and lyase activities (129,130).

As noted at the beginning of the Introduction, eLOX3 performs a vital function in epidermal barrier formation. Where do our new findings stand in relation to this physiological role, and what is their importance? When the hydroperoxide isomerase activity of eLOX3 was discovered originally, it was presumed that this atypical isomerase activity, acting on a hydroperoxide product of its partner 12*R*-LOX, represents the function of eLOX3 *in vivo*. As the evidence stands at present, we continue to favor this interpretation, although whether this dioxygenase activity in eLOX3 is physiologically relevant should be considered in future studies. In our view the latent dioxygenase activity of eLOX3 is a reflection of mechanistic issues biasing eLOX3 towards hydroperoxide isomerase activity.
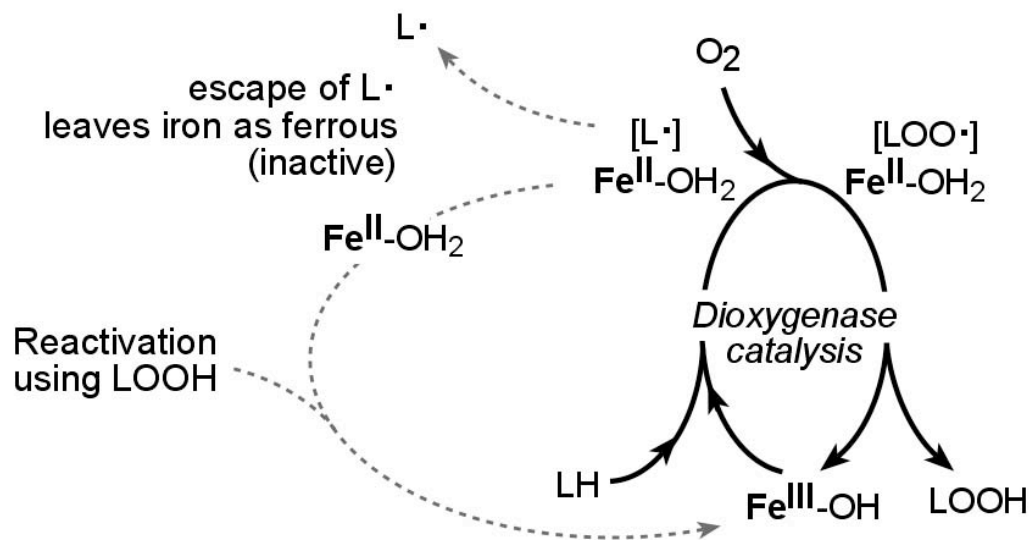


**Figure 25**: LOX catalytic cycle. Solid lines: when oxygen access is not limited. Dotted lines: when oxygen access is limited.

# CHAPTER III

# COMPARISON AND CONTRAST OF ELOX3 WITH SOYBEAN LOX-1: ELUCIDATION OF THE ROLE OF MOLECULAR OXYGEN IN LOX ACTIVATION

## Introduction

Lipoxygenases (LOX) are a class of non-heme iron dioxygenases that incorporate molecular oxygen into polyunsaturated fatty acids to give fatty acid hydroperoxides (11). Widely expressed in animals and plants, and also in some bacteria and fungi, LOX enzymes participate in diverse physiological and pathological processes. Mammalian 12$R$-LOX and epidermal lipoxygenase-3 (eLOX3), for example, play an indispensable role in skin barrier formation (96,99), whereas plant LOX enzymes are involved in stress responses and development (131). A distinctive characteristic of LOX enzymes in general is that the resting enzyme requires activation before catalytic reactions with fatty acids and molecular oxygen can begin (4,5,132).

Mechanistically, soybean LOX-1 is the most extensively studied and generally considered as the prototypical LOX enzyme. The non-heme iron of soybean LOX-1 exists in two oxidation states, ferric and ferrous. The ferric enzyme is responsible for the catalytic activity (19) and preferentially oxygenates polyunsaturated fatty acids (PUFA) with an ω6 and ω9 pentadiene unit at the "$S$" face of the ω6 carbon, e.g., to convert linoleic acid to 13$S$-hydroperoxy-octadecadienoic acid (13$S$-HPODE). The ferrous

enzyme is inactive with fatty acids but can react with fatty acid hydroperoxides such as 13$S$-HPODE to become the ferric enzyme (102,133). Since the newly isolated enzyme is usually in the ferrous state, such a reaction with fatty acid hydroperoxides is required for the enzyme to enter the catalytic cycle, hence being known as the LOX activation step. In this activation process, as the proportion of ferric enzyme gradually increases, the rate of fatty acid oxygenation will also increase, manifesting itself in the progress curve of fatty acid oxygenation as a lag phase (20). A distinctive feature of LOX activation is that it is a single turnover event; once the enzyme is oxidized to the ferric form, it will no longer react with fatty acid hydroperoxides (18). Because of this single-turnover nature of the reaction, the products from LOX activation are formed in minute amounts and have not been identified. Although substantial evidence suggests that an alkoxyl radical is produced in LOX activation (134), the fate of this alkoxyl radical is poorly understood. **Figure 26** illustrates transformation of a fatty acid hydroperoxide to an alkoxyl radical as well as subsequent reactions and rearrangement discussed throughout the paper.

eLOX3, on the other hand, is an atypical LOX with a prominent hydroperoxide isomerase activity (37). Using this hydroperoxide isomerase activity, ferrous eLOX3 converts fatty acid hydroperoxides via an alkoxyl radical intermediate to epoxyalcohols and ketones  (**Figure 26**). Unlike the single-turnover LOX activation step, this hydroperoxide isomerase activity fulfills a catalytic cycle so that the free ferrous enzyme will be regenerated upon product release. Although previously unknown, the dioxygenase activity of eLOX3 has recently been reexamined and uncovered in this laboratory (135). Using this dioxygenase activity, ferric eLOX3 oxygenates the synthetic fatty acid, 9$E$,11$Z$,11$Z$-20:3ω6, to the specific 9$S$-hydroperoxide, and oxygenates arachidonic acid

to a mixture of HPETEs including the bis-allylic 7-HPETE. However, we have found this dioxygenase activity unusual in exhibiting a very pronounced lag phase, which points to a deficiency in eLOX3 activation by fatty acid hydroperoxides. We have also found that this long lag phase is partially alleviated by introduction of an Ala-to-Gly mutation at a conserved residue (Ala451) that has been implicated in the control of $O_2$ access in LOX active site (13-16,115,136).

An alkoxyl radical is postulated as a common intermediate in both the hydroperoxide isomerase cycling pathway and the single turnover LOX activation step (**Figure 26**). $O_2$ is not involved in hydroperoxide isomerase cycling, but I questioned whether $O_2$ might be directly involved in LOX activation. Oxygen uptake has been observed in aerobic incubations of soybean LOX-1 with fatty acid hydroperoxides (137). The participation of $O_2$ in LOX activation has also been suggested in a kinetic study of rabbit reticulocyte 15-LOX (126). If $O_2$ is involved in activation, I postulated further, a lack of or limited $O_2$ access in the enzyme active site could be the explanation for both the prominent hydroperoxide isomerase activity and the inefficient enzyme activation observed in eLOX3. To explore these ideas, here using kinetic and analytical chemical approaches I compared and contrasted the rates and the products of reactions of soybean LOX-1, the Ala451Gly eLOX3 and wild-type eLOX3 with fatty acid hydroperoxides at various oxygen concentrations.
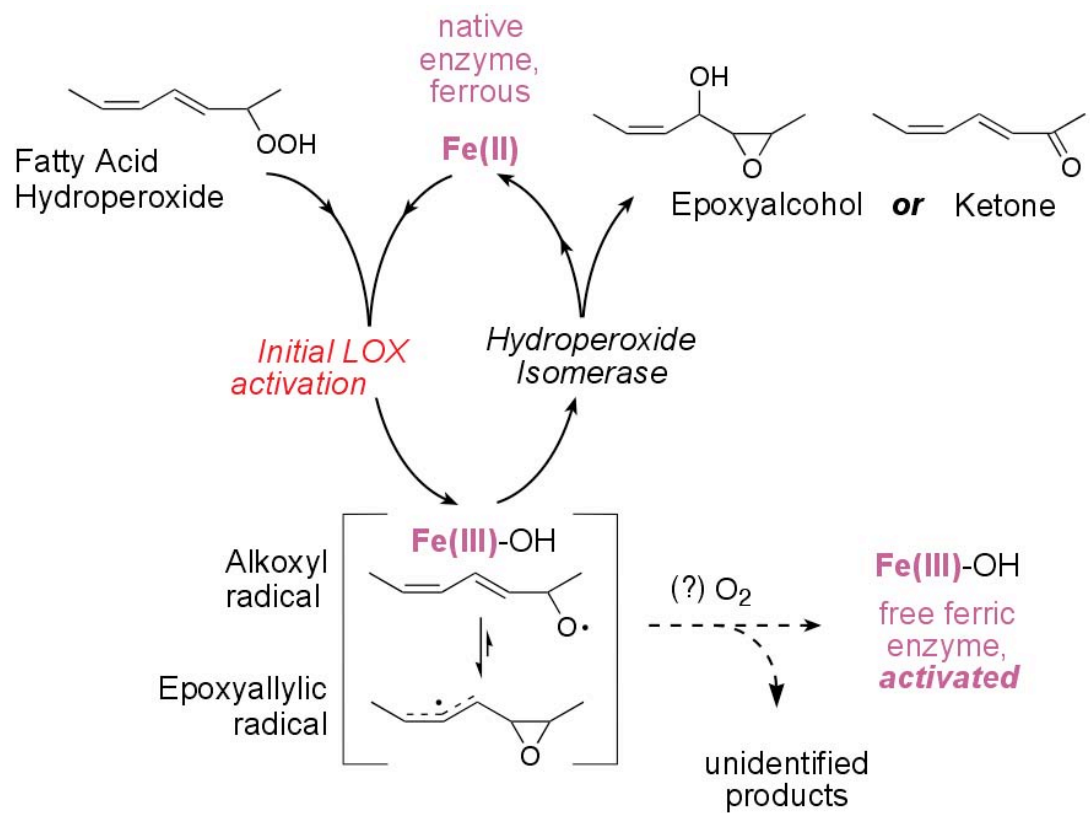
**Figure 26**: Comparison and contrast of LOX activation and hydroperoxide isomerase activity

**Experimental Procedures**

<u>Materials</u>

Arachidonic and linoleic acids and methyl esters were purchased from NuChek Prep Inc. (Elysian, MN). 15$S$-HPETE or 13$S$-HPODE was synthesized by reacting soybean LOX-1 with arachidonic acid or linoleic acid at pH 9 followed by SP-HPLC purification (103). Nordihydroguaiaretic acid (NDGA) was purchased from Cayman Chemical, Co Inc (Ann arbor, MI). Triphenylphosphine (TPP) was purchased from Sigma-Aldrich (St. Louis, MO). Soybean LOX-1 was purchased from Sigma-Aldrich (St. Louis, MO) and Cayman Chemical, Co Inc (Ann arbor, MI), labeled as type V and P1 purified respectively. The enzyme from both sources gave identical products, although in our hands the Sigma enzyme was about ten times as active as the Cayman purified enzyme (138). The concentration label in the current manuscript refers to the Sigma enzyme assuming 80% purity of the preparation.

*<u>Expression and purification of human eLOX3</u>*

The cDNA of human eLOX3 with an N-terminal His$_6$ tag was subcloned into the pCW vector, and the protein was expressed in *E. coli* and purified according to a previously published protocol (105). The Ala451Gly mutagenesis in eLOX3 was performed using QuikChange$^{TM}$ Site-Directed Mutagenesis Kit. The mutation was verified by DNA sequencing. Then the Ala451Gly eLOX3 was expressed and purified as the wild-type eLOX3.

Initial incubations were conducted on an analytical scale in 100 mM sodium phosphate buffer pH 7.5 at various $O_2$ concentrations at room temperature and were monitored using a Perkin-Elmer spectrophotometer. The typical reaction volume is 1 ml. $O_2$-saturated buffer was made by bubbling ~ 40 ml buffer in a 50-ml conical tube with $O_2$ for 30 minutes. The $O_2$-saturated buffer was used for the incubations only when the buffer temperature reverted to room temperature. For the anaerobic incubations, the buffer was rendered anaerobic using an oxygen-consuming system consisting of glucose, glucose oxidase and catalase according to a previously published protocol (138). To verify the results, each anaerobic reaction was also repeated in $N_2$-saturated phosphate buffer inside a $N_2$-inflated glovebag in the absence of the glucose-glucose oxidase-catalase system (138), and identical results were found. If methyl arachidonate is one of the substrates, sodium deoxycholate (final concentration 1-2 mM) was used to help solubilize the methyl ester. The incubation mixture was acidified to pH 5 and then extracted using an Oasis HLB cartridge (Waters Corp.).

For structural identification of the products of LOX activation by 13$S$-HPODE, large-scale incubations of Cayman unpurified soybean LOX-1 (250 μl of the commercial preparation, Catalog No. 60712) with 13$S$-HPODE (66 μM) in the presence of NDGA (80 μM) was performed in 60 ml of air-saturated 50 mM sodium borate pH 10 buffer for 15 minutes. Although borate would form a complex with NDGA and thus reduce the reaction efficiency (27), we found the reaction was largely complete under the used conditions. (Other buffers can be used to eliminate this problem.) In addition, 20 μl of bovine liver catalase (the commercial preparation, Sigma-Aldrich, C3155) was added to

the incubation to eliminate hydrogen peroxide generated from NDGA autoxidation. The reaction mixture was acidified to ~ pH 4 and extracted by methylene chloride.

## HPLC-diode array analysis

RP-HPLC analysis generally used a Waters Symmetry C18 column (0.46 cm × 25 cm), a flow rate of 1 ml/min, and a solvent system of methanol/water/acetic acid (80:20:0.01, by volume). For better resolution of the epoxyalcohol or epoxyallylic hydroperoxide products, we performed SP-HPLC analysis using a Beckman Silica Ultrasphere column (0.46 cm × 25 cm), a flow rate of 1 ml/min and a solvent system of hexane/isopropyl alcohol/acetic acid (100:2:0.02 v/v/v). The monomeric and dimeric products from the anaerobic reaction of soybean LOX-1 or Ala451Gly eLOX3 can be conveniently separated using a Waters Symmetry C18 column (0.46 cm × 25 cm), a flow rate of 1 ml/min and a solvent system of methanol/water/acetic acid (95:5:0.01, by volume) (data not shown in the Results).

## Derivatization and GC-MS analysis

Free fatty acid products were dissolved in a small volume of methanol and then converted to the methyl ester by adding ethereal diazomethane. TMS ether derivatives were prepared by treatment with *bis*(trimethylsilyl)-trifluoracetamide (10 μl) and pyridine (2 μl) at room temperature for 2 h. Subsequently, the reagents were evaporated under a stream of nitrogen and the samples were dissolved in hexane for GC-MS.

Analysis of the methyl ester trimethylsilyl ether derivatives of the products was carried out in the positive ion electron impact mode (70 eV) using a Thermo Finnigan Trace DSQ ion trap GC-MS with the Xcalibur data system. Samples were injected at 150 °C, and after 1 min the temperature was programmed to 300 °C at 20 °C/min. Spectra

collected during elution of the GC peak (typically about 10 spectra) were averaged for calculation of the isotopic compositions.

ESI-LC-MS

ESI-LC-MS was performed using a Thermo Finnigan LC Quantum or LTQ instrument. For analysis of the aerobic reactions of soybean LOX-1 or Ala451Gly eLOX3 with 13$S$-HPODE or 15$S$-HPETE in the presence of NDGA, a Waters Symmetry C$_{18}$ column (0.2 × 15 cm) was eluted with acetonitrile/water/ammonium acetate (50:50:10 mM) at 0.2 ml/min. Mass spectra were acquired over the mass range m/z 200-500 at 2 s per scan under the negative ion mode. For analysis of monomer products from the anaerobic reactions of soybean LOX-1 or Ala451Gly eLOX3 with 13$S$-HPODE and arachidonic acid, we used a Phenomenex C18 column (2.6 μm, 0.3 cm × 10 cm), methanol/water/ammonium acetate (80:20:10 mM) and a flow rate of 0.3 ml/min. These conditions were held for 5 minutes and a gradient started from the weak solvent to pure methanol during which the remaining arachidonic acid substrate and dimer products were eluted. Mass spectra were acquired over the mass range m/z 200-700 at 2 s per scan under the negative ion mode. For detailed analysis of the dimer products, we used a Phenomenex C18 column (2.6 μm, 0.3 cm × 10 cm), a flow rate of 0.3 ml/min and a solvent system of methanol/water/ammonium acetate (90:10:10 mM), with MS detecting negative ions in the range from m/z 500 to m/z 650. HPLC-diode array analysis was also performed for each reaction under identical LC conditions.

*NMR-* ^{1}H and ^{1}H,^{1}H-COSY NMR spectra were recorded on a Bruker DXR 600 MHz spectrometer at 298K. The ppm values are reported relative to residual non-deuterated solvent ($\delta$ = 7.16 ppm for $C_6H_6$).

## Results

Effect of $O_2$ concentration or the Ala451Gly mutation on the lag phase of eLOX3

Our previous study showed that eLOX3 is capable of oxygenating the synthetic fatty acid, 9*E*,11*Z*,14*Z*-20:3$\omega$6 to a specific hydroperoxide, and that the reaction exhibits a pronounced lag phase during which the enzyme is slowly activated by trace amounts of fatty acid hydroperoxides (135). As known with other LOX enzymes (4,5,132), this lag phase can be eliminated using exogenous fatty acid hydroperoxide activators such as 13*S*-HPODE (135). To elucidate the role of $O_2$ in eLOX3 activation, first we compared the reactions of eLOX3 with 9*E*,11*Z*,14*Z*-20:3$\omega$6 in air- and $O_2$-saturated buffer ([$O_2$] ~240 $\mu$M and ~1.2 mM respectively). We found a consistently shorter lag phase in $O_2$-saturated buffer than in air-saturated buffer (**Figure 27**). Only the duration of the lag phase, not the maximal oxygenation rate, was affected. Thus, $O_2$ appeared to promote eLOX3 activation. We also found that the eLOX3 mutant, Ala451Gly eLOX3, shows a shorter lag phase than wild-type eLOX3 (**Figure 27**). Mutation of Ala to Gly in this position is implicated in oxygenation control in many other LOX enzymes (13-16,115,136) and the result in Figure 1 is consistent with this mutation in eLOX3 improving the access of $O_2$ within the enzyme active site.
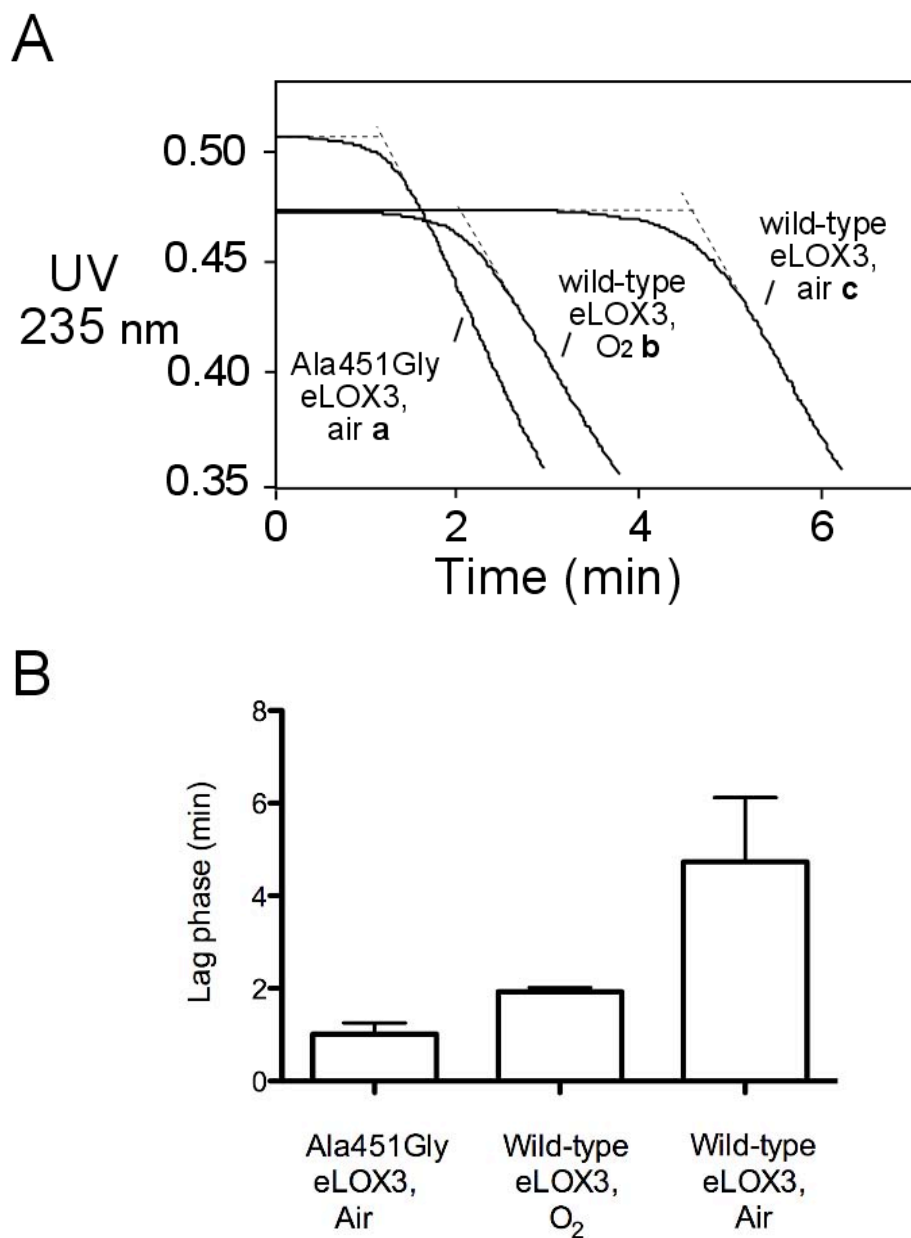
**Figure 27**: Increased $O_2$ concentration or the Ala451Gly mutation shortened the lag phase in the reaction of eLOX3 with 9*E*,11*Z*,14*Z*-20:3ω6. **A**, reaction progress curves monitored at 235 nm. Reaction was conducted in sodium phosphate pH 7.5 buffer at room temperature and was started by addition of enzyme. Wild-type eLOX3 concentration: 0.10 μM. Ala451Gly eLOX3 concentration: 0.13 μM. 9*E*,11*Z*,11*Z*-20:3 ω6 concentration: 18-20 μM. **B**, statistical bar representation of the lag phase duration of the reactions in A. The lag phase duration is defined as the time axis intercept of a straight line through the portion of the reaction progress curve where the rate is maximal. The data are presented as the mean ± the standard deviation. Each of the reactions of wild-type eLOX3 in air- and $O_2$-saturated buffer: n=4. The reaction of Ala451Gly eLOX3 in air-saturated buffer: n=3. P < 0.01 for every pair of reactions.

Effect of $O_2$ concentration or the Ala451Gly mutation on the rate of reaction of eLOX3 with 13S-HPODE

Fatty acid hydroperoxide activators of LOX-catalyzed oxygenation of polyunsaturated substrates are consumed in the activation process (123). This also occurs in 13*S*-HPODE activated eLOX3-catalyzed oxygenations, as we demonstrated previously (135). Here we studied the influence of $O_2$ concentration or the Ala451Gly mutation on the consumption of 13S-HPODE when incubated by itself with the enzyme. We observed an increased rate of 13S-HPODE disappearance on shifting from $O_2$-saturated buffer to normoxic buffer, and a further dramatic ~9 fold increase in rate under anaerobic conditions (**Figure 28**, curves a, b, and c). Thus, the initial rate of reaction with 13*S*-HPODE was inversely related to the oxygen concentration. We also found that compared to wild-type eLOX3 in air-saturated buffer, Ala451Gly eLOX3 reacted very slowly with 13*S*-HPODE (**Figure 28**, curves b and d), a result compatible with improved access to $O_2$ within the Ala451Gly mutant active site.

Although counterintuitive, this inhibitory effect of $O_2$ or the Ala451Gly mutation on the rate of 13*S*-HPODE consumption (**Figure 28**) is in fact consistent with its stimulatory effect on eLOX3 activation (**Figure 27**). Because $O_2$ or the Ala451Gly mutation promotes eLOX3 activation, i.e., the single turnover reaction of ferrous eLOX3 with 13*S*-HPODE to give ferric eLOX3, it will necessarily impede the ferrous enzyme cycling pathway, i.e., the far more productive pathway of 13*S*-HPODE consumption (cf. **Figure 26).**
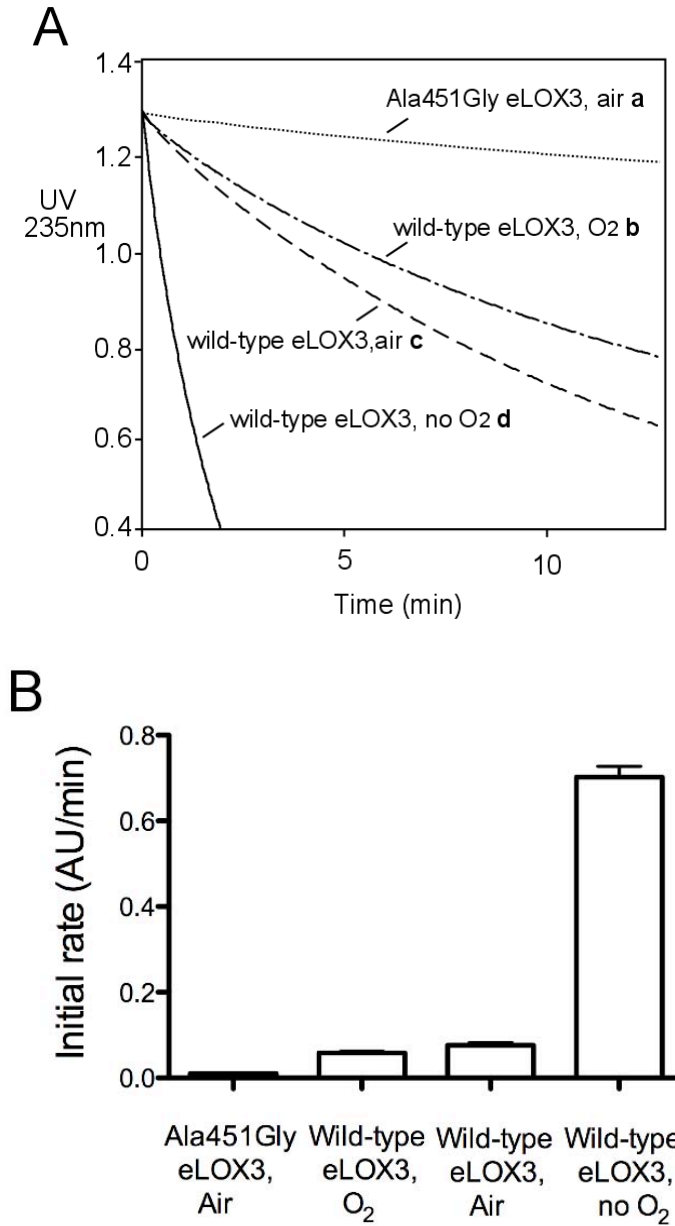
**Figure 28**: Increased $O_2$ concentration or the Ala451Gly mutation decreased the rate of the reaction of eLOX3 with 13*S*-HPODE. **A**, reaction progress curves monitored at 235 nm. Reaction was conducted in sodium phosphate buffer pH7.5 at room temperature and was started by addition of enzyme. Wild-type eLOX3 concentration: 0.25 μM. Ala451Gly eLOX3 concentration: 0.32 μM. Note that the oxygenation rate of wild-type eLOX3 at 0.25 μM is similar to the oxygenation rate of Ala451Gly eLOX3 at 0.32 μM (Figure 1). 13*S*-HPODE concentration: 52-55 μM. **B**, statistical bar representation of the initial rate of the reactions in A. The data are presented as the mean ± the standard deviation. Each of the reactions of wild-type eLOX3 in air- and $O_2$-saturated buffer: n=4. The reaction of wild-type eLOX3 under anaerobic conditions: n=3. The reaction of Ala451Gly eLOX3 in air-saturated buffer: n=3. P < 0.01 for every pair of reactions.

Identification of the products in LOX activation by 13S-HPODE

As noted in the Introduction, for LOX enzymes such as soybean LOX-1 that are efficiently activated to the ferric state, the activation process is a single turnover event that produces only traces of hydroperoxide-derived products. NDGA affords an opportunity to obtain the products in LOX activation in large amounts, since it helps regenerate the ferrous enzyme and thus accelerates transformation of the activating hydroperoxide (27), in our experiments 13$S$-HPODE (**Figure 33A**). Hence, we incubated soybean LOX-1 with 13$S$-HPODE in the presence of NDGA and identified the products by RP- and SP-HPLC, LC- and GC-MS, and NMR. The keto derivative 13-KODE (product **3** in **Figure 29E**) was only a minor product. The major products (**1** and **2** in **Figure 29E**) showed end absorbance at 205 nm and similar retentions times on RP-HPLC to $C_{18}$ epoxyalcohol standards. On SP-HPLC, **1** and **2** were further resolved into four products (I and II, 23% and 58% respectively (a ratio of 28:72), and Ia and IIa 6% and 13% respectively **Figure 29J**). Upon TPP reduction, I and II were converted to Ia and IIa respectively. LC-MS showed that products Ia and IIa both have the relative molecular mass of 312, consistent with the structure of a linoleic acid-derived epoxyalcohol, and that product I and II both have the relative molecular mass of 328, which, together with the TPP reduction experiment, suggests that I and II are hydroperoxide counterparts of Ia and IIa, i.e., epoxyallylic hydroperoxides. GC-MS analysis indicated that both Ia and IIa are stereoisomers of 9-hydroxy-12,13$S$-epoxyoctadecenoic acid (**Figure 30A, 30B**). $^1$H and $^1$H,$^1$H-COSY NMR analysis confirmed such a structure and further revealed that both Ia and IIa contain a *trans* epoxide between C-12 and C-13 (J = 2.0 Hz) and a *trans* double bond between C-10 and

72
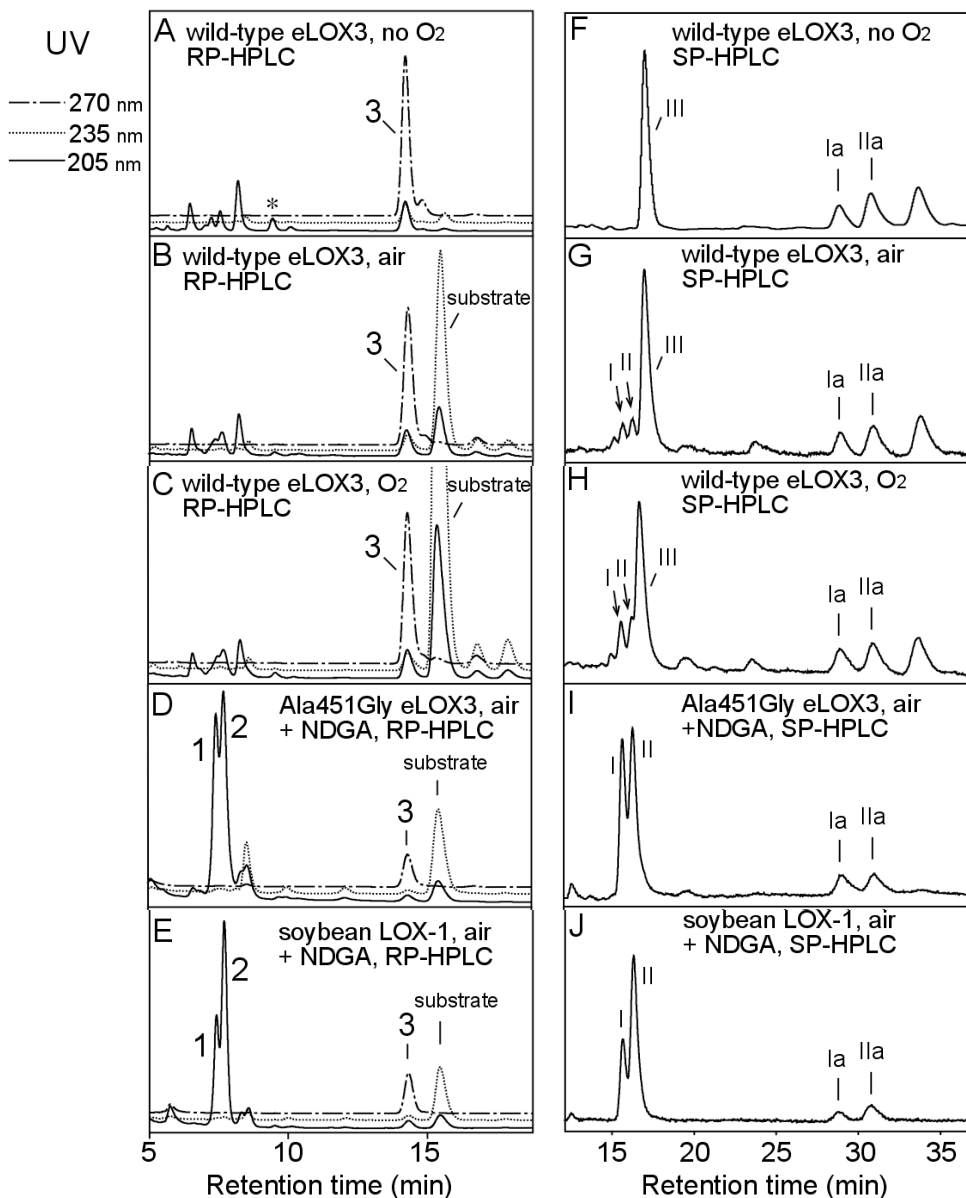
**Figure 29**: RP- and SP-HPLC analysis of the products from the reactions with 13*S*-HPODE. Analysis of wild-type eLOX3 (panels **A**, **B**, **C** and panels **F**, **G**, **H**), Ala451Gly eLOX3 (panels **D** and **I**) and soybean LOX-1 following reaction with 13*S*-HPODE (panels **E** and **J**). For wild-type eLOX3, $O_2$ concentration was varied in the incubation, from 0 (panel **A** and **F**) to 240 μM (panel **B** and **G**) to 1.2 mM (panel **C** and **H**). For Ala451Gly eLOX3 and soybean LOX-1, NDGA was included in the incubation. RP-HPLC analysis used a Water Symmetry C18 column (0.46 cm × 25 cm), a flow rate of 1 ml/min and a solvent system of methanol/water/acetic acid (80:20:0.01, by volume). SP-HPLC analysis used a Beckman Silica Ultrasphere column (0.46 cm × 25 cm), a flow rate of 1 ml/min and a solvent system of hexane/isopropyl alcohol/acetic acid (100:2:0.02). ∗ Control experiments indicated that this peak was not an enzymatic product.

73
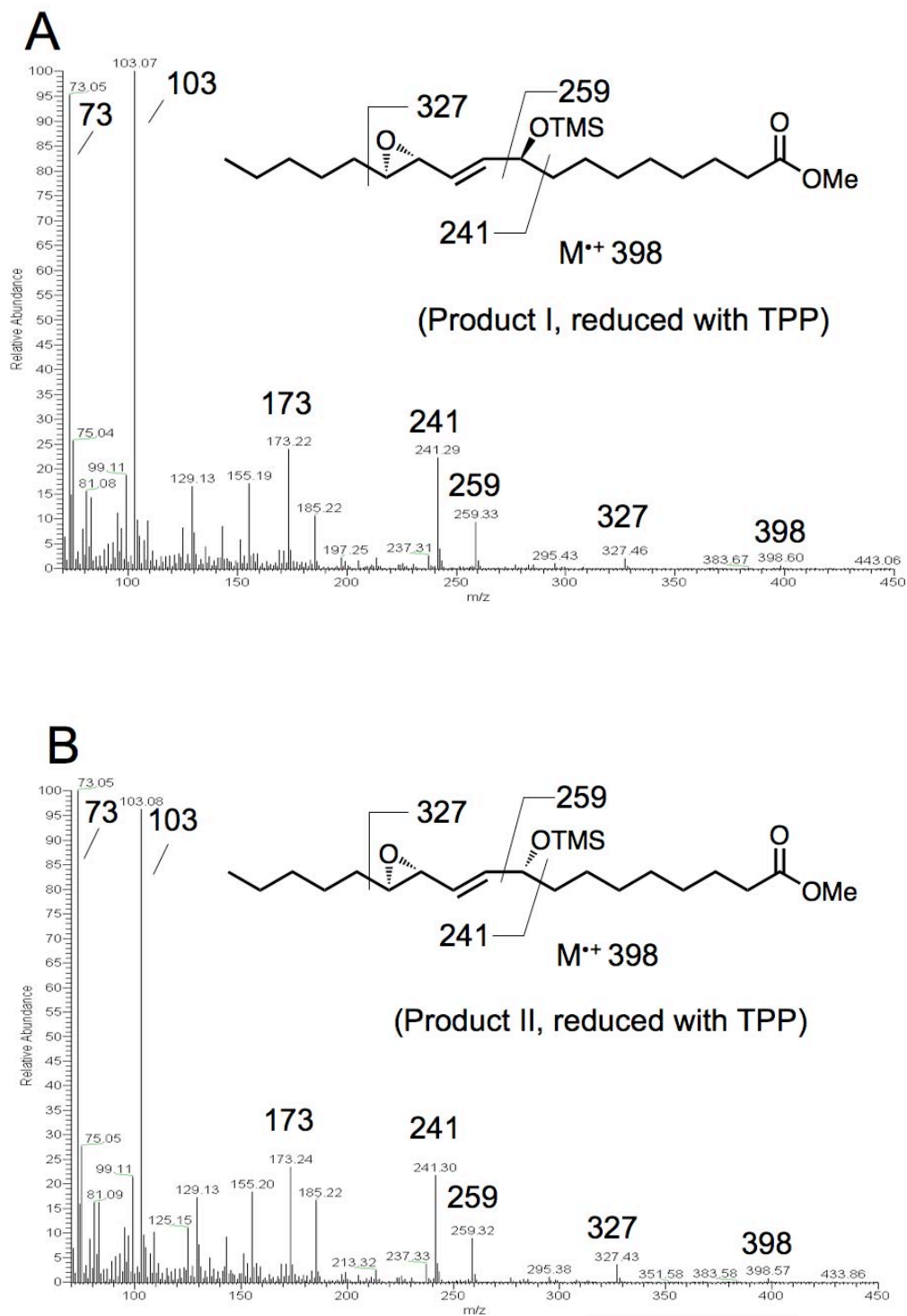
**Figure 30:** GC-MS analysis of products I and II**.** Mass spectra of the TMS ether methyl ester derivative of the TPP-reduced major products (product I and II in figure 3) from the reaction of soybean LOX-1 or Ala451Gly eLOX3 with 13S-HPODE in the presence of NDGA. **A**, product I. **B**, product II.

C-11 (J = 15.5 Hz) (**Figure 31**). Finally, the stereochemistry of the 9-hydroxyl in Ia and IIa was assigned as 9*S* and 9*R* respectively based on their order of elution on silica SP-HPLC (139). Thus, the major products in the activation of soybean LOX-1 by 13*S*-HPODE, I and II, are 9*S* and 9*R*-hydroperoxy-12*S*,13*S*-*trans*-epoxyoctadec-10*E*-enoic acid respectively (**Figure 32**).

Similarly to soybean LOX-1, Ala451Gly eLOX3 barely reacted with 13*S*-HPODE alone and NDGA stimulated this reaction by ~90 fold (**Figure 33B**). As the reaction proceeded, the enzyme was quickly and irreversibly inactivated (**Figure 33B**). This type of LOX inactivation has been documented for soybean LOX-1 and is partly ascribed to hydrogen peroxide generated from reaction of NDGA-derived radical intermediates with $O_2$ (27). RP-HPLC, SP-HPLC, LC-MS analyses and also TPP reduction of the products from the reaction of Ala451Gly eLOX3 in the presence of NDGA revealed that 13*S*-HPODE was converted to the same major products I and II as in the reaction of soybean LOX-1, albeit with a different ratio of 42:58 (**Figure 29D, 29I, Figure 32**). On prolonged incubations with an excess of enzyme, the epoxyallylic hydroperoxide products I and II were further converted by Ala451Gly eLOX3 to an epoxyketone compound (9-keto-12*S*,13*S*-*trans*-epoxyoctadec-10*E*-enoic acid), the structure of which was identified by $^1$H-NMR and $^1$H,$^1$H-COSY NMR and $NaBH_4$ reduction (data not shown).

For the reaction of wild-type eLOX3 with 13*S*-HPODE, a considerable stimulation (~23 fold) was also observed in the presence of NDGA (**Figure 33C**). However, whether NDGA was present or not, 13*S*-HPODE was converted to a different set of products, among which the two most prominent were 13-KODE (product 3 in Figure **29**) and one stereoisomer of 11-hydroxy-12,13*S*-epoxy-octadec-9*Z*-enoic acid

**Figure 31A**
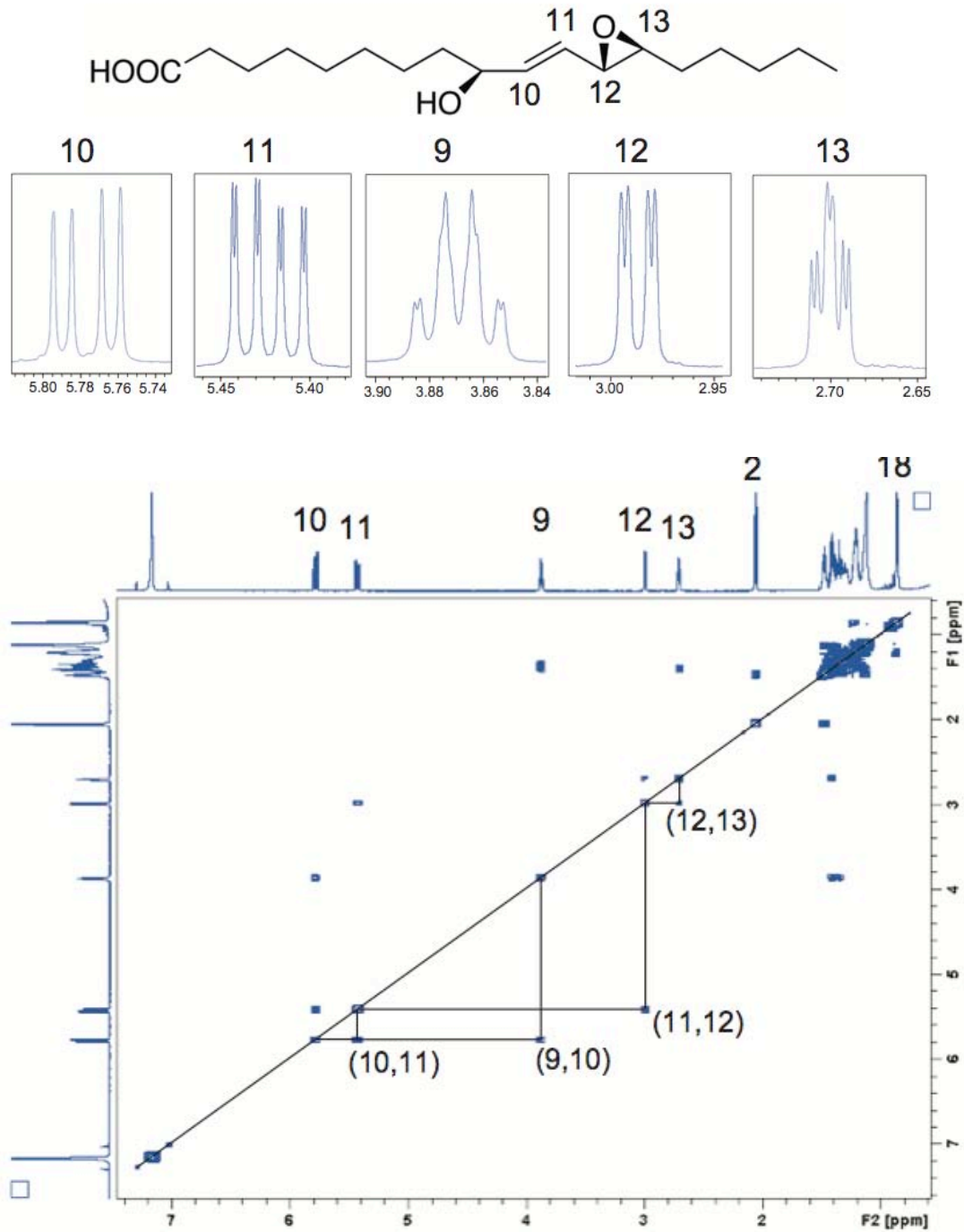
**Figure 31B**
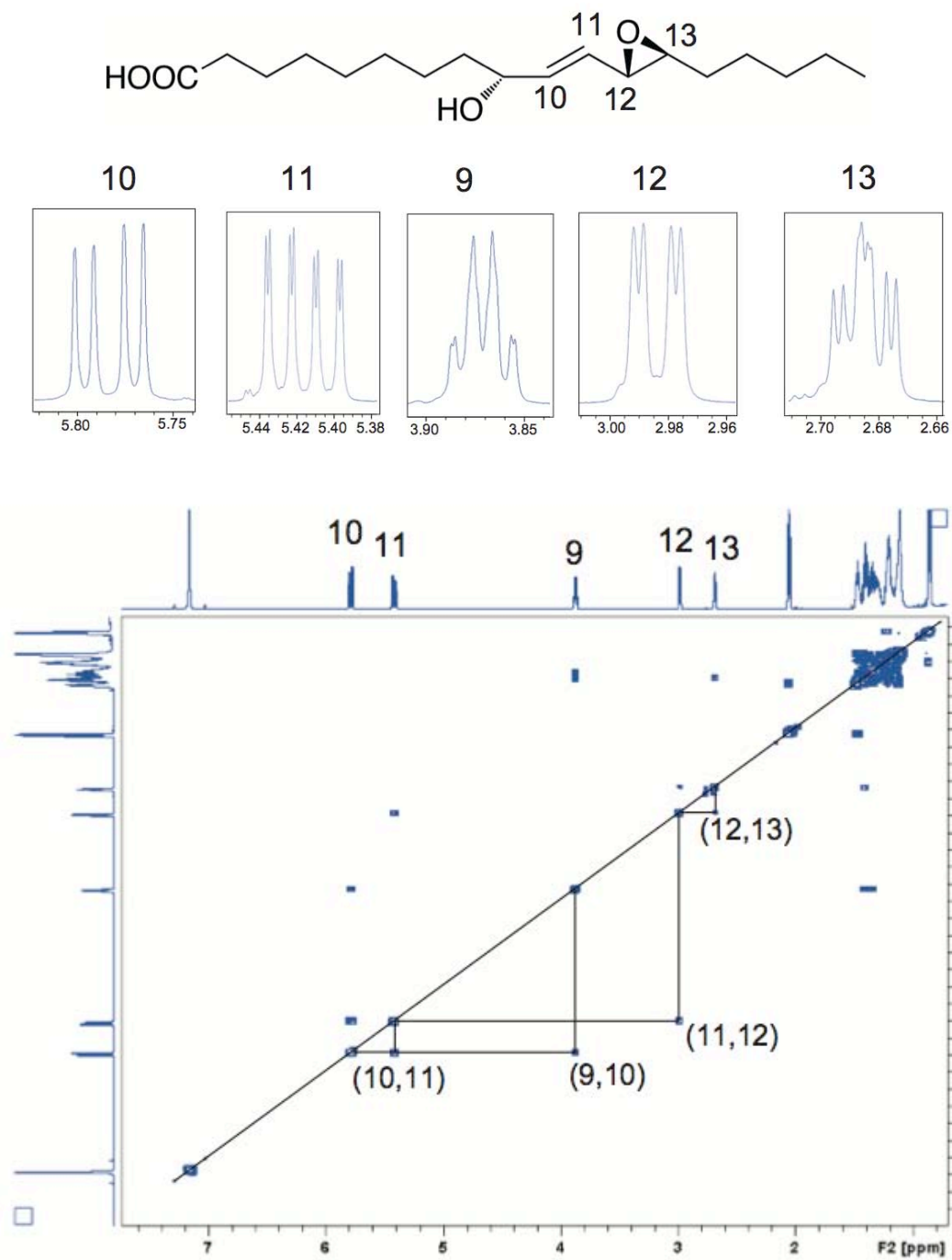


**Figure 31 (A)** $^1$H and $^1$H,$^1$H-COSY NMR spectra of TPP-reduced product I (Figure 29) in $C_6D_6$. **(B)** $^1$H and $^1$H,$^1$H-COSY NMR spectra of TPP-reduced product II (Figure 29) in $C_6D_6$.
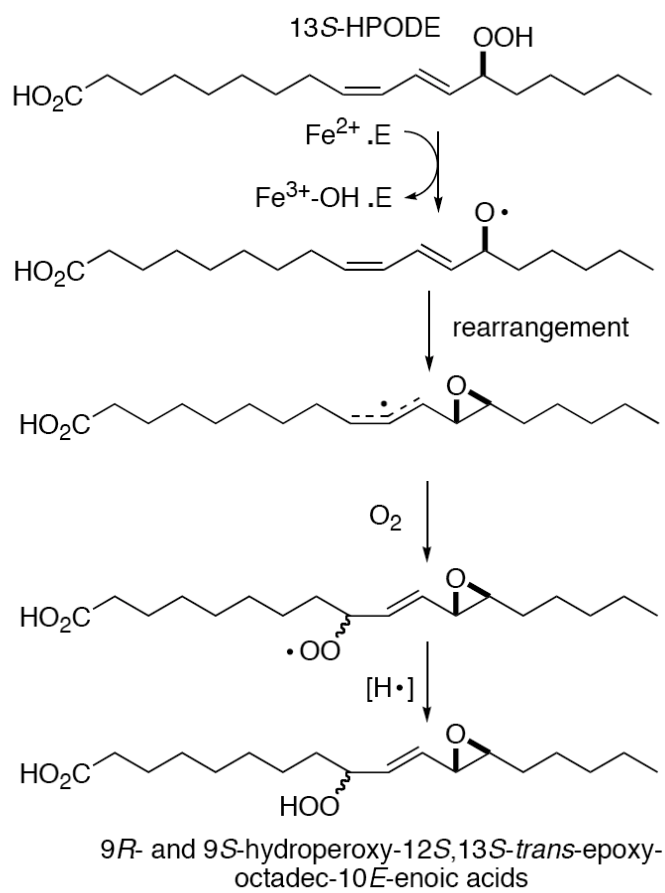
**Figure 32**: The major products formed in LOX activation by 13*S*-HPODE.
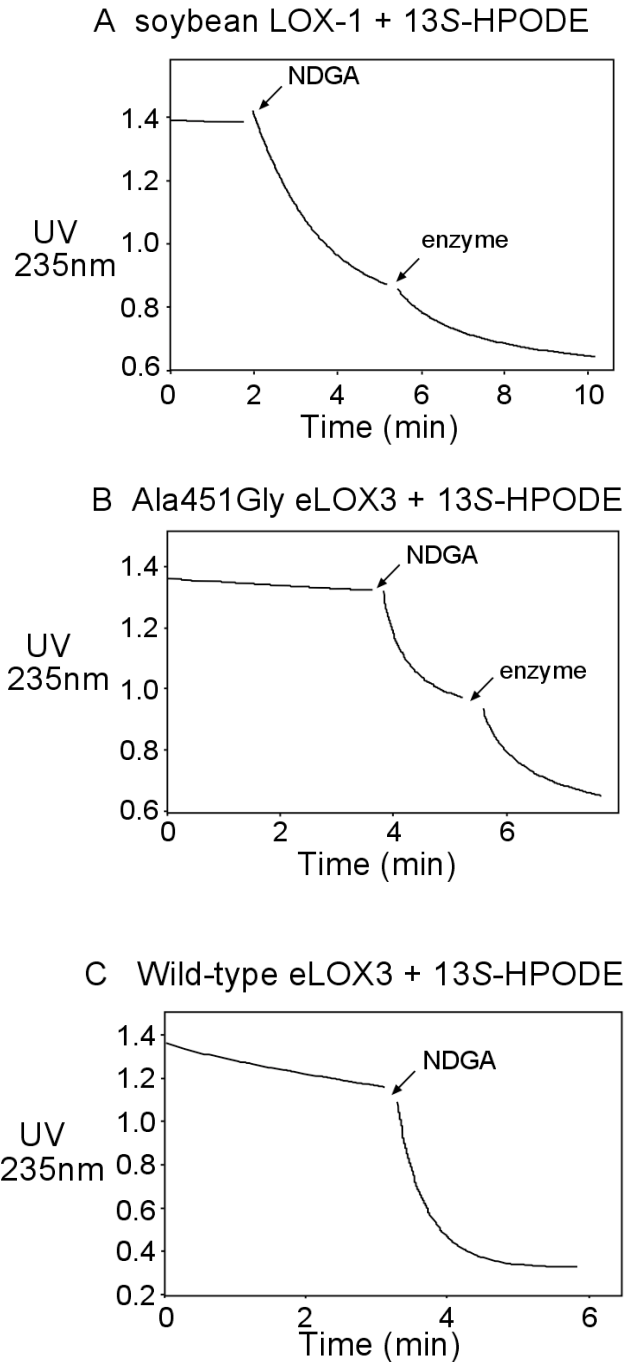
**Figure 33**: Effect of NDGA on the rates of reaction with 13*S*-HPODE. NDGA (20 μM) stimulated the reaction of soybean LOX-1 (0.06 μM panel A), Ala451Gly eLOX3 (0.32 μM, panel B), or wild-type eLOX3 (0.25 μM, panel C) with 13*S*-HPODE (55 μM). The incubations were performed in sodium phosphate buffer pH 7.5 and initiated by addition of enzyme. NDGA was added at the indicated point. For the reaction of Ala451Gly eLOX3 or soybean LOX-1, a second equal aliquot of enzyme was added at the indicated point.

(product III in **Figure 29**, identified by GC-MS in **Figure 34**). Despite this, careful examination revealed that the epoxyallylic hydroperoxides I and II were also present as minor products. On TPP reduction, these two products were converted to the epoxyalcohols Ia and IIa. Importantly, the production of I and II by wild-type eLOX3 was $O_2$-dependent: under anaerobic conditions, I and II were absent and only 13-KODE and epoxyalcohols were produced (**Figure 29F**); in air-saturated buffer, I and II constituted 7% of total products (**Figure 29G**); in $O_2$-saturated buffer, the yield of I and II was increased to 11% (**Figure 29H)**.

Identification of the products in LOX activation by 15S-HPETE

Similarly, soybean LOX-1 or Ala451Gly eLOX3 reacted with 15*S*-HPETE in air-saturated buffer in the presence of NDGA to give a non-specific mixture consisted of mainly epoxyallylic hydroperoxides (**Figure 35A, 35B, Figure 36**). Wild-type eLOX3, on the other hand, gave a specific epoxyalcohol, *threo*-13*R*-hydroxy-14*S*,15*S*-*trans*-epoxyeicosa-5Z,8Z,11Z-trienoic acid followed by 15-KETE (**Figure 35C and ref. (37)**).

Reaction of soybean LOX-1 or Ala451Gly eLOX3 with 13S-HPODE under anaerobic conditions

As already demonstrated for wild-type eLOX3, the conversion of 13*S*-HPODE by wild-type eLOX3 was dramatically accelerated under anaerobic conditions giving exclusively epoxyalcohols and 13-KODE (**Figures 28, 29A and 29F**). I questioned whether the same applies to soybean LOX-1 and Ala451Gly eLOX3. The anaerobic reaction of soybean LOX-1 with 13*S*-HPODE has been extensively investigated (30,31,33) and these findings were confirmed in the present study. The anaerobic
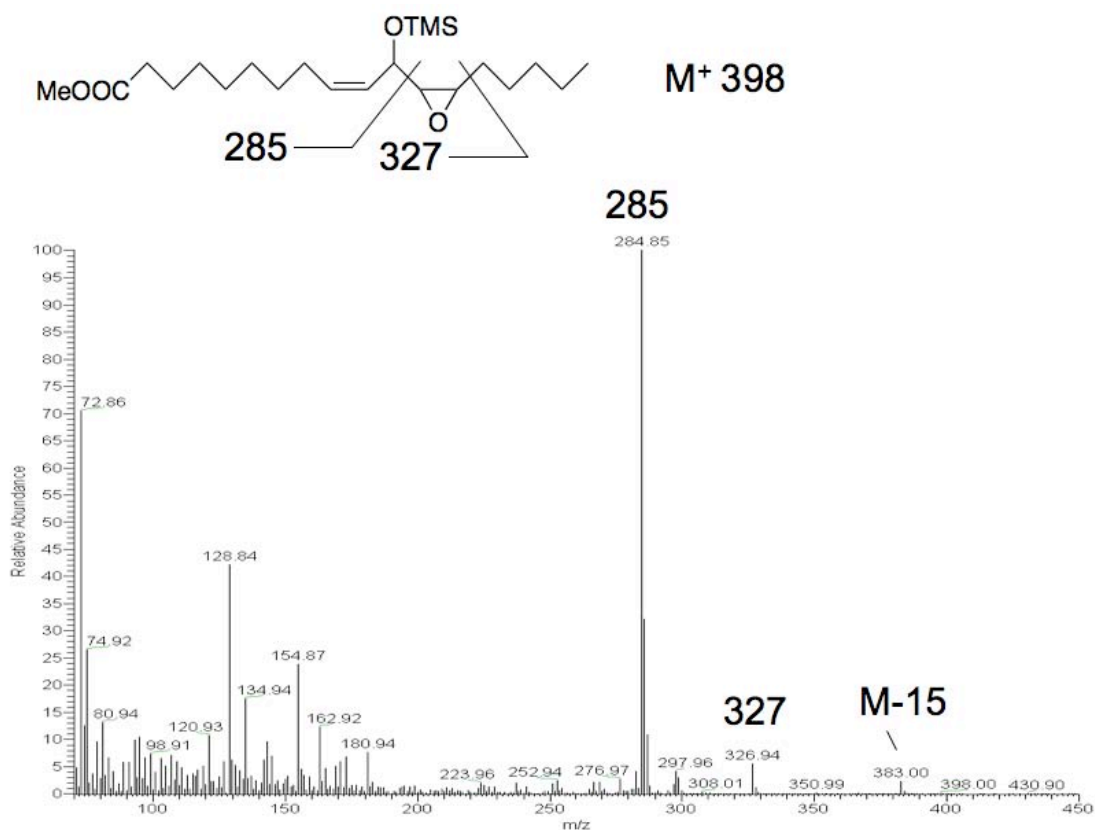
**Figure 34**: GC-MS analysis of the TMS ether methyl ester derivative of the major product (product III in Figure 29) from the reaction of wild-type eLOX3 with 13*S*-HPODE.
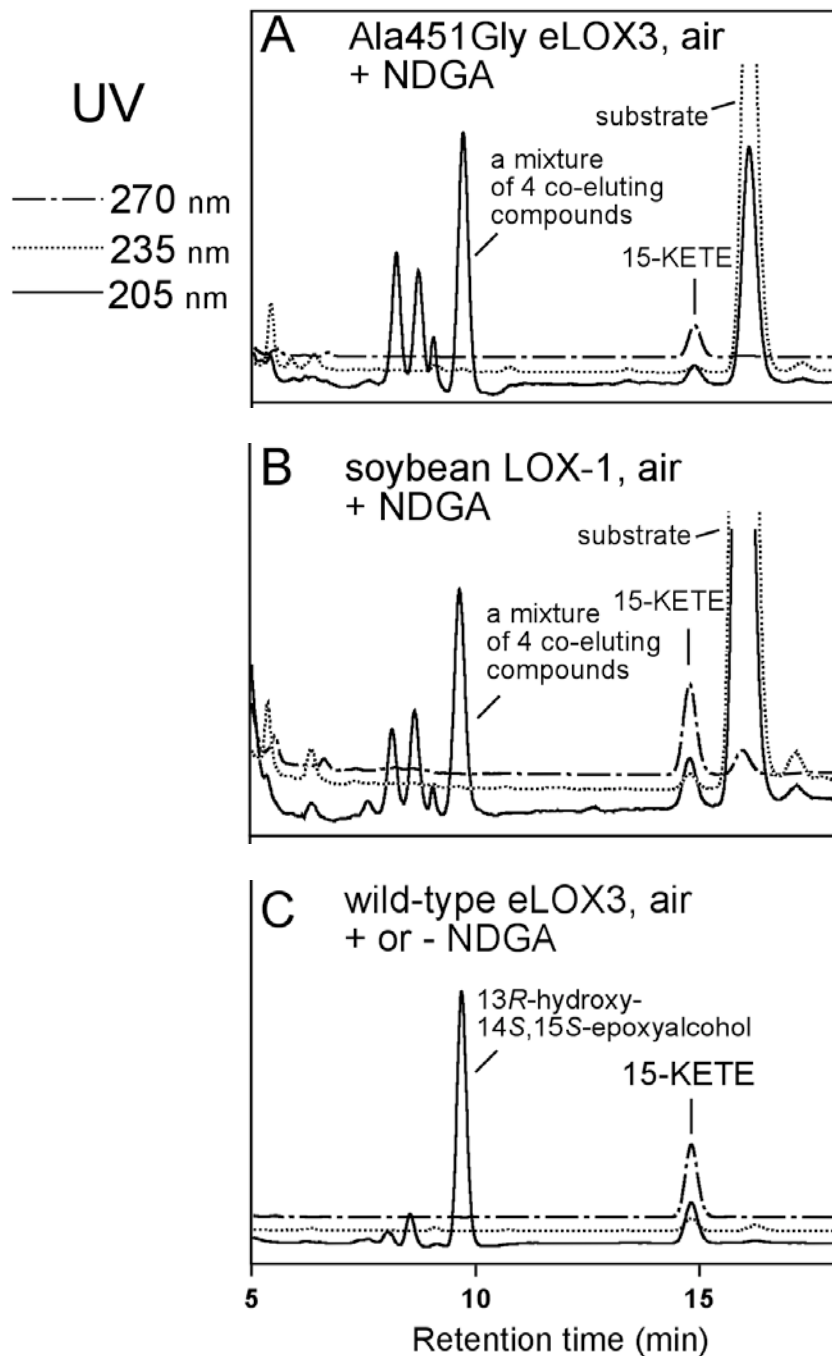
**Figure 35**: RP-HPLC analysis of the products from the reactions with 15*S*-HPETE. Products from reaction of 15*S*-HPETE with Ala451Gly eLOX3 (panel A), soybean LOX-1 (panel B), and wild-type eLOX3 (panel C). RP-HPLC analysis used a Waters Symmetry C18 column (0.46 cm × 25 cm), a flow rate of 1 ml/min and a solvent system of methanol/water/acetic acid (80:20:0.01, by volume).
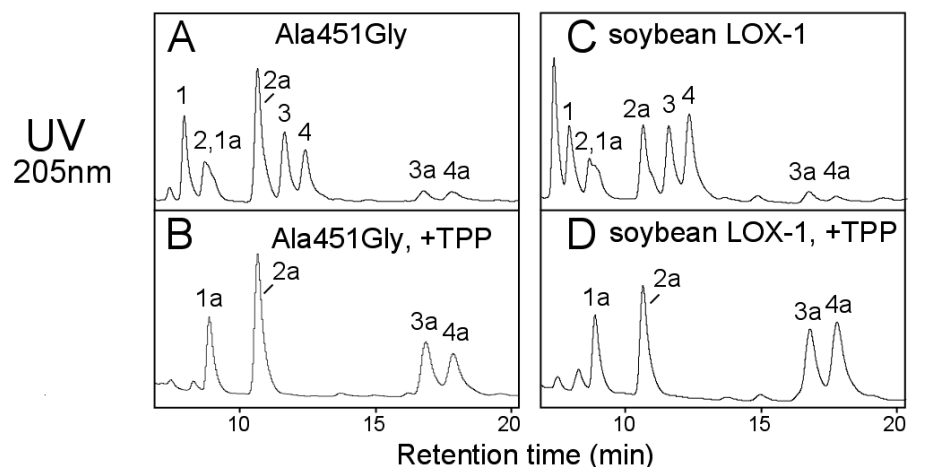
**Figure 36**: SP-HPLC analysis of the products from the aerobic reactions of Ala451Gly eLOX3 and soybean LOX-1 with 15*S*-HPETE before and after TPP reduction. (A) Ala451Gly eLOX3, before TPP reduction. (B) Soybean LOX-1, before TPP reduction. (C) Ala451Gly eLOX3, after TPP reduction. (D) Soybean LOX-1, after TPP reduction. SP-HPLC analysis used a Beckman Silica Ultrasphere column (0.46 cm × 25 cm), a flow rate of 1 ml/min and a solvent system of hexane/isopropyl alcohol/acetic acid (100:2:0.02). The epoxyalcohol products were identified by comparison with authentic standards (140).

conditions afforded only a mild stimulation on the reaction of soybean LOX-1 with 13*S*-HPODE alone (33,137); at sub-micromolar enzyme concentrations, the rate of consumption of 13*S*-HPODE by soybean LOX-1 was negligible even under anaerobic conditions compared to wild-type eLOX3. When further stimulated by linoleic acid or arachidonic acid (which serves as a LOX reducing agent under anaerobic conditions), the reaction yielded not only epoxyalcohols and 13-KODE, but also significant amounts of $C_{13}$ aldehydes and fatty acid dimers.

Although considered later in Discussion, it might be helpful to note at this stage that both the anaerobic and aerobic behavior of soybean LOX-1 and Ala451Gly eLOX3 is consistent with the concept that their reaction with hydroperoxides is often followed by dissociation of the fatty acid radicals produced, leaving the enzyme in the activated ferric state and thus able to oxygenate polyunsaturated substrates, while unable to further react with hydroperoxides.

Consistent with this, we found that Ala451Gly eLOX3 also required a LOX reducing agent in order to react with 13*S*-HPODE under anaerobic conditions (**Figure 37**) and gave products qualitatively similar to those from soybean LOX-1 yet with one notable exception. In addition to epoxyalcohols, 13-KODE, $C_{13}$ aldehydes and fatty acid dimers, the reaction of Ala451Gly eLOX3 with 13*S*-HPODE and arachidonic acid or methyl arachidonate unexpectedly gave considerable amounts of (methyl) HETEs (**Figure 38, Figure 39**, **Figure 40**). These were hydroxy products, not hydroperoxides. The relative amounts of these HETE products (5-HETE + 9-HETE > 15-HETE + 11-HETE > 8-HETE + 12-HETE) were consistent with the preference of this enzyme in
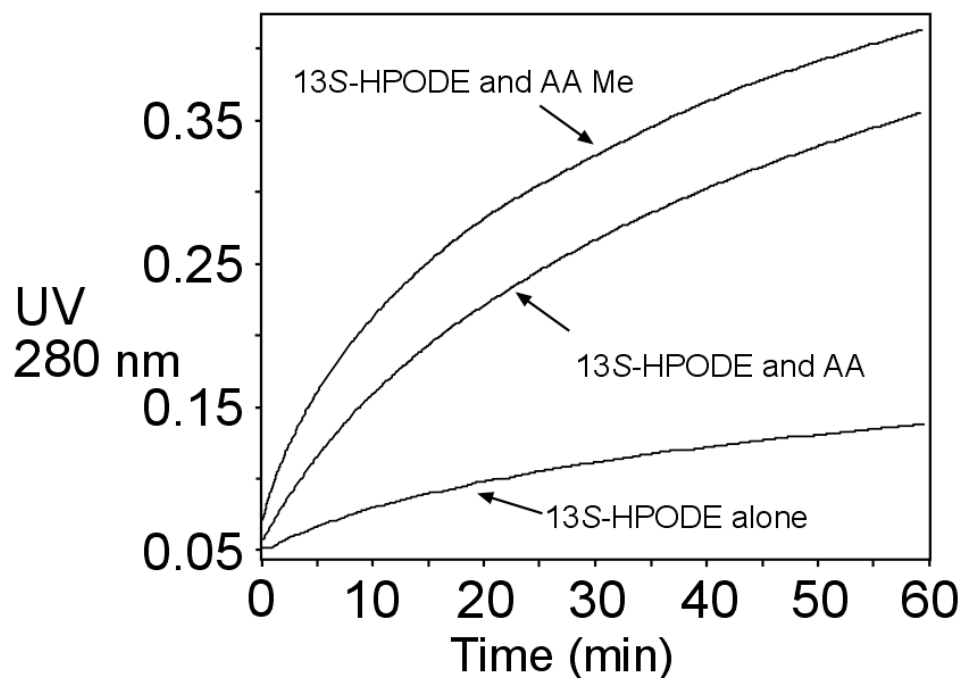
**Figure 37**: Progress curves of the anaerobic reactions of Ala451Gly eLOX3 (0.23 μM) with 13S-HPODE (90 μM). Reactions were conducted in the absence or presence of fatty acids (arachidonic acid or methyl arachidonate, 70 μM) in sodium phosphate buffer pH 7.5, were started by addition of enzyme, and were monitored at 280 nm. The anaerobic conditions are described in the Materials and Methods.
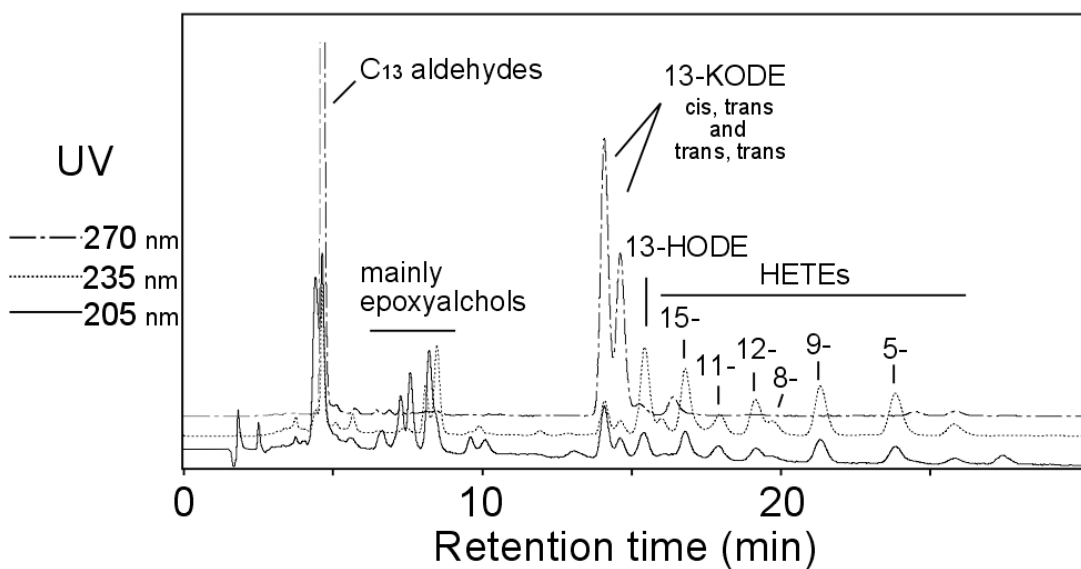
**Figure 38**: RP-HPLC analysis of the monomeric products from the anaerobic reaction of Ala451Gly eLOX3 with 13*S*-HPODE and arachidonic acid. RP-HPLC analysis used a Waters Symmetry C18 column (0.46 cm × 25 cm), a flow rate of 1 ml/min and a solvent system of methanol/water/acetic acid (80:20:0.01, by volume).
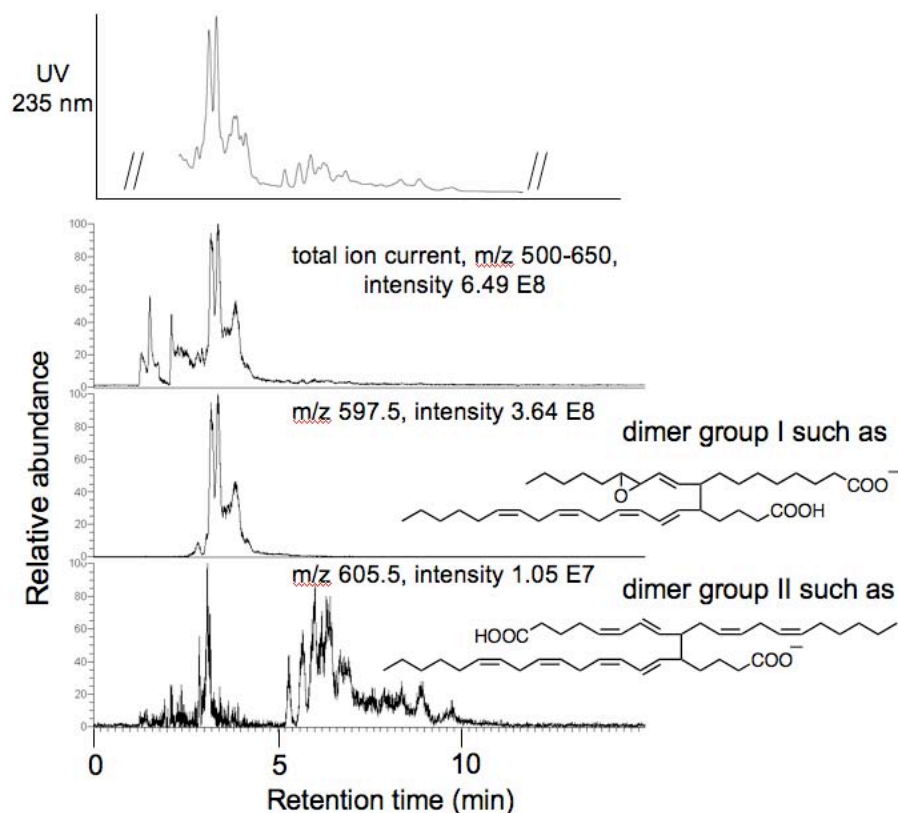
**Figure 39**: RP-HPLC-UV and LC-ESI-MS analysis of the dimer products from the anaerobic reaction of Ala451Gly eLOX3 with 13*S*-HPODE and arachidonic acid. RP-HPLC analysis used a Phenomenex C18 column (2.6 μm, 0.3 cm × 10 cm), a flow rate of 0.3 ml/min and a solvent system of methanol/water (90:10 by volume) containing 10 mM ammonium acetate. MS analysis detected negative ions in the range from m/z 500 to m/z 650. Under these conditions, arachidonic acid eluted at 3.0 min (data not shown).
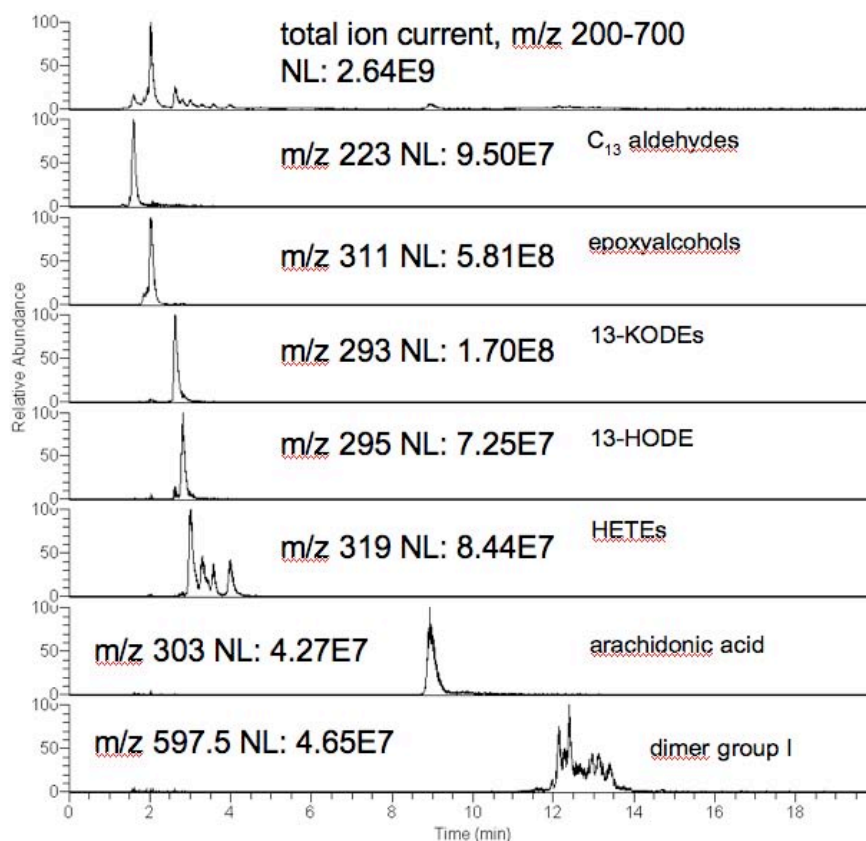
**Figure 40**: LC-ESI-MS analysis of the products from the anaerobic reaction of Ala451Gly eLOX3 with 13*S*-HPODE and arachidonic acid. The RP-HPLC used a Phenomenex C18 column (2.6 μm, 0.3 cm × 10 cm), a flow rate of 0.3 ml/min and initially an isocratic solvent system of methanol/water/ammonium acetate (90:10:10 mM) for 5 minutes followed by a gradient elution from the weak solvent to pure methanol. MS analysis detected negative ions in the range from m/z 200 to m/z 700.

hydrogen abstraction under aerobic conditions (H-7 > H-13 > H-10) (135), pointing to a similar hydrogen abstraction step during this anaerobic HETE synthesis. Incubations with [$^{18}$O]-13$S$-HPODE or in $H_2{}^{18}O$ followed by LC-MS analysis led to the unexpected finding that the hydroxyl of these HETE products was derived exclusively from water (**Figure 41**). The mechanism of formation of these HETE products is considered in the Discussion. As to the leading question, we concluded that for soybean LOX-1 or Ala451Gly eLOX3, epoxyalcohols and ketone are formed from 13$S$-HPODE in better yields anaerobically than aerobically, yet the synthesis of these compounds is prevented by other factors from being the only mechanism in operation. Their formation may be hindered by spontaneous dissociation of the radical intermediates from the enzyme, see Discussion.

As a control, incubation of wild-type eLOX3 with both 13$S$-HPODE and methyl arachidonate under identical anaerobic conditions showed that 13$S$-HPODE was converted to the same set of epoxyalcohols and 13-KODE as in the absence of methyl arachidonate, whereas methyl arachidonate remained unconverted. This can be explained if wild-type eLOX3 reacts with 13$S$-HPODE strictly through the cycling pathway under anaerobic conditions and thus remains in the ferrous state when in the free enzyme form, which is inactive towards methyl arachidonate. Similarly, Ala451Gly eLOX3 failed to metabolize methyl arachidonate when 12$R$-HPETE instead of 13$S$-HPODE was co-incubated under anaerobic conditions. Unlike 13$S$-HPODE, 12$R$-HPETE was converted by Ala451Gly eLOX3 to epoxyalcohol and ketone products (8$R$-hydroxy-11$R$,12$R$-epoxyeicosa-5$Z$,9$E$,14$Z$-trienoic acid and 12-KETE) whether $O_2$ is present or not,
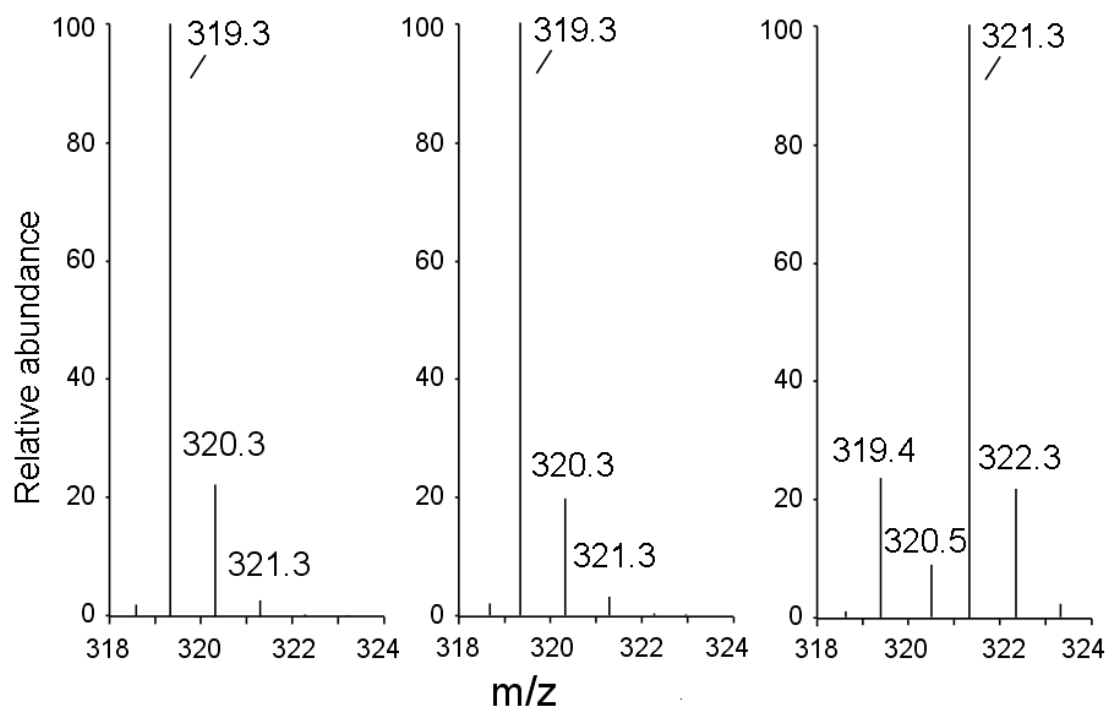
**Figure 41:** Mass spectra of 15-HETE formed in the reaction of Ala451Gly eLOX3 with 13*S*-HPODE and arachidonic acid. **A,** the reaction with [$^{16}$O]-13*S*-HPODE in H$_2$$^{16}$O. **B,** the reaction with [$^{18}$O]-13*S*-HPODE in H$_2$$^{16}$O. **C,** the reaction with [$^{16}$O]-13*S*-HPODE in 83% H$_2$$^{18}$O. The mass spectra were obtained in LC-ESI-MS analysis using a Phenomenex C18 column (2.6 μm, 0.3 cm × 10 cm), a flow rate of 0.3 ml/min and a solvent system of methanol/water (80:20, by volume), containing 10 mM ammonium acetate. MS analysis detected negative ions in the range from m/z 200 to m/z 700.

implying that with 12*R*-HPETE the hydroperoxide isomerase activity of Ala451Gly eLOX3 is dominant. Taken together, these results emphasized the importance of the enzyme shuttling between the two oxidation states during the synergistic conversion of (methyl) arachidonate and 13*S*-HPODE by Ala451Gly eLOX3 or soybean LOX-1.

Reaction of soybean LOX-1 or Ala451Gly eLOX3 with 15S-HPETE under anaerobic conditions

When 15*S*-HPETE alone was used as substrate, significant conversion by either soybean LOX-1 or Ala451Gly eLOX3 did occur under anaerobic conditions. Part of the reason could be that 15*S*-HPETE itself serves as a reducing agent to stimulate the reaction, due to the presence of the C5-C9 and C8-C12 pentadiene systems on the molecule. Strikingly, for both soybean LOX-1 and Ala451Gly eLOX3, the major product (>50% yield) is the single epoxyalcohol *threo*-13*R*-hydroxy-14*S*,15*S*-*trans*-epoxyeicosa-5Z,8Z,11Z-trienoic acid (product IV, **Figure 42A and 42B**), the same molecule as found in the reaction of wild-type eLOX3 with 15*S*-HPETE either aerobically or anaerobically (**Figure 35C and Figure 42C**). **(**The identification of product IV has been described in detail in Ref. (138)). Yet unlike in wild-type eLOX3 reaction, besides the epoxyalcohol and 15-KETE (product V), other products were also present, including $C_{15}$ aldehydes (product I), leukotriene-type 8,15-diols (product II and III), and for soybean LOX-1, two unusual 5,15-diols (138). Thus, for soybean LOX-1 and Ala451Gly eLOX3, anaerobic conditions promoted specific epoxyalcohol synthesis from 15*S*-HPETE, yet the "perfected" epoxyalcohol synthesis as catalyzed by wild-type eLOX3 was still not achieved.
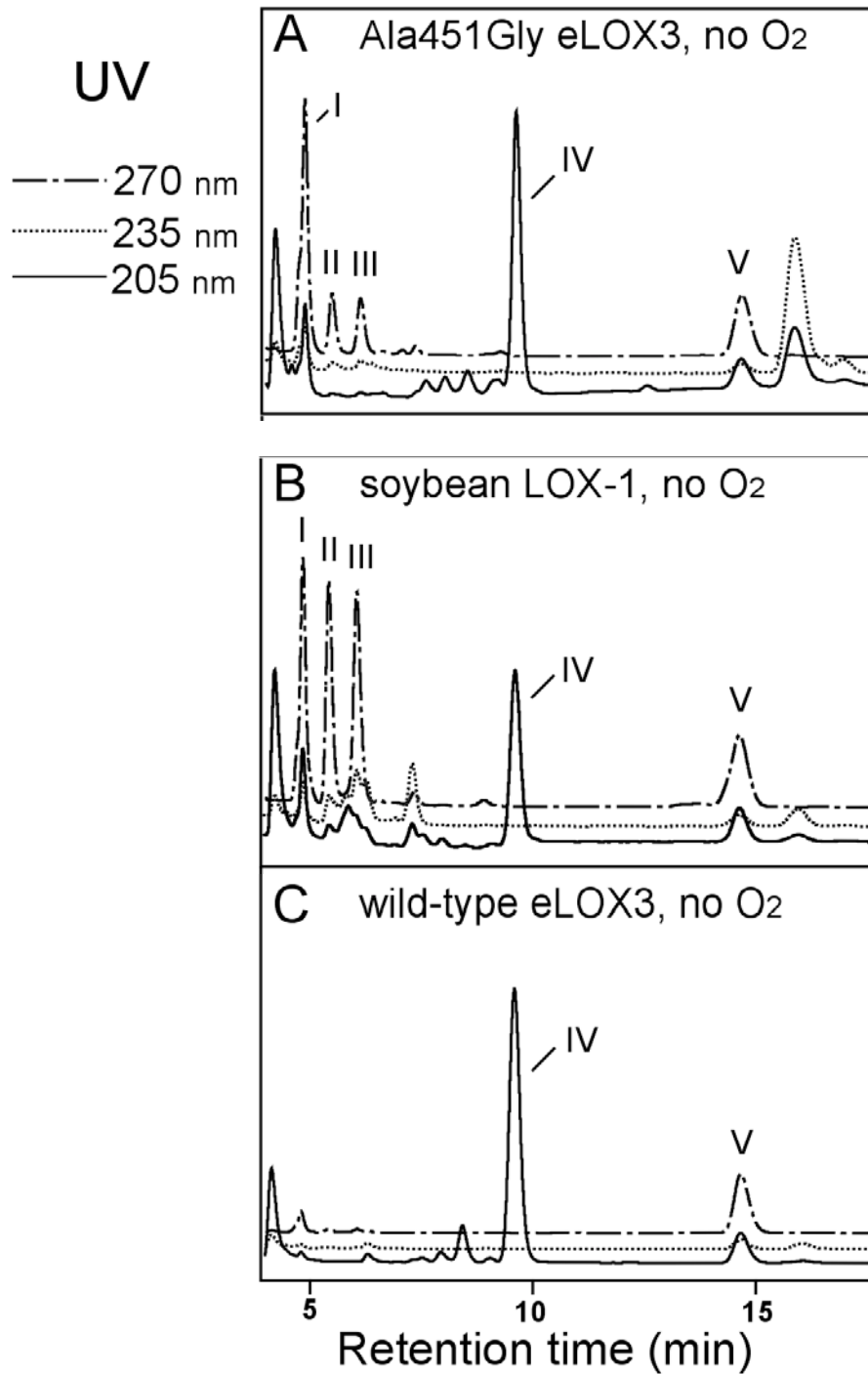
**Figure 42.** RP-HPLC analysis of the products from anaerobic reactions with 15*S*-HPETE. **A**, Ala451Gly eLOX3. **B**, soybean LOX-1. **C**, wild-type eLOX3. RP-HPLC analysis used a Waters Symmetry C18 column (0.46 cm × 25 cm), a flow rate of 1 ml/min and a solvent system of methanol/water/acetic acid (80:20:0.01, by volume).

**Discussion**

In this study, we have demonstrated that $O_2$ is involved in LOX activation, a central piece of evidence being that $O_2$ itself is incorporated into the products from LOX activation. Our study also demonstrates that for eLOX3, the enzyme activation and the hydroperoxide isomerase activity are in competition and are reciprocally regulated by $O_2$. To explain the preponderance of the hydroperoxide isomerase activity over the enzyme activation in eLOX3 under normoxic conditions, we propose a model of limited $O_2$ access in its enzyme active site. For soybean LOX-1, although complexity arises to suggest that the enzyme activation may occur to some extent even under anaerobic conditions, $O_2$ if present will penetrate into the enzyme active site and help maximize the efficiency of enzyme activation. In a context of enzyme evolution, we suggest that restricting $O_2$ access to the enzyme active site is one crucial mechanism that enables eLOX3 to develop the unique hydroperoxide isomerase activity that distinguishes itself from soybean LOX-1 and other typical LOX enzymes.

A chemical model of LOX activation

It has long been recognized that ferrous ion, whether in aqueous solutions, in model complexes or in proteins, readily induces homolytic cleavage of the peroxide bond in an alkyl hydroperoxide to give an alkoxyl radical and a hydroxide, with itself being converted to the ferric ion (38,39,141-143). A PUFA-derived alkoxyl radical usually exists in equilibrium with an epoxyallylic radical and the fate of such an alkoxyl/epoxyallylic radical is usually one of the following: 1) combination of the epoxyallylic radical with other radicals, favored in the presence of an efficient radical

trap; 2) loss of the β-hydrogen from the alkoxyl radical to become a ketone, favored in the presence of a strong oxidant that helps abstract the β-hydrogen; 3) carbon-carbon chain cleavage resulting in an aldehyde and an alkyl radical, favored if a γ double bond exists to help stabilize the alkyl radical fragment (144,145). Despite these complexities, the pioneering work led by Gardner and colleagues suggests that in a simple system such as aqueous ferrous ion, cysteine, and 13$S$-HPODE, the major route of the alkoxyl/epoxyallylic radical under aerobic conditions is the combination of the epoxyallylic radical with $O_2$, an efficient radical trap, followed by hydrogen abstraction to give epoxyallylic hydroperoxides, which, in the cysteine/$Fe^{2+}$ system, will be further converted to epoxyketones (141,146-148).

The mechanism of LOX activation

Based on the above chemical precedence, we suggest for LOX activation a similar mechanism from an alkoxyl radical to the epoxyallylic hydroperoxide products, with $O_2$ playing the central role as a radical trap. Yet it merits attention that the ratio of the two epoxyallylic hydroperoxide products from soybean LOX-1 epimeric at C-9 (28:72, **Figure 29J**) is clearly deviated from the ratio of 50:50 as predicted in the chemical system. We surmise that in LOX activation, the combination of the epoxyallylic radical with $O_2$ occurs largely under the enzymatic control, i.e., within the enzyme active site where oxygen supplies to the two faces of the molecule are often unequal. Once produced, these epoxyallylic peroxyl radicals will then be released into the solution, leaving the enzyme in the activated ferric state and free to react with polyunsaturated fatty acid substrates.

Up to this point, the enzyme activation is complete yet the fate of the epoxyallylic peroxyl radical in the solution is uncertain. It is often suggested in the literature that two such epoxyallylic peroxyl radicals in solution would combine by the Russell mechanism to give epoxyketone, epoxyalcohol and singlet oxygen (143), or that the epoxyallylic peroxyl radical would transfer an oxygen atom to certain susceptible compounds (e.g., to epoxidize a double bond) with itself being converted to an epoxyalcohol (21,149). Although we cannot exclude these possibilities, here we have demonstrated, in agreement with the chemical model, that the major route for an epoxyallylic peroxyl radical in solution is to abstract a hydrogen atom from certain source to become an epoxyallylic hydroperoxide. It might be argued that this could be an artifact brought by NDGA we used in the study to regenerate the enzyme and thus to amplify the reaction, since NDGA is also a free radical scavenger. However, we consider this rather unlikely, because we found in an analogous reaction of *Anabaena* LOX that when a large quantity of purified enzyme instead of NDGA was used, the product pattern of the *Anabaena* LOX activation by 9*R*-HPODE remained largely unchanged (although in this case, the epoxyallylic hydroperoxides were further dehydrated to epoxyketones as in the chemical model, Zheng and Brash, unpublished observations). The chemical transformations involved in LOX activation are summarized in **Scheme 32**.

Is $O_2$ required for LOX activation?

It is natural to ask whether the observed incorporation of $O_2$ into the products is necessary for LOX activation/oxidation. An alternative scenario is that the alkoxyl radical is produced in the enzyme active site and then simply released into the solution resulting in LOX activation. The present study unexpectedly provides two different answers to this

question for the two enzymes, eLOX3 and soybean LOX-1, suggesting variability within the LOX family.

For eLOX3, $O_2$ is required for the enzyme activation, as suggested by three lines of evidence. First, increasing $O_2$ concentration promotes the enzyme activation in the oxygenation of 9*E*,11*Z*,14*Z*-20:3ω6 (**Figure 27**). Second, the anaerobic incubation of eLOX3 with 13*S*-HPODE and methyl arachidonate results in the production of exclusively epoxyalcohols and 13-KODE from 13*S*-HPODE with no conversion of methyl arachidonate, the latter suggesting that the enzyme is never activated to the ferric form under anaerobic conditions. From a different perspective, for eLOX3, the hydroperoxide isomerase activity with 13*S*-HPODE operates at full speed only when the competing enzyme activation pathway is fully suppressed under the anaerobic conditions (**Figure 28**). Third, in sharp contrast to the second point, in the presence of $O_2$, eLOX3 will be activated by 13*S*-HPODE and will then convert (methyl) arachidonate into a mixture of (methyl) HPETEs (135). Given this stringent $O_2$ requirement, we further deduce that the relative low efficiency of eLOX3 activation is a consequence of limited oxygen access in the enzyme active site.

For soybean LOX-1, however, $O_2$ seems only to help maximize the efficiency of enzyme activation. Although the hydroperoxide isomerase activity as indicated by epoxyalcohol and ketone synthesis is indeed promoted by the anaerobic conditions, it is not the only mechanism in operation. That the enzyme activation/oxidation occurs to some extent even in the absence of $O_2$ is suggested by the observations that linoleic or arachidonic acid is converted via the corresponding fatty acid radical to fatty acid dimers in the presence of 13*S*-HPODE under anaerobic condition or that 15*S*-HPETE is

96

converted via either C-7 or C-10 centered radicals to allylic epoxides such as 14,15-LTA$_4$ (**Figure 42B**), both of which have been ascribed to the ferric enzyme form (28,125,138). This O$_2$-independent enzyme activation is best explained if a fraction of the alkoxyl/epoxyallylic radical intermediate is released into the solution, probably due to a low affinity of the enzyme for this radical intermediate, leaving the enzyme in the activated, ferric state. Indeed, some of the released alkoxyl/epoxyallylic radicals are subsequently trapped in fatty acid dimers, which have been shown to form in the solution as opposed to in the enzyme active site (32). Nevertheless, it is beyond doubt that the efficiency of enzyme activation will be maximized under aerobic conditions, when the fatty acid hydroperoxide is efficiently utilized for enzyme activation with minimal conversion to epoxyalcohols and ketones.

The effect of the Ala451Gly mutation on eLOX3 activation

Strikingly, the single amino acid substitution Ala451Gly causes eLOX3 to switch from the hydroperoxide isomerase cycling pathway to the single turnover enzyme activation pathway in the reaction with 13*S*-HPODE or 15*S*-HPETE. The close resemblance of Ala451Gly eLOX3 to soybean LOX-1 in the chemistry of enzyme activation by 13*S*-HPODE or 15*S*-HPETE is evident either under aerobic conditions or under anaerobic conditions. To explain this effect of the Ala451Gly mutation, we have considered two possibilities not mutually exclusive. In the first possibility, this mutation opens up space either directly or indirectly, thereby allowing O$_2$ to react with the epoxyallylic radical intermediate in the enzyme active site. Consistent with this possibility is the finding by Oliw and colleagues that the opposite mutation in the fungal Mn LOX, Gly316Ala, produces the opposite effect, i.e., a switch from dioxygenase to

hydroperoxide isomerase activity (114). Presumably, $O_2$ is barred from reacting with the epoxyallylic radical intermedate when Gly316 is replaced with Ala in Mn LOX.

In the second possibility, the Ala451Gly mutation results in a lower affinity of the enzyme for the alkoxyl/epoxyallylic radical intermediate, which once released will also lead to enzyme activation. This will not be unexpected since this residue lies on the surface of the active site and may be directly involved in the substrate/intermediate/product binding. Consistent with this possibility, the two epoxyallylic hydroperoxide products from 13$S$-HPODE are in a ratio of 42:58 (cf. 28:72 in soybean LOX-1) and thus may derive comparatively more from combination of the epoxyallylic radical with $O_2$ in the solution. Also, as already explained for soybean LOX-1, the formation of dimers containing an epoxyallylic structure in the anaerobic reaction of Ala451Gly eLOX3 with 13$S$-HPODE and arachidonic acid (**Figure 39**) is strong evidence for the occurrence of the alkoxyl/epoxyallylic radical leakage.

It should be emphasized, however, that this switch to the enzyme activation pathway does not apply to every fatty acid hydroperoxide. 12$R$-HPETE, for example, is still predominantly converted to an epoxyalcohol and 12-KETE by Ala451Gly eLOX3. This probably explains why this mutation only partially alleviates the pronounced lag phase exhibited by wild-type eLOX3 in fatty acid oxygenation (**Figure 27** and (135)).

A novel mechanism of HETE synthesis

In this study, the anaerobic reaction of Ala451Gly eLOX3 with 13$S$-HPODE and (methyl) arachidonate unexpectedly gives significant amounts of HETEs. LOX enzymes are known to operate through free radical mechanisms. The free radical nature of this HETE synthesis is also suggested by the product pattern (5-HETE + 9-HETE > 11-HETE

+ 15-HETE > 8-HETE + 12-HETE) that is consistent with the preference of this enzyme in hydrogen atom abstraction (H-7 > H-13 > H-10) (135). Thus, it seems paradoxical that the HETEs generated in a free radical reaction derive the hydroxyl group from water, which is often considered as evidence for an ionic mechanism.

We suspect that what is actually incorporated into the HETE products is the hydroxide ligand of the non-heme ferric iron in the enzyme active site rather than water in the bulk solvent. The hydroxide ligand of the non-heme iron can be conceived as a trapped hydroxyl radical, and its combination with an arachidonate carbon radical to give HETEs seems feasible on chemical grounds. (In fact it mimics the rebound hydroxylation step in the hydroperoxide isomerase cycle producing epoxyalcohols (37).) Notably, for HETE synthesis this mechanism necessitates two molecules of the ferric enzyme to generate one molecule of HETE: the first molecule of ferric enzyme abstracts a hydrogen from arachidonic acid to generate the corresponding carbon radical and then releases it into the solution; this released arachidonic acid radical then fetches the trapped hydroxyl radical from a second molecule of ferric enzyme and becomes the final HETE product. In addition, this mechanism assumes that the hydroxide ligand of the non-heme iron readily exchanges with water in the bulk solvent. It would be of interest to further investigate the mechanism of this unusual HETE synthesis. Also, it remains to be ascertained whether this type of HETE synthesis is unique to Ala451Gly eLOX3 or is general among LOX enzymes. In the anaerobic reaction of soybean LOX-1 with arachidonic acid and 13$S$-HPODE, 15-HETE and 11-HETE were also observed among the minor products, but the origin of the hydroxyl group in these HETE products was not investigated here due to their minute amounts.

Conclusions

In the present study, we have established the role of $O_2$ in LOX activation and elucidated the chemistry involved (**Figure 43**). The key event leading to LOX activation is dissociation of a ferric LOX-radical intermediate complex. $O_2$ facilitates this dissociation and arrests the competing hydroperoxide isomerase cycling pathway by reacting with the epoxyallylic radical intermediate to give an epoxyallylic peroxyl radical, which, due to its limited reactivity within the enzyme active site, will leave the enzyme resulting in enzyme activation.
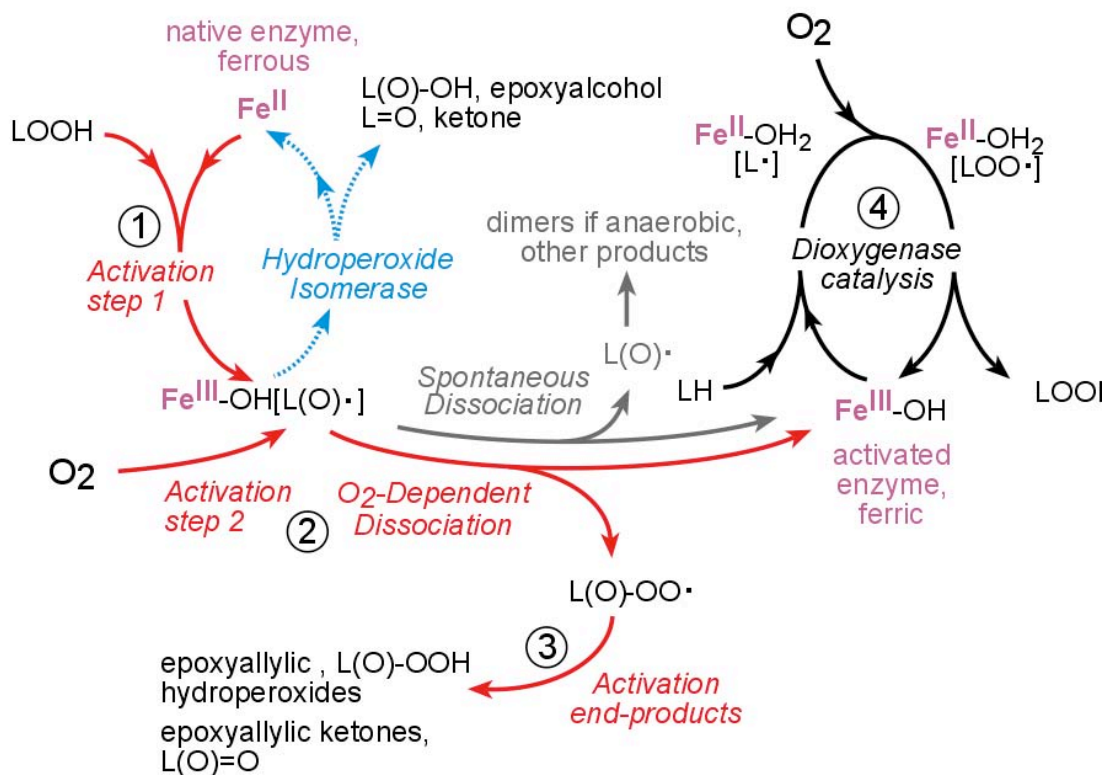


**Figure 43** Proposed model explaining the role of $O_2$ in promoting LOX activation and inhibiting hydroperoxide isomerase activity.

# CHAPTER IV

## ESSENTIAL FATTY ACIDS, 12R-LOX AND ELOX3, AND EPIDERMAL BARRIER FORMATION

### Introduction

In 1929, Burr & Burr famously reported the existence of essential fatty acids (EFA), and noted the most obvious symptom of EFA deficiency as "an abnormal scaly condition of the skin" (49). This phenotype is associated with defects in barrier function and trans-epidermal water loss (51,52), and thus resembles the human genetic disorders of ichthyosis, diseases with a dry, thickened, scaly skin. Linoleate is by far the most abundant EFA in the epidermis, being mainly esterified to the omega hydroxyl of the very long chain FA in two classes of sphingolipids unique to the epidermis, namely acylceramides and acylglucosylceramides. The most abundant subclass of these are esterified omega-hydroxyacyl-sphingosine (EOS) and Gluc-EOS, respectively (Scheme) (150). Acylglucosylceramides are the precursor of acylceramides (75) and a portion of acylceramides will be further converted to ω-hydroxyceramides (mainly omega-hydroxyacyl-sphingosine, OS) that will then be covalently attached to the cross-linked proteins in the cornified cell envelope (CE) (69,70). These covalently bound ω-hydroxyceramides are the main component of the corneocyte lipid envelope (CLE), and together with the underlying CE, constitute a specialized structure indispensable for the integrity of the water barrier (72,150,151).

*ALOX12B* and *ALOXE3* are the only human lipoxygenase genes that, if mutated to inactive forms, will cause a disease (86,100). The disease, autosomal recessive congenitial ichthyosis (ARCI), occurs in response to a defective skin barrier, and exhibits a typical ichthyosiform scaly skin. Because the same phenotype is caused by mutation of either gene, the encoded proteins, 12*R*-lipoxygenase (12*R*-LOX) and epidermal lipoxygenase-3 (eLOX3), are proposed to function in the same pathway during epidermal barrier formation. The recent 12*R*-LOX-/- and eLOX3-/- mouse models confirm their importance in epidermal barrier formation; indeed, deletion of either *alox12b* or *aloxe3* is neonatal lethal, the pups dying of dehydration within hours of birth (89-91). Biochemical studies also suggest that the two enzymes act in tandem: 12*R*-LOX first makes a specific hydroperoxide from a fatty acid substrate, and eLOX3 in turn converts the 12*R*-LOX product into a specific epoxyalcohol (37). The physiological substrate of 12*R*-LOX and eLOX3 in the epidermis, however, remains to be identified. And why does the lack of LOX products lead to an impaired barrier function?

Two further observations led me to propose a model that may explain simultaneously the role of 12*R*-LOX and eLOX3 and the role of EFA in the epidermis. In essential fatty acid deficient epidermis, where the linoleate moiety of acylceramides and acylglucosylceramides is replaced by oleate, the covalently bound ω-ceramides are significantly decreased (78). In 12*R*-LOX-/- mouse epidermis, the covalently bound ω-ceramides, as detected by thin layer chromatography, are greatly depleted (89). Putting all this information together, I propose that the two LOX enzymes oxygenate the linoleate esterified in acylglucosylceramdes or acylceramides. I further propose, in turn, that this LOX-catalyzed oxygenation is required to facilitate hydrolysis of the (oxidized) linoleate

102

moiety and leave free the very long chain FA omega hydroxyl for coupling to the CE proteins. To test this hypothesis, I first examined the proposed reactions *in vitro*, then looked for LOX metabolites in both pig and mouse epidermis, and finally with the aid of a 12*R*-LOX-/- mouse model, evaluated the impact of the putative 12*R*-LOX-eLOX3 pathway on the profiles of both free and covalently bound ceramides, and on the CLE structure in the stratum corneum of mouse epidermis.

## Experimental Procedures

Materials

HODE methyl ester standards were synthesized by autoxidation of methyl linoleate (NuChek Prep Inc.) followed by triphenylphosphine reduction and HPLC purification. HODE free acid standards were generated by alkaline hydrolysis of the corresponding methyl esters or by reacting soybean LOX-1 (Sigma-Aldrich) or *Anabaena* LOX (16) with linoleic acid (NuChek Prep Inc.). Epoxyalcohol standards were synthesized by reacting hematin with 9*S*-HPODE. 4-Hydroxy-TEMPO and CHAPS were purchased from Sigma-Aldrich. Generation of 12*R*-LOX-deficient mice via N-ethyl-N-nitrosourea mutagenesis has been described previously (91). Human 12*R*-LOX and human eLOX3 were expressed and purified as described previously (14).

Preparation of epidermis

Sections of pig skin (ca. 10 cm × 10 cm) were immersed in 65 °C water for 2 min, and then the epidermis was separated from the dermis using a razor blade. Mouse epidermis was isolated after treating the skin with 1.5 mg/ml Dispase II (Roche) in phosphate buffered saline at 4°C overnight.

Lipid extraction

The epidermis was homogenized in chloroform-methanol mixtures (1:1 and 2:1, v/v). The organic layer was separated from the protein pellet by centrifugation. This was repeated four times. The lipids were extracted by the Bligh and Dyer method (152). The lipid extract was dried using a rotary evaporator or under a stream of $N_2$ and then redissolved in chloroform-hexane (1:1, v/v). The lipid extract was then loaded onto a pre-equilibrated solid phase silica column (Bond Elut, Varian, Inc.), washed with chloroform-hexane (1:1, v/v), and eluted with chloroform and chloroform-methanol (2:1, v/v).

Recovery of ester-linked protein-bound lipids

After removal of free (and reversibly bound) lipids, protein pellets were incubated in 1M KOH in 95% methanol at room temperature overnight. The methanolic layer was removed after centrifugation, neutralized with 1N HCl, and then extracted by the Bligh & Dyer method. The protein pellet was washed by chloroform-methanol (1:1, v/v), which was then extracted by the Bligh & Dyer method. The organic phases were combined, dried, and redissolved in the LC solvent.

Isolation of glucosyl-Cer[EOS] and Cer[EOS] from pig epidermis

Glucosyl-Cer[EOS] and Cer[EOS] were isolated from the lipid extract by SP-HPLC with APCI-MS detection (153). SP-HPLC used a Waters 2695 pump, a Beckman Silica Ultrasphere column (5 μm, 10 mm × 25 cm), a gradient program from chloroform to chloroform-isopropanol (1:1, v/v) in 15 min, and a flow rate of 5 ml/min. An Upchurch Scientific TEE was used to split the flow between the fraction collector and the mass spectrometer, a Finnigan LCQ deca XP or a Finnigan LTQ instrument (Thermo Electron). The APCI vaporizer temperature was set to 500 °C and the capillary

temperature to 150 °C. The spectra were obtained in full scan mode monitoring positive ions between m/z 400 and m/z 1500.

**Reaction of 12*R*-LOX and eLOX3 with glucosyl-Cer[EOS] or Cer[EOS].**

Isolated glucosyl-Cer[EOS] (final concentration: 60 μM) or Cer[EOS] (final concentration: 40 μM), together with the antioxidant 4-hydroxy-TEMPO (final concentration: 1 mM), was taken to dryness under a stream of $N_2$. The lipids were dispersed in 2 ml of sodium phosphate pH 6.0 with 10 mM CHAPS by sonication on ice and then incubated with 12*R*-LOX (final concentration: 5 μM) at room temperature for 2 h. To study the reaction of eLOX3, HPLC-purified 12*R*-LOX products (final concentration: 10-15 μM) were dispersed in 1 ml of sodium phosphate pH 6.0 with 10 mM CHAPS by sonication on ice, and then incubated with eLOX3 (final concentration: 5 μM) at room temperature for 2h. Both 12*R*-LOX and eLOX3 products were extracted by the Bligh and Dyer method.

HPLC-UV and LC-MS analysis of 12*R*-LOX and eLOX3 reactions

All HPLC-UV analyses used an Agilent 1100 or 1200 system with diode array detection. Reactions with glucosyl-Cer[EOS] were analyzed by RP-HPLC-UV analysis using a Zorbax Eclipase XDB-C8 column (5 μm, 4.6 mm × 15 cm), an isocratic solvent system of methanol/hexane (10:1, v/v) for 12*R*-LOX reaction or methanol/water (100:2, v/v) for eLOX3 reaction, and a flow rate of 1 ml/min. For reactions with Cer[EOS], we used SP-HPLC analysis instead, as described in the next section. Prior to LC-MS analysis, 12*R*-LOX products were reduced with excess triphenylphosphine, because hydroperoxides were not stable under the used APCI conditions. LC-MS analysis used

the same chromatography conditions as the corresponding HPLC-UV analysis, and the same APCI-MS conditions as described above.

<u>HPLC-UV and LC-MS analysis of epidermal ceramides</u>

SP-HPLC-UV analysis used a Beckman Silica Ultrasphere column (5 μm, 4.6 mm × 25 cm), a solvent system of hexane/isopropanol/acetic acid (90:10:0.1, v/v/v), and a flow rate of 1 ml/min. LC-MS analysis used the same chromatography conditions. For MS analysis of free and reversibly protein-bound ceramides, we used the same APCI conditions as described above. For analysis of ester-linked protein-bound ω-hydroxyceramides, the APCI vaporizer temperature was set to 275 °C and the capillary temperature to 250 °C.

<u>Transesterification of oxygenated acyl(glucosyl)ceramides and HPLC-UV analysis of the methyl esters</u>

HPLC-purified samples were incubated with 0.16 M sodium methoxide in chloroform-methanol (2:1, v/v) at room temperature for 1h. After the reaction, the mixture was acidified by 1M $KH_2PO_4$ and the organic phase was washed with water before being dried and redissolved in the HPLC solvent. SP-HPLC-UV analysis of HODE methyl esters used a Beckman Silica Ultrasphere column (5 μm, 4.6 mm × 25 cm), a solvent system of hexane/isopropanol (100:2, v/v), and a flow rate of 1 ml/min. Chiral HPLC-UV analysis of HODE methyl esters used a solvent system of hexane/methanol/ethanol (100:5:5, v/v/v), with either a Chiralpak AD column (5 μm, 4.6 mm × 25 cm) eluted at 1 ml/min, or a Chiralpak AD column (5 μm, 2.1 mm × 15 cm) eluted at 0.2 ml/min. SP-HPLC-UV analysis of epoxyalcohol methyl esters used a

Beckman Silica Ultrasphere column (5 μm, 4.6 mm × 25 cm), a solvent system of hexane/isopropanol (100:2 or 100:1.5, v/v), and a flow rate of 1 ml/min.

GC-MS analysis

Derivatization and GC-MS analysis of epoxyalchols were performed as described previously (138).

# Results

## 12R-LOX and eLOX3 react with glucosyl-EOS or EOS *in vitro*

The species of glucosyl-EOS purified from pig skin were detected by RP-HPLC with UV absorbance at 205 nm as a series of structural analogues eluting at 7-11 min (**Figure 44a, lower panel**) and by RP-HPLC-APCI-MS with major ions m/z 1175, 1201, 1203, and 1229, corresponding to very long-chain acyl fatty acid components of C30:0, C32:1, C32:0 and C34:1 respectively, as reported (61,154). Incubation with human 12R-LOX at pH 6 led to the formation of a similar pattern of more polar products eluting at 3.5 – 5 min and displaying UV absorbance at 235 nm (**Figure 44a**, upper panel). The UV spectrum of these products was characteristic of conjugated dienes ($\lambda_{max}$ = 235 nm), and was very subtly altered upon triphenylphosphine treatment ($\lambda_{max}$ = 234 nm), consistent with the reduction of the original hydroperoxy product to hydroxy. The pattern of ions of the reduced product on APCI-MS was also very similar to the substrate, except that the major ions were observed at 2 a.m.u. (atomic mass units) lower, at m/z 1173, 1199, 1201,

and 1227 (**Figure 44b**, upper panel); whereas the substrate exhibits major ions at $[M+H]^+$, the hydroxy product readily ionizes with loss of $H_2O$, giving ions corresponding to $[M-H_2O+H]^+$, an apparent loss of 2 a.m.u. compared to the substrate.

To ascertain the position and stereo-configuration of the hydro(pero)xyl group introduced by 12R-LOX in the linoleate moiety, I transesterified the reduced products into hydroxyoctadecadienoate (HODE) methyl esters, which could then be conveniently analyzed by SP-HPLC and chiral-HPLC in comparison with authentic standards. As shown in **Figure 44c**, 9-HODE methyl ester was predominantly formed over 13-HODE methyl ester, and showed almost exclusively the 9R chirality. Thus, the linoleate in glucosyl-EOS was specifically oxygenated by 12R-LOX *in vitro* to the 9R-hydroperoxide (9R-HPODE). Incubations with 12R-LOX using non-glucosylated EOS as substrate were also carried out, and the same 9R-hydroperoxide was produced.

Next, I incubated the 9R-HPODE-glucosyl-EOS produced from the 12R-LOX reaction with eLOX3. RP-HPLC-APCI-MS analysis identified a group of products with retention times shorter than those of the 9R-HPODE-glucosyl-EOS substrate and molecular masses 32 a.m.u. (i.e., the mass of two oxygen atoms) higher than glucosyl-EOS. When transesterified into the methyl esters, these compounds gave rise to a single epoxyalcohol methyl ester as the major product, which was identified by SP-HPLC and GC-MS analysis in comparison with authentic standards (and assuming a 9R configuration) as methyl 13R-hydroxy-9R,10R-epoxyoctadeca-11E-enoate (**Figure 44d and 44e**). In addition, the 9-keto derivative, 9-KODE-glucosyl-EOS, was also formed in the reaction as a minor product. Non-glucosylated 9R-HPODE-EOS reacted similarly with eLOX3. Thus, these results together suggested an *in vitro* pathway in which 12R-

LOX and eLOX3 act in tandem on the linoleate moiety of glucosyl-EOS or EOS with remarkable regio- and stereospecificity to give the 13*R*-hydroxy, 9*R*,10*R*-epoxy derivative (**Figure 44f**).

**Figure 44**

**Figure 44**



c  12R-LOX products, transesterified

SP-HPLC

UV 235 nm

9-HODE

13-HODE

Chiral-HPLC

9(R)-HODE

9(S)-HODE

Retention Time (min)

d  eLOX3 reaction, transesterified

SP-HPLC

9-keto

unreacted 9-HPODE/9-HODE

main product

UV

270 nm

235 nm

205 nm

Retention Time (min)
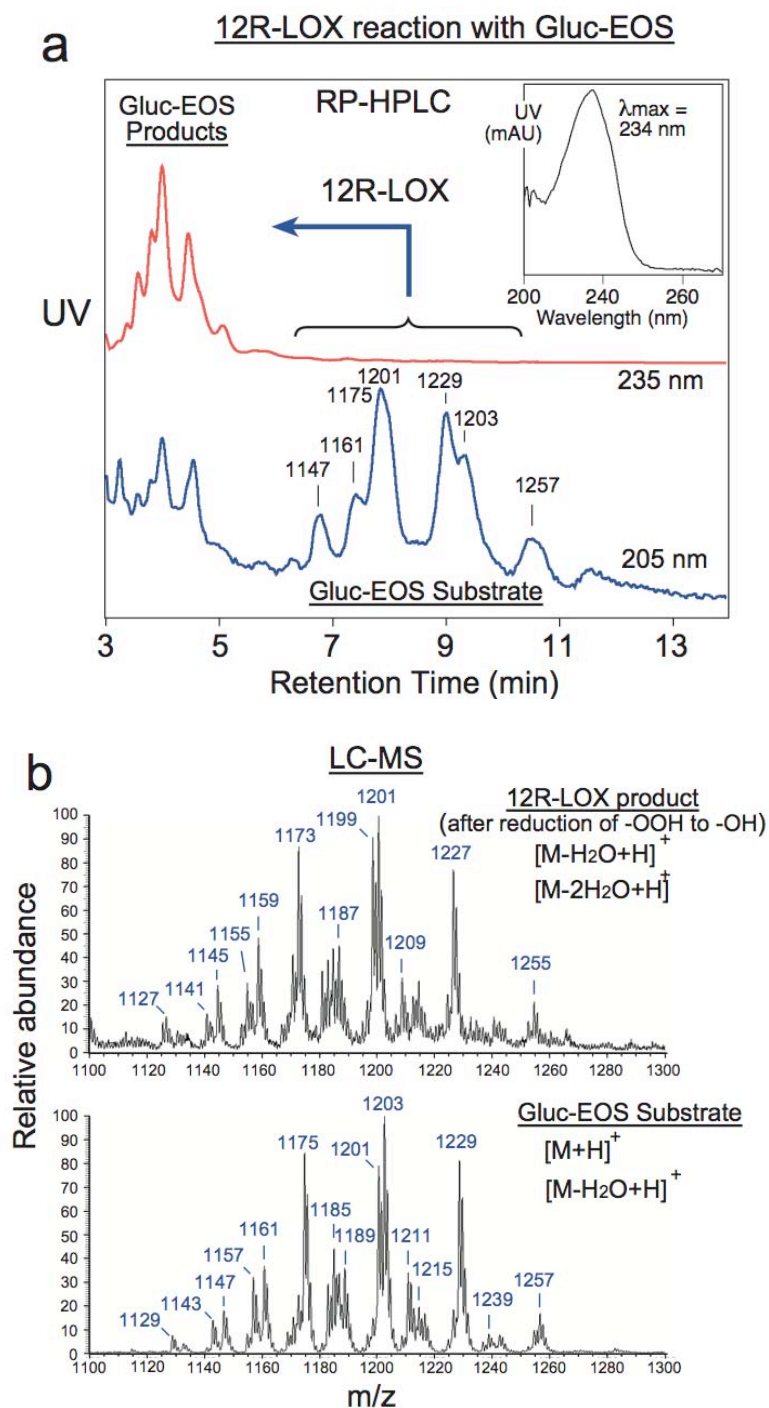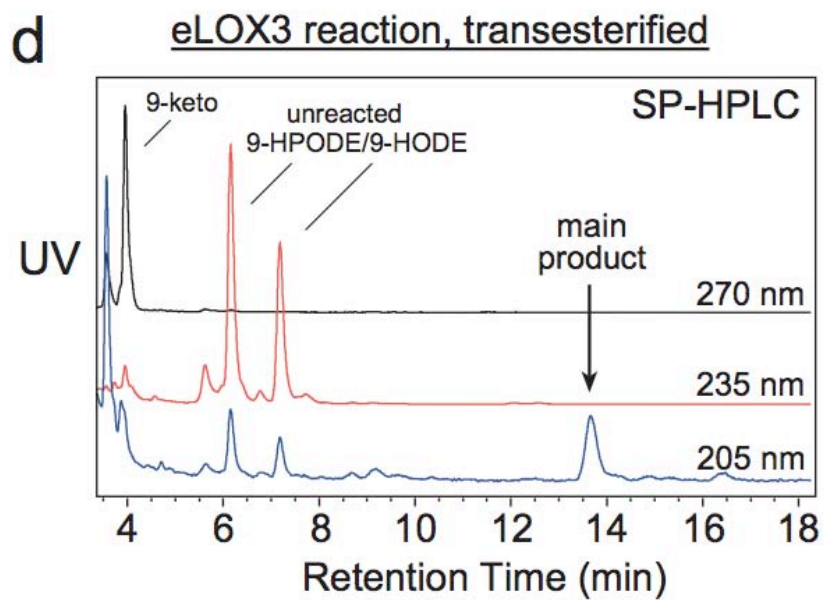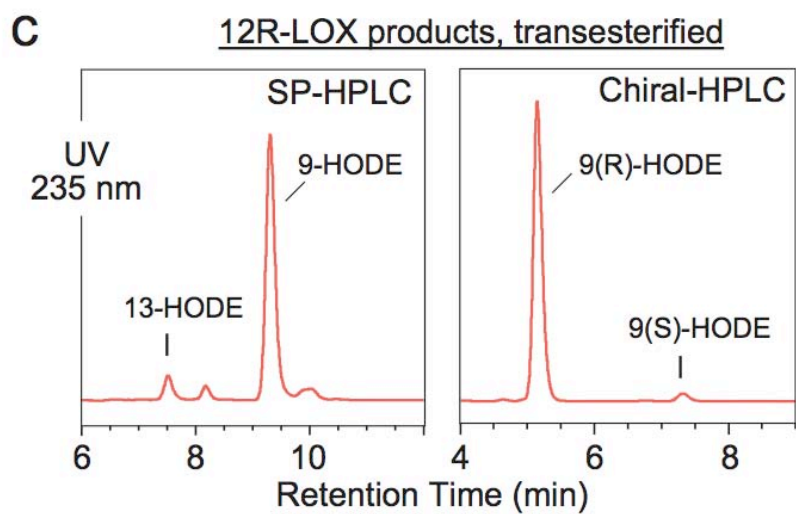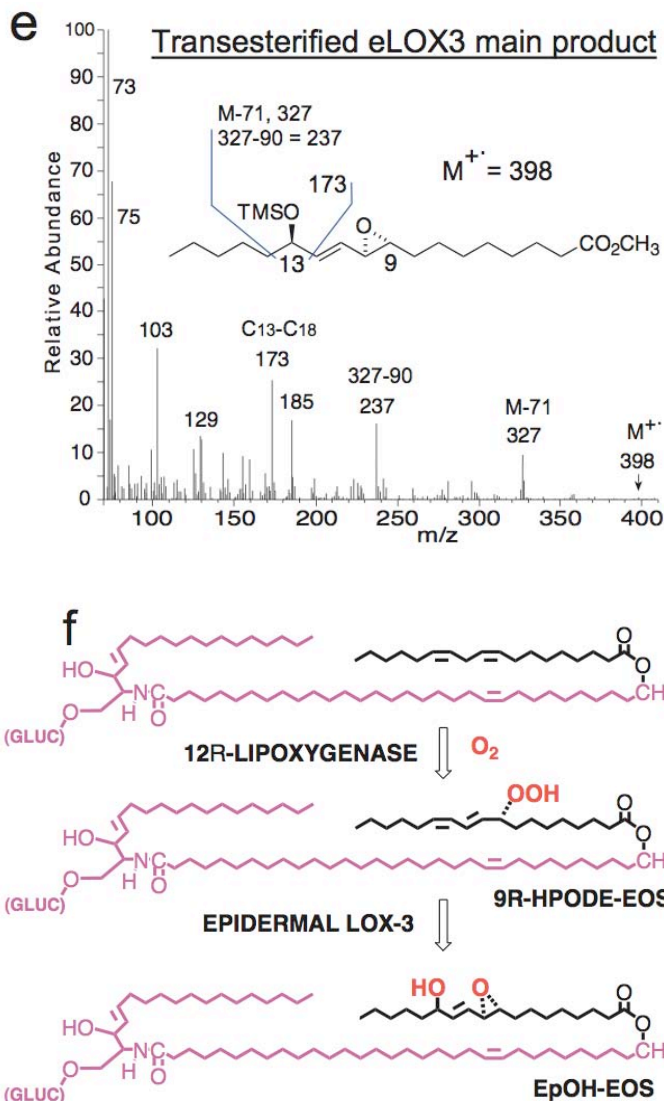
**Figure 44**



**Figure 44:** Reaction of 12*R*-LOX and epidermal LOX-3 with glucosyl-EOS. (**a**) Reversed-phase HPLC analysis of the oxygenation of glucosyl-EOS by 12*R*-LOX. Inset: UV spectrum of the products. (**b**) Combined mass spectra of the substrates (lower) and products (upper). (**c**) SP-HPLC (left panel) and chiral HPLC (right) of the reduced and transesterified 12*R*-LOX products as methyl esters. (**d**) Analysis of the eLOX3 reaction with the hydroperoxy products of the 12*R*-LOX reaction with glucosyl-EOS. (**e**) GC-MS analysis of the main eLOX3 product as the methyl ester trimethylsilyl (TMS) ether derivative. The retention time on GC and the mass spectrum (electron impact, positive ion), in comparison with authentic standards identifies the product as the epoxyalcohol, 9*R*,10*R*-epoxy-13*R*-hydroxy-octadeca-11*E*-enoate. (**f**) Scheme showing reaction of 12*R*-LOX and eLOX3 with glucosyl-EOS.

Occurrence of 12*R*-LOX and eLOX3 metabolites of acylceramides in pig epidermis

Having observed the reaction of 12*R*-LOX and eLOX3 with the acylglucosylceramides *in vitro*, I then went on to search for potential metabolites of the two enzymes *in vivo*, first in pig epidermis. Considering that the LOX metabolites, if present, might exist in minor amounts, I developed a sensitive method for ceramide analysis involving an isocratic SP-HPLC elution followed by either diode array or APCI-MS detection. Using this method, I detected in pig epidermis three groups of novel ceramides with UV spectra and SP-HPLC mobility suggestive of LOX metabolites of the acylceramides EOS (**Figure 45a**). Subsequent LC-MS analysis confirmed that these three groups of compounds were, on the order of elution, keto, hydroxy, and epoxyalcohol derivatives of EOS (abbreviated to KODE-EOS, HODE-EOS, and epOH-EOS respectively). For example, the molecular masses of epOH-EOS differed from those of EOS by +32 amu, corresponding to the two incorporated oxygen atoms in epOH-EOS (**Figure 45b**). Upon transesterification with sodium methoxide, analysis of the methyl esters revealed a specificity reminiscent of the *in vitro* reactions of 12*R*-LOX and eLOX3: predominantly 9-HODE was recovered from the EOS ceramides in pig epidermis, and it was almost purely 9*R* in chirality (**Figure 45c**). Similarly, the single prominent epoxyalcohol recovered from epOH-EOS in pig epidermis was identified in comparison to synthetic standards as 13*R*-hydroxy-9*R*,10*R*-epoxy (making the assumption of the *R* chirality at C-9) (**Figure 45d**), and in KODE-EOS the 9-keto-linoleate was the major species. This remarkable specificity suggested an enzymatic origin of these oxygenated metabolites of EOS, and, as it matches well to the specificity

of 12*R*-LOX and eLOX3 *in vitro,* it also points to a likely involvement of the two LOX enzymes.

**Figure 45**
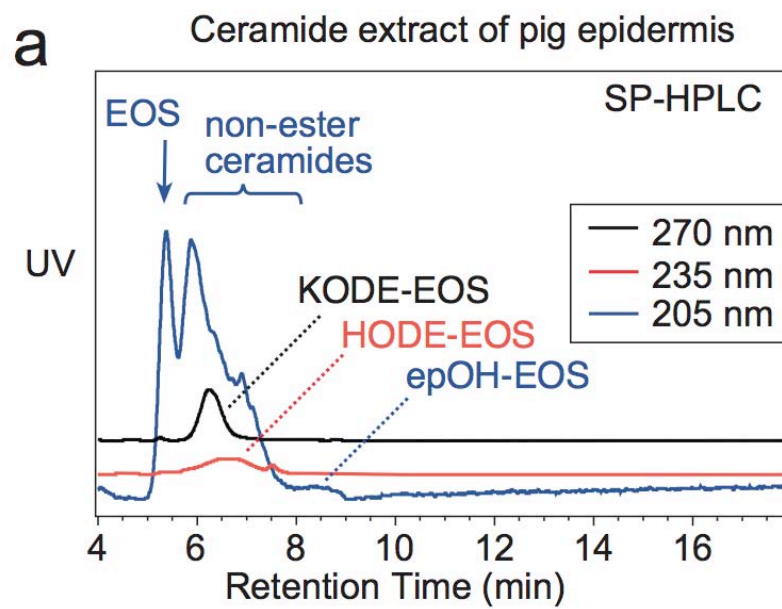
**Figure 45**
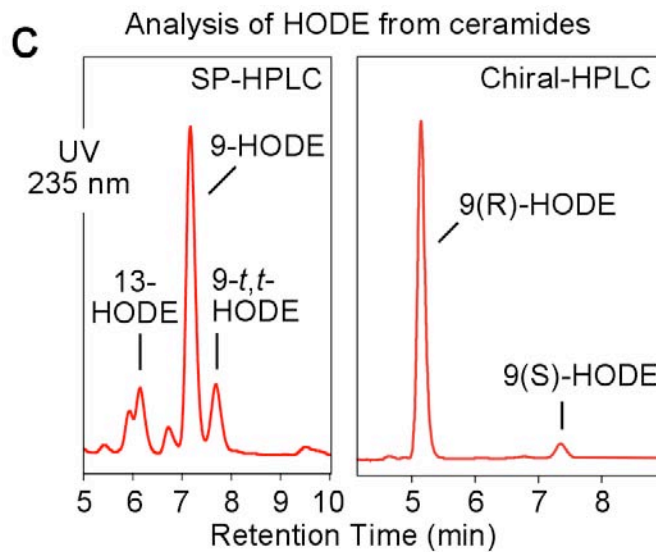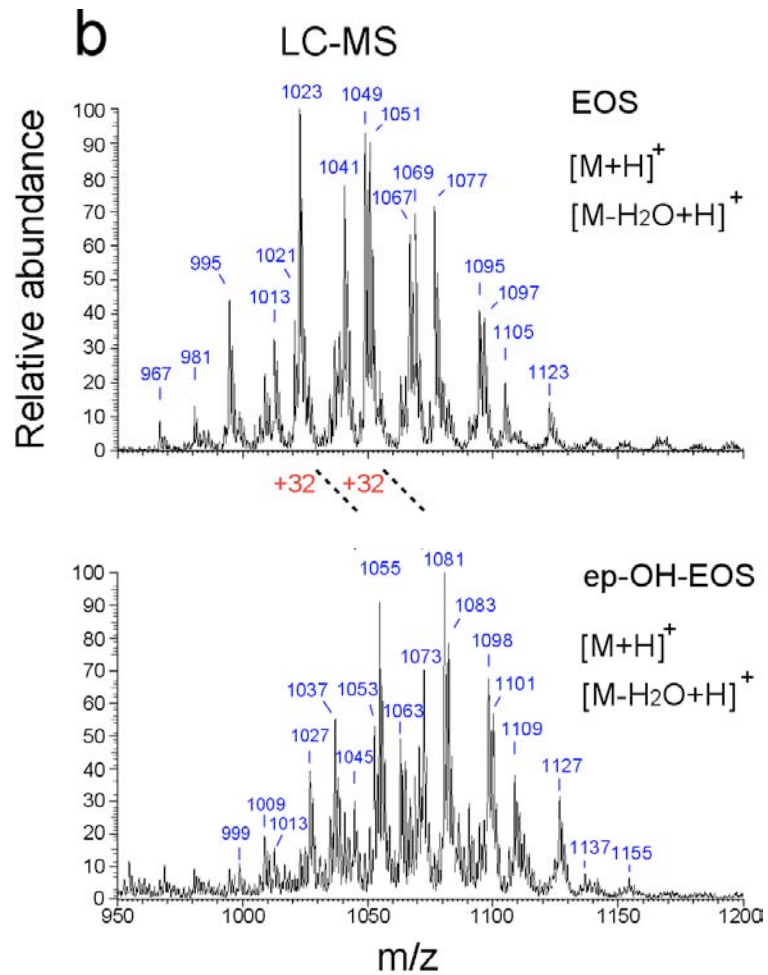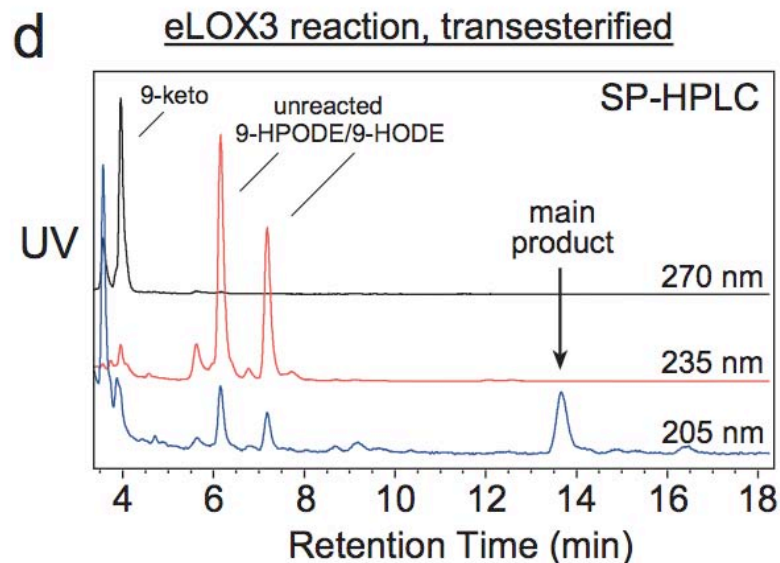
**Figure 45:** Natural occurrence of specifically oxygenated EOS ceramides in pig epidermis. (**a**) SP-HPLC analysis with diode-array UV detection reveals oxygenated species of EOS in pig epidermal extracts. KODE-EOS, containing a keto derivative of linoleate is detected at 270 nm (black trace). HODE-EOS, containing hydroxy-linoleate is detected at 235 nm (red trace). At 205 nm (blue trace), unmodified EOS and other known ceramides elute at 5-7 min, with a later peak of epOH-EOS eluting at 8-9 min. (**b**) Mass spectra of unmodified EOS (top) and epOH-EOS (below). (**c**) Following transesterification of the ceramides from panel **a** to the methyl ester derivatives, SP-HPLC with UV detection at 235nm in comparison to authentic standards identifies the main oxygenated product as 9-hydroxy-linoleate (9-HODE), and chiral HPLC reveals this is predominantly 9*R*-HODE. (**d**) SP-HPLC analysis of the transesterified epOH-EOS peak from panel **a** shows a single peak (top panel) corresponding to 9*R*,10*R*-epoxy-13*R*-hydroxy-octadeca-11*E*-enoate, the first of a mixture of authentic standards (lower panel).

LOX metabolites of acylceramides in mouse epidermis

Using similar analytical approaches, I also analyzed the epidermal ceramides from mouse neonates. As noted by others, the epidermal ceramide composition varies from species to species; not surprisingly, the HPLC profile of the epidermal ceramides

from mouse epidermis was markedly different from that from pig epidermis (cf. **Figure 45a and Figure 46a**).

Comparison of the ceramide profiles from wild-type and 12*R*-LOX-/- mouse epidermis immediately revealed two dramatic differences. First, the level of EOS in 12*R*-LOX-/- mice was at least twice as much as in wild-type mice, whereas other known epidermal ceramides were present at similar or slightly reduced levels in 12*R*-LOX-/- mice. This selective accumulation of EOS in 12*R*-LOX-/- mice is expected if EOS is to be metabolized by 12*R*-LOX and eLOX3 as suggested in our hypothesis. Second, a novel class of ceramides was found in wild type mice but not in 12*R*-LOX-/- mice, and thus was likely to be the metabolites of 12*R*-LOX and/or eLOX3 in mouse epidermis (**Figure 46a**). The UV spectrum of these compounds, although showing λmax at ~230 nm, was clearly distinct from that of HODE-EOS, and similar instead to the UV spectra of authentic standards with an epoxyenone structure (i.e., an epoxide group adjacent to a double bond adjacent to a keto group) (155). On LC-MS, the prominent ions in these compounds had m/z values 30 a.m.u. higher than in EOS, also consistent with an epoxyenone derivative of EOS (**Figure 46b**). To define the precise structure, an HPLC fraction containing these compounds was reduced with sodium borohydride followed by transesterification using sodium methoxide. The methyl esters thus formed consisted of two diastereomers in ~50:50 ratio, identified by SP-HPLC (**Figure 46c**) and GC-MS in comparison to authentic standards as methyl 13*R*-hydroxy-9,10-*trans*-epoxyoctadeca-11*E*-enoate and methyl 13*S*-hydroxy-9,10-*trans*-epoxyoctadeca-11*E*-enoate. Thus, prior to the borohydride reduction these putative LOX metabolites were deduced to be the 13-keto, 9,10-*trans*-epoxy derivative of EOS (**Figure 46d**). I have often observed such

epoxyenone derivatives as a minor product in reactions of eLOX3 with fatty acid hydroperoxides.

Although not as prominent as the epoxyenone-EOS, KODE-EOS and HODE-EOS were also present in wild type mouse epidermis. Whereas KODE-EOS seemed to be a mixture of 9-keto and 13-keto isomers, the remarkable 9R specificity seen both *in vitro* and in pig epidermis recurred in the HODE-EOS isolated from wild-type mouse epidermis. In 12R-LOX-/- mouse epidermis, KODE-EOS and HODE-EOS amounted to less than 25% and 30% respectively of the wild-type level, and HODE-EOS were ~50:50 mixture of 9- and 13 isomers. Due to their relatively small quantities, the stereospecificity of KODE-EOS or HODE-EOS from 12R-LOX-/- mouse epidermis was not analyzed. Their presence in 12R-LOX-/- mouse epidermis might be partly attributed to non-enzymatic oxygenation or to one of the additional LOX enzymes that are detectable in mouse epidermis, none of which, it should be noted, produce the 9R enantiomer of 9-HPODE as product (97).

In addition to the noted differences between wild-type and 12R-LOX-/- mice in the ceramide fraction of the epidermal lipid extract, a difference was also seen in the free (unoxidized and oxidized) fatty acid fraction (**Figure 47**). In wild-type mouse epidermis, HODE free acid existed predominantly as the 9R isomer, whereas in 12R-LOX-/- mouse epidermis, it occurred at ~ 15% of the wild-type level and was a mixture of 13-HODE and 9-HODE in a ratio of ~ 60:40. Since mouse 12R-LOX has been shown to be inactive towards free linoleic acid (97,115), the observed concurrence of 9R-HODE free acid and 12R-LOX activity is best explained by a sequence of events in which linoleic acid is first incorporated into acylceramides such as EOS, then converted by 12R-LOX and a

peroxidase to the 9*R*-HODE derivative, and finally hydrolyzed by an esterase to yield 9*R*-

HODE free acid.

**Figure 46**
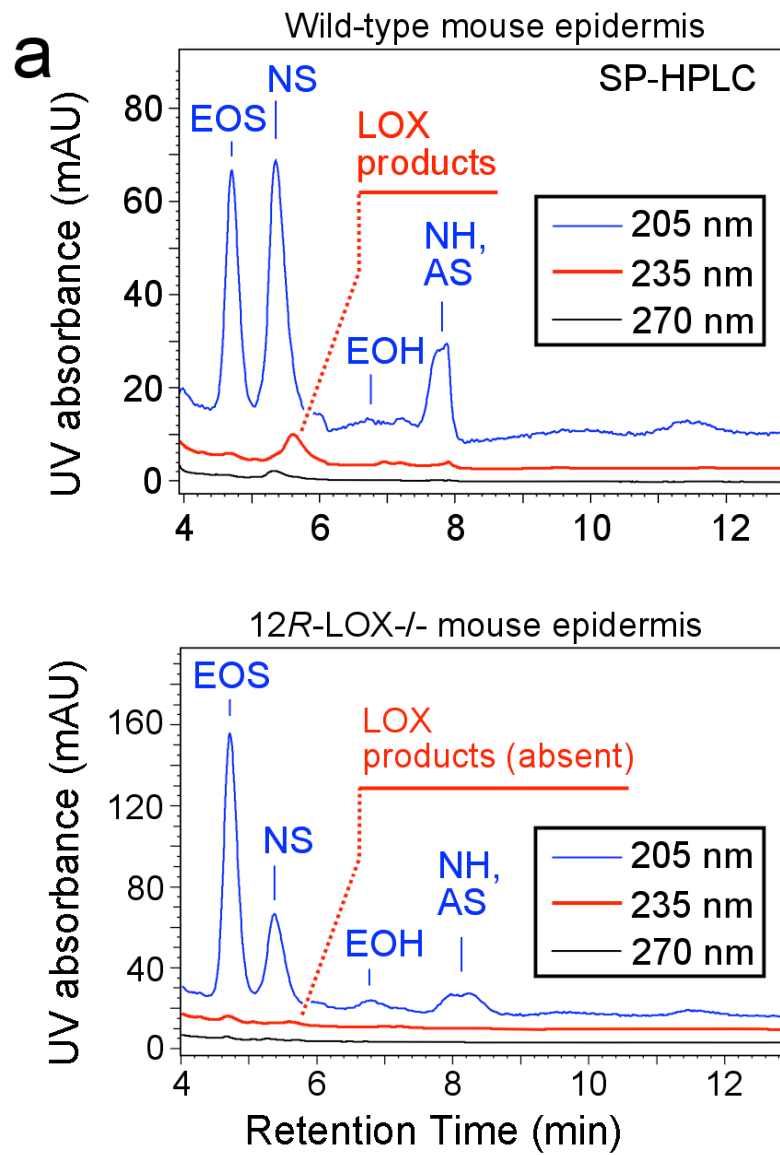
**Figure 46**
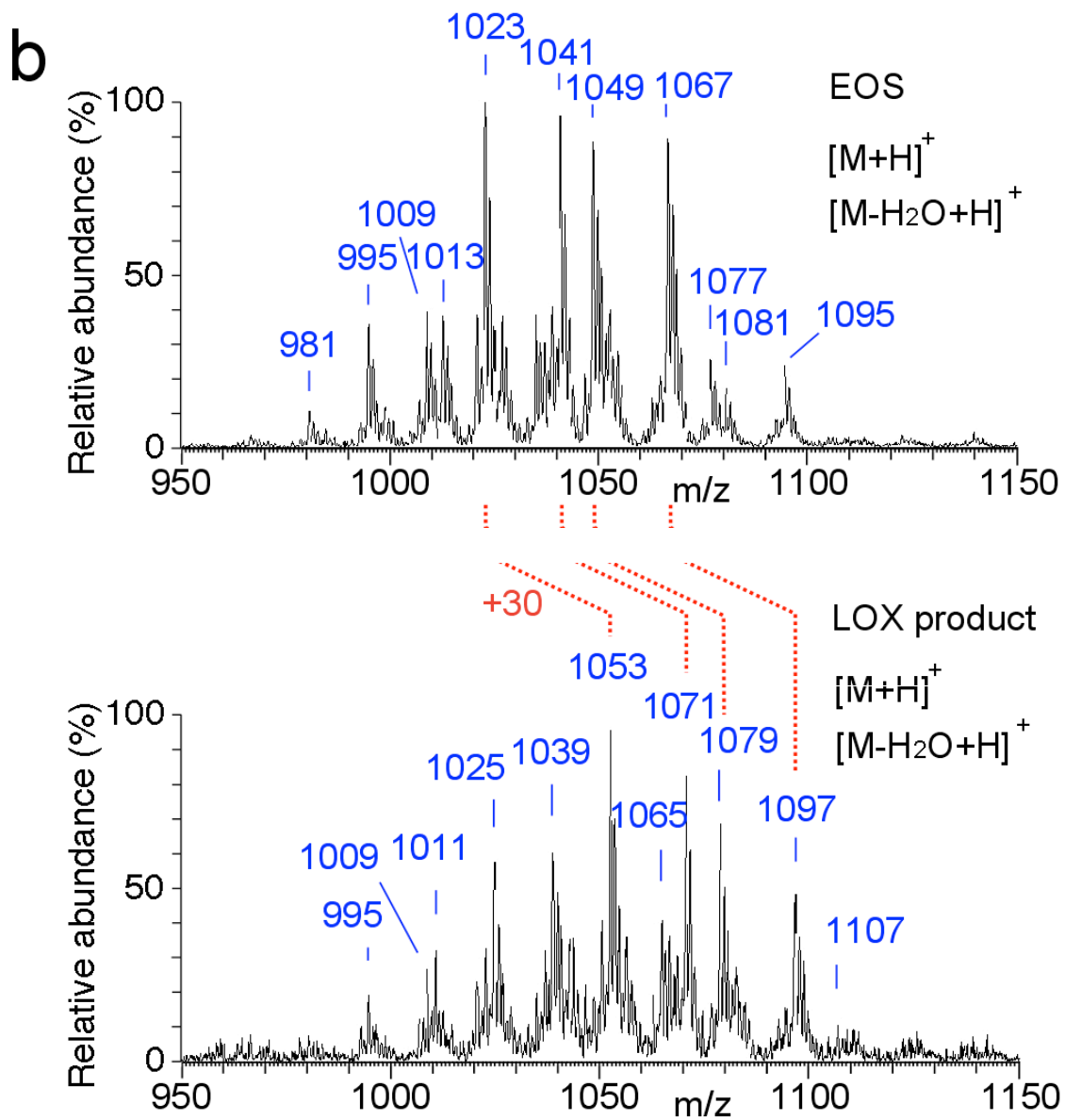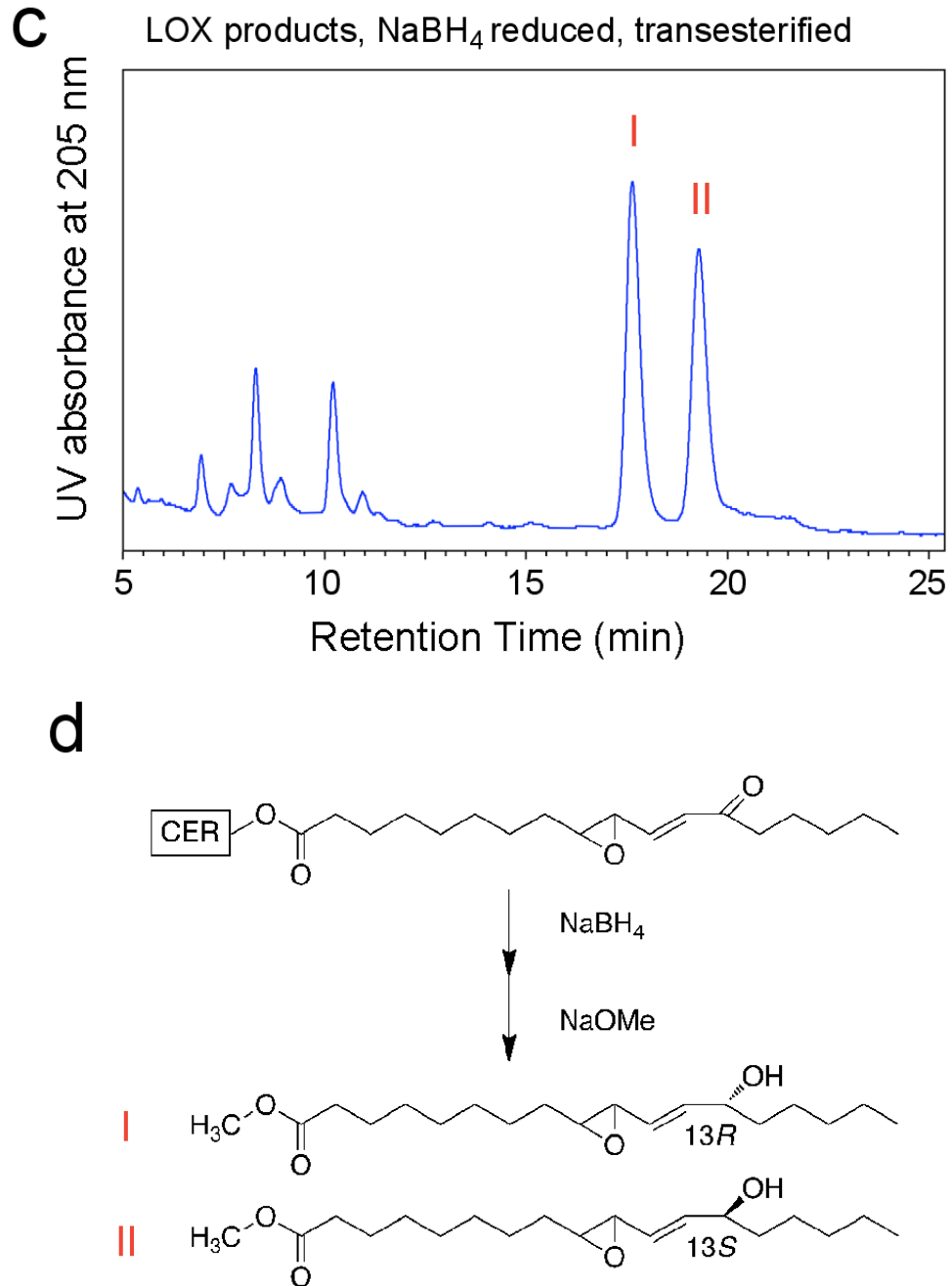
**Figure 46:** Occurrence of LOX metabolites in wild-type mouse epidermis, and absence in 12*R*-LOX-/- mouse epidermis. (**a**) SP-HPLC analysis of ceramides from wild-type (top) and from 12*R*-LOX-/- (bottom) mouse epidermis. (**b**) SP-HPLC-APCI-MS analysis of EOS (top) and LOX product (bottom) from wild-type mouse epidermis. (**c**) SP-HPLC analysis of the methyl esters transesterified from NaBH$_4$-reduced LOX product. (**d**) Scheme of LOX product indentification.
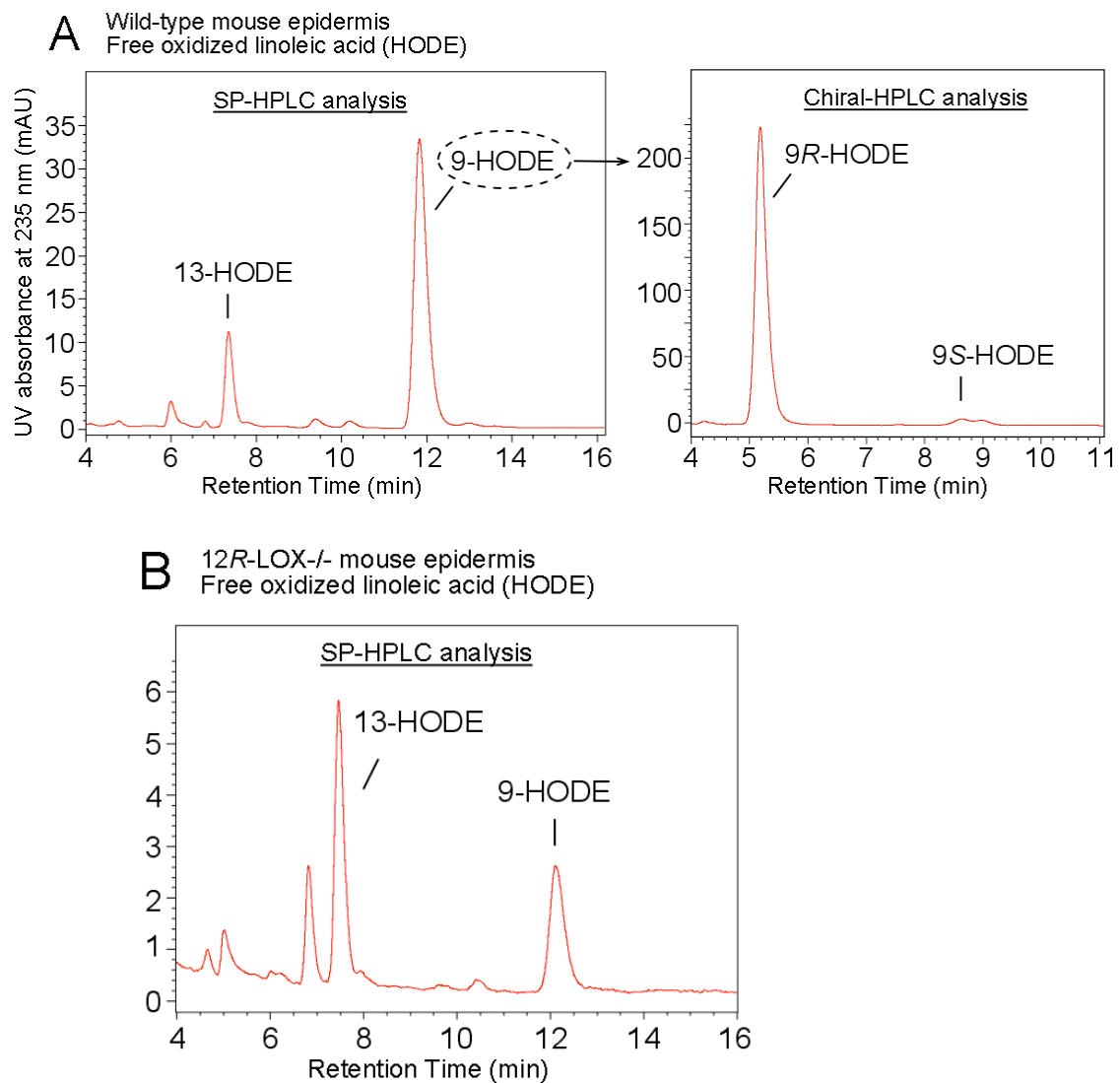
**Figure 47:** Comparison of free oxidized fatty acids from wild-type and 12*R*-LOX-/- mouse epidermis. (**A**) SP- and chiral HPLC analysis of HODE free acid from wild-type mouse epidermis. (**B**) SP-HPLC analysis of HODE free acid from 12*R*-LOX-/- mouse epidermis.

Covalently bound lipids in mouse epidermis

Central to our hypothesis is that the ester-linked protein bound ω-hydroxyceramides and ω-hydroxy VLFA, which constitute the corneocyte lipid envelope, should be reduced in 12$R$-LOX-/- mice. Although this has been indicated by thin layer chromatography in the study by Krieg and colleagues (89), definitive evidence is lacking as the multiple spots on the TLC were not characterized. Therefore, here using LC-MS we analyzed and compared the levels of the ester-linked protein-bound ω-hydroxyceramides and ω-hydroxy VLFA in wild-type and 12$R$-LOX-/- mouse epidermis. These ester-linked lipids were obtained by mild-alkaline hydrolysis of the protein pellet extensively extracted so as to be devoid of any free or reversibly bound lipids (**Figure 48a**). Using SP-HPLC-APCI-MS analysis, we were able to discern two classes of covalently bound ω-hydroxyceramides in wild-type mouse epidermis, namely OS (**Figure 48b, c**) and OH, the latter of which as a minor component has not been previously recognized in mouse epidermis. Using RP-HPLC-ESI-MS analysis, covalently bound ω-hydroxy VLFA was also detected in wild-type mouse epidermis. It is noteworthy that similar to the reversibly bound lipids (*vide infra*), the principal VLFA in these irreversibly ester-linked lipids differed from the composition of the free lipids, the most abundant species being 34:1.

In sharp contrast to wild-type epidermis, the level of covalently bound OS or OH in 12$R$-LOX-/- mice was less than 2% of the wild-type level (**Figure 48d**). Similarly, covalently bound ω-hydroxy VLFA was reduced by more than 100 fold in 12$R$-LOX-/- mice. Consistent with these biochemical results, examination of the stratum corneum by electron microscopy revealed that the CLE was virtually absent in 12$R$-LOX-/- mice

(Results of Debra Crumrine and Peter Elias, UCSF). These results prove unambiguously that 12*R*-LOX and eLOX3 are indispensably involved in the metabolic pathway of EOS that leads to the formation of covalently bound ω-hydroxy-ceramides and ω-hydroxy VLFA. As noted previously (89,91), additional structural abnormalities are evident in the 12*R*-LOX-/- epidermis, including malformed lamellar granules (89), and their relative absence in our samples, indicating either that compensatory responses feedback to early steps in the epidermal barrier formation, or indeed that production of the oxygenated ceramides may be initiated prior to fusion of lamellar granules with the plasma membrane and extrusion of their contents.

**Figure 48**



a

Covalently bound ceramide

OS = Omega-hydroxy-acyl Sphingosine

amide-linked C34:1 fatty acid
exact mass 803.77, M+1  =  m/z 805

b    Mass spectra of OS ceramide species
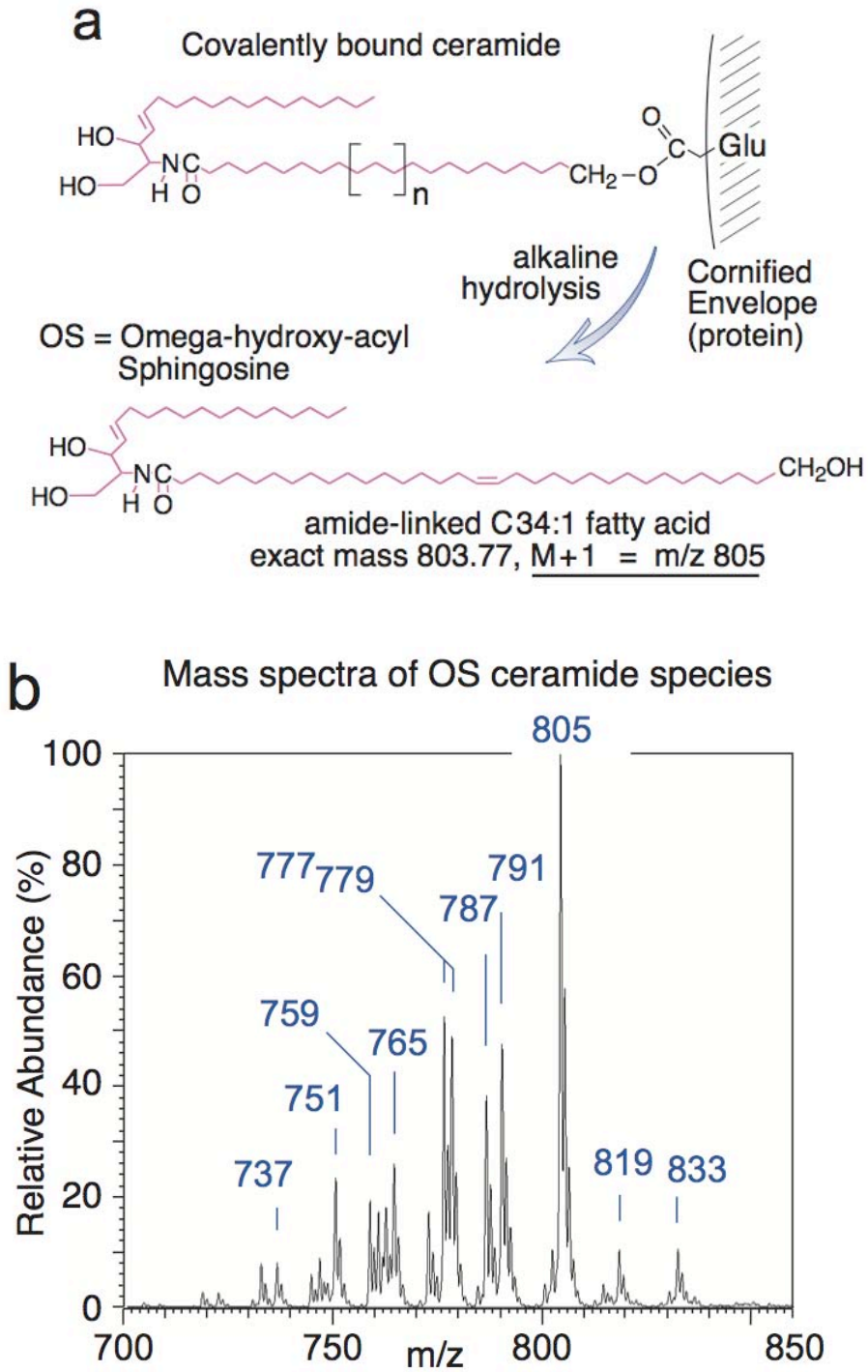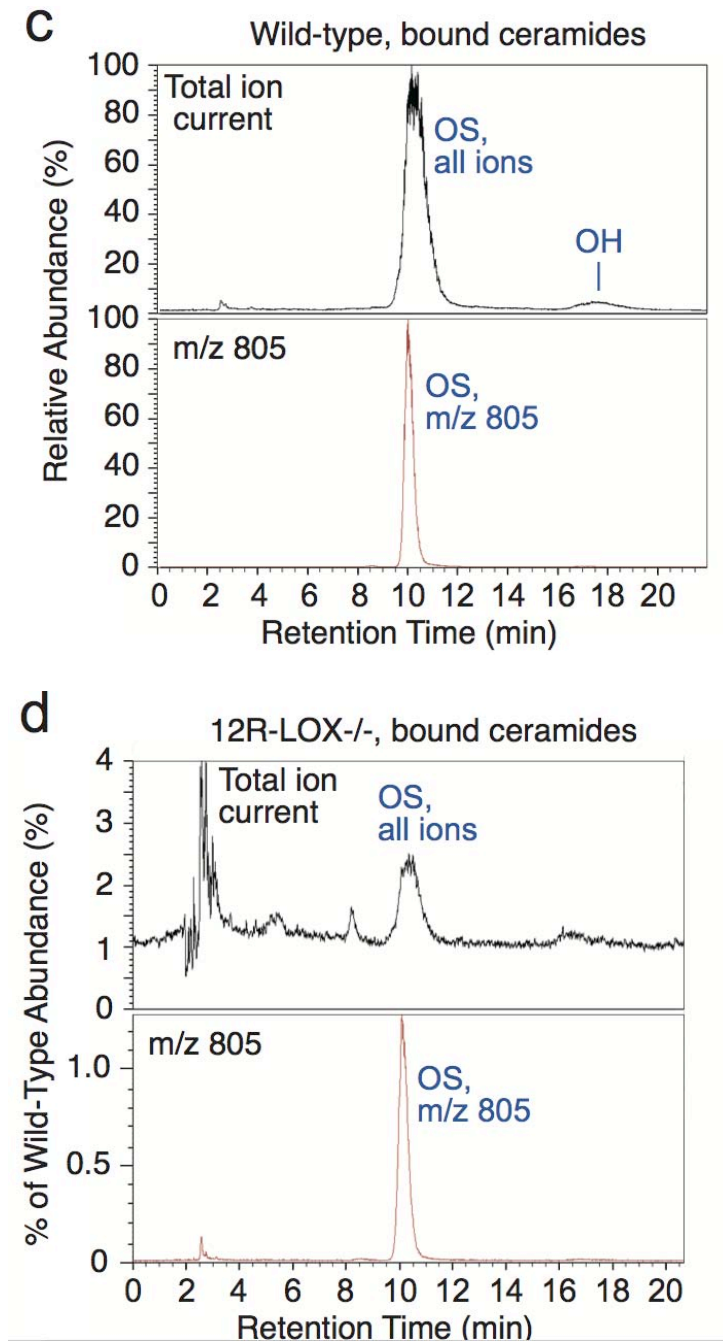
**Figure 48:** Analysis of covalently bound ceramides in mouse skin. (**a**) Protein-bound ceramide species are released by mild alkaline hydrolysis of the ester linkage and identified by LC-MS mainly as OS, omega-hydroxy-acyl sphingosine. (**b**) Combined mass spectra of the OS species from wild-type mouse skin. (**c**) Analysis of bound ceramides from wild-type mouse epidermis showing LC-MS recordings of total ion current (top) and m/z 805, corresponding to the most prominent of the OS species. (**d**) Analysis of bound ceramides from 12*R*-LOX-/- epidermis.

LOX metabolites reversibly coupled to protein in mouse epidermis

A surprising observation was made during our procedures to exhaustively extract the free lipids from mouse epidermis. Following 4-5 cycles of sonication and extraction with chloroform/methanol (1:1 or 2:1) for 1-2 hours at 0 °C, HPLC analysis indicated no further detectable free lipid in the later extracts. However, upon a further soak of the sonicated protein pellet in chloroform/methanol (1:1) at room temperature overnight, a specific pair of SP-HPLC peaks showing the UV absorbance profile of epoxyenone derivatives were evident (denoted as **I** and **II** in **Figure 49**, upper panel). To completely extract this pool of lipids, 6-7 cycles of such prolonged incubations at room temperature were required. Notably, these products were completely absent in the extracts of protein from 12R-LOX-/- mice (**Figure 49, lower panel**). LC-MS analysis indicated that the early eluting peak **I** comprised very long-chain omega-hydroxy fatty acids containing esterified epoxyenone (an acyl acid derivative), and peak **II** as EOS esterified with epoxyenone (an acyl ceramide). Compared to the unbound epoxyenones, for both **I** and **II**, mass spectrometry revealed a bias towards the longer 34:1 species in the ω-hydroxy VLFA component  (**Figure 49**). The esterified epoxyenone in **I** and **II** was further characterized following NaBH$_4$ reduction and transesterification as already described above for analysis of the free ceramides, and the identical epoxyenone structure was revealed, i.e. 9,10-*trans*-epoxy, 11-*trans*, 13-keto-linoleate. Based on the SP-HPLC analysis, I estimated that the ratio of free over reversibly protein-bound epoxyenone-EOS in the wild-type was approximately 1:1.

To explain this unusual observation of slowly releasable lipids, I suspect that these products are covalently bound to proteins, yet the linkage must be slowly reversible so that they would partition into the organic phase on prolonged incubations. Michael addition of the enone moiety to histidine might account for the coupling and slow release. These novel observations indicate an additional mode of linking the lipids and proteins in the neonatal mouse epidermis, perhaps preceding or concurrent with the ester linkage through the omega-hydroxyl that is already established (156).

**Figure 49**
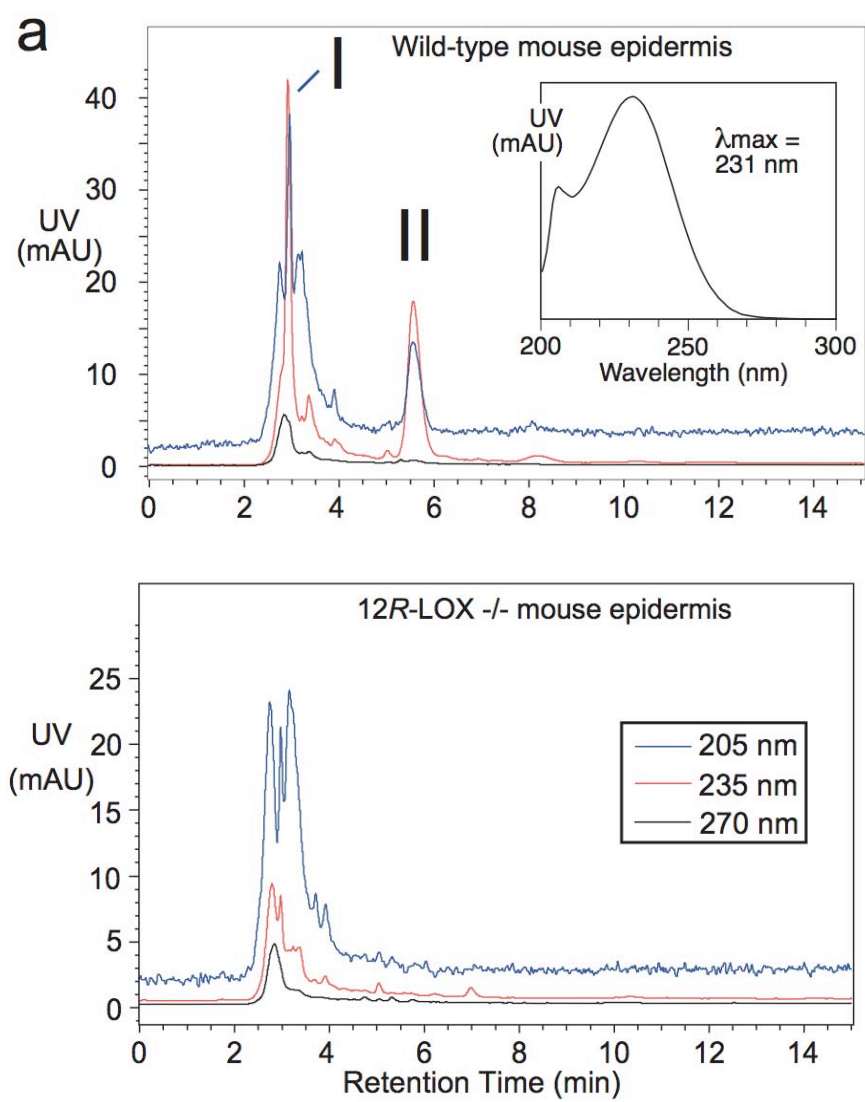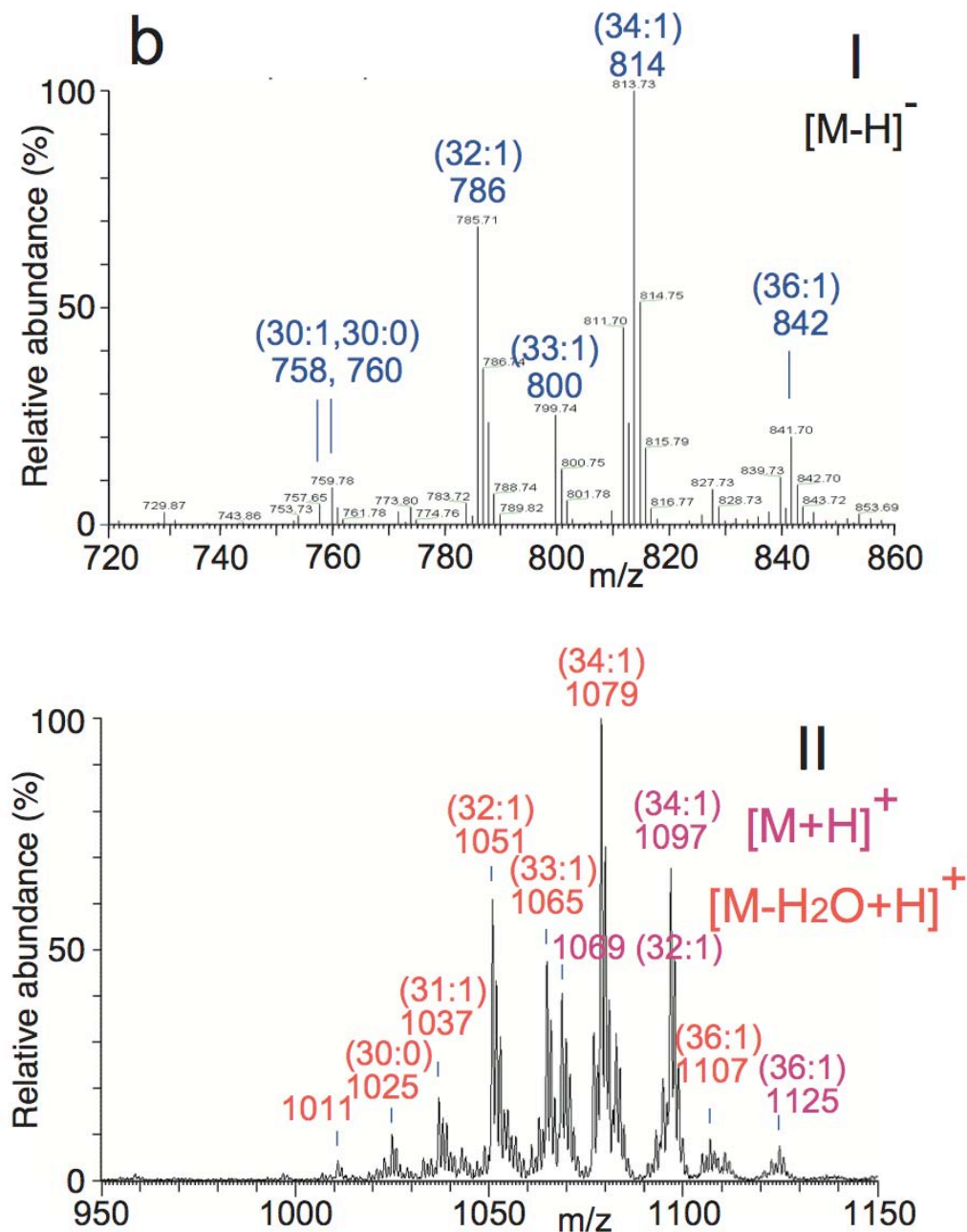
**Figure 49:** Identification of epoxy-enone fatty acid bound to protein. (**a**) SP-HPLC analysis of wild-type (top panel) and 12R-LOX-/- (lower panel) neonatal mouse epidermal lipids recovered from a final soak for 24 hr at room temperature following prior MeOH/CHCl₃ extractions. Top panel inset, UV spectrum of products I and II. (**b**) Mass spectral analysis of I (top panel) and II (lower panel). (**c**) Potential binding of I and II to protein as a slowly reversible covalent Michael adduct, and structures of the major species of the free products I and II.

**Discussion**

Our study provides a model that explains the role of 12*R*-LOX and eLOX3 in skin barrier formation, and ties this together with the long-known and not well-understood need for an EFA in the skin ceramides (**Figure 50**). We have demonstrated both *in vitro* and *in vivo* the existence of a novel metabolic pathway, where 12*R*-LOX oxygenates the linoleate-containing acyl(glucosyl)ceramides to give the 9*R* hydroperoxide, and eLOX3 in turn converts the 12*R*-LOX product to the specific 9*R*,10*R*-epoxy-13*R*-hydroxy-epoxyalcohol. We have further deduced, from our biochemical and EM evidence that the CLE is missing in 12*R*-LOX-/- mice in correlation with a complete absence of LOX metabolites, that this LOX-catalyzed oxygenation is required to facilitate hydrolysis of the (oxidized) linoleate moiety and leave free the ω-hydroxyl on the ceramides for coupling to the cross-linked proteins of CE. This covalent coupling is an important step in sealing the water barrier (47,150). If EFA are deficient, there is no LOX substrate available and thus the fatty acid cannot be cleaved. Absence of one or the other of the LOX enzymes has a similar effect. Thus in both cases, the CLE is either missing or defective, leading to a skin barrier defect.

Our model linking EFA with the action of 12*R*-LOX and eLOX3 also provides a simple explanation on the finding by Houtsmuller and colleagues that for a fatty acid (natural or synthetic) to be an EFA in the skin, it has to have at least two *cis* double bonds in the arrangement of bond-CH$_2$-bond and placed at about the ω6 position from the end of the carbon chain (54), which fits perfectly with the structural requirement of LOX substrates. Thus, although other fatty acids such as 9*trans*,12*cis*-18:2ω6 or 9*trans*,12*cis*-18:2ω6 (which differs from linoleic acid only in the configuration of one double bond)

will be incorporated into acylceramides if topically applied to essential fatty acid deficient skin, they invariably fail to cure the skin defects because they are not LOX substrates (80).

It was once assumed that arachidonic acid is the natural substrate of the putative 12*R*-LOX-eLOX3 pathway in the epidermis, being converted via 12*R*-HPETE to 8*R*-hydroxy-11*R*,12*R*-epoxyeicosa-5*Z*,9*E*,14*Z*-trienoic acid (37). A major problem for this assumption was that arachidonic acid is not a substrate of mouse 12*R*-LOX (97). Instead, the enzyme prefers to use fatty acid esters such as methyl arachidonate as substrate. This no longer presents as a problem, as we now suggest in this study that arachidonic acid oxygenation by 12*R*-LOX and eLOX3 is probably of little relevance in the physiological setting of skin barrier formation. Nonetheless, the 12*R*-LOX products of arachidonic acid do occur in the inflammatory skin disease of psoriasis (96), and may have a separate role in that condition.

It is worth mentioning at this point that acylceramides were proposed to be LOX substrates 25 years ago (80), at a time when this class of ceramides was newly discovered (58), the potential role of prostaglandins in mediating the effect of EFA in the epidermis just ruled out (54), and 12*R*-LOX and eLOX3 to be discovered more than ten years later (83,101). In this study by Nugteren and colleagues, [$^{14}$C-1]linoleic acid was topically applied to rat skin and some of the radioactivity was found two or three days later in a group of oxidized acylceramides that were suggested to be LOX metabolites. Unfortunately, due to technical limitations at that time, these putative LOX metabolites were not structurally defined. Our present study extended this finding by demonstrating that the oxygenated metabolites of EOS found *in vivo* exhibit the same remarkably high

regio- and stereospecificity as the LOX products *in vitro*, thus having definitively resolved the arguments (81) over whether the oxygenated metabolites were truly of enzymatic origin. Moreover, we have advanced a further step in rationalizing the functions these LOX metabolites may serve in the skin, i.e., to help build the CLE.

Confusion may arise as to which of the two, acylceramides or acylglucosylceramides, are the LOX substrates. We have shown in our *in vitro* experiment that acylglucosylceramides are substrates of 12*R*-LOX and eLOX3, yet the LOX metabolites we have detected *in vivo* are oxygenated derivatives of acylceramides. Biochemical studies on LOX reactions with large esters suggest that the polar groups on a large ester substrate, such as the glucose in acylglucosylceramide does not directly interact with the enzyme active site and thus will play no major effect on LOX catalysis (106). Moreover, studies on mice deficient in β-glucocerebrosidase or the activator proteins indicate that deglycosylation is not a requisite step for formation of the CLE (although the CLE will remain glycosylated and thus defective) (73,74). Accordingly, we suggest that both acylceramide and acylglucosylceramide are accepted by 12*R*-LOX and eLOX3 as substrates. Within the context of our model (**Figure 50**), the acylglucosylceramide newly delivered to the plasma membrane is demanded by its own structure to span the entire membrane bilayer, with the glucose group protruding into the extracellular space where β-glucocerebrosidase resides and the linoleate moiety placed instead at inner leaflet of plasma membrane where the two LOX enzymes should reside. Thus, our model predicts that cleavage of the glucose group and cleavage of oxidized linoleate moiety may be two independent events separated by membrane compartmentation.

The LOX metabolites we have detected *in vivo* are at low levels, those in pig epidermis amounting in all to ~5% of the acylceramide substrate, EOS. Of note, despite numerous studies of epidermal ceramide composition in the past, the specific derivatives we have identified have not been previously characterized. In our case, the application of multiple wavelength UV detection on HPLC provided crucial insights that are absent in the forest of products detectable on thin layer chromatography and upon mass spectral analysis. The low abundance of these oxidized ceramides in fact consistent with our hypothesis that these LOX metabolites are obligatory intermediates rather than the end products of the pathway, being selectively subject to ester-bond cleavage with concomitant formation of ω-hydroxyceramides that will be covalently coupled to proteins. As noted earlier, such a hydrolysis event is strongly suggested by the observation in 12*R*-LOX-/- mice that the CLE is missing in correlation with a complete absence of LOX metabolites. In addition, since linoleic acid, similar to arachidonic acid, is not a substrate of mouse 12*R*-LOX, the 9*R*-HODE free acid present in wild-type and absent in 12*R*-LOX-/- mouse epidermis must stem from hydrolysis of the 9*R*-HODE-acylceramide products. Further supporting our hypothesis, there accumulated many papers over the years showing that oxidized polyunsaturated fatty acid esters are more susceptible to hydrolysis, and indeed nowadays it is generally accepted that oxidation disrupts membranes and provokes clearance of oxidized lipids. It is also possible that the specific oxygenation pattern brought by 12*R*-LOX and eLOX3 may be stringently required by the downstream esterase for hydrolysis to occur.

We have noted considerable differences in the pattern of LOX products between those from the *in vitro* reactions, those detected in pig epidermis and those detected in

mouse epidermis, although the specificity of the individual products is strikingly similar. For example, in the eLOX3 reaction with glucosyl-EOS *in vitro*, the epoxyalcohol derivative is the major product and the 9-KODE derivative is a minor product, whereas in pig epidermis, this relationship is reversed. In mouse epidermis, the epoxyalcohol derivative was not detected at all and instead the major LOX metabolite identified is 9,10-epoxy-13-keto-EOS. Such epoxyenone compounds are often formed as byproducts in the reactions of eLOX3. Since the detected LOX metabolites *in vivo* are likely to be "leftovers" from the downstream hydrolysis, the emerging picture seems to be one in which the epoxyalcohol derivative is preferentially hydrolyzed, whereas the byproducts are hydrolyzed to a less extent and thus accumulate.

An intriguing result of this study is that in mouse epidermis some epoxyenone-EOS ceramides, together with epoxyenone-acyl acids, are directly coupled to proteins through a reversible linkage. Most likely, the chemistry involves Michael addition of the α,β-unsaturated ketone to His on proteins (155). Notably, the CE protein Involucrin is enriched in His (72). We have estimated that this type of covalently bound epoxyenone-EOS products account for ~ 8% of total covalently bound ceramides. The physiological relevance of this reversible covalent coupling remains to be determined.

Finally, it should be emphasized that the model proposed here is by no means all-inclusive. We note the special physical properties brought by linoleate itself in acylceramides that may contribute to the proper phase behavior of intercellular lamellar membranes (68). Also, the unexpected finding of protein-bound epoxyenone-EOS products in mouse epidermis opens up the possibilities that LOX products may be directly attached to proteins. For example, both the epoxide group with an adjacent

double bond and the $\alpha,\beta$-unsaturated keto group in the epoxyalcohol-EOS or ketone-EOS products are excellent electrophiles, naturally prone to attack by nucleophilic amino acid residues such as His, Cys and Lys. Notably, these potential non-ester-bound species cannot be distinguished from the ester-bound $\omega$-hydroxyceramides using mild alkaline hydrolysis, since free $\omega$-hydroxyceramides will also be recovered while the oxidized linoleate will remain attached to proteins even if the actual bound species are LOX products themselves.
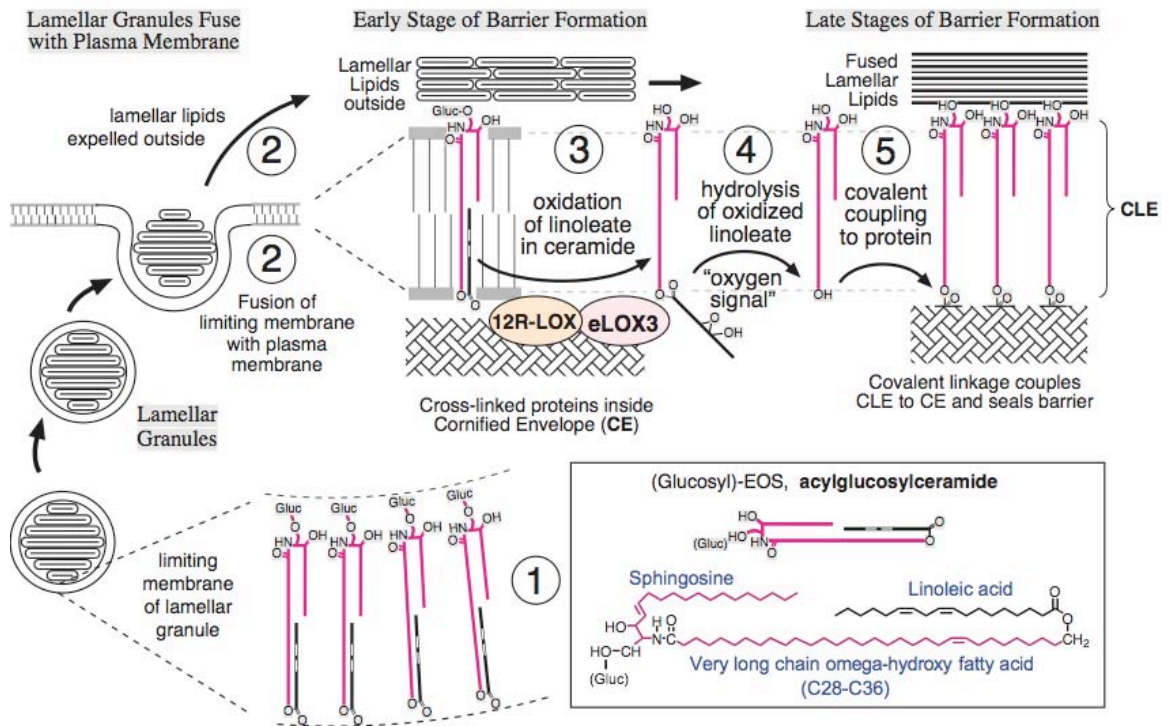
**Figure 50:** A model connecting ceramides, EFA and LOX in the Stratum Corneum. (1) Lamellar granules containing lamellar lipid discs have Gluc-EOS (with linoleate coupled to the omega-hydroxyl) in the limiting membrane. (2) Fusion extrudes the lamellar contents extracellularly and combines the lamellar limiting membrane with the cell plasma membrane, initiating formation of the cornified lipid envelope (CLE, shown greatly expanded). (3) Progression towards the mature barrier entails LOX-catalyzed oxygenation of the linoleate, the resultant "oxygen signal" permits esterase-catalyzed hydrolysis of the oxidized linoleate, freeing the ceramide omega-hydroxyl for (4) transglutaminase-catalyzed covalent coupling of the CLE to the cross-linked proteins of the CE, thus helping to seal the barrier. Lipoxygenase-catalyzed oxygenation of (Gluc)-EOS may be initiated earlier in the process than illustrated here.

# CHAPTER V

# AN UNEXPECTED FINDING IN THE DISSERTATION RESEARCH: FORMATION OF A CYCLOPROPYL EPOXIDE VIA A LEUKOTRIENE A SYNTHASE-RELATED PATHWAY IN AN ANAEROBIC REACTION OF SOYBEAN LOX-1 WITH 15*S*-HPETE

## Introduction

Lipoxygenases (LOX) are named for their oxygenase activity with polyunsaturated fatty acids yet they also catalyze other types of reaction. One of the most important in a biological context is leukocyte 5-LOX-catalyzed further conversion of the hydroperoxide product 5*S*-HPETE to leukotriene $A_4$ (LTA$_4$) (157). LTA$_4$, an unstable epoxide, will then be subject to metabolism of downstream enzymes in the pathway to more stable and biologically active LTs including the dihydroxy LTB$_4$ and the peptidyl LTC$_4$, D$_4$ and E$_4$ (2). Parallels of the LTA synthase activity of 5-LOX also exist in some other LOX enzymes. Mammalian 15-LOX-1, for example, can further convert 15*S*-HPETE to a structural analogue of LTA$_4$, named 14,15-LTA$_4$ based on the position of the epoxide group between C-14 and C-15 . This 14,15-epoxide was recently given the name of eoxin A$_4$ on account of its production by eosinophils and its further transformation, analogous to LTA$_4$, to a series of biologically active peptidyl derivatives, 14,15-LTC$_4$, D$_4$ and E$_4$ (eoxins C$_4$, D$_4$, E$_4$) ((158).

Despite the general parallels between leukocyte 5-LOX and mammalian 15-LOX-1 within the physiological context, the two enzymes exhibit notable differences in their reactions towards 5$S$-HPETE and 15$S$-HPETE respectively. Leukocyte 5-LOX gives almost exclusively LTA$_4$ from 5$S$-HPETE, whereas the reaction of mammalian 15-LOX-1 with 15$S$-HPETE leads, in addition to 14,15-LTA$_4$, to several other products including two fatty acid dihydroperoxides, 8$S$,15$S$-diHPETE and 5$S$,15$S$-diHPETE (159). On the other end of the spectrum of reactivity compared to leukocyte 5-LOX is the prototypical plant lipoxygenase, soybean LOX-1. It converts 15$S$-HPETE exclusively to 8$S$,15$S$-diHPETE and 5$S$,15$S$-diHPETE (160). These diHPETEs are often referred to as "double oxygenation" products, since they are formed, in essence, by oxygenation of arachidonic acid twice in succession at two different positions.

In the present study, I aimed to understand the mechanistic basis for the different preferences of LOX enzymes for LTA synthesis or double oxygenation. Some clues can be gleaned from the literature. Rabbit reticulocyte 15-LOX or porcine leukocyte 12-LOX (both being homologs of human 15-LOX-1), when incubated with 15$S$-HPETE under anaerobic reactions, gives a higher yield of 14,15-LTA$_4$ at the expense of the double oxygenation products (159,161). Conversely, under higher than normal oxygen pressures, potato 5-LOX can be forced to perform double oxygenation on 5$S$-HPETE (162). These studies imply that LTA synthesis and double oxygenation are in competition, and the concentration of molecular oxygen is a critical determinant on which process dominates. The latter point can be better understood when one considers that LTA synthesis does not involve molecular oxygen whereas the double oxygenation reaction uses molecular oxygen as one of the two substrates. Since the catalysis should be influenced by oxygen

concentrations in the enzyme active site, rather than in the atmosphere *per se*, I hypothesized that the different preferences of LOX isoenzymes for LTA synthesis or double oxygenation stem from different oxygen concentrations in their active sites.

With this hypothesis, I reasoned that soybean LOX-1, which catalyzes only double oxygenation with 15*S*-HPETE under usual aerobic conditions, might show 14,15-LTA$_4$ synthase activity when molecular oxygen is excluded. In this paper, I described such an anaerobic reaction of soybean LOX-1 with 15*S*-HPETE. As anticipated, I observed the formation of the hydrolysis products of the putative 14,15-LTA$_4$. Moreover, as a mechanistically informative finding, I identified among the reaction products two novel 5,15-dihydroxy compounds and their δ-lactone derivatives. Based on their chemical structures, conditions of formation, and evidence from H$_2$$^{18}$O incubations, I suggested that the 5,15-dihydroxy compounds and their δ-lactone derivatives result from nucleophilic attack by water (hydrolysis) and by the terminal carboxylate anion (lactonization) respectively of a novel cyclopropyl epoxide formed via a LTA-synthase related mechanism.

## EXPERIMENTAL PROCEDURES

### Materials

Soybean LOX-1 (soybean P1, purified) and nordihydroguaiaretic acid (NDGA) were purchased from Cayman Chemical, Co Inc (Ann Arbor, MI). We determined that the purified soybean LOX-1 employed in this work was of 10-fold lower specific activity than advertised (possibly due to two cycles of freeze-thawing), ~20 μmol/min/mg using

the Axelrod assay with sodium linoleate (127). Linoleic and arachidonic acids were purchased from NuChek Prep Inc. (Elysian, MN). [1-$^{14}$C]Arachidonic acid was purchased from PerkinElmer Life Sciences. 15$S$-HPETE and 13$S$-HPODE were synthesized by reacting soybean LOX-1 with arachidonic acid at pH 9 under the normal aerobic conditions followed by SP-HPLC purification (103). 5($RS$)-HETE was chemically synthesized from arachidonic acid (163) and the enantiomers resolved by chiral column HPLC as described (164). 5,15-diHETE was prepared similarly using 5$S$-HETE and/or 5$R$-HETE as substrate for soybean LOX-1, followed by reduction using NaBH$_4$ and SP-HPLC purification. The Aldrich Atmosbag used for conducting the anaerobic incubations was purchased from Sigma-Aldrich (St. Louis, MO).

Reaction incubations and extraction

The initial anaerobic reactions on an analytical scale were conducted inside a N$_2$-inflated Aldrich Atmosbag. First, placed into the Aldrich Atmosbag were an open vial containing the enzyme solution (0.76 μM soybean LOX-1 in 1 ml of sodium phosphate pH 7.5), an open vial containing the substrate solution (20 μM to 440 μM 15$S$-HPETE in 1 ml of sodium phosphate pH 7.5), syringes, vial caps and a bottle of methanol. The Atmosbag was then sealed, and subjected to vacuuming and N$_2$ inflation for three cycles. Twenty minutes was given for the enzyme and substrate solutions to reach equilibrium with the N$_2$ atmosphere. Then the reaction was started by mixing the enzyme and the substrate. Reaction was stopped by addition of an equal volume of methanol, followed by extraction using an Oasis HLB cartridge (Waters Corp.).

For the reactions in the presence of NDGA or 13$S$-HPODE, 80 μM NDGA or 13$S$-HPODE was included in the substrate solution. For structural analysis of the

products, the incubations were scaled up to a volume of 20 ml using otherwise the same conditions. For incubations in $^{18}$O-enriched buffer, a volume of 0.5 ml was used, which is comprised of 0.4 ml of 96% H$_2$$^{18}$O and 0.1 ml of 500 mM sodium phosphate pH 7.5.

Kinetic measurements

For kinetic measurements, the anaerobic reaction of soybean LOX-1 (usually 0.2 μM unless noted otherwise) with 15$S$-HPETE (50 μM to 500 μM) was monitored at 280 nm in an enclosed quartz cuvette using a Perkin-Elmer Lambda-35 spectrophotometer. N$_2$ saturated sodium phosphate buffer (pH 7.5), glucose oxidase, glucose and catalase were used to achieve the anaerobic conditions; subsequently, HPLC analyses verified that no oxygenation products were formed. The reaction volume is usually 1.1 ml. To avoid potential inhibition of alcohols on the enzyme activity, 15$S$-HPETE originally dissolved in methanol was first added to the quartz cuvette and then taken to dryness under a stream of N$_2$. The cuvette was then placed to the bottom of a plastic bag filled with argon. 1 ml of N$_2$ saturated buffer, 25 μl of glucose oxidase (stock concentration: 827 sigma units/ml), 1 μl of catalase (the stock solution was 5X diluted from the commercial solution of bovine liver catalase purchased from Sigma-Aldrich, C3155, ≥35,000 units/mg protein), and 50 μl of glucose (2 M stock, N$_2$ saturated) were then added to the cuvette. The cuvette was then capped, taken out of the bag, shaken for a few seconds and let stand for about 1 minute. Reaction was started by quick addition of 6 μl of soybean LOX-1 stock solution (final concentration: 0.38 μM).

## HPLC analysis and purification

The extracted products were analyzed by RP-HPLC and SP-HPLC using an Agilent 1100 HPLC system equipped with a diode array detector. The products from [1-$^{14}$C]15$S$-HPETE were analyzed simultaneously by the diode array detector and by a Flo-One A-100 radioactive detector (Radiomatic Instruments and Chemical, Meridian, CT). The RP-HPLC analysis used a Waters Symmetry $C_{18}$ column (5 μm, 0.46 × 25 cm), an isocratic solvent system of methanol/water/acetic acid (80:20:0.01 by volume) and a flow rate of 1 ml/min. The SP-HPLC analysis used a Beckman Ultrasphere Silica column (5 μm, 0.46 × 25 cm), an isocratic solvent system of hexane/isopropanol/acetic acid (100:2:0.1 by volume for less polar products followed by a strong solvent wash, or 100:5:0.1 for polar products), and a flow rate of 1 ml/min. Products **2**, **3**, **4** and **5** were purified by SP-HPLC. Products **1**, **6**, **7** were purified by SP-HPLC followed by RP-HPLC. Separation of the two diastereomers of product 4 was achieved using a Chiralpak AD-RH column (5 μm, 0.46 × 15 cm), an isocratic solvent system of methanol/water/acetic acid (95:5:0.01 by volume) and a flow rate of 0.5 ml/min. For analysis of product **5**, we used the same column, methanol/acetic acid (100:0.01, by volume) and a flow rate of 1 ml/min.

## Synthesis of HETEs and diHETE with trans-trans conjugated dienes

Thiyl radical induced isomerization (mercaptoethanol, UV light, room temperature (165,166)), was used to convert *cis-trans* to *trans-trans* conjugated dienes. Reaction conditions had the starting material (2.5 mg, methyl ester of HETE or diHETE) in 0.5 ml isopropanol containing 0.5 μl mercaptoethanol in a quartz UV cuvette with telfon cap. The cuvette was submerged in a solution of aqueous 1M NaCl that served

both to stabilize the temperature at <25°C and absorb UV radiation below 220 nm. A low pressure immersion UV lamp rated with 3.5 Watts output at 254 nm (part no. 12128-15, Ace Glass Inc., Vineland, NJ) [caution: harmful UV radiation] was placed about 15 cm above the cuvette. Aliquots of the reaction were analyzed at 30 min intervals by argentation HPLC using a cation exchange column (Sepralyte SCX 5-µm, 25 x 0.46 cm, originally purchased from Analytichem International, later owned by Varian) in the silver form (167,168) with a solvent of hexane/isopropanol/acetic acid in the proportions 70:30:0.1 (by volume) for mono-HETE methyl esters and 5,15-diHETE methyl ester, a flow rate of 1 ml/min, and with UV monitoring using an Agilent 1100 series diode array detector. 5-HETE and 15-HETE were isomerized in the conjugated diene, leading to accumulation of the *trans,trans*-HETEs (with two *trans* and two *cis* double bonds) with very minor peaks for the more highly isomerized derivatives. 5,15-diHETE was isomerized in one conjugated diene and, after 2-3 hours irradiation in both, giving the all-*trans* derivative as the major product.

Derivatization and GC-MS analysis

Catalytic hydrogenations were performed in 100 µl of ethanol using about 1 mg of palladium on alumina and bubbling with hydrogen for 2 min at room temperature. The hydrogenated products were recovered by the addition of water and extraction with ethyl acetate. TMS ester TMS ether derivatives were prepared by treatment with *bis*(trimethylsilyl)-trifluoracetamide (10 µl) and pyridine (2 µl) at room temperature for 2 h. Subsequently, the reagents were evaporated under a stream of nitrogen and the samples were dissolved in hexane for GC-MS.

Analysis of the methyl ester trimethylsilyl ether derivatives of the products was carried out in the positive ion electron impact mode (70 eV) using a Thermo Finnigan Trace DSQ ion trap GC-MS with the Xcalibur data system. Samples were injected at 150 °C, and after 1 min the temperature was programmed to 300 °C at 20 °C/min. Spectra collected during elution of the GC peak (typically about 20 spectra) were averaged for calculation of the isotopic compositions.

ESI-LC-MS

ESI-LC-MS of purified product **4** and product **5** was performed using a Thermo Finnigan LC Quantum instrument. A Waters Symmetry $C_{18}$ column (0.2 × 15 cm) was eluted with acetonitrile/water/ammonium acetate (50:50:10 mM) at 0.2 ml/min. The heated capillary ion lens was operated at 220 °C. Nitrogen was used as a nebulization and desolvation gas. The electrospray potential was held at 4 kV. Source-induced dissociation was set − 10 eV. Mass spectra were acquired over the mass range m/z 100-500 at 2 s per scan under the negative ion mode.

NMR

$^1$H and $^1$H,$^1$H-COSY NMR spectra were recorded on a Bruker DXR 600 MHz spectrometer at 298K. The ppm values are reported relative to residual non-deuterated solvent (δ = 7.16 ppm for $C_6H_6$).

# RESULTS

An anaerobic reaction of soybean LOX-1 with 15S-HPETE

To test the hypothesis that soybean LOX-1 is capable of catalyzing LTA synthesis in the absence of oxygen, initially we incubated the enzyme (0.38 μM) with various concentrations of 15S-HPETE (20 μM to 440 μM) at pH 7.5 under $N_2$ for two hours. [Although analysis of reaction rates is complicated by the mixture of products formed (see below), subsequent analyses indicated that, for example, 100 μM 15S-HPETE is fully consumed within 10 min. Observed rates are presented in the Supplemental data]. Reactions were stopped by addition of an equal volume of methanol, followed by extraction using an Oasis HLB cartridge. RP-HPLC analysis revealed that the substrate 15S-HPETE, at all concentrations tested, was completely converted to seven new compounds, designated **1-7** based on the order of elution (**Figure 51**). We also examined the reaction carefully for the production of fatty acid dimers, as their formation would be predicted if this reaction follows the same mechanism as the well-studied anaerobic reaction of soybean LOX-1 with linoleic acid and 13S-HPODE (30,31,125). However, SP-HPLC and RP-HPLC analyses showed that this reaction gave no appreciable amounts of C-C linked dimers and confirmed that products **1-7** constitute the main products.

Contribution of the Fe(II) enzyme to the anaerobic reaction with 15S-HPETE

Since soybean LOX-1 exists in two oxidation states, Fe(II) and Fe(III), we next questioned which enzyme form is responsible for the formation of the products. NDGA, as a redox-based LOX inhibitor, inhibits the oxygenase activity of LOX by reduction of
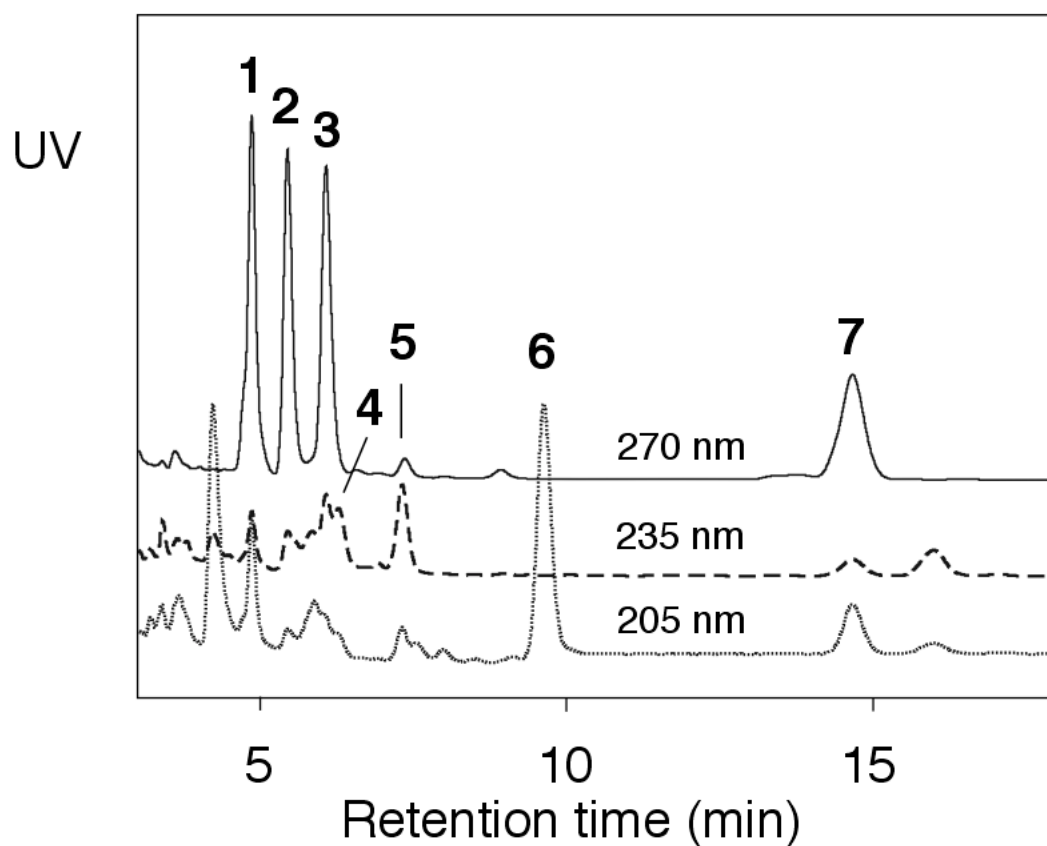
**Figure 51**: RP-HPLC analysis of products from the anaerobic reaction of soybean LOX-1 (0.38 μM) with 15S-HPETE (40 μM). The products were eluted using a Waters Symmetry $C_{18}$ column (0.46 × 25 cm), a solvent system of methanol/water/acetic acid (80:20:0.01 by volume) and a flow rate of 1 ml/min. Shown are the UV traces at 205 nm, 235 nm and 270 nm monitored by an Agilent diode array detector. The products are designated **1-7** based on the order of elution.

Fe(III) LOX to Fe(II) LOX (27); therefore, in the presence of NDGA, soybean LOX-1 would be kept in the Fe(II) state and only the products from the Fe(II) enzyme would be observed.

The anaerobic reaction of soybean LOX-1 (0.38 μM) with 15S-HPETE (40 μM) was performed in the presence of NDGA (80 μM) and subsequently analyzed by RP-HPLC. As shown in **Figure 52**, only products **1**, **6**, **7** were formed in the presence of NDGA, indicating that these are the products from the Fe(II) enzyme. In addition, we noted that NDGA significantly accelerated the rate of reaction, especially at substrate concentrations lower than 100 μM.

Under anaerobic conditions, linoleic acid also reduces Fe(III) soybean LOX-1 to Fe(II) soybean LOX-1, with itself being converted to a carbon-centered radical and then released from the enzyme active site (28). Accordingly, linoleic acid should have the same effect as NDGA does on the anaerobic reaction of soybean LOX-1 with 15S-HPETE. Indeed, in the presence of linoleic acid (150 μM), 15S-HPETE was converted to essentially the same set of products as in the presence of NDGA (data not shown).

Identification of the Fe(II) enzyme products **1**, **6** and **7**

Products **1**, **6** and **7** were identified by UV, LC-MS, and NMR. Product **1** is the $C_{15}$ aldehyde 15-oxopentadeca-5Z,8Z,11Z,13E-tetraenoic acid, product **6** is 13R-hydroxy-14S,15S-epoxyeicosa-5Z,8Z,11Z-trienoic acid, and product **7** is 15-oxoeicosa-5Z,8Z,11Z,13E-tetraenoic acid (15-KETE) (**Figure 53**). Formation of the $C_{15}$ aldehyde (product **1**) and 15-KETE (product **7**) is expected, as they are structural analogues of the major $C_{13}$ aldehyde and 13-KETE formed in the anaerobic reaction of the Fe(II) enzyme with 13S-HPODE (30). Product **7** is a direct analogue of *threo*-11-hydroxy-12,13S-*trans*-

epoxyoctadec-9*Z*-enoic acid, another known compound derived from 13*S*-HPODE by soybean LOX-1 (34), and this *threo*-13-hydroxy-14,15-*trans*-epoxyalcohol was originally identified by Corey and Mehrotra in 1983 (169).

Contribution of the Fe(III) enzyme to the anaerobic reaction with 15S-HPETE

To examine the products from the Fe(III) enzyme, we took advantage of the fact that 13*S*-HPODE reacts with Fe(II) soybean LOX-1 stoichiometrically to give Fe(III) soybean LOX-1 (18). Thus, soybean LOX-1 (0.2 μM) was reacted with [1-$^{14}$C]-15*S*-HPETE (40 μM*)* in the presence 13*S*-HPODE (80 μM). SP-HPLC with both UV and radioactivity detection revealed that **2**, **3**, **4** and **5** were the main products from the Fe(III) enzyme reaction (**Figure 54**), the complementary set of products compared to those formed from reactions of the Fe(II) enzyme in the presence of NDGA or linoleic acid.

Identification of the Fe(III) enzyme products **2** and **3**

Products **2** and **3** were identified as 8*R*,15*S*-dihydroxyeicosa-5*Z*,9*E*,11*E*,13*E*-tetraenoic acid (8*R*,15*S*-Z,E,E,E-diHETE) and 8*S*,15*S*-dihydroxyeicosa-5*Z*,9*E*,11*E*,13*E*-tetraenoic acid (8*S*,15*S*-Z,E,E,E-diHETE) respectively, based on the same UV, mass spectra (**Figure 55** and **Figure 56**), and chromatographic properties they exhibited as the authentic standards. These 8,15-diols with an all-*trans* conjugated triene are characteristic hydrolysis products of the unstable allylic epoxide, 14,15-LTA$_4$.

Identification of the Fe(III) enzyme products **4** and **5**

Products **4** and **5** display unusual UV spectra similar to, yet distinguishable from, that of the well-known double oxygenation product 5,15-dihydroxyeicosa-6*E*,8*Z*,11*Z*,13*E*-tetraenoic acid (5,15-diHETE). In SP-HPLC solvents, the differences are the more striking (cf. **Figure 57A, 57B**). LC-ESI-MS (negative ion mode) showed that
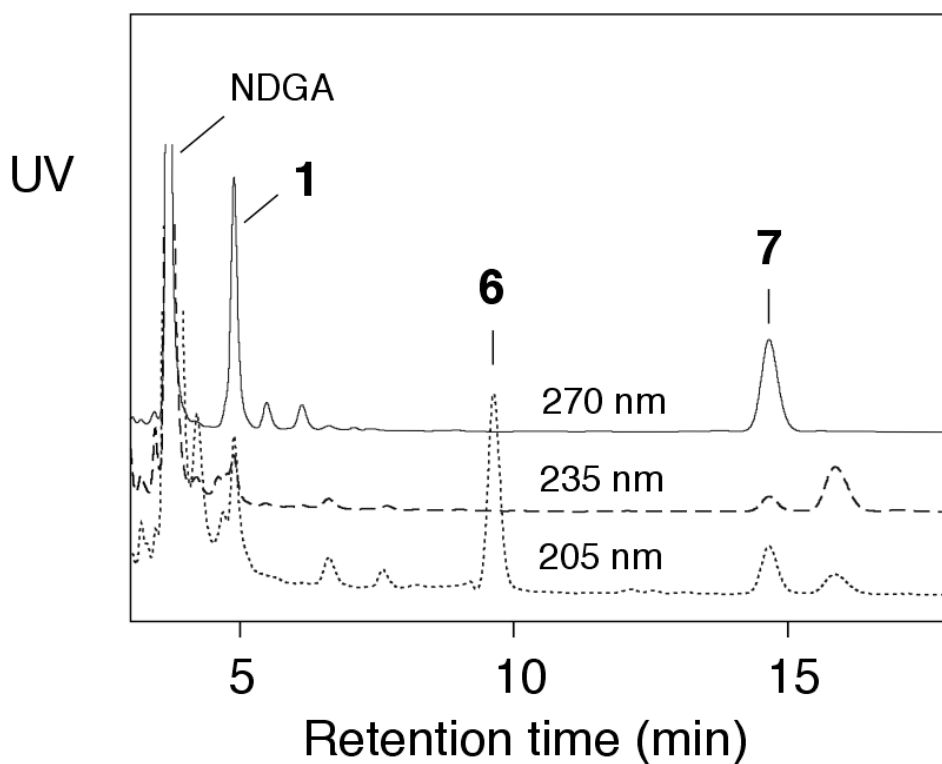
**Figure 52:** RP-HPLC analysis of products from the anaerobic reaction of soybean LOX-1 (0.38 μM) with 15S-HPETE (40 μM) in the presence of NDGA (80 μM). As in **Fig. 51**, the products were eluted using a Waters Symmetry $C_{18}$ column (0.46 × 25 cm), a solvent system of methanol/water/acetic acid (80:20:0.01 by volume) and a flow rate of 1 ml/min. Shown are the UV traces at 205 nm, 235 nm and 270 nm monitored by an Agilent diode array detector.
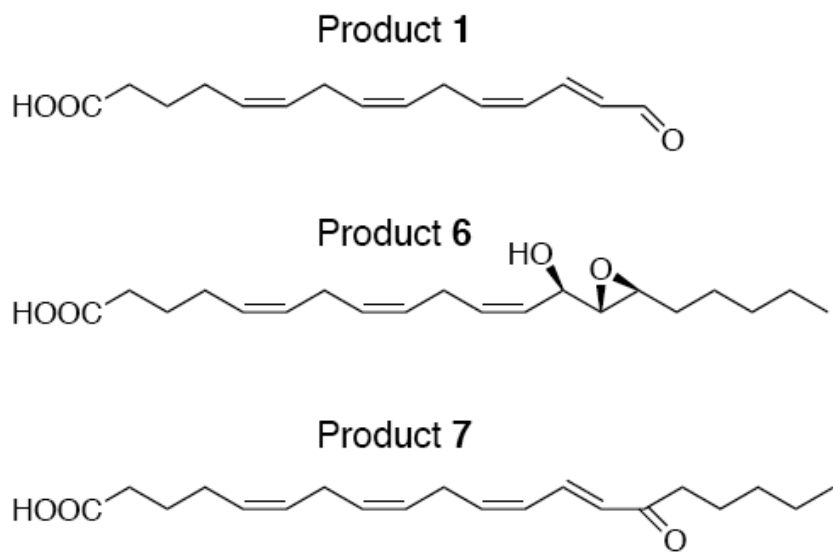
**Figure 53**: Chemical structures of product **1**, **6**, and **7**.
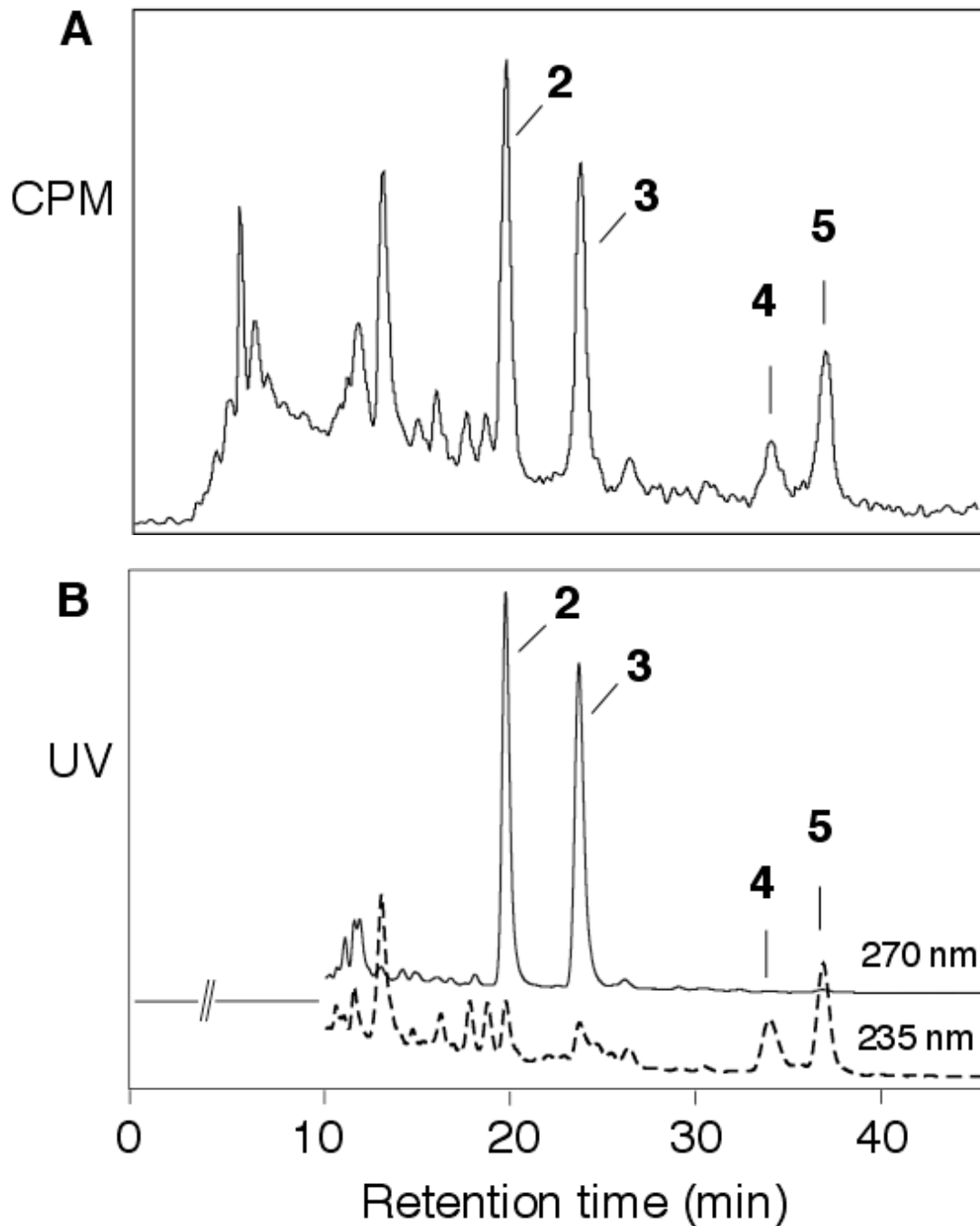
**Figure 54**: SP-HPLC analysis of products from the anaerobic reaction of soybean LOX-1 (0.38 μM) with [1-^{14}C]15S-HPETE (40 μM) in the presence of 13S-HPODE (80 μM). **(A)** The ^{14}C radiochromatogram recorded by a radioactive detector. **(B)** The UV chromatogram at 235 nm and 270 nm recorded by a diode array detector. The products were eluted using a Beckman Silica Ultrasphere column (0.46 × 25 cm), a solvent system of hexane/isopropanol/acetic acid (100:5:0.1 by volume) and a flow rate of 1 ml/min.
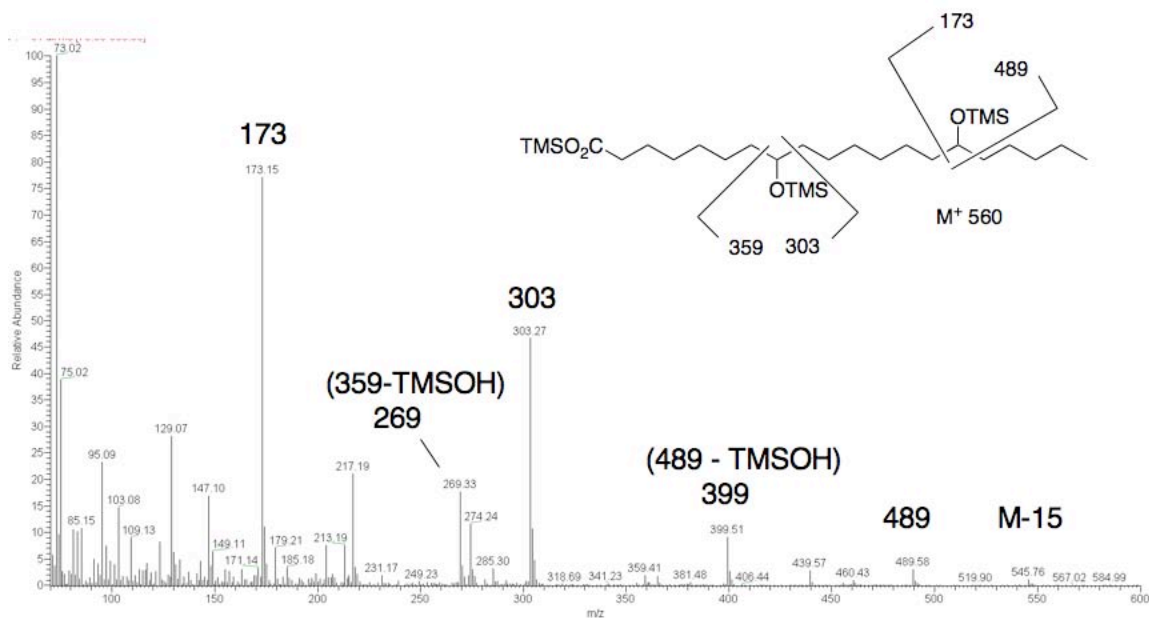
**Figure 55**: GC-MS analysis of the TMS ether TMS ester of hydrogenated product 2



**Figure 56**: GC-MS analysis of the TMS ether TMS ester of hydrogenated product 3
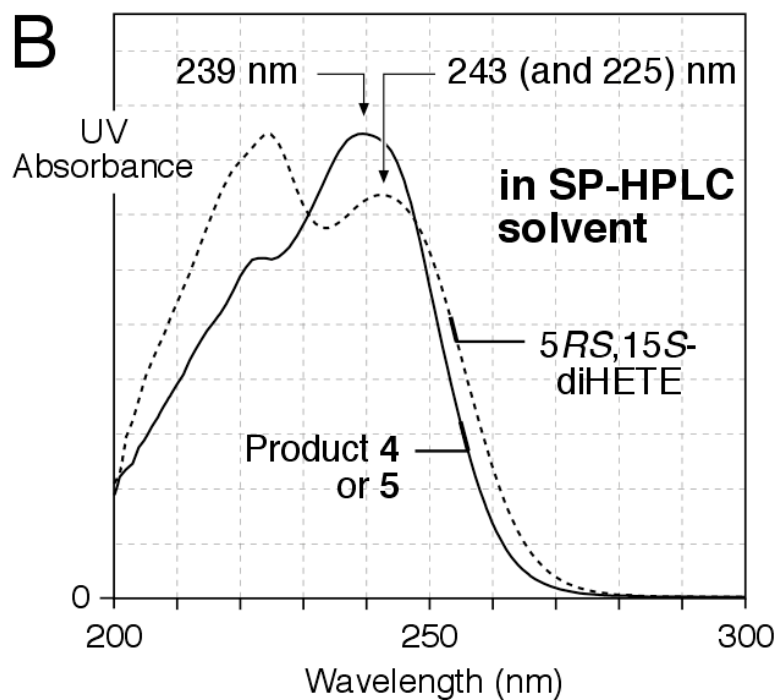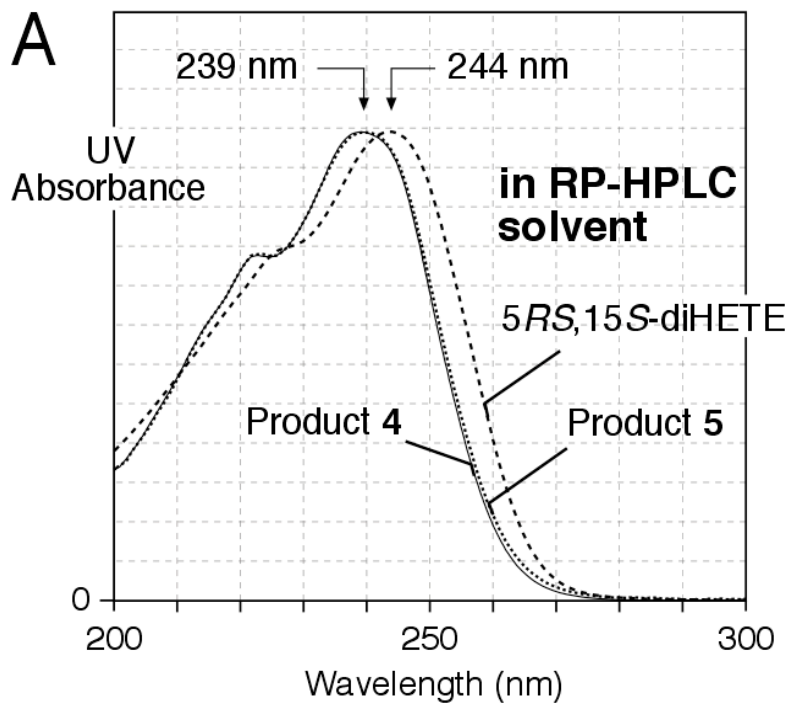
**Figure 57:** Comparison of the UV spectra of product **4** and **5** with that of 5,15-(E,Z,Z,E)-diHETE. **(A)** The spectra in RP-HPLC solvent, methanol/water/acetic acid (80:20:0.01 by volume). **(B)** The spectra in SP-HPLC solvent, hexane/isopropanol/acetic acid (100:5:0.1 by volume).

153

product **4** has the same molecular mass, 336, as 5,15-diHETE (whereas under the same conditions, product **5** was not detected, see below). GC-MS analysis of the TMS ester TMS ether derivative of hydrogenated product **4** established the 5,15-dihydroxy structure (**Figure 58**): the prominent ions at m/z 401 and 261 arise from α-cleavage at the 5-hydroxyl, and m/z 173 and 489 come from α-cleavage at the 15-hydroxyl. Thus, product **4** is a geometric isomer of 5,15-diHETE. Unlike the well-known 5,15-diHETE containing two *cis-trans* conjugated diene chromophores (160), product **4** contains four double bonds, all in the *trans* configuration as indicated by the coupling constants (J ≈ 15 Hz) obtained from $^1$H NMR (**Figure 59A**) and $^1$H,$^1$H-COSY NMR analysis.

To confirm the structure of product **4**, we synthesized all-*trans*-5,15-diHETE by thiyl radical-induced isomerization of the *cis* double bonds in 5,15-diHETE (See Experimental Procedures). The UV, chromatographic, and NMR properties of the synthetic compound were identical to product **4**. In addition, comparison of the olefin regions of the NMR spectra of synthetic 6*E*,8*E*-5-HETE and 11*E*,13*E*-15-HETE helped with assignment of the individual olefin protons in all-*trans*-diHETE, in particular confirming that the H-6 signal is more upfield of H-14, and thus allowing assignment of the rest of the double bond proton signals from the COSY analysis.

Unlike product **4**, product **5** had eluded detection by ESI-MS, suggesting the lack of ionizable groups in the structure (e.g., as esters, including lactones). This was confirmed by GC-MS analysis of the TMS ether derivative of hydrogenated product **5**, which gave a spectrum identical to that published for the TMS ether derivative of hydrogenated δ-lactone of 5,15-diHETE (170) (**Figure 60**). Diagnostic ions include m/z 99, 173 and 327. $^1$H NMR and $^1$H,$^1$H-COSY NMR analysis of product **5** determined the
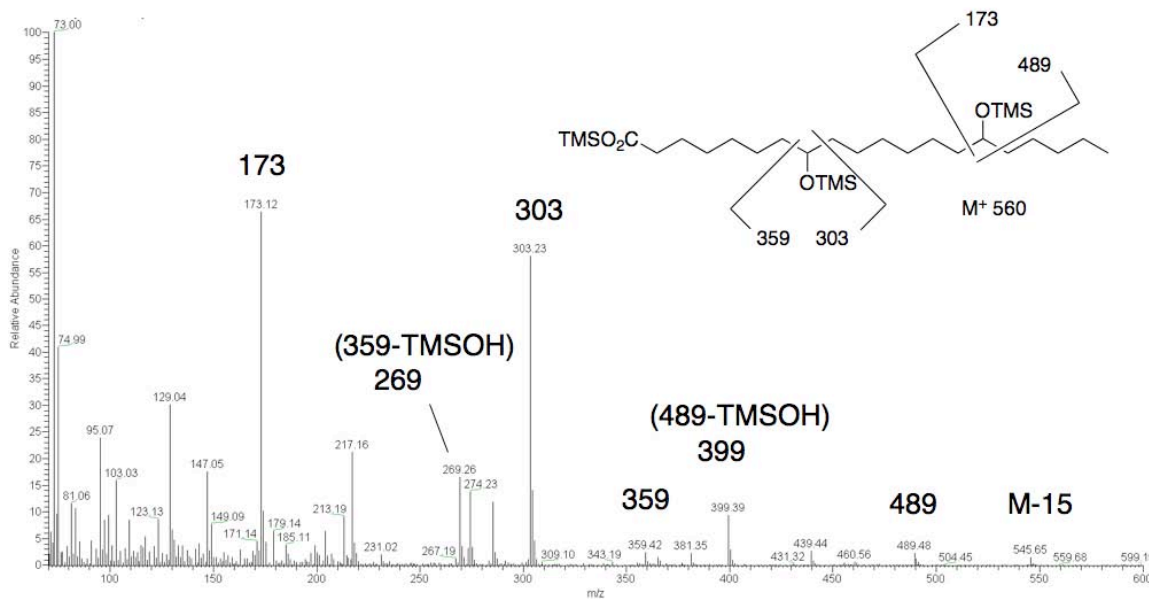
**Figure 58:** GC-MS analysis of the TMS ether TMS ester of hydrogenated product **4**.
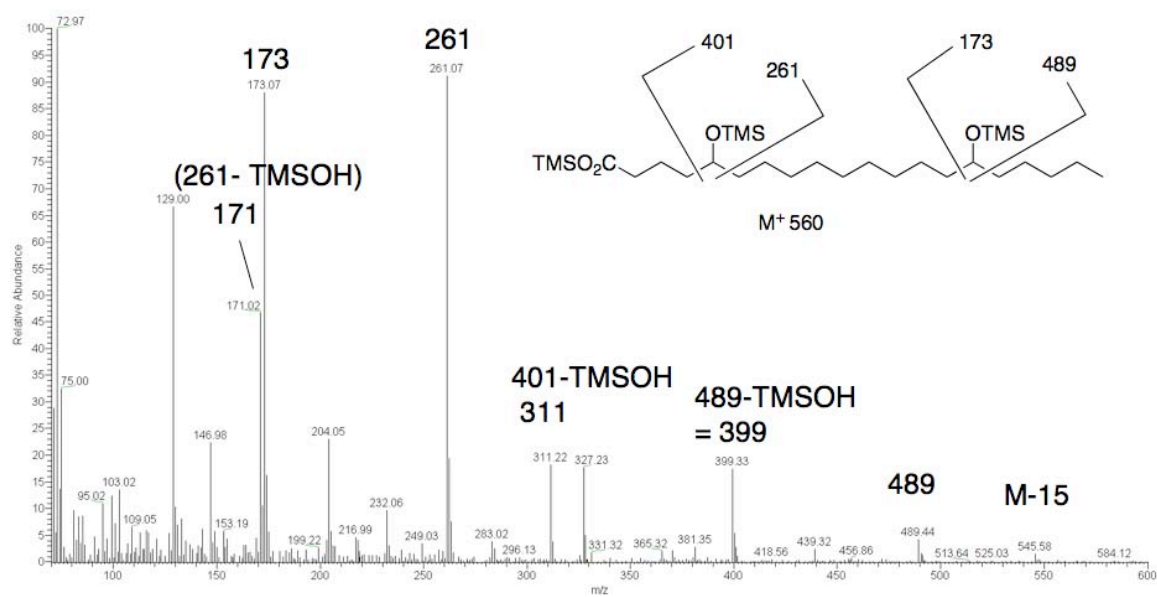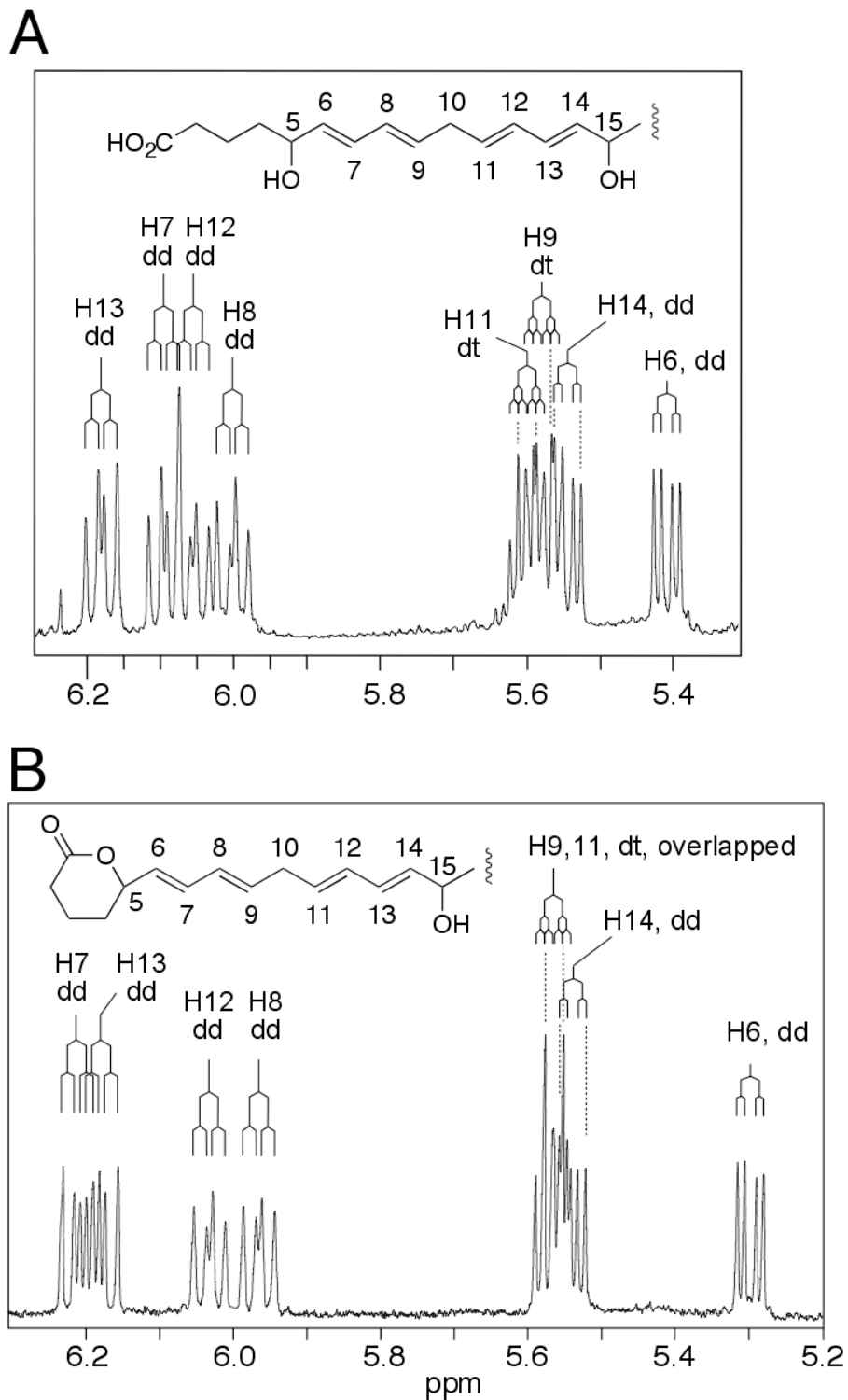
**Figure 59:** ^{1}H-NMR analysis of product **4** (panel **A**) and **5** (panel **B**) in $d_6$-benzene. Shown is an expanded view of the region corresponding to olefinic protons. The splitting pattern of each olefinic proton is also illustrated. The proton signals are assigned with aid of [1]H[1]H-COSY NMR.
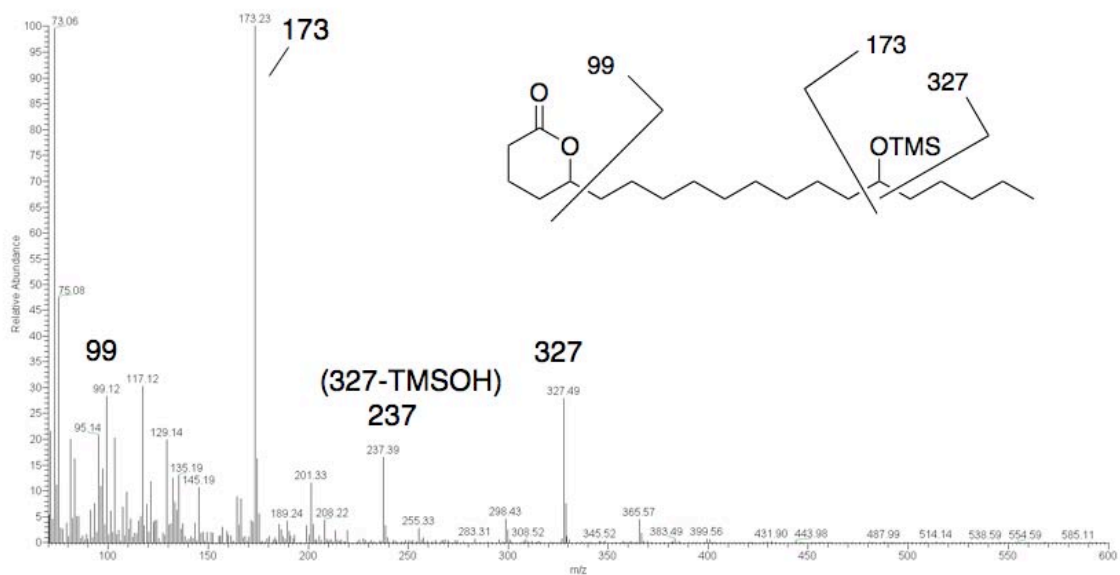
**Figure 60**: GC-MS analysis of the TMS ether of hydrogenated product **5**.

configurations of the four double bonds to be all *trans* (**Figure 59B**, **Figure 61**). Thus, product **4** is 5,15-dihydroxyeicosa-6*E*,8*E*,11*E*,13*E*-tetraenoic acid (5,15-all *trans*-diHETE) and product **5** is the corresponding δ-lactone.

<u>Products **4** and **5** are each a mixture of diastereomers</u>

Although each appeared as a single peak on RP-HPLC and SP-HPLC, each could be further resolved using a chiral HPLC column into a 50:50 mixture of two peaks with identical UV spectra. (Their NMR spectra are also identical, since there were no indications of a mixture of two sets of signals in the spectra of products **4** or **5**). Based on the reasonable assumption that the original *S* configuration of the substrate 15*S*-HPETE is retained in the 15-hydroxyl, we conclude that the peaks resolved on the chiral column are diastereomers rather than enantiomers, epimeric at C-5. This was confirmed using synthetic all-*trans*-diHETE prepared from a 2:1 mixture of 5*S*,15*S*- and 5*R*,15*S*-diHETE diastereomers. Similar to product **4**, this synthetic all-*trans*-diHETE chromatographed as a single peak on RP- and SP-HPLC. On the Chiralpak AD-RH column it resolved into the larger, earlier-eluting peak of 5*S*,15*S* followed by the later-eluting 5*R*,15*S* diastereomer. Mechanistic considerations that follow from the $H_2^{18}O$ experiments further support the conclusion that products **4** and **5** are each a mixture of diastereomers.

<u>The anaerobic reaction in $H_2^{18}O$</u>

To understand the origin of the hydroxyls in products **2**, **3**, **4** and **5**, we conducted the anaerobic reaction of soybean LOX-1 with 15*S*-HPETE in $^{18}O$-enriched water (80% $H_2^{18}O$), followed by HPLC purification of the individual products, catalytic hydrogenation, TMS ether TMS ester derivatization, and GC-MS analysis.
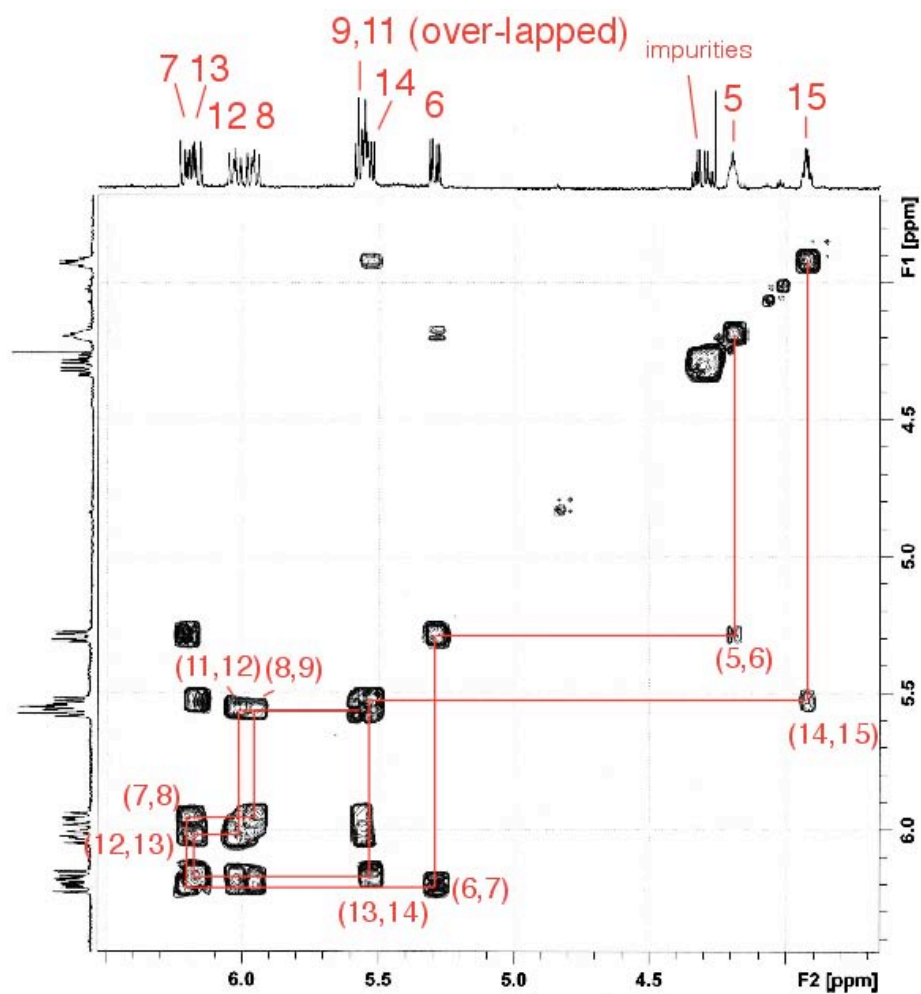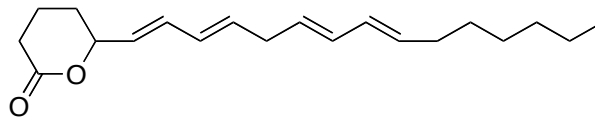
**Figure 61**: $^1$H,$^1$H-COSY NMR analysis of product **5** in d$_6$-benzene. Shown is an expanded view of the region corresponding to olefinic protons and protons on hydroxylated carbons. Assignment of H-6 and H-5 has been aided by comparison with the NMR spectra of chemically synthesized 5-trans,trans-HETE lactone (data not shown).

In the mass spectrum of the derivatized pair of 8,15-diols with all-*trans* conjugated trienes (products **2** and **3**) from the $H_2^{18}O$ reaction, the ions containing the 8-hydroxyl were all shifted by +2 mass units (i.e., ions at m/z 303 to 305, 359 to 361 and 489 to 491), while the m/z 173 fragment containing the 15-hydroxyl remained unchanged (**Figure 62, 63**). Quantitative analysis of the isotopic ratios revealed that the 8-hydroxyl derives exclusively from water, while the 15-hydroxyl derives from the 15-hydroperoxyl of the substrate.

In accord with the results on the 8,15-diols, and in sharp contrast to the known mechanisms of formation of 5,15-diHETE via double oxygenation, GC-MS analysis of derivatized all-*trans* 5,15-diHETE (product **4**), established that the 5-hydroxyl comes from water and the 15-hydroxyl from 15-hydroperoxyl group in the substrate, **Figure 64A**. Ions containing the 5-hydroxyl were shifted by +2 mass units (to m/z 263, 313 and 491), while m/z 173, the characteristic fragment ion of the 15-hydroxyl, remained unchanged.

By contrast, GC-MS analysis of the derivatized product **5**, the δ-lactone of all-*trans* 5,15-diHETE, indicated no $^{18}O$ incorporation in the molecule, **Figure 64B**. (The mass spectrum is identical to that of product **5** from $H_2^{16}O$ incubations). The lack of $^{18}O$ in the δ-lactone ring clearly demonstrated that product **5** was not formed by lactonization of product **4**. Instead, we surmise that the C-5 oxygen in the δ-lactone ring of product **5** must derive from the free carboxylate group in the substrate.

A cyclopropyl epoxide as the enzymatic product

The formation of products **4** and **5** can be explained if the true enzymatic product is an allylic 14,15-epoxide with a cyclopropane ring (**Figure 66**, Discussion). This
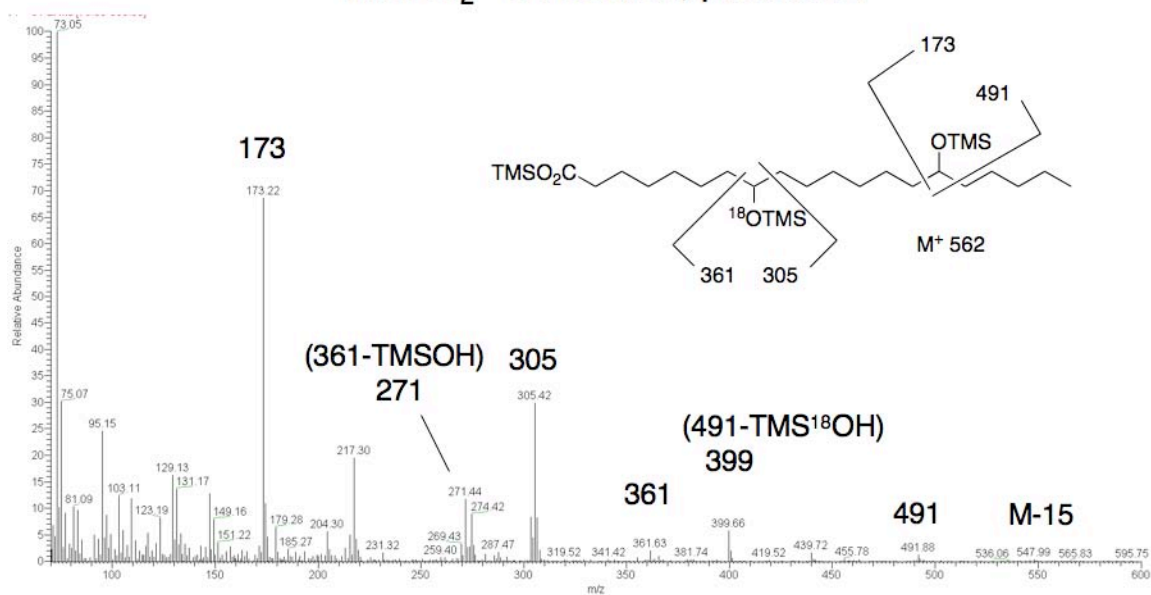
**Figure 62**: GC-MS analysis of the TMS ether TMS ester of hydrogenated product **2** from the H$_2^{18}$O incubation.
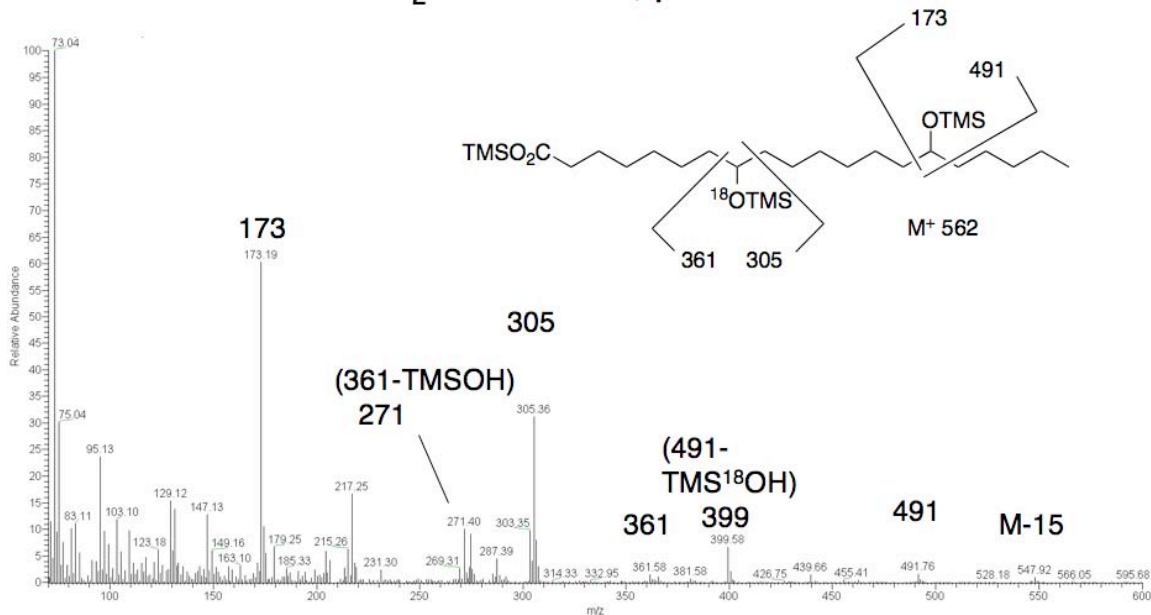


**Figure 63**: GC-MS analysis of the TMS ether TMS ester of hydrogenated product **3** from the H$_2^{18}$O incubation.

**A**



80% H$_2$$^{18}$O reaction, product **4**

**B**



80% H$_2$$^{18}$O reaction, product **5**
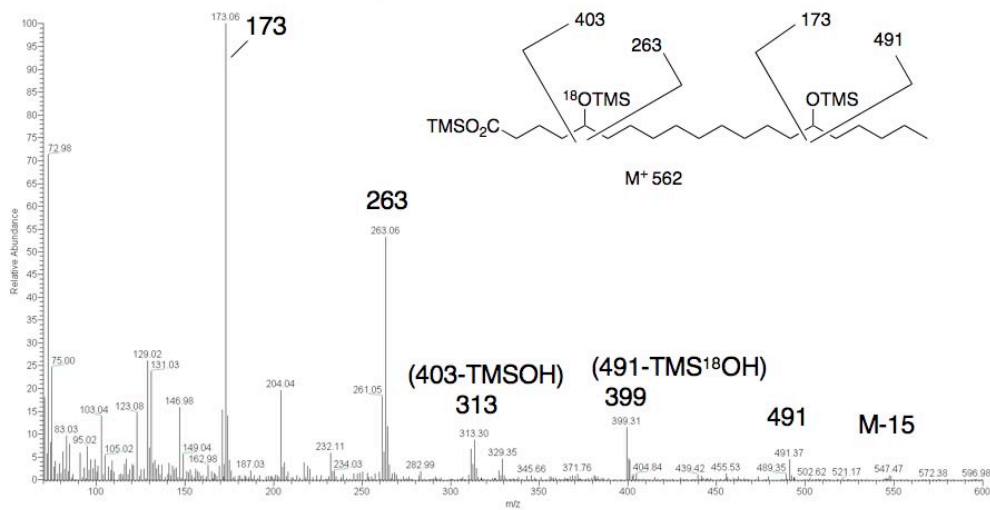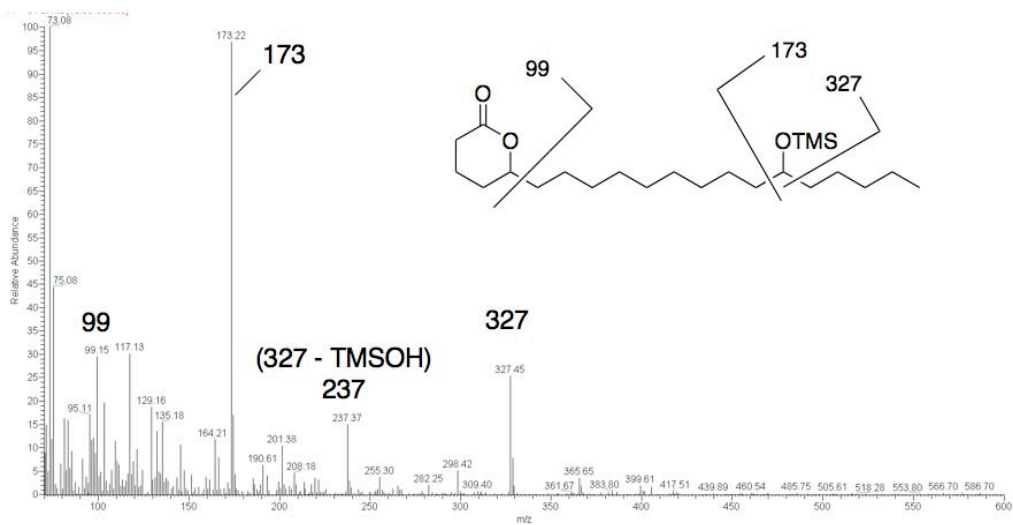
**Figure 64:** GC-MS analysis of TMS derivatized products **4** and **5** from the anaerobic reaction in H$_2$$^{18}$O. **(A)** The mass spectrum of the TMS ether TMS ester derivative of product **4**. **(B)** The mass spectrum of the TMS ether derivative of product **5**.

epoxide is opened up in one of two ways. Either water reacts at the end of the conjugated system to yield product **4** (with corresponding incorporation of $^{18}O$ from $H_2{}^{18}O$ at C-5), or nucleophilic attack by the free carboxylate yields the δ-lactone derivative with no involvement of water in the transformation.

## DISCUSSION

Background of this study

Soybean LOX-1 was the first LOX to be discovered and has since received the most extensive mechanistic studies among the LOX enzymes (5,171). Typically, the hallmarks of LOX catalysis, such as the antarafacial relationship between hydrogen abstraction and oxygen insertion, were first demonstrated for soybean LOX-1 and then recapitulated in studies on other LOX enzymes. One notable exception, however, is the LTA synthase-type activity. From a historical point of view, because no such chemistry had been described for soybean LOX-1, it was not immediately recognized at the time of the discovery of $LTA_4$ that the same enzyme, 5-LOX, catalyzes the formation of 5*S*-HPETE and $LTA_4$. The recognition came a number of years later when it was demonstrated that both 5-LOX and $LTA_4$ synthase activities involve stereoselective hydrogen abstraction as the initial step, always co-elute during purification, and are inhibited to similar extents by LOX inhibitors (172,173).

LTA synthase activity and LOX dual specificity

Both the primary LOX activity and the secondary LTA synthase activity start with hydrogen abstraction, yet at two different positions. Therefore, it has been suggested that

LTA synthase activity is a consequence of dual specificity, i.e., the ability of the enzyme to abstract hydrogens from two different positions and thus make two distinct hydroperoxides (173). Consistent with this suggestion, leukocyte 5-LOX gives the 8*S*-hydroperoxide from 8,11,14-eicosatrienoic acid (compared with the 5*S*-hydroperoxide from arachidonic acid) (174,175). Similarly, mammalian 15-LOX-1 usually gives a mixture of 15*S*-HPETE and 12*S*-HPETE from arachidonic acid (176). However, dual specificity alone does not ensure LTA synthase type activity; for instance, the dual specificity of soybean LOX-1 is evidenced by the formation of 8*S*,15*S*-diHPETE and 5*S*,15*S*-diHPETE in its double oxygenation reaction with 15*S*-HPETE (160), yet no LTA synthase type activity has ever been detected for this enzyme under the usual aerobic conditions.

## LTA synthase activity and active site oxygen

We hypothesize that oxygen concentration in the enzyme active site is an additional factor that determines whether LTA synthase type activity will be present in a LOX or not, through influence on the rate of the competing process, double oxygenation. When oxygen concentration is low, as we would propose in the 5-LOX active site, double oxygenation barely occurs due to deprivation of oxygen co-substrate, so LTA synthase activity will occur without interference. By contrast, at high active site oxygen concentrations, as in soybean LOX-1, double oxygenation occurs so fast that LTA synthase type activity will be fully suppressed. To relieve this potential suppression of LTA synthase type activity imposed by molecular oxygen, here we performed the reaction of soybean LOX-1 with 15*S*-HPETE under anaerobic conditions. Consistent with our hypothesis, we observed under these conditions the formation of 8(*RS*),15*S*-

*Z,E,E,E*-diHETEs, the expected hydrolysis products from 14,15-LTA$_4$ (or the *cis* epoxide isomer, see below). This result strongly supports our view that the soybean LOX-1 has all the essential elements to fulfill the role of a LTA synthase, yet this potential has been obscured by the presence of high concentrations of oxygen in the active site, which favors the double oxygenation reaction.

An oxygen channel in the LOX protein might normally target O$_2$ to the correct position on the reacting substrate (10,177), or alternatively there could be an appropriately positioned oxygen pocket in the active site (11). Either way, oxygen could be well positioned for one substrate (e.g. arachidonic acid in mammalian 5-LOX) and out of place for another (5*S*-HPETE in 5-LOX), while adequately positioned for either arachidonic acid or 15*S*-HPETE in soybean LOX. It is expected that the K$_m$(O$_2$) for soybean LOX-1 using 15*S*-HPETE as substrate would be considerably lower than the K$_m$(O$_2$) for mammalian 15-LOX using the same substrate, or the K$_m$(O$_2$) for 5-LOX using 5*S*-HPETE. These values for fatty acid hydroperoxide substrates remain to be determined. Yet, evidence does exist that suggests a high K$_m$(O$_2$) for LOX that normally exhibit LTA synthase activity; for example, a large K$_m$(O$_2$) can be deduced from the observation that potato 5-LOX shows double oxygenation activity with 5*S*-HPETE only under high oxygen pressures (162). It would be of interest to test whether a similar switch occurs with mammalian 5-LOX or 15-LOX under hyperbaric conditions.

<u>The oxidation state of the enzyme involved in LTA synthesis</u>

Next, we questioned which enzyme form, Fe(III) or Fe(II) soybean LOX-1, is responsible for the formation of 8(*RS*),15*S*-*Z,E,E,E*-diHETEs. Although it is widely accepted that the Fe(III) LOX accounts for LTA synthesis, an alternative Fe(II) LOX

165

pathway, originally proposed for LT formation in fatty acid autoxidation (178) and in hemoglobin-catalyzed transformation of fatty acid hydroperoxides (179,180), is also feasible on purely chemical grounds (**Figure 65**). The key difference of the two pathways is the order of the two chemical steps, hydrogen abstraction and peroxide bond cleavage; while the Fe(III) LOX pathway involves hydrogen abstraction followed by peroxide bond cleavage, the Fe(II) LOX pathway employs the same two steps in the reverse order. To clarify this issue in the present case, we dissected the anaerobic reaction of soybean LOX-1 with 15*S*-HPETE into two components: one catalyzed by the Fe(II) enzyme and the other by the Fe(III) enzyme, using NDGA and 13*S*-HPODE to keep the enzyme ferrous and ferric, respectively. We found that 8(*RS*),15*S*-Z,E,E,E-diHETEs are formed in the presence of 13*S*-HPODE but not in the presence of NDGA, thus determining unambiguously that the Fe(III) enzyme is the catalytic species in the soybean LOX-1 catalyzed formation of 14,15-LTA$_4$ and the corresponding 8,15-diol hydrolysis products. Our result agrees well with the early studies using stereospecifically tritium-labeled arachidonic acid that established hydrogen abstraction as the first irreversible step in LT synthesis (172), and also agrees with the studies using LOX inhibitors that demonstrated the inhibitory effect of NDGA on LT formation from HPETEs, although at these early times the mechanism of inhibition of NDGA (159,173), i.e., by reduction of Fe(III) LOX to Fe(II) LOX, had yet to be clarified (27).

The proposed cyclopropyl epoxide intermediate leading to 5(RS),15S-all trans-diHETEs and the δ--lactone derivatives

The most intriguing finding in the present study is probably the detection of the novel compounds, 5(*RS*),15*S*-all *trans*-diHETEs and the δ--lactone derivatives. Inspired

166

by the structural similarities of 5(*RS*),15*S*-all *trans*-diHETEs to 8(*RS*),15*S*-*Z,E,E,E*-diHETEs, the shared involvement of the Fe(III) enzyme in the formation of both, and similar incorporations of $H_2^{18}O$, we propose that the 5(*RS*),15*S*-all *trans*-diHETEs are also hydrolysis products of an unstable intermediate, formed in a mechanism with parallels to the synthesis of 14,15-LTA$_4$. A feature of our proposal is involvement of first the ferric enzyme and then the ferrous species in activation at the two pentadiene units, followed by intramolecular coupling of two radicals to give un unstable epoxide which, upon hydrolysis, gives the 5,15-diols containing four *trans* double bonds. Notably, a directly analogous mechanism can explain LTA$_4$ or 14,15-LTA$_4$ synthesis.

As illustrated in **Figure 66**, similar to 14,15-LTA$_4$ formation, hydrogen abstraction by the Fe(III) enzyme is the initial step, but it occurs at C-7 rather than C-10 to form a carbon-centered radical delocalized over the C5-C9 pentadiene. This initial step produces the Fe(II) enzyme which then induces homolytic cleavage of the O-O bond of the 15-hydroperoxide group to give an alkoxyl radical at the C11-C15 pentadiene. At this stage the reacting intermediate exists as an oxygen-centered and carbon-centered biradical. Due to its intrinsic instability, this biradical would rearrange, by reacting the oxygen-centered radical with the nearby double bonds to form an epoxide group and a second carbon- centered radical, followed by combination of the two carbon-centered radicals to form a new C-C bond, to give a covalently complete compound, an allylic 14,15-epoxide with a cyclopropane ring comprised of C-9, C-10, and C-11, namely 14,15-epoxy-[9,10,11-cyclopropyl]- eicosa-5*Z*,7*E*,13*E*-trienoic acid.
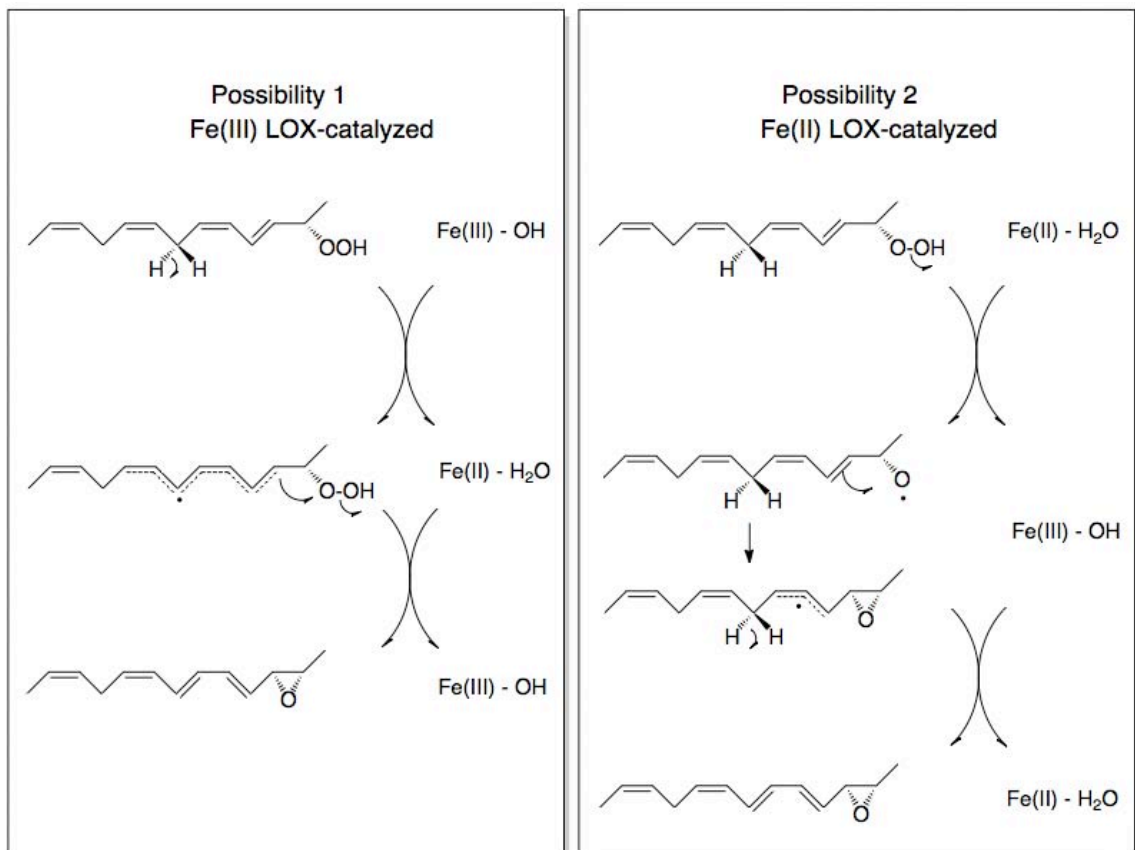
Figure 65: Two possible pathways of LTA formation on purely chemical grounds.
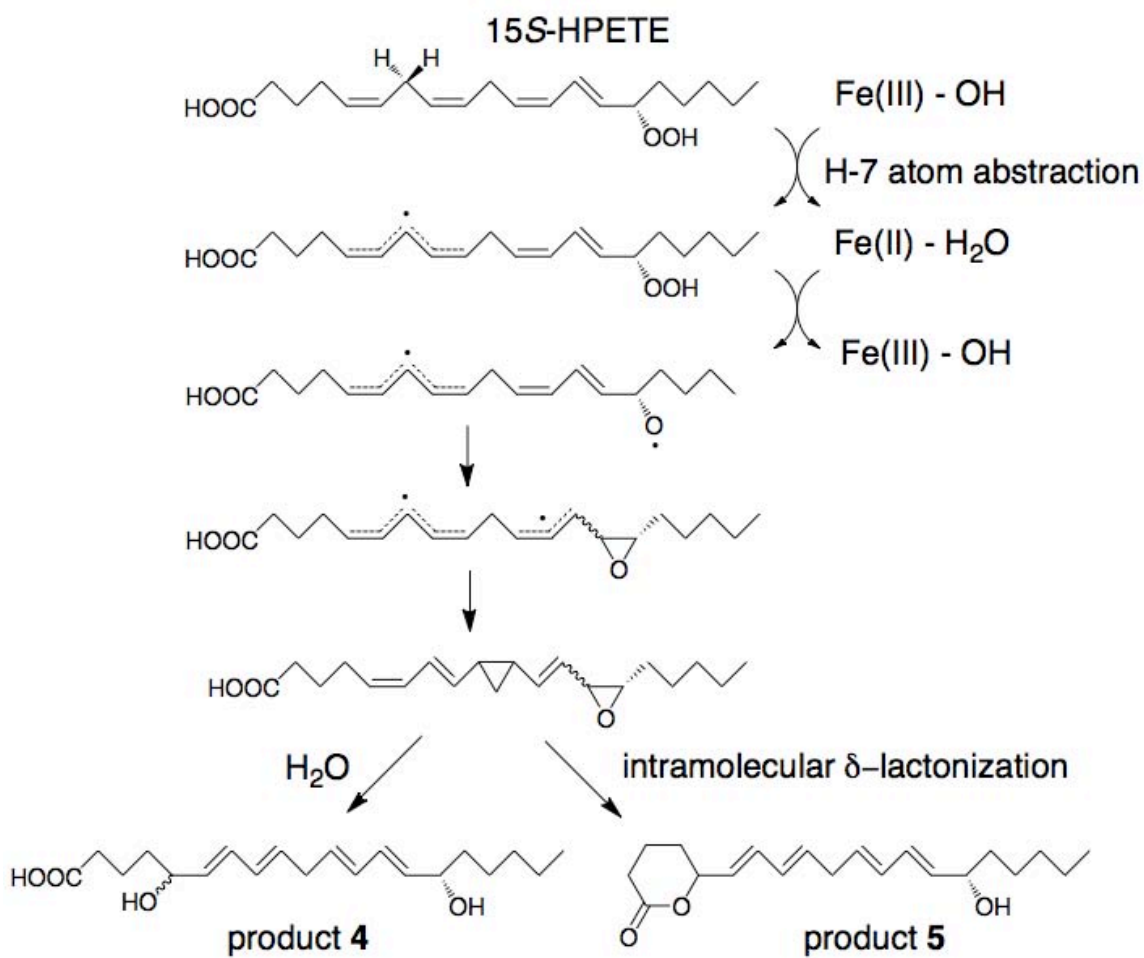
**Figure 66**: Proposed mechanism of formation of products 4 and 5.

Similar to other allylic epoxides, at non-alkaline pHs this cyclopropyl epoxide may react with even the weakest nucleophiles, such as water in aqueous solutions to give 5(*RS*),15*S*-all *trans*-diHETEs, or the carboxylate group in the molecule itself to give the corresponding δ--lactones. As water is involved in the former but not the latter process, only the 5(*RS*),15*S*-diols and not the δ--lactones incorporate water at C-5, exactly what we found using $H_2^{18}O$. Finally, as a subtle point of the proposed mechanism, the cyclopropane ring is formed only in the covalently complete final product, as opposed to in any radical intermediates, because such radical intermediates containing a cyclopropane ring and an adjacent radical would be highly energetically unfavorable (181).

The stereochemistry of the epoxide group in the putative 14,15-LTA$_4$ and the cyclopropyl epoxide intermediates cannot be determined based on the analysis of the hydrolysis products in the present study. Although perhaps not widely recognized, LOX-catalyzed formation of the *cis* epoxy isomer of allylic epoxides has been documented and the *cis* epoxy isomer would hydrolyze to the same set of products as the *trans* epoxide isomer, with only a subtle difference in the product ratios (162).

Concluding remarks

In summary, our study demonstrates the competition between dioxygenation, which requires the presence of appropriately positioned molecular oxygen in the LOX active site, and leukotriene biosynthesis, which proceeds anaerobically. For an enzyme such as soybean LOX-1 in which O$_2$ is readily available for dioxygenation reactions, leukotriene biosynthesis is not observed until the enzyme is placed in an anaerobic environment. Conversely, we surmise that in LOX enzymes in which leukotriene

synthesis occurs under aerobic conditions, molecular oxygen is less readily available in the active site. In the case of soybean LOX-1, the dioxygenase reactions on 15$S$-HPETE are initiated via hydrogen abstractions at C-7 and C-10, giving 5$S$,15$S$-diHETE and 8$S$,15$S$-diHETE respectively, and the LTA synthase type of reactions are initiated in the same way under anaerobic conditions (**Figure 67**). The hydrogen abstraction at C-7 leads to formation of the novel cyclopropyl-containing epoxide, which in turn gives the 5,15-diols with all-*trans* double bonds and the corresponding δ-lactones.

In addition to driving reaction reaction initiated by the Fe(III) enzyme down the LT synthase pathway, a lack of active site oxygen may play a role in other non-canonical reactions of lipoxygenases. An example from the present study is formation by the Fe(II) enzyme of the *threo*-13-hydroxy-14,15-*trans*-epoxyalcohol, the 15-ketone and $C_{15}$ aldehyde. These reactions strongly resemble those of two unusual lipoxygenases that appear to be structurally intact and yet catalyze no detectable formation of fatty acid hydroperoxides with any natural polyunsaturated fatty acid. One of these, a specific LOX enzyme in maize (ZmLOX6) acts as a hydroperoxide lyase (129), forming aldehydes of the type found with the anaerobic soybean LOX-1. The other is the epidermal LOX-3 of mammalian skin, known from genetic studies to be required for proper differentiation in the epidermis and which displays hydroperoxide isomerase activity (37,96), forming epoxyalcohols and ketones, again similarly to the anaerobic soybean LOX-1. In both cases, a lack of available oxygen within the active site may contribute to both the lack of activity with natural fatty acids and the acquisition of new activities with fatty acid hydroperoxides. The concept of a limited access to oxygen within the lipoxygenase active site as a basis for new activities might also be extended to include the plant "type-II"

LOX enzymes such as soybean LOX-3 that catalyze mainly non-specific peroxidation of fatty acids and their esters and further conversion of the hydroperoxide products to ketones (127,128). In their case it appears that hydrogen abstraction is followed by release of the fatty acid radical and that reaction with oxygen occurs outside the LOX active site. The enzyme, being left in the ferrous state, would in turn react with fatty acid hydroperoxides to give alkoxyl radicals that lead eventually to ketones. A lack of access to oxygen within the active site may prompt this outcome.

Finally, we note the implications for the mechanism of leukotriene $A_4$ synthesis based on the proposed mechanism of formation of the epoxy-cyclopropyl fatty acid. The involvement of both the ferric and ferrous iron and the production of a fleeting biradical species in both types of reaction are strongly implied.

**AEROBIC REACTIONS**

**15S-HPETE**

pro-R H-7
abstraction / $O_2$     $O_2$ \ pro-R H10
abstraction

**5S,15S-diHPETE**          **8S,15S-diHPETE**

**ANAEROBIC REACTIONS**

**15S-HPETE**

pro-R H-7
abstraction     $H_2O$     $H_2O$     pro-R H10
abstraction

**14,15-epoxy-5Z,7E,12E**          **14,15-epoxy-5,8,10,12-20:4**
**(9,10,11)-cyclopropyl-20:3**          **(14,15-LTA$_4$)**

$H_2O$          $H_2O$

**5,15-diHETE**          **8,15-diHETE**
**6E,8E,11E,13E**          **5Z,9E,11E,13E**
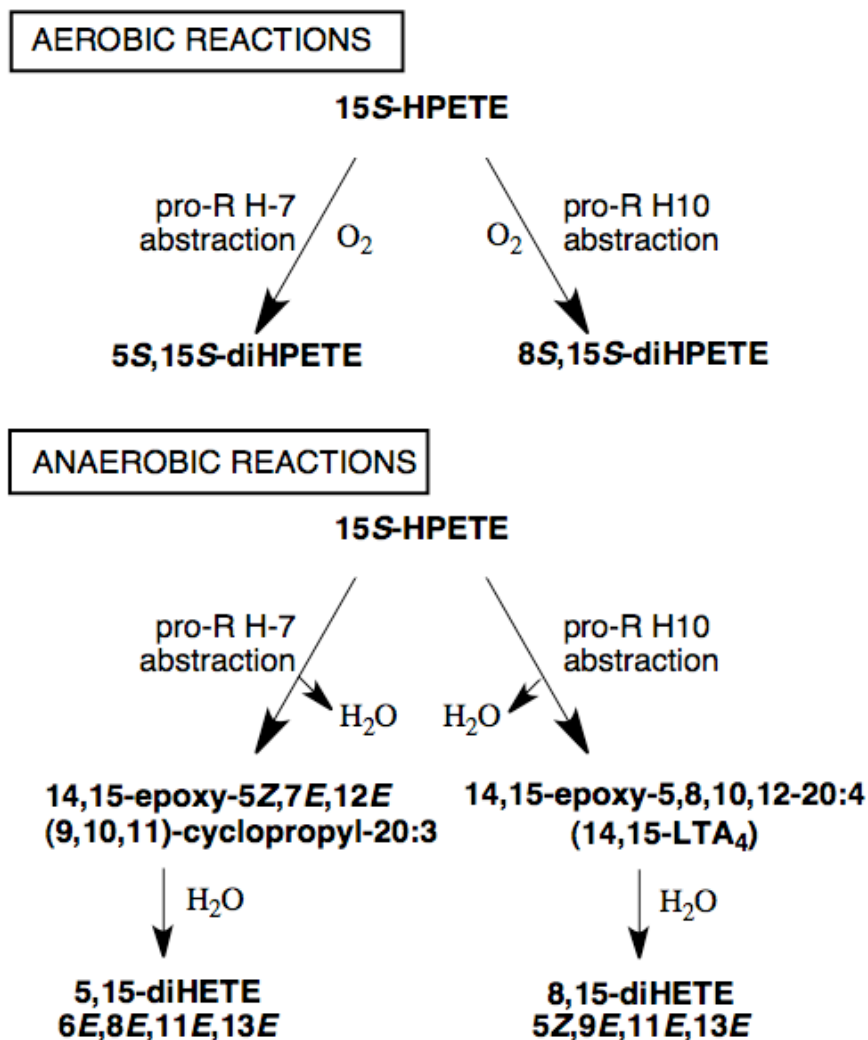
**Figure 67**: Comparison of the aerobic and anaerobic reactions of soybean LOX-1 with 15S-HPETE. Aerobic reaction is initiated by the H-7 and H-10 hydrogen abstractions (pro-R hydrogens, designated as in arachidonic acid rather than 15S-HPETE) with 15S-HPETE in the reversed orientation, antarafacial oxygenation giving the 5S,15S-diHPETE and 8S,15S-diHPETE products, respectively (1,160,182). Anaerobically, analogous hydrogen abstractions can account for formation of the cyclopropyl epoxide and 14,15-LTA$_4$, respectively, followed by non-enzymatic hydrolysis to give the stable diol end products.

# CHAPTER VI

## PARTIALLY RESOLVED ISSUES, OPEN QUESTIONS, AND FUTURE

## DIRECTIONS

**1.** Why does not eLOX3 make a single product? In its classical reaction with 12*R*-HPETE, the epoxyalcohol and 12-KETE are formed in a ratio of 60:40. Both derive from a common alkoxyl/epoxyallylic radical intermediate. Ketone is formed by loss of a hydrogen atom, whereas epoxyalcohol is formed via "oxygen rebound". One is dehydration, the other isomerization. (A similar problem exists for allene oxide synthase, see ref. (183)) One possible explanation is that two orientations can be used by eLOX3 with the same substrate. Consistent with this, I found that 9*R*-HPODE or 11*R*-HPETE is by eLOX3 converted to a mixture of a type A epoxyalcohol and 9-KODE, but 9*R*-HPODE/lyso PC or 11*R*-HPETE/lyso PA (a large ester, head-first orientation prohibited) is converted by the enzyme nearly exclusively to the epoxyalcohol derivative (**Figure 68**).

Interestingly, I also found that Ala451Gly or Phe409Leu mutations in eLOX3 specifically diminished type-A epoxyalcohol products while retaining type-B epoxyalcohol and ketone products from the reactions of eLOX3 with all fatty acid hydroperoxides tested, including 12*R*-HPETE, 15*S*-HPETE, 12*S*-HPETE, 8*R*-HPETE (methyl ester), 11*R*-HPETE and 9*R*-HPODE. (Although Ala451Gly eLOX3 converts 15*S*-HPETE to mostly epoxyallylic hydroperoxides under aerobic conditions, its ability to make type-B epoxyalcohol and 15-KETE as the wild-type enzyme is revealed under

anaerobic conditions, Chapter II.) This suggests that formation of type-A epoxyalcohol is an event independent of formation of type-B epoxyalcohol and ketone, and the former is more readily perturbed by active site mutations.

Finally, I noted that with the exception of 12*S*-HPETE, every *R*-hydroperoxide is transformed by eLOX3 to type-A epoxyalcohol, and every *S*-hydroperoxide to type-B epoxyalcohol. The mechanistic basis for this remains to be explored.

**A**
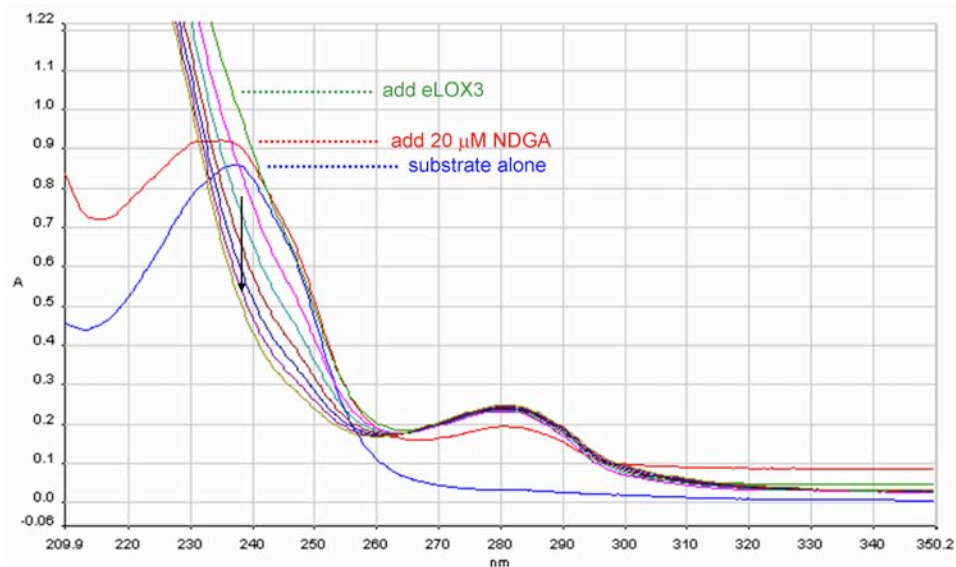


**B**
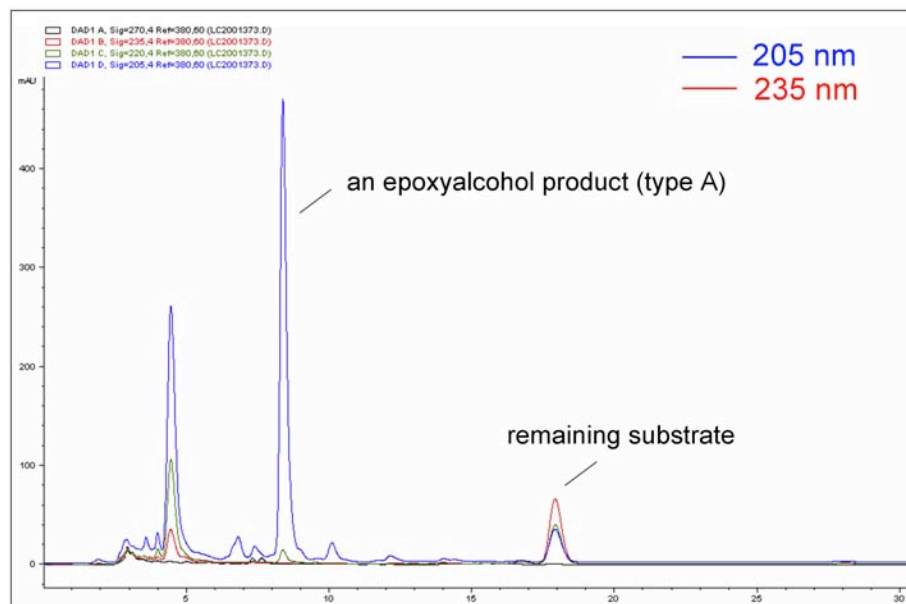


**Figure 68**: Reaction of human eLOX3 with 11*R*-HPETE/lyso PA. (**A**) UV scans. The reaction was carried out in 0.5 ml of 50 mM sodium phosphate pH 7.5. 11*R*-HPETE/lyso PA was synthesized by reacting Anabaena LOX with AA/lyso PA. After adding the enzyme, a scan was immediately taken (t ~ 15 s). The subsequent scans were taken every 2 min. (**B**) RP-HPLC analysis. The reaction products were hydrolyzed to free acids by mild alkaline hydrolysis. Similar results were obtained using 9*R*-HPODE/lyso PC as substrate.

176

**2.** While the influence of substrate orientation on product specificity of eLOX3 is largely unexplored (Future Direction **1**, above), the influence of substrate orientation on product specificity of conventional LOX enzymes has been studied extensively. From these and other studies, Dr. Coffa and Dr. Brash in this group have proposed a general model to explain the regio- and stereospecificity of most LOX enzymes (12). This model predicts that 9*S*-HPODE/lyso PC will not made by any LOX in reacting with LA/lyso PA, because "9*S*" specificity is associated with "head-first" substrate orientation, which is strongly disfavored by LA/lyso PA due to its bulky polar head group. In contrast to this prediction, in the reaction of Arabidopsis 9*S*-LOX with LA/lyso PA, I identified 9*S*-HPODE/lyso PA as a major product (9*S*:9*R*~ 63:37) (**Figure 69**). Does this imply that at least some LOX enzymes have a U-shaped substrate channel with both ends open (17)?

**Figure 69A**
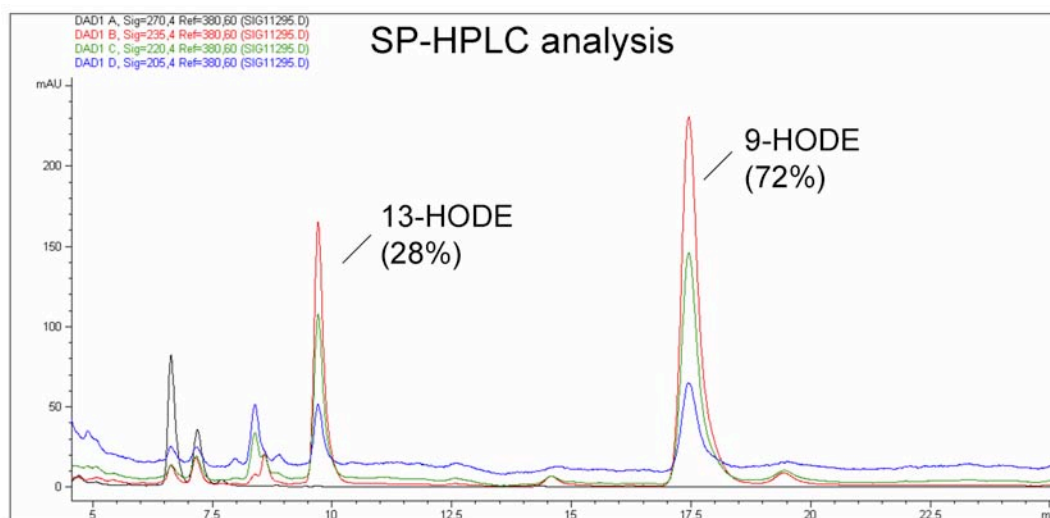
**B**
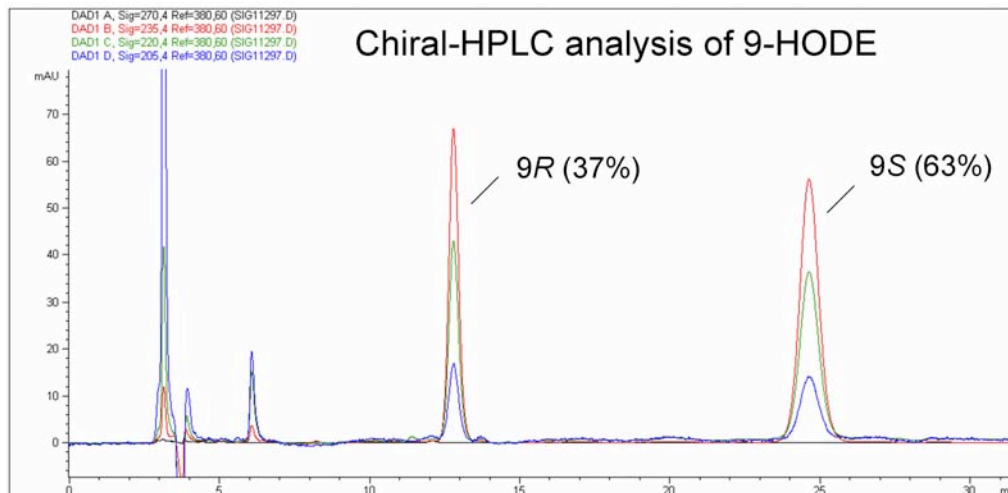


**C**
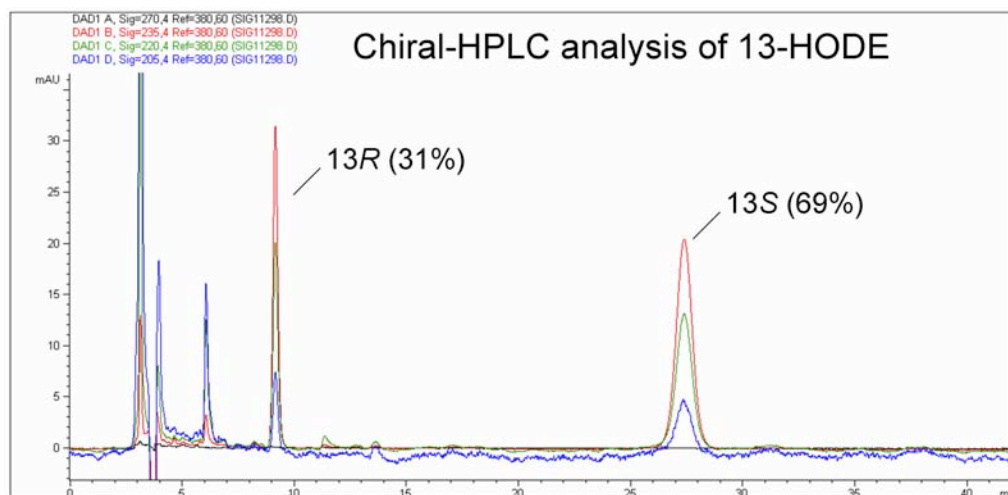


**Figure 69**: Reaction of Arabidopsis LOX with LA/lyso PC in the presence of 4-hydroxy-TEMPO. The products were reduced with TPP and then hydrolyzed to free acids by mild alkaline hydrolysis. (**A**) SP-HPLC analysis. (**B**)&(**C**) Chiral HPLC analysis of 9-HODE and 13-HODE products respectively.

**3.** One finding that has intrigued me is that a specific epoxyalcohol is formed in the so-called purple enzyme degradation (Purple enzyme refers to the complex between ferric soybean LOX-1 and 13$S$-HPODE, see Chapter I). Related to this reaction is the not well-known linoleic acid-independent anaerobic reaction of soybean LOX-1 with 13$S$-HPODE, which was reported to give a specific epoxyalcohol. Because the purple enzyme is in the ferric state and the enzyme after the degradation remains ferric, I once considered that the epoxyalcohol is made by the ferric enzyme rather than the ferrous enzyme, via a mechanism similar to that of hematin, from non-heme $Fe^{3+}$ to $Fe^{4+}$-OH, then back to $Fe^{3+}$. However, there is no indication in the literature that the non-heme iron in LOX enzymes could exist in higher oxidation states. My repeated attempts to reproduce the purple enzyme degradation and the related LA-independent anaerobic reactions proved to be futile, and it seemed that I always obtained a mixture of epoxyalcohols rather than a single one. Possibilities include: 1) my enzyme brought from Cayman Chemical was in bad shape – this is not entirely impossible since I have detected a "gain-of-function" activity in the Cayman enzyme, which I will describe later; 2) in the early days, the standard protocol often stated acidification to pH 2-3 before extraction, and this might have selectively retained one epoxyalcohol and destroyed others.

One explanation for linoleic acid-independent anaerobic reaction of soybean LOX-1 with 13$S$-HPODE is that whereas the ferrous enzyme reacts with the fatty acid hydroperoxide to give an alkoxyl/epoxyallylic radical, the ferric enzyme reacts with the fatty acid hydroperoxide to give a peroxyl radical. This hypothesis predicts that the epoxyallylic radical should readily combine with the peroxyl radical to give peroxide-linked dimers. Using Cayman soybean LOX-1 (Cayman Chemical Item Number 60700),

I was able to identify a group of peroxide-linked dimers as the major products in its reaction with 13$S$-HPODE methyl ester. Kinetic measurements clearly showed that this reaction was catalytic. Addition of NDGA to the incubation resulted instead in self-combination of the epoxyallylic radical forming C-C linked dimers, further suggesting that the ferric enzyme was involved in making the peroxyl radical. This finding fascinated me and was thus followed by extensive analytical chemical work that culminated in unambiguous identification of the structure of the major dimer by GC-MS, LC-MS, and NMR (**Figure 70**, **Figure 71**, LC-MS analysis of the hydrolyzed sample showed m/z 605.5, not shown). However, it seems that this reaction could not be reproduced using Sigma soybean LOX. Thus questions remain as to whether this observation was an artifact brought by impurities/additives in the "purified" Cayman soybean LOX-1 or was a bona fide reaction readily inhibited by impurities in the Sigma soybean LOX preparation.

# Figure 70A
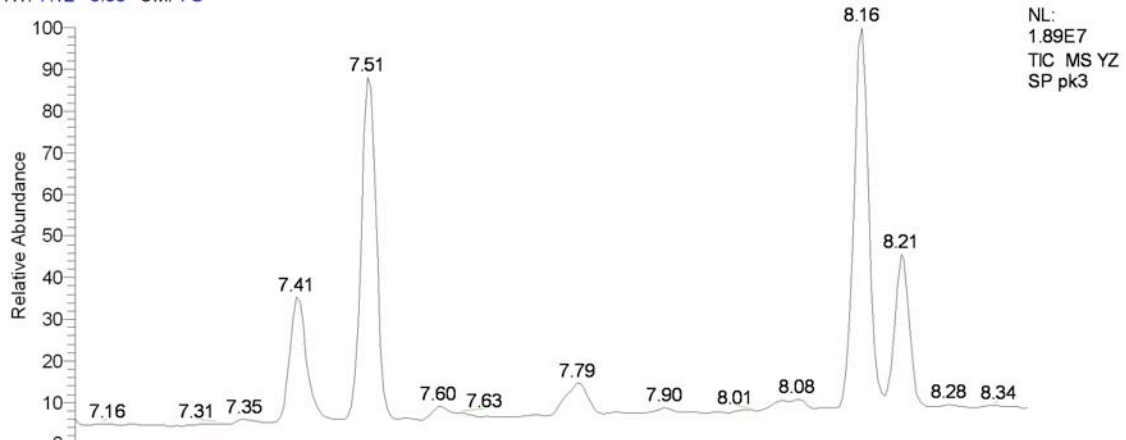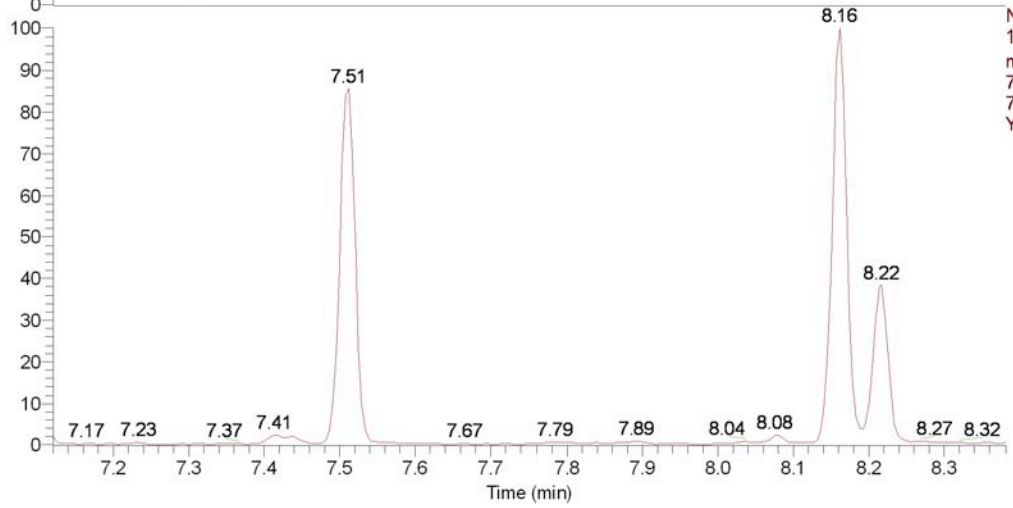
# Figure 70B



YZ SP pk3 #1398-1415  RT: 7.47-7.54  AV: 18  SB: 50 6.16-6.26 , 6.52-6.62  NL: 1.35E6
T: + c Full ms [70.00-600.00]
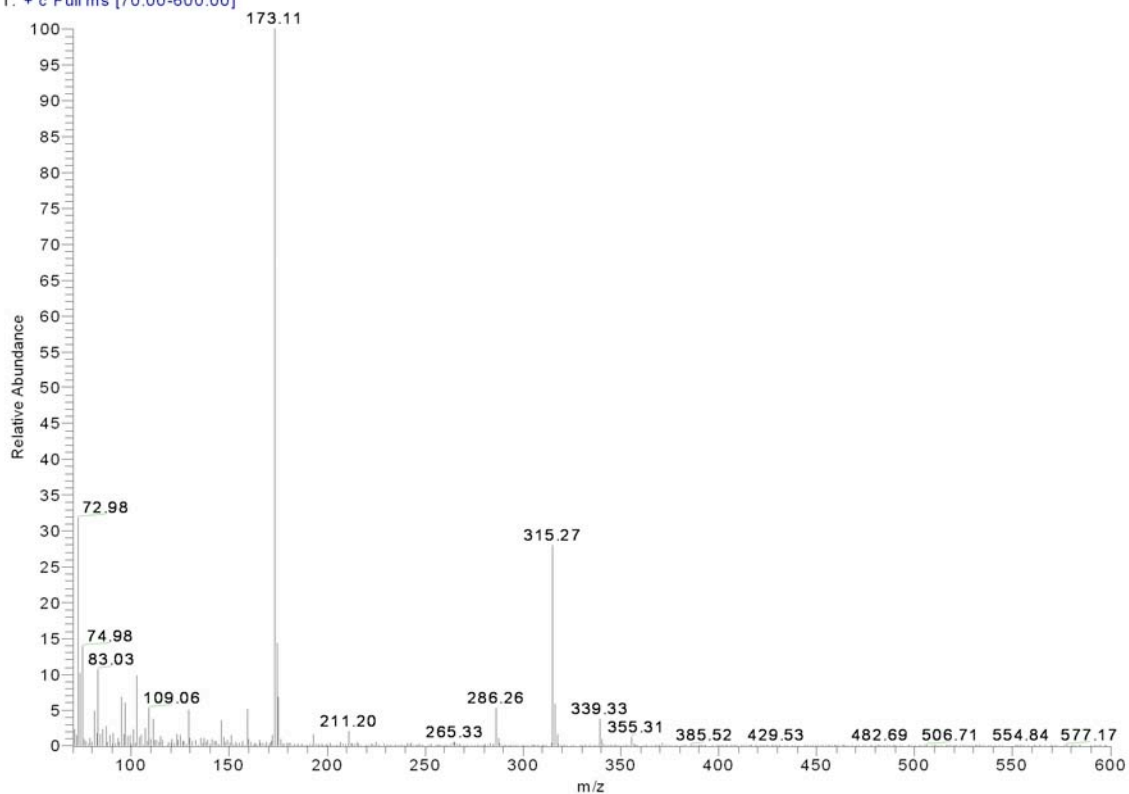
# Figure 70C
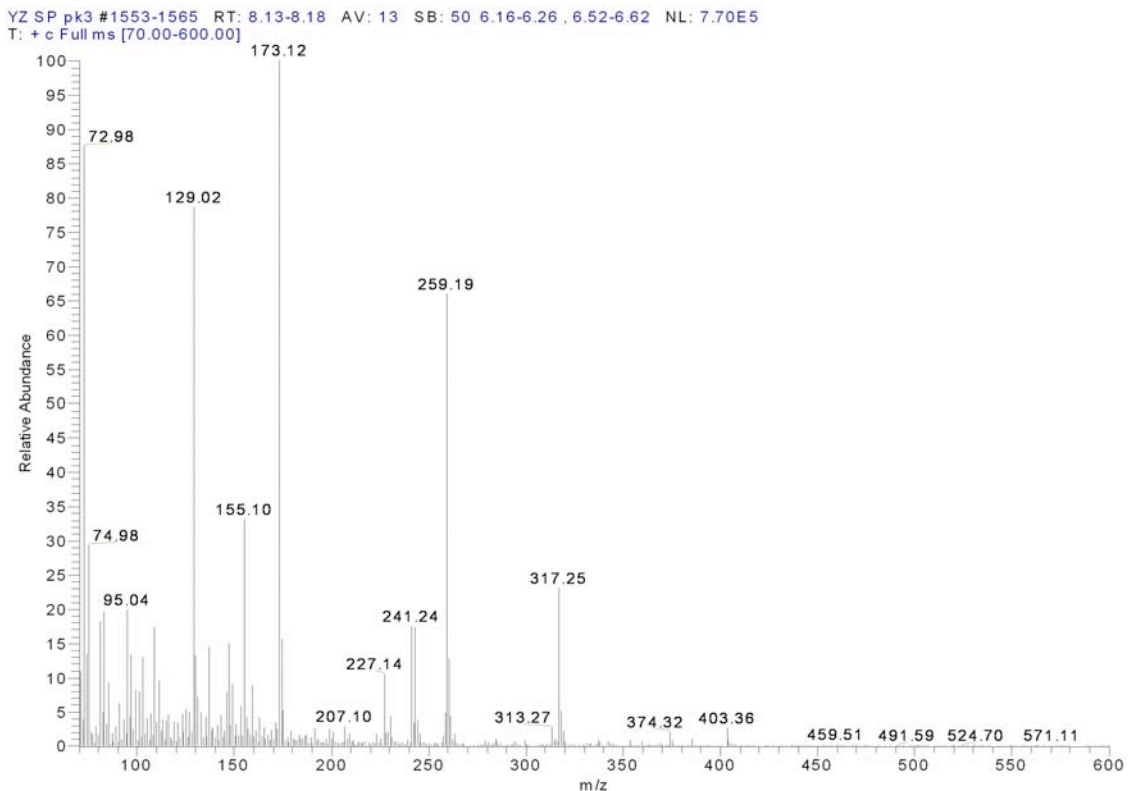


**Figure 70:** GC-MS analysis of the major peroxide-linked dimer after catalytic hydrogenation and TMS derivatization. The major dimer was purified by both RP- and SP-HPLC. Hydrogenation reduces peroxide bonds and double bonds, and opens up the epoxide group. (**A**) Top: total ion trace. Bottom: selective ion trace at m/z 73, showing compounds with TMS group. (**B**) Mass spectrum of the eluate at 7.51 min, which identified the peak as 18:0, 13-OTMS. (**C**) Mass spectrum of the eluate at 8.16 min, which identified the peak as 18:0, 9-OTMS, 13-OTMS.

**(A)**
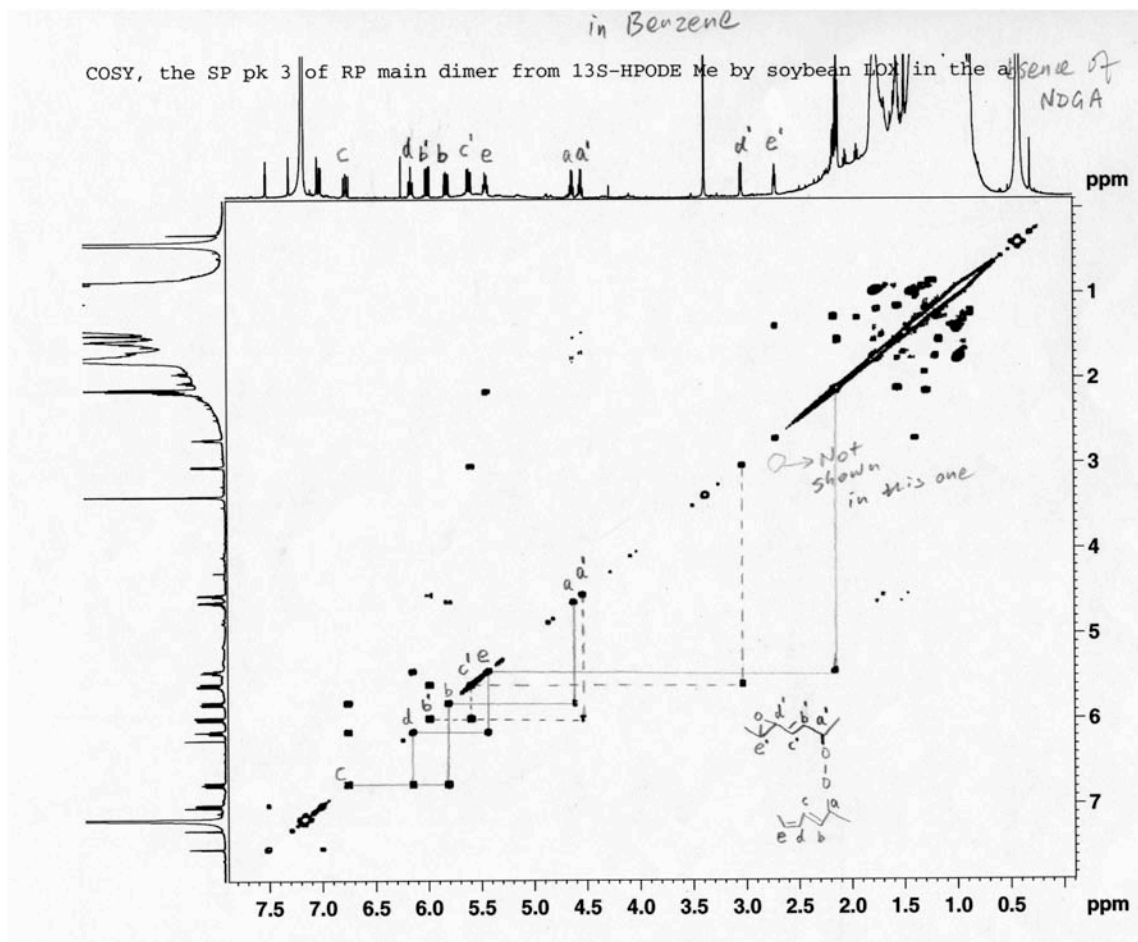


**(B)**
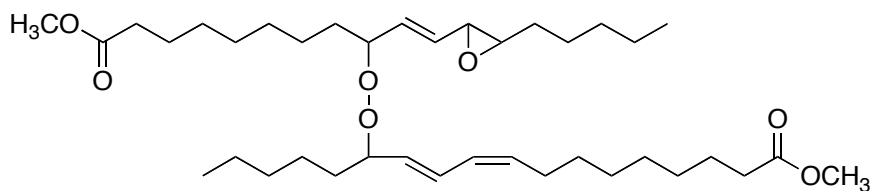


**Figure 71**: **(A)** $^1$H,$^1$H-COSY NMR spectrum of the major peroxide-linked dimer from the anaerobic reaction of Cayman soybean LOX-1 with 13*S*-HPODE methyl ester. **(B)** Chemical structure of the compound as established by GC-MS (after catalytic hydrogenation), LC-MS (after alkaline hydrolysis), and NMR.

184

**4.** Almost every conjugated HPETE or HPODE is an eLOX3 substrate, how about bisallylic hydroperoxides (e.g., 7-HPETE, a major oxygenation product of eLOX3)? Cumene hydroperoxide? The alkoxyl radicals derived from these hydroperoxides show different chemistry from those derived from conjugated HPETEs. These experiments were considered in 2007, but were not actually done.

**5.** An incidental finding: conversion of 13-*cis,trans*-HPODE by sodium dithionite to 9-*trans,trans*-HODE (**Figure 72**). Sodium dithionite was newly purchased from Sigma-Aldrich. 13-*cis,trans*-HODE did not react with sodium dithionite. What surprised me was 1) that very little, if any, 13-*trans,trans*-HODE was formed in this reaction; 2) using newly purified [1-$^{13}$C]-13$S$-HPODE, I found that ~ 50% radioactivity remained in the aqueous phase after acidification to pH 3 and extraction by methylene chloride. Control experiments showed that no radioactivity remained in the aqueous phase if sodium dithionite was omitted. The radioactive metabolite in the aqueous phase seemed not to be volatile and remains to be identified.
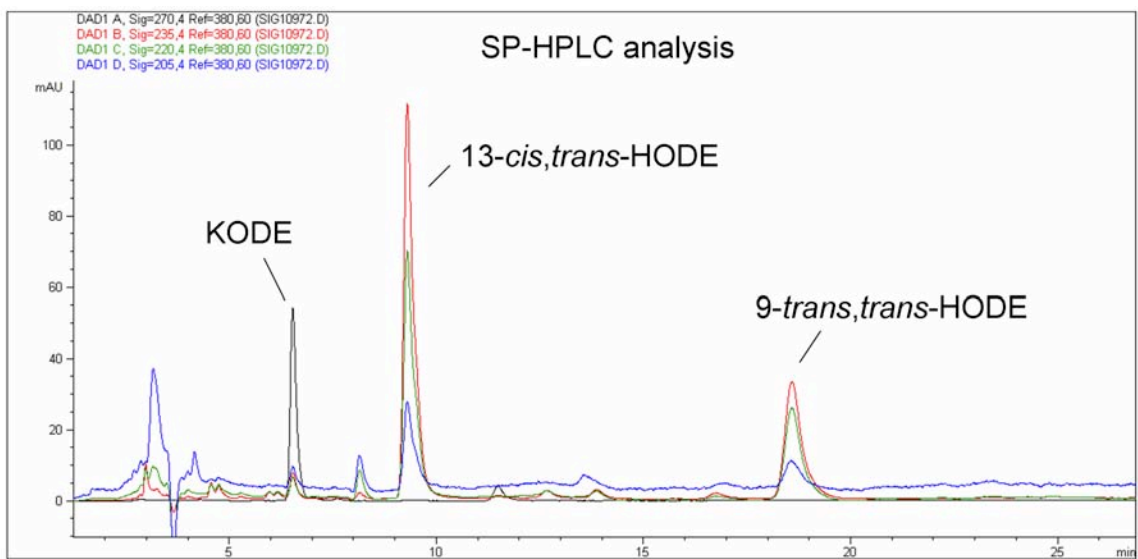
**Figure 72**: SP-HPLC analysis of the reaction of 13-HPODE (100 μM) and sodium dithionite (1 mM) in 50 mM sodium phosphate pH 7.5. Incubation time was 30 min.

## REFERENCES

1.      Brash, A. R. (1999) *J. Biol. Chem.* **274**, 23679-23682

2.      Funk, C. D. (2001) *Science* **294**, 1871-1875

3.      Samuelsson, B., Dahlen, S. E., Lindgren, J. A., Rouzer, C. A., and Serhan, C. N. (1987) *Science* **237**, 1171-1176

4.      Schewe, T., Rapoport, S. M., and Kuhn, H. (1986) *Adv. Enzymol.* **58**, 191-272

5.      Vliegenthart, J. F. G., and Veldink, G. A. (1982) *Free Radic. Biol.* **5**, 29-64

6.      Que, L., Jr., and Ho, R. Y. (1996) *Chem. Rev.* **96**, 2607-2624

7.      Pratt, D. A., Mills, J. H., and Porter, N. A. (2003) *J. Am. Chem. Soc.* **125**, 5801-5810

8.      Nelson, M. J. (1988) *Biochemistry* **27**, 4273-4278

9.      Knapp, M. J., Seebeck, F. P., and Klinman, J. P. (2001) *J. Am. Chem. Soc.* **123**, 2931-2932

10.     Saam, J., Ivanov, I., Walther, M., Holzhutter, H. G., and Kuhn, H. (2007) *Proc. Natl. Acad. Sci. U S A* **104**, 13319-13324

11.     Schneider, C., Pratt, D. A., Porter, N. A., and Brash, A. R. (2007) *Chem. Biol.* **14**, 473-488

12.     Coffa, G., Schneider, C., and Brash, A. R. (2005) *Biochem. Biophys. Res. Commun.* **338**, 87-92

13.     Andreou, A. Z., Vanko, M., Bezakova, L., and Feussner, I. (2008) *Phytochemistry* **69**, 1832-1837

14.     Coffa, G., and Brash, A. R. (2004) *Proc. Natl. Acad. Sci. U S A* **101**, 15579-15584

15.     Coffa, G., Imber, A. N., Maguire, B. C., Laxmikanthan, G., Schneider, C., Gaffney, B. J., and Brash, A. R. (2005) *J. Biol. Chem.* **280**, 38756-38766

16.     Zheng, Y., Boeglin, W. E., Schneider, C., and Brash, A. R. (2008) *J. Biol. Chem.* **283**, 5138-5147

17.     Neau, D. B., Gilbert, N. C., Bartlett, S. G., Boeglin, W., Brash, A. R., and Newcomer, M. E. (2009) *Biochemistry* **48**, 7906-7915

18.     de Groot, J. J. M. C., Garssen, G. J., Veldink, G. A., Vliegenthart, J. F., and Boldingh, J. (1975) *FEBS Lett.* **56**, 50-54

19.     Schilstra, M. J., Veldink, G. A., and Vliegenthart, J. F. (1994) *Biochemistry* **33**, 3974-3979

20.     Haining, J. L., and Axelrod, B. (1958) *J. Biol. Chem.* **232**, 193-202

21.     Qian, S. Y., Yue, G. H., Tomer, K. B., and Mason, R. P. (2003) *Free Radic. Biol. Med.* **34**, 1017-1028

22.     Chamulitrat, W., Mason, R. P., and Riendeau, D. (1992) *J. Biol. Chem.* **267**, 9574-9579

23.     Clapp, C. H., Banerjee, A., and Rotenberg, S. A. (1985) *Biochemistry* **24**, 1826-1830

24.     Mansuy, D., Cucurou, C., Biatry, B., and Battioni, J. P. (1988) *Biochem. Biophys. Res. Commun.* **151**, 339-346

25.     Nelson, M. J., Batt, D. G., Thompson, J. S., and Wright, S. W. (1991) *J. Biol. Chem.* **266**, 8225-8229

26.     Riendeau, D., Falgueyret, J. P., Guay, J., Ueda, N., and Yamamoto, S. (1991) *Biochem. J.* **274**, 287-292

27.     Kemal, C., Louis-Flamberg, P., Krupinski-Olsen, R., and Shorter, A. L. (1987) *Biochemistry* **26**, 7064-7072

28.     de Groot, J. J. M. C., Garssen, G. J., Vliegenthart, J. F. G., and Boldingh, J. (1973) *Biochim. Biophys. Acta* **326**, 279-284

29.     Glickman, M. H., and Klinman, J. P. (1996) *Biochemistry* **35**, 12882-12892

30.     Garssen, G. J., Vliegenthart, J. F., and Boldingh, J. (1971) *Biochem. J.* **122**, 327-332

31.     Garssen, G. J., Vliegenthart, J. F., and Boldingh, J. (1972) *Biochem. J.* **130**, 435-442

32.     van der Heijdt, L. M., van der Lecq, F., Lachmansingh, A., Versluis, K., van der Kerk-van Hoof, A., Veldink, G. A., and Vliegenthart, J. F. (1993) *Lipids* **28**, 779-782

33.     Verhagen, J., Bouman, A. A., Vliegenthart, J. F. G., and Boldingh, J. (1976) *Biochim. Biophys. Acta* **486**, 114-120

34. Garssen, G. J., Veldink, G. A., Vliegenthart, J. F., and Boldingh, J. (1976) *Eur. J. Biochem.* **62**, 33-36

35. Slappendel, S., Veldink, G. A., Vliegenthart, J. F., AASA, R., and Malmstrom, B. G. (1983) *Biochim. Biophys. Acta* **747**, 32-36

36. Krieg, P., Siebert, M., Kinzig, A., Bettenhausen, R., Marks, F., and Furstenberger, G. (1999) *FEBS Lett.* **446**, 142-148

37. Yu, Z., Schneider, C., Boeglin, W. E., Marnett, L. J., and Brash, A. R. (2003) *Proc. Natl. Acad. Sci. U S A* **100**, 9162-9167

38. Dix, T. A., and Marnett, L. J. (1985) *J. Biol. Chem.* **260**, 5351-5357

39. O'Brien, P. J. (1969) *Can. J. Biochem.* **47**, 485-492

40. Elias, P. M., Williams, M. L., Holleran, W. M., Jiang, Y. J., and Schmuth, M. (2008) *J. Lipid Res.* **49**, 697-714

41. Fuchs, E. (2009) *Cell Stem Cell* **4**, 499-502

42. Elias, P. M., and Menon, G. K. (1991) *Adv. Lipid Res.* **24**, 1-26

43. Akiyama, M., and Shimizu, H. (2008) *Exp. Dermatol.* **17**, 373-382

44. Kalinin, A. E., Kajava, A. V., and Steinert, P. M. (2002) *Bioessays* **24**, 789-800

45. Nemes, Z., Marekov, L. N., Fesus, L., and Steinert, P. M. (1999) *Proc. Natl. Acad. Sci. U S A* **96**, 8402-8407

46. Landmann, L. (1986) *J. Invest. Dermatol.* **87**, 202-209

47. Madison, K. C. (2003) *J. Invest. Dermatol.* **121**, 231-241

48. Burr, G. O., and Burr, M. M. (1930) *J. Biol. Chem.* **86**, 587-621

49. Burr, G. O., and Burr, M. M. (1929) *J. Biol. Chem.* **82**, 345-367

50. De Thomas, M. E., Branner, R. R., and Peluffo, R. D. (1963) *Biochim. Biophys. Acta* **70**, 472

51. Prottey, C. (1976) *Br. J. Dermatol.* **94**, 579-585

52. Prottey, C. (1977) *Br. J. Dermatol.* **97**, 29-38

53. Hansen, H. S., and Jensen, B. (1985) *Biochim. Biophys. Acta* **834**, 357-363

54. Houtsmuller, U. M., and van der Beek, A. (1981) *Prog. Lipid Res.* **20**, 219-224

55. Ziboh, V. A., and Hsia, S. L. (1972) *J. Lipid Res.* **13**, 458-467

56. Houtsmuller, U. M. (1981) *Prog. Lipid Res.* **20**, 889-896

57. Gray, G. M., White, R. J., and Majer, J. R. (1978) *Biochim. Biophys. Acta* **528**, 127-137

58. Wertz, P. W., and Downing, D. T. (1982) *Science* **217**, 1261-1262

59. Wertz, P. W., and Downing, D. T. (1983) *J. Lipid Res.* **24**, 1135-1139

60. Wertz, P. W., and Downing, D. T. (1983) *J. Lipid Res.* **24**, 759-765

61. Wertz, P. W., and Downing, D. T. (1983) *J. Lipid Res.* **24**, 753-758

62. Bowser, P. A., Nugteren, D. H., White, R. J., Houtsmuller, U. M., and Prottey, C. (1985) *Biochim. Biophys. Acta* **834**, 419-428

63. Bowser, P. A., and White, R. J. (1985) *Br. J. Dermatol.* **112**, 1-14

64. Wertz, P. W., Cho, E. S., and Downing, D. T. (1983) *Biochim. Biophys. Acta* **753**, 350-355

65. Hansen, H. S., Jensen, B., and von Wettstein-Knowles, P. (1986) *Biochim. Biophys. Acta* **878**, 284-287

66. Chapkin, R. S., and Ziboh, V. A. (1984) *Biochem. Biophys. Res. Commun.* **124**, 784-792

67. Landmann, L., Wertz, P. W., and Downing, D. T. (1984) *Biochim. Biophys. Acta* **778**, 412-418

68. Bouwstra, J. A., Gooris, G. S., Dubbelaar, F. E., and Ponec, M. (2002) *J. Invest. Dermatol.* **118**, 606-617

69. Wertz, P. W., and Downing, D. T. (1987) *Biochim. Biophys. Acta* **917**, 108-111

70. Wertz, P. W., Madison, K. C., and Downing, D. T. (1989) *J. Invest. Dermatol.* **92**, 109-111

71. Swartzendruber, D. C., Wertz, P. W., Madison, K. C., and Downing, D. T. (1987) *J. Invest. Dermatol.* **88**, 709-713

72. Downing, D. T. (1992) *J. Lipid Res.* **33**, 301-313

73.     Doering, T., Holleran, W. M., Potratz, A., Vielhaber, G., Elias, P. M., Suzuki, K., and Sandhoff, K. (1999) *J. Biol. Chem.* **274**, 11038-11045

74.     Doering, T., Proia, R. L., and Sandhoff, K. (1999) *FEBS Lett.* **447**, 167-170

75.     Hedberg, C. L., Wertz, P. W., and Downing, D. T. (1988) *J. Invest. Dermatol.* **91**, 169-174

76.     Doering, T., Brade, H., and Sandhoff, K. (2002) *J. Lipid Res.* **43**, 1727-1733

77.     Madison, K. C., Swartzendruber, D. C., Wertz, P. W., and Downing, D. T. (1989) *J. Invest. Dermatol.* **93**, 10-17

78.     Meguro, S., Arai, Y., Masukawa, Y., Uie, K., and Tokimitsu, I. (2000) *Arch. Dermatol. Res.* **292**, 463-468

79.     Tobias, L. D., and Hamilton, J. G. (1979) *Lipids* **14**, 181-193

80.     Nugteren, D. H., Christ-Hazelhof, E., van der Beek, A., and Houtsmuller, U. M. (1985) *Biochim. Biophys. Acta* **834**, 429-436

81.     Wertz, P. W., and Downing, D. T. (1990) *J. Lipid Res.* **31**, 1839-1844

82.     Nugteren, D. H., and Kivits, G. A. (1987) *Biochim. Biophys. Acta* **921**, 135-141

83.     Boeglin, W. E., Kim, R. B., and Brash, A. R. (1998) *Proc. Natl. Acad. Sci. U S A* **95**, 6744-6749

84.     Brash, A. R., Boeglin, W. E., and Chang, M. S. (1997) *Proc. Natl. Acad. Sci. U S A* **94**, 6148-6152

85.     Heidt, M., Furstenberger, G., Vogel, S., Marks, F., and Krieg, P. (2000) *Lipids* **35**, 701-707

86.     Jobard, F., Lefevre, C., Karaduman, A., Blanchet-Bardon, C., Emre, S., Weissenbach, J., Qzquc, M., Lathrop, M., Prud'homme, J. F., and Fischer, J. (2002) *Hum. Mol. Genet.* **11**, 107

87.     Eckl, K. M., de Juanes, S., Kurtenbach, J., Natebus, M., Lugassy, J., Oji, V., Traupe, H., Preil, M. L., Martinez, F., Smolle, J., Harel, A., Krieg, P., Sprecher, E., and Hennies, H. C. (2009) *J. Invest. Dermatol.* **129**, 1421-1428

88.     Eckl, K. M., Krieg, P., Kuster, W., Traupe, H., Andre, F., Wittstruck, N., Furstenberger, G., and Hennies, H. C. (2005) *Hum. Mutat.* **26**, 351-361

89.	Epp, N., Furstenberger, G., Muller, K., de Juanes, S., Leitges, M., Hausser, I., Thieme, F., Liebisch, G., Schmitz, G., and Krieg, P. (2007) *J. Cell Biol.* **177**, 173-182

90.	Krieg, P., de Juanes, S., Epp, N., Rosenberger, S., Furstenberger, G., Hausser, I., Thieme, F., Liebisch, G., Schmitz, G., and Stark, H. (2010) *The 12th International Winter Eicosanoid Conference* abstract, Baltimore, MD

91.	Moran, J. L., Qiu, H., Turbe-Doan, A., Yun, Y., Boeglin, W. E., Brash, A. R., and Beier, D. R. (2007) *J. Invest. Dermatol.* **127**, 1893-1897

92.	Pace-Asciak, C. R., Reynaud, D., and Demin, P. M. (1995) *Lipids* **30**, 107-114

93.	Woollard, P. M. (1986) *Biochem. Biophys. Res. Commun.* **136**, 169-176

94.	Yu, Z., Schneider, C., Boeglin, W. E., and Brash, A. R. (2007) *Lipids* **42**, 491-497

95.	Schmuth, M., Schoonjans, K., Yu, Q. C., Fluhr, J. W., Crumrine, D., Hachem, J. P., Lau, P., Auwerx, J., Elias, P. M., and Feingold, K. R. (2002) *J. Invest. Dermatol.* **119**, 1298-1303

96.	Brash, A. R., Yu, Z., Boeglin, W. E., and Schneider, C. (2007) *FEBS J.* **274**, 3494-3502

97.	Siebert, M., Krieg, P., Lehmann, W. D., Marks, F., and Furstenberger, G. (2001) *Biochem. J.* **355**, 97-104

98.	Yu, Z., Schneider, C., Boeglin, W. E., and Brash, A. R. (2006) *Arch. Biochem. Biophys.* **455**, 188-196

99.	Furstenberger, G., Epp, N., Eckl, K. M., Hennies, H. C., Jorgensen, C., Hallenborg, P., Kristiansen, K., and Krieg, P. (2007) *Prostaglandins Other Lipid Mediat.* **82**, 128-134

100.	Fischer, J. (2009) *J. Invest. Dermatol.* **129**, 1319-1321

101.	Kinzig, A., Heidt, M., Furstenberger, G., Marks, F., and Krieg, P. (1999) *Genomics* **58**, 158-164

102.	Schilstra, M. J., Veldink, G. A., and Vliegenthart, J. F. (1993) *Biochemistry* **32**, 7686-7691

103.	Brash, A. R., and Song, W. (1996) *Methods Enzymol.* **272**, 250-259

104.	Nugteren, D. H., and Christ-Hazelhof, E. (1987) *Prostaglandins* **33**, 403-417

105. Boutaud, O., and Brash, A. R. (1999) *J. Biol. Chem.* **274**, 33764-33770

106. Huang, L. S., Kim, M. R., and Sok, D. E. (2006) *Arch. Biochem. Biophys.* **455**, 119-126

107. Brash, A. R., Boeglin, W. E., Capdevila, J. H., Yeola, S., and Blair, I. A. (1995) *Arch. Biochem. Biophys.* **321**, 485-492

108. Brash, A. R., Ingram, C. D., and Harris, T. M. (1987) *Biochemistry* **26**, 5465-5471

109. Brash, A. R., Yokoyama, C., Oates, J. A., and Yamamoto, S. (1989) *Arch. Biochem. Biophys.* **273**, 414-422

110. Clapp, C. H., Strulson, M., Rodriguez, P. C., Lo, R., and Novak, M. J. (2006) *Biochemistry* **45**, 15884-15892

111. Pistorius, E. (1974) *PhD thesis, Purdue University*

112. Salzmann, U., Kuhn, H., Schewe, T., and Rapoport, S. M. (1984) *Biochim. Biophys. Acta* **795**, 535-542

113. Butovich, I. A., and Reddy, C. C. (2001) *Biochim. Biophys. Acta* **1546**, 379-398

114. Cristea, M., and Oliw, E. H. (2006) *J. Biol. Chem.* **281**, 17612-17623

115. Meruvu, S., Walther, M., Ivanov, I., Hammarstrom, S., Furstenberger, G., Krieg, P., Reddanna, P., and Kuhn, H. (2005) *J. Biol. Chem.* **280**, 36633-36641

116. Kuhn, H., Saam, J., Eibach, S., Holzhutter, H. G., Ivanov, I., and Walther, M. (2005) *Biochem. Biophys. Res. Commun.* **338**, 93-101

117. Gardner, H. W. (1989) *Biochim. Biophys. Acta* **1001**, 274-281

118. Brash, A. R. (2000) *Lipids* **35**, 947-952

119. Tallman, K. A., Pratt, D. A., and Porter, N. A. (2001) *J. Am. Chem. Soc.* **123**, 11827-11828

120. Su, C., and Oliw, E. H. (1998) *J. Biol. Chem.* **273**, 13072-13079

121. Andreou, A., Gobel, C., Hamberg, M., and Feussner, I. (2010) *J. Biol. Chem.* **285**, 14178-14186

122. Cristea, M., and Oliw, E. H. (2007) *J. Lipid. Res.* **48**, 890-903

123. Kuhn, H., Wiesner, R., Stender, H., Schewe, T., Lankin, V. Z., Nekrasov, A., and Rapoport, S. M. (1986) *FEBS Lett.* **203**, 247-252

124. Perez-Gilabert, M., Sanchez-Felipe, I., Morte, A., and Garcia-Carmona, F. (2005) *J. Agric. Food Chem.* **53**, 6140-6145

125. de Groot, J. J. M. C., Veldink, G. A., Vliegenthart, J. F. G., Boldingh, J., Wever, R., and van Gelder, B. F. (1975) *Biochim. Biophys. Acta.* **377**, 71-79

126. Ivanov, I., Saam, J., Kuhn, H., and Holzhutter, H. G. (2005) *FEBS J.* **272**, 2523-2535

127. Axelrod, B., Cheesbrough, T. M., and Laakso, S. (1981) *Methods Enzymol.* **71**, 441-451

128. Fukushige, H., Wang, C., Simpson, T. D., Gardner, H. W., and Hildebrand, D. F. (2005) *J. Agric. Food Chem.* **53**, 5691-5694

129. Gao, X., Stumpe, M., Feussner, I., and Kolomiets, M. (2008) *Planta* **227**, 491-503

130. Senger, T., Wichard, T., Kunze, S., Gobel, C., Lerchl, J., Pohnert, G., and Feussner, I. (2005) *J. Biol. Chem.* **280**, 7588-7596

131. Feussner, I., and Wasternack, C. (2002) *Annu. Rev. Plant Biol.* **53**, 275-297

132. Ford-Hutchinson, A. W., Gresser, M., and Young, R. N. (1994) *Annu. Rev. Biochem.* **63**, 383-417

133. Schilstra, M. J., Veldink, G. A., Verhagen, J., and Vliegenthart, J. F. (1992) *Biochemistry* **31**, 7692-7699

134. Qian, S. Y., Yue, G. H., Tomer, K. B., and Mason, R. P. (2003) *Free Radic. Biol. Med.* **34**, 1017-1028

135. Zheng, Y., and Brash, A. R. (2010) *J. Biol. Chem., in press*

136. Boeglin, W. E., Itoh, A., Zheng, Y., Coffa, G., Howe, G. A., and Brash, A. R. (2008) *Lipids* **43**, 979-987

137. Verhagen, J., Veldink, G. A., Vliegenthart, J. F. G., and Boldingh, J. (1979) *Advances in the Biochemistry and Physiology of Plant Lipids* Appelqvist, L. (editor) and Liljenberg C. (editor) 231-236

138. Zheng, Y., and Brash, A. R. (2010) *J. Biol. Chem.* **285**, 13427-13436

139. Van Os, C. P., Vliegenthart, J. F. G., Crawford, C. G., and Gardner, H. W. (1982) *Biochim. Biophys. Acta.* **713**, 173-176

140. Chang, M. S., Boeglin, W. E., Guengerich, F. P., and Brash, A. R. (1996) *Biochemistry* **35**, 464-471

141. Gardner, H. W., Weisleder, D., and Kleiman, R. (1978) *Lipids* **13**, 246-252

142. Hamberg, M. (1975) *Lipids* **10**, 87-92

143. Reeder, B. J., and Wilson, M. T. (1998) *Biochem. J.* **330**, 1317-1323

144. Gardner, H. W. (1989) *Free Radic. Biol. Med.* **7**, 65-86

145. Marnett, L. J., and Wilcox, A. L. (1995) *Biochem. Soc. Symp.* **61**, 65-72

146. Gardner, H. W., and Crawford, C. G. (1981) *Biochim. Biophys. Acta* **665**, 126-133

147. Gardner, H. W., and Jursinic, P. A. (1981) *Biochim. Biophys. Acta* **665**, 100-112

148. Gardner, H. W., and Kleiman, R. (1981) *Biochim. Biophys. Acta* **665**, 113-124

149. Dix, T. A., Fontana, R., Panthani, A., and Marnett, L. J. (1985) *J. Biol. Chem.* **260**, 5358-5365

150. Uchida, Y., and Holleran, W. M. (2008) *J. Dermatol. Sci.* **51**, 77-87

151. Elias, P. M. (2005) *J. Invest. Dermatol.* **125**, 183-200

152. Bligh, E. G., and Dyer, W. J. (1959) *Can. J. Biochem. Physiol.* **37**, 911-917

153. Farwanah, H., Wohlrab, J., Neubert, R. H., and Raith, K. (2005) *Anal. Bioanal. Chem.* **383**, 632-637

154. Hamanaka, S., Asagami, C., Suzuki, M., Inagaki, F., and Suzuki, A. (1989) *J. Biochem.* **105**, 684-690

155. Lin, D., Zhang, J., and Sayre, L. M. (2007) *J. Org. Chem.* **72**, 9471-9480

156. Marekov, L. N., and Steinert, P. M. (1998) *J. Biol. Chem.* **273**, 17763-17770

157. Radmark, O., Werz, O., Steinhilber, D., and Samuelsson, B. (2007) *Trends Biochem. Sci.* **32**, 332-341

158. Feltenmark, S., Gautam, N., Brunnstrom, A., Griffiths, W., Backman, L., Edenius, C., Lindbom, L., Bjorkholm, M., and Claesson, H. E. (2008) *Proc. Natl. Acad. Sci. U S A* **105**, 680-685

159. Bryant, R. W., Schewe, T., Rapoport, S. M., and Bailey, J. M. (1985) *J. Biol. Chem.* **260**, 3548-3555

160. Van Os, C. P., Rijke-Schilder, G. P., Van Halbeek, H., Verhagen, J., and Vliegenthart, J. F. (1981) *Biochim. Biophys. Acta* **663**, 177-193

161. Yokoyama, C., Shinjo, F., Yoshimoto, T., Yamamoto, S., Oates, J. A., and Brash, A. R. (1986) *J. Biol. Chem.* **261**, 16714-16721

162. Corey, E. J., Wright, S. W., and Matsuda, S. P. T. (1989) *J. Am. Chem. Soc.* **111**, 1452-1455

163. Corey, E. J., Albright, J. O., Barton, A. E., and Hashimoto, S. I. (1980) *J. Am. Chem. Soc.* **102**, 1435-1436

164. Schneider, C., Boeglin, W. E., and Brash, A. R. (2000) *Anal. Biochem.* **287**, 186-189

165. Ferreri, C., Samadi, A., F., S., Landi, L., and Chatgilialoglu, C. (2004) *J. Am. Chem. Soc.* **126**, 1063-1072

166. Moussebois, C., and Dale, J. (1966) *J. Chem. Soc. C.*, 260-264

167. Powell, W. S. (1982) *Methods Enzymol.* **86**, 530-543

168. Christie, W. W., and Breckenridge, G. H. M. (1989) *J. Chromatogr. A.* **469**, 261-269

169. Corey, E. J., and Mehrotra, M. M. (1983) *Tetrahedron Lett.* **24**, 4921-4922

170. Maas, R. L., Turk, J., Oates, J. A., and Brash, A. R. (1982) *J. Biol. Chem.* **257**, 7056-7067

171. Gardner, H. W. (1991) *Biochim. Biophys. Acta* **1084**, 221-239

172. Maas, R. L., and Brash, A. R. (1983) *Proc. Natl. Acad. Sci. U S A* **80**, 2884-2888

173. Shimizu, T., Radmark, O., and Samuelsson, B. (1984) *Proc. Natl. Acad. Sci. U S A* **81**, 689-693

174. Borgeat, P., Hamberg, M., and Samuelsson, B. (1976) *J. Biol. Chem.* **251**, 7816-7820

175. Shimizu, T., Izumi, T., Seyama, Y., Tadokoro, K., Radmark, O., and Samuelsson, B. (1986) *Proc. Natl. Acad. Sci. U S A* **83**, 4175-4179

176. Bryant, R. W., Bailey, J. M., Schewe, T., and Rapoport, S. M. (1982) *J. Biol. Chem.* **257**, 6050-6055

177. Knapp, M. J., and Klinman, J. P. (2003) *Biochemistry* **42**, 11466-11475

178. Hamberg, M. (1983) *Biochim. Biophys. Acta* **752**, 353-356

179. Hamberg, M. (1983) *Biochim. Biophys. Acta* **752**, 191-197

180. Sok, D. E., Chung, T., and Sih, C. J. (1983) *Biochem. Biophys. Res. Commun.* **110**, 273-279

181. Griller, D., and Ingold, K. U. *Acc. Chem. Res.* **13**, 317-323

182. Maas, R. L., Ingram, C. D., Porter, A. T., Oates, J. A., Taber, D. F., and Brash, A. R. (1985) *J. Biol. Chem.* **260**, 4217-4228

183. Brash, A. R. (2009) *Phytochemistry* **70**, 1522-1531